

# Targeting the TRAF6-Ubc13 interaction for therapeutic intervention

Dissertation

der Fakultät für Biologie

der Ludwig-Maximilians-Universität München

zur Erlangung des Doktorgrades der Naturwissenschaften

angefertigt am

**Helmholtz Zentrum München**

Deutsches Forschungszentrum für Gesundheit und Umwelt

unter der Leitung von

Prof. Dr. Daniel Krappmann

vorgelegt von

**Jara Kerstin Brenke**

München, den 26.02.2015



1. Gutachter:	Prof. Dr. Daniel Krappmann
2. Gutachter:	Prof. Dr. Elisabeth Weiß

Tag der mündlichen Prüfung:	30.07.2015
-----------------------------	------------

Mitglieder der Prüfungskommission:	Prof. Dr. Heinrich Jung Prof. Dr. Ruth Brack-Werner
------------------------------------	--

Weitere Gutachter:	Prof. Dr. Charles David Prof. Dr. Benedikt Grothe
--------------------	--

For Henry, Karla and Tilman



---

## Table of Content

<b>1 Summary.....</b>	<b>1</b>
<b>2 Introduction.....</b>	<b>3</b>
2.1 The Ubiquitin Proteasome System.....	3
2.1.1 The ubiquitination cascade.....	3
2.1.2 Types and functions of ubiquitination.....	4
2.1.3 E3 Ubiquitin ligases.....	5
2.1.4 Deubiquitinases.....	6
2.2 NF- $\kappa$ B signaling.....	7
2.2.1 The NF- $\kappa$ B transcription factor family.....	7
2.2.2 Canonical NF- $\kappa$ B signaling.....	9
2.2.2.1 Activation of the transcription factor NF- $\kappa$ B.....	9
2.2.2.2 Membrane proximal interactions.....	11
2.2.2.2.1 Signaling cascades triggered by the TLR/IL-1R superfamily.....	11
2.2.2.2.2 Signaling via the TNF receptor superfamily.....	14
2.2.2.3 Regulation of NF- $\kappa$ B by Deubiquitinases.....	14
2.2.3 Noncanonical NF- $\kappa$ B signaling.....	15
2.2.4 NF- $\kappa$ B signaling in diseases.....	16
2.2.4.1 NF- $\kappa$ B signaling in inflammatory disorders and cancer.....	16
2.2.4.2 NF- $\kappa$ B signaling in metabolic diseases.....	17
2.3 TRAF6 in cellular signaling.....	19
2.3.1 The TRAF protein family.....	19
2.3.2 TRAF6.....	20
2.3.2.1 Structure of the TRAF6 protein.....	20
2.3.2.2 Functions of TRAF6 in signaling pathways.....	21
2.3.2.3 Counteracting TRAF6 activity by DUBs.....	23
2.3.2.4 TRAF6 in diseases.....	24
2.3.2.4.1 TRAF6 in obesity and insulin resistance.....	24
2.4 The TRAF6 - Ubc13 interaction in NF- $\kappa$ B signaling.....	25
2.4.1 The ubiquitin-conjugating enzyme Ubc13.....	25
2.4.2 The direct interaction of TRAF6 and Ubc13.....	27
2.5 Protein-protein-interactions and the UPS in drug discovery.....	29
<b>3 Aim of this thesis.....</b>	<b>31</b>

---

<b>4 Results</b>	<b>32</b>
4.1 Establishment of a TRAF6-Ubc13 interaction assay for High-Throughput-Screening	32
4.1.1 Biochemical validation of the TRAF6-Ubc13 interaction	32
4.1.2 Establishment of the ALPHAScreen TRAF6-Ubc13 binding assay for HTS	33
4.2 HTS, Hit identification and Hit verification	36
4.2.1 HTS – Hit identification	36
4.2.2 HTS – Hit verification	37
4.3 Biochemical and cell-based Hit validation	38
4.3.1 Biochemical hit validation	38
4.3.2 Cell-based hit validation	39
4.4 Validation of C27 in biochemical and cell-based assays	42
4.4.1 Biochemical validation of C27	43
4.4.2 Cell-based validation of C27	44
4.5 Validation of C25 in biochemical and cell-based experiments	50
4.5.1 Biochemical analysis of C25	51
4.5.2 Verification of C25 in cell-based assays	52
4.6 Hit optimization	56
4.6.1 Biochemical Structural activity relationships (SAR) of C25	56
4.6.2 Verification of the three best analogs of C25 in cell-based assays	58
4.7 In-depth analysis of C25-0140	60
4.7.1 Biochemical studies of C25-0140	61
4.7.2 Investigation of C25-0140 in cell-based assays	62
4.7.3 Analysis of the effect of C25-0140 in an obese mouse model	67
<b>5 Discussion</b>	<b>71</b>
5.1 Targeting the TRAF6-Ubc13 interaction: a novel approach for interfering with E3 ligase activity by protein-protein-interaction inhibition	71
5.2 Identification and verification of TRAF6-Ubc13 inhibitors <i>in vitro</i>	75
5.2.1 High-Throughput assays for screening of selective TRAF6-Ubc13 inhibitors	75
5.2.2 Low-Throughput assays for verifying selected TRAF6-Ubc13 inhibitors	78
5.3 Verification of the newly identified TRAF6-Ubc13 inhibitors in cell-based assays	79
5.4 Selectivity of compounds targeting the RING-Zincfinger1 domain of TRAF6	81
5.5. Targeting the RING-Zincfinger1 domain of TRAF6	84
5.6 Targeting the TRAF6-Ubc13 interaction for therapeutic intervention	86

---

5.6.1 Targeting TRAF6 in Obesity.....	86
5.6.2 Targeting TRAF6 in autoimmune disorders.....	90
5.6.3 Targeting TRAF6 in cancer.....	91
<b>6 Outlook.....</b>	<b>93</b>
<b>7. Material and Methods.....</b>	<b>94</b>
7.1 Material.....	94
7.1.1 Instruments and Equipment.....	94
7.1.2 Chemicals.....	96
7.1.3 Antibodies.....	99
7.1.4 Enzymes and Kits.....	99
7.1.5 Bacteria strains.....	100
7.1.6 Eukaryotic cell lines.....	101
7.1.7 Mouse strains.....	101
7.1.8 Recombinant proteins.....	101
7.1.9 Vectors and generated plasmids.....	101
7.1.10 Oligonucleotides.....	102
7.1.11 Buffers.....	103
7.1.12 Software.....	105
7.1.13 Screening libraries and small molecules.....	105
7.2 Methods.....	107
7.2.1 Molecular biological methods.....	107
7.2.1.1 Polymerase chain reaction (PCR).....	107
7.2.1.2 Agarose Gel Electrophoresis and DNA extraction from gel.....	107
7.2.1.3 Restriction digest.....	108
7.2.1.4 Ligation.....	108
7.2.1.5 Transformation of bacteria cells.....	108
7.2.1.6 Plasmid preparation.....	108
7.2.1.7 RNA extraction.....	108
7.2.1.8 cDNA synthesis and Quantitative Realtime PCR.....	109
7.2.2 Cell biological methods.....	110
7.2.2.1 Cultivation of eukaryotic cells.....	110
7.2.2.2 Compound treatment and stimulation of MEF cells.....	110

---

7.2.2.3 Toxicity assays.....	111
7.2.2.4 Storage of eukaryotic cells.....	112
7.2.2.5 p65 translocation assay.....	112
7.2.2.6 Yeast-Two-Hybrid- (Y2H) assay.....	112
7.2.3 Biochemical and immunological methods.....	113
7.2.3.1 Recombinant protein purification.....	113
7.2.3.1.1 Purification of TRAF6Strepll.....	113
7.2.3.1.2 Purification of untagged TRAF6 protein.....	113
7.2.3.1.3 Purification of Ubc13FH.....	114
7.2.3.1.4 Purification of GST-tagged TRAF6, OTUB1 and RNF8 proteins.....	115
7.2.3.2 SDS-Polyacrylamid-Gelectrophoresis (SDS-PAGE).....	115
7.2.3.3 Coomassie and Silverstain.....	115
7.2.3.4 Western Blot and Immunodetection.....	116
7.2.3.5 Gel-filtration assay.....	116
7.2.3.6 <i>In vitro</i> Ubiquitination assay.....	116
7.2.3.7 Pulldown assay.....	117
7.2.3.8 Saturation-Transfer-Difference-Nuclear-Magnetic-Resonance.....	117
7.2.3.9 ALPHAScreen assay.....	117
7.2.3.10 High-Throughput-Screening.....	118
7.2.3.11 Electro-Mobility-Shift-Assay (EMSA).....	119
7.2.3.12 Immunoprecipitation of TRAF6 for endogenous ubiquitination.....	120
7.2.3.13 IKK kinase assay.....	121
7.2.3.14 ALPHASurefire.....	121
7.2.4 Diet-Induced-Obesity (DIO) mouse study.....	122
7.2.4.1 Treatment of DIO-mice.....	122
7.2.4.2 Glucose Tolerance Test (GTT).....	122
7.2.4.3 Isolation of protein from epidermal white adipose tissue of DIO.....	122
<b>8 References.....</b>	<b>123</b>
<b>9 Abbreviations.....</b>	<b>140</b>
<b>10 Supplement.....</b>	<b>145</b>

---

<b>11 Appendix.....</b>	
11.1 Publications.....	155
11.2 Curriculum Vitae.....	156
11.3 Acknowledgements.....	157



## 1 Summary

Receptor stimulation by IL-1 $\beta$  and LPS initiates the interaction of the E3 Ligase TRAF6 and the E2-conjugating enzyme Ubc13, which is required to mediate signal progression towards NF- $\kappa$ B activation. Interfering with the TRAF6-Ubc13 complex formation by small molecules could help to relieve symptoms of diseases associated with elevated NF- $\kappa$ B activation including autoimmune diseases, metabolic disorders and cancer. To identify specific inhibitors of TRAF6-Ubc13 interaction, a High-Throughput-Screening involving the ALPHAScreen technology was established. Screening of small molecule libraries consisting of ~25,000 compounds led to the identification of several selective inhibitors of TRAF6-Ubc13 interaction. Two of the most potent compounds (C27 and C25) were selected for further studies of their effects on TRAF6-Ubc13 *in vitro* and on TRAF6 function and NF- $\kappa$ B signaling in cells. Both compounds are directly binding to TRAF6 and are capable of disrupting TRAF6 binding to Ubc13 in a dose dependent manner. Cell based assays revealed a strong but non-pathway selective effect on NF- $\kappa$ B signaling after C27 treatment. In contrast, C25 led to a milder, but IL-1 $\beta$ /TLR specific impairment of NF- $\kappa$ B activation in EMSA as well as target gene experiments. Studies of the structure activity relationships of C25 highlighted the analog C25-0140 as a compound with a strongly enhanced inhibitory potential in cells. Biochemical experiments proved that C25-0140 is directly binding to the RING-Zincfinger1 domain of TRAF6 and inhibits the TRAF6-Ubc13 interaction with an IC<sub>50</sub> of ~ 2.6 $\mu$ M. In cells, C25-0140 diminished TRAF6 auto-ubiquitination as well as the activity of the IKK complex after IL-1 $\beta$  stimulation and it thereby exhibited strong effects on NF- $\kappa$ B activation. However, despite the augmented effectiveness of compound C25-0140, the selectivity of the compound was decreased. Besides affecting TRAF6-dependent IL-1 $\beta$  and LPS pathways, TNF $\alpha$ -induced NF- $\kappa$ B activation was impaired as well. Based on studies describing the pharmacological disposition of C25-0140, the compound was tested in a diet-induced obesity (DIO) mouse model that is characterized by low-grade chronic inflammation leading to increased glucose intolerance. Indeed, C25-0140 administration reduced the weight gain without affecting food uptake of the animals, but did not improve glucose tolerance. There was a tendency for a slight relieve of the chronic inflammatory symptoms in the animals indicating that the compound affects innate immune signaling *in vivo*. Taken together, the identification of the first small molecules specifically inhibiting the TRAF6-Ubc13 interaction *in vitro* by directly targeting the TRAF6 RING-Zincfinger1 domain provides a proof of concept for the feasibility of small molecule targeting of an E2-E3 interaction. The identified compounds

inhibit TRAF6 activity and NF- $\kappa$ B signaling in cells and first *in vivo* data indicate an effect in a TRAF6-dependent mouse model of diet-induced obesity. However, cellular studies indicate that the identified small molecules are not highly selective for TRAF6-Ubc13 inhibition. Further investigations will be necessary to unravel the exact mode of action and to further improve effectiveness and selectivity of the compounds.

## **2 Introduction**

### **2.1 The Ubiquitin Proteasome System**

The ubiquitin proteasome system (UPS) is a key regulator of cellular functions in eukaryotes ranging from proteasome-dependent proteolysis to modulation of protein function in cell signaling, autophagy and DNA damage response as well as structure assembly and localization of cellular proteins (Deshaies and Joazeiro, 2009). Ubiquitination is a posttranslational modification that covalently attaches ubiquitin molecules to substrates. Ubiquitin is a small (8.5kDa) regulatory protein consisting of 76 amino acids forming a compact globular structure with an exposed C-terminal tail that can be covalently linked to another ubiquitin molecule or to other substrate proteins (Husnjak and Dikic, 2012). In the human ubiquitin-modified proteome more than 4,000 to 5,000 proteins are shown to be modified by ubiquitin (Husnjak and Dikic, 2012). Ubiquitin substrates can be modified by either monoubiquitination at one or multiple sites or polyubiquitination with the different linkage types of ubiquitin chains leading to various functional consequences (Komander and Rape, 2012).

#### **2.1.1 The ubiquitination cascade**

Within the ubiquitination cascade, ubiquitin is covalently bound to substrate lysines in a three-enzyme cascade involving E1, E2 and E3 enzymes. The process of ubiquitination is displayed in Figure 2.2. In the humane proteome two E1 enzymes, approximately 40 E2 and around 600 E3 enzymes are described (Husnjak and Dikic, 2012). E1 enzymes are ubiquitin-activating proteins and catalyze the activation of an ubiquitin molecule, which is the first step within the ubiquitination process. E2s are ubiquitin-conjugating enzymes. Their active-site cysteine forms a thioester linkage with the C-terminus of the ubiquitin molecule (Deshaies and Joazeiro, 2009). E3 ubiquitin ligases bind E2 and substrate and mediate the transfer of ubiquitin from the E2 to the substrate (Deshaies and Joazeiro, 2009). The ubiquitination cascade begins with ATP-dependent charging of the ubiquitin-activating enzyme E1 resulting in the formation of a thioester bond between the C-terminus of the ubiquitin and the active site cysteine of the E1 enzyme. In a transthioesterification reaction, ubiquitin is then transferred to the active site cysteine of the ubiquitin-conjugating enzyme E2. Next, an E3 ubiquitin ligase catalyzes the transfer of the ubiquitin from the E2 to the substrate resulting in an isopeptide linkage between the C-terminus of the ubiquitin molecule and the  $\epsilon$ -aminogroup of the substrate lysine or methionine (Berndsen and Wolberger, 2014). Deubiquitinating enzymes (DUBs) can remove the ubiquitin from the substrate to recycle the ubiquitin molecules. Multiple ubiquitination cycles lead to polyubiquitination of the substrates.

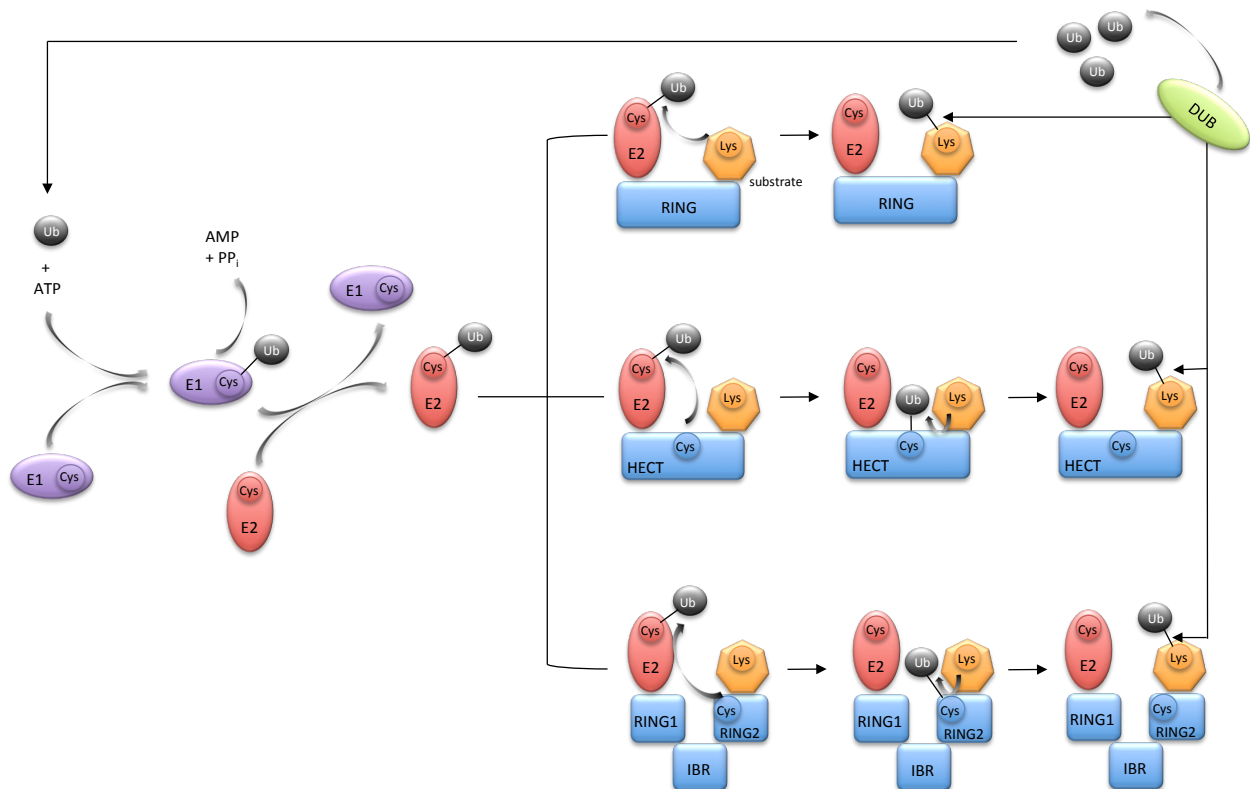


**Figure 2.1: The ubiquitination process.** Schematic overview of the ubiquitination process. First, ubiquitin (grey) is activated in an ATP-dependent manner and bound to the E1 activating enzyme (purple). After transfer of the ubiquitin to the E2 conjugating enzyme (red), E3 ligases (blue) remove the ubiquitin from the E2 and attach it to the substrate. Thereby, RING E3 ligases use a one-step reaction whereas HECT and RBR E3 ligases operate via a two-step reaction to transfer the ubiquitin to the substrate. In the end, deubiquitinating enzymes (green) remove the ubiquitin molecules.

### 2.1.2 Types and functions of ubiquitination

Ubiquitin is primarily attached to lysine residues, but it can also bind to the  $\epsilon$ -amino group at the N-terminus of the substrate as well as to cysteine, serine and threonine residues of target proteins (Husnjak and Dikic, 2012). Attaching of single (monoubiquitination) or several independent ubiquitin molecules (multiple monoubiquitination) to target proteins are shown to regulate signaling, endocytosis and DNA repair (Husnjak and Dikic, 2012). Polyubiquitin chains can be formed on methionine 1 and all seven internal lysine residues within an ubiquitin molecule (Lys6, Lys11, Lys 27, Lys29, Lys33, Lys48 and Lys63). Homotypic ubiquitin chains that contain only one linkage type per polymer or heterotypic ubiquitin chains that include multiple linkage types per polymer can be generated (Husnjak and Dikic, 2012; Komander and Rape, 2012). Depending on the type of linkage, polyubiquitination leads to a variety of functions. Whereas Lys48-linked chains are well known to target the substrate for proteasomal degradation via the 26S proteasome (Finley, 2009), Lys63-linked chains are implicated in a

variety of non-proteolytic functions like trafficking, DNA damage response as well as signaling for NF- $\kappa$ B activation in innate and adaptive immunity (Haglund and Dikic, 2005). Up to now, the roles of the other linkages have not been studied in great detail but these “atypical” polyubiquitin chains become more and more subject of investigation. For example, Lys11 chains are known to promote proteasomal degradation of substrate proteins during cell cycle progression (Jin et al., 2008) as well as regulating the endoplasmic reticulum-associated degradation (ERAD) (Xu et al., 2009). Even a regulatory function of Lys11 chains in NEMO-dependent NF- $\kappa$ B activation upon TNF $\alpha$  stimulation is described (Dynek et al., 2010). During stress response Lys27 and Lys33 polyubiquitin chains are assembled (Hatakeyama et al., 2001). Lys29-linked chains appear to function in ubiquitin fusion degradation (Johnson et al., 1995). Ubiquitin molecules can also be linked head to tail forming Met1-linked (linear) polyubiquitin chains. To date, only one E3 ligase complex, LUBAC (linear ubiquitin assembly complex) has been shown to assemble such chains (Kirisako et al., 2006) and plays a crucial role in NF- $\kappa$ B signaling (Rahighi et al., 2009). The existence of heterotypic ubiquitin chains has been demonstrated *in vitro*, but their role *in vivo* is not clear, yet (Kulathu and Komander, 2012).

### **2.1.3 E3 Ubiquitin ligases**

E3 ubiquitin ligases are divided into three classes each characterized by conserved structural domains and the distinct mechanism to transfer ubiquitin from the E2 to the substrate: the RING, the HECT and the RBR E3 ligases. The RING (really interesting new gene) E3 ligases contain a RING domain that mediates both binding of the ubiquitin charged E2 conjugating enzyme as well as the ubiquitin transfer from the E2 to the substrate (Lorick et al., 1999) (see Figure 2.1). Representative RING E3 ligases involved in TLR/IL-1R and TNFR signaling are TRAF2, TRAF5, TRAF6 and cIAP1/2 (Deshaies and Joazeiro, 2009). Their RING domain folds into a conserved cross-brace structure and incorporates two zinc ions. The basic sequence expression of the canonical RING domain is Cys-X<sub>2</sub>-Cys-X<sub>(9-39)</sub>-Cys-X<sub>(1-3)</sub>-His-X<sub>(2-3)</sub>-Cys-X<sub>2</sub>-Cys-X<sub>(4-48)</sub>-Cys-X<sub>2</sub>-Cys (where X is any amino acid). The conserved cysteine and histidine residues are buried within the domains core in order to maintain the overall structure through binding of the two zinc atoms (Deshaies and Joazeiro, 2009). The E2-E3 interaction appears to be transient and to compete with binding of the E1 enzyme to E2 depending on the presence or absence of an E2-bound ubiquitin (Elektr et al., 2005). Most RING E3 ligases contain a domain to recruit the substrate for ubiquitin conjugation in addition to the E2-binding RING domain (Deshaies and Joazeiro, 2009). However, a subset of RING E3 ligases known as cullin E3s are multi-subunit complexes and use three proteins to facilitate E2-Ubiquitin and substrate binding (Lydeard et

al., 2013; Skaar et al., 2013): the cullin protein presents the scaffold protein, the RING-box protein that is similar to the RING domain found in single-polypeptide E3 ligases, and the bridging F-box protein that facilitates binding of substrates (Lydeard et al., 2013; Skaar et al., 2013). The need to specifically target a broad variety of substrates accounts for the great diversity among the estimated 600 human E3 ligases. E3 ligases need to modify specific lysine residue of ubiquitin. As E3 ligases harboring a RING can synthesize different chain types depending on the E2, the linkage specificity is determined by the E2 (Kim et al., 2007; Ye and Rape, 2009). Therefore, RING E3s that interact with a single E2 generally display the specificity of this particular E2 enzyme.

The HECT (homology to E6AP C terminus) and the RING-between-RING (RBR) ubiquitin ligases use a two-step reaction to first transfer ubiquitin from the E2 to an active site cysteine within the E3 and then from the E3 to the substrate (Berndsen and Wolberger, 2014) (see Figure 2.1). For that, HECT and RBR E3 ligases contain an intrinsic catalytic cysteine (Rotin and Kumar, 2009). The E2 enzyme charges this cysteine with ubiquitin before it is used for modification. In this case, the linkage specificity is not determined by the E2 but by the HECT and RBR E3 ligases. HECT E3 ligases consist of a C-terminal HECT domain and a N-terminal domain that harbors binding sites for the E2 enzyme and as well the catalytic cysteine residue (Huang et al., 1999; Kee et al., 2007).

Unlike RING or HECT E3 ligases, the RBR E3 ligase group consists of complex multidomain proteins and share a common structure of three domains: RING1, In-Between-RING and RING2 (Marin and Ferrus, 2002). The RING2 domain possesses a single cysteine residue for binding an ubiquitin molecule from the E2, forming a thioester linkage with ubiquitin and transferring it to the substrate (Spratt et al., 2014). The domain between the RING domains folds as the RING2 domain but lacks the catalytic cysteine residue as well as ubiquitination activity. The RING1 domain also contains multiple cysteine residues to coordinate zinc ions and shows similarities to the RING E3 ligase consensus sequence (Marin and Ferrus, 2002). These three domains are invariable found in that specific order indicating that all three domains are required for ubiquitination (Marin and Ferrus, 2002; Marin et al., 2004). The proteins HOIL-1 and HOIP of the LUBAC complex represent two members of the RBR E3 ligases (Tokunaga et al., 2011).

#### **2.1.4 Deubiquitinases**

Deubiquitinases (DUBs) are a family of around 100 enzymes that counteract ubiquitination and play a critical role in regulating the majority of the ubiquitin-dependent processes (Komander and Rape, 2012; Clague et al., 2012). Besides processing the ubiquitin precursor protein into

monoubiquitin, DUBs are also responsible for recycling ubiquitin molecules as well as reversing ubiquitination of ubiquitin modification of target proteins (Reyes-Turcu et al., 2009). DUBs are subdivided into five families according to the architecture of their catalytic domains: JAB1/MPN/MOV34 family (JAMMs), Josephins, ovarian tumor proteases (OTUs), ubiquitin COOH-terminal hydrolases (UCHs) and ubiquitin specific proteases (USPs) (Clague et al., 2013). Whereas UCHs, USPs, OTUs and Josephins function as cysteine proteases, JAMMs are zinc-dependent metalloproteases (Harhaj and Dixit, 2012). Most DUBs are covalently modified by phosphorylation, ubiquitination or sumoylation to regulate their activity, localization or half-life (Reyes-Turcu et al., 2009). The extent of linkage specificity varies among the DUB families. While Ubiquitin-specific protease (USP) family DUBs do not exhibit linkage specificity (Faesen et al., 2011), most human OTU enzymes reveal linkage specificity for a defined subset of linkage subtypes (Mevisen et al., 2013). OTUB1 prefers K48-linked polyubiquitin chains in DNA damage response (Edelmann et al., 2009), whereas OTULIN shows Met1 specificity in TNF $\alpha$  signaling (Keusekotten et al., 2013). This specificity is mediated by the selectivity of the catalytic core, the ubiquitin-binding domains of the DUBs or adaptor proteins.

## **2.2 NF- $\kappa$ B signaling**

The eukaryotic transcription factor nuclear factor “kappa-light-chain-enhancer” of activated B cells (NF- $\kappa$ B) plays a critical role in regulating the expression of a large variety of genes that are involved in several cellular processes including innate and adaptive immune response, cell growth as well as cell development (Napetschnig and Wu, 2013). Several signals including cytokines, pathogens, injuries and other stress conditions induce activation of the NF- $\kappa$ B transcription factors that are tightly regulated (Napetschnig and Wu, 2013). Inappropriate NF- $\kappa$ B signaling is described to cause autoimmunity, chronic inflammation and various cancers (Toubi et al., 2004, Bassères et al., 2006). NF- $\kappa$ B signaling can be divided in the canonical and noncanonical NF- $\kappa$ B pathway depending on the stimulus. The canonical NF- $\kappa$ B signaling is induced by most physiological NF- $\kappa$ B stimuli whereas the noncanonical NF- $\kappa$ B signaling arises only from certain ligands (Figure 2.2) (Oeckinghaus et al., 2011).

### **2.2.1 The NF- $\kappa$ B transcription factor family**

NF- $\kappa$ B is a heterodimeric protein composed of different combinations of members of the Rel family transcription factors including RelA (p65), RelB, c-Rel, p50 (p105 precursor), p52 (p100 precursor) and Relish (Gilmore, 2006). All members share a conserved DNA-binding and dimerization domain termed Rel homology region (RHR) that is responsible for homo- or

heterodimerization among the Rel proteins (Hoffmann et al., 2006). Whereas RelA, RelB and c-Rel contain a C-terminal transactivation domain (TAD) to activate gene expression, p50, p52 and Relish harbor a long, ankyrin repeat-containing domain (ARD) and are therefore not able to activate target gene expression as a homodimer (Vallabhapurapu and Karin, 2009; Oeckinghaus et al., 2011). NF- $\kappa$ B proteins bind as a homo- or heterodimer to a specific DNA target sequence requiring the C-terminal domain for dimerization as well as for making phosphate contact with the DNA (Chen and Ghosh, 1999).

In unstimulated cells, NF- $\kappa$ B is either retained in the cytoplasm by the inhibitors of the  $\kappa$ B (I $\kappa$ B) family that mask the nuclear localization signal (NLS) of NF- $\kappa$ B and therefore prevent NF- $\kappa$ B from binding to DNA (canonical NF- $\kappa$ B signaling) or it is sequestered like in the case of the inactive precursor p100 (noncanonical NF- $\kappa$ B signaling) (Figure 2.2) (Vallabhapurapu and Karin, 2009; Oeckinghaus et al., 2011).

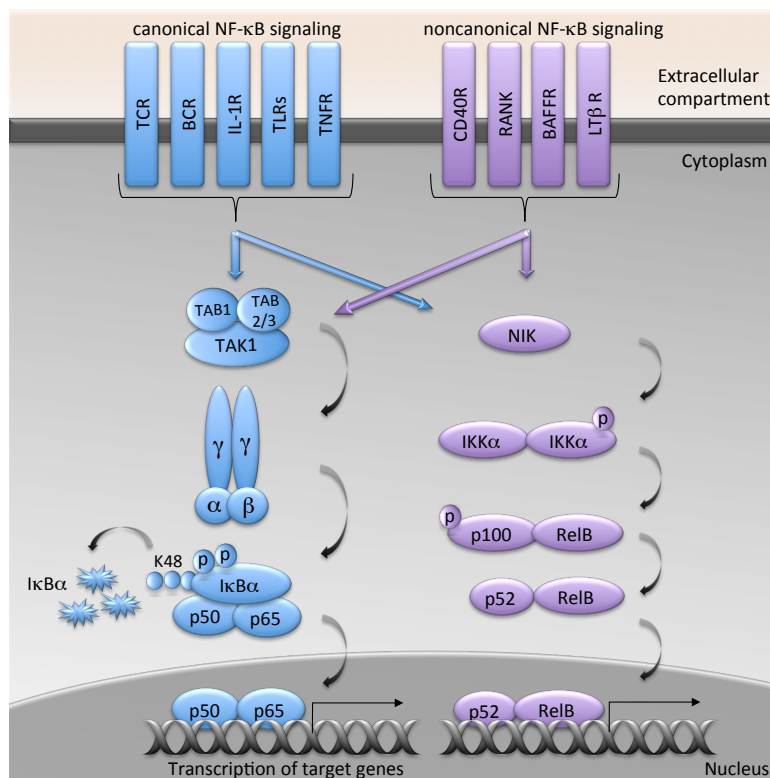


**Figure 2.2: Canonical and noncanonical signaling to NF- $\kappa$ B.** Schematic illustration of the pathways activating NF- $\kappa$ B signaling. Canonical NF- $\kappa$ B signaling is induced by TLR, IL-1R, TNFR and antigen receptors leading to the activation of the TAK1 complex followed by IKK signaling to activate NF- $\kappa$ B. In noncanonical NF- $\kappa$ B signaling, stimulation of cell-type specific receptors including CD40 and RANK initiate NIK activation resulting in phosphorylation of IKK $\alpha$  and processing of p100 to p52 to allow NF- $\kappa$ B activation.

The family of I $\kappa$ B consists of the classical I $\kappa$ B proteins (I $\kappa$ B $\alpha$ , I $\kappa$ B $\beta$  and I $\kappa$ B $\epsilon$ ), the NF- $\kappa$ B precursor proteins p100 and p105 as well as the nuclear I $\kappa$ Bs (I $\kappa$ B $\zeta$ , Bcl-3 and I $\kappa$ BNS). These proteins serve as inhibitors and regulators of NF- $\kappa$ B activity. The cytosolic I $\kappa$ B $\alpha$  protein regulates the activation and inactivation of NF- $\kappa$ B whereby its transcription in turn is regulated by NF- $\kappa$ B (Napetschnig and Wu, 2013). The classical I $\kappa$ B subfamily exhibits binding preference



for NF- $\kappa$ B dimers containing a p65 or c-Rel subunit whereas the nuclear I $\kappa$ Bs prefer p50 and p52 homodimers (Huxford and Ghosh, 2009; Ohno et al., 1990).

The transcription factor NF- $\kappa$ B regulates a broad spectrum of target genes due to its involvement in a variety of cellular processes. Immune regulatory proteins including adhesion molecules (Intracellular Adhesion Molecule 1 (ICAM-1) and Vascular Adhesion Molecule (VCAM)), cytokines (TNF $\alpha$ , IL-1 $\beta$ , IL-6), regulators of apoptosis (Bcl-XL and IAP), cyclins, growth factors that are responsible for proliferation and regulators of NF- $\kappa$ B (I $\kappa$ B $\alpha$ , c-Rel and p105) are coordinated in a NF- $\kappa$ B dependent manner (Oeckinghaus and Ghosh, 2009). These NF- $\kappa$ B target genes enable the organism to respond effectively to external stimuli including infections, cytokines and genotoxic stress (Oeckinghaus and Ghosh, 2009).

The biological function of NF- $\kappa$ B involves crosstalk between the canonical and noncanonical NF- $\kappa$ B pathways at different levels including upstream signaling crosstalk as well as nuclear interactions (Sun, 2012). The positive and negative interplays between the two NF- $\kappa$ B signaling pathways may control the kinetics and magnitude of the expression of NF- $\kappa$ B regulated target genes (Sun, 2012).

### **2.2.2 Canonical NF- $\kappa$ B signaling**

#### **2.2.2.1 Activation of the transcription factor NF- $\kappa$ B**

In canonical NF- $\kappa$ B signaling, proinflammatory stimuli like tumor necrosis factor  $\alpha$  (TNF $\alpha$ ), Interleukin (IL-1), lipopolysaccharide (LPS) or antigens lead to stimulation of a variety of receptors such as TNF receptor (TNFR1), Interleukin-1 receptors (IL-1R), Toll-like receptor (TLR) as well as antigen receptors including B cell receptor (BCR) and T cell receptor (TCR). Figure 2.3 illustrates the schematic process of canonical NF- $\kappa$ B signaling. Upon receptor stimulation, the TAK1 complex consisting of the kinase TAK1 (TGF $\beta$ -activated kinase 1) and the TAK1 binding proteins TAB1, TAB2 and TAB3 is activated (Landström et al., 2010). TAK 1 is a member of the MAPKKK family and requires the TAB proteins for its kinase activity (Kishimoto et al., 2000). The Zincfinger domains of TAB2 and TAB3 specifically recognize K63-linked polyubiquitin chains that are either unanchored or attached to substrate proteins including TRAF6, RIP1 and NEMO (Wang et al., 2001). Recruitment of multiple TAK1 complexes brings the kinase domains of TAK1 proteins close to each other resulting in auto-phosphorylation and activation of the TAK1 kinase, which in turn can activate the IKK complex. The IKK complex consists of the two catalytic subunits IKK $\alpha$ , IKK $\beta$  and the regulatory subunit IKK $\gamma$  also called NEMO (NF- $\kappa$ B essential modifier) (Karin, 1999). Two NEMO molecules assemble a dimer and associate with the one

IKK $\alpha$  and one IKK $\beta$  molecule. Binding of NEMO to polyubiquitin is crucial for IKK recruitment and subsequent NF- $\kappa$ B activation (Napetschnig and Wu, 2013). These polyubiquitin chains serve as extended scaffolds for recruitment of signaling molecules and enhance higher-order oligomerization (Ferraro et al., 2012). Whereas the N-terminus of NEMO is required for binding the catalytic IKK subunits, its C-terminal region is responsible for ubiquitin chain recognition (Hadian et al., 2011; Xu et al., 2011). The NEMO dimer preferentially binds linear (Met1-linked) ubiquitin chains with the highest affinity and shows modest binding to K63-linked ubiquitin whereas K48-kinked Ubiquitin is not recognized (Hadian et al., 2011; Yoshikawa et al., 2009).

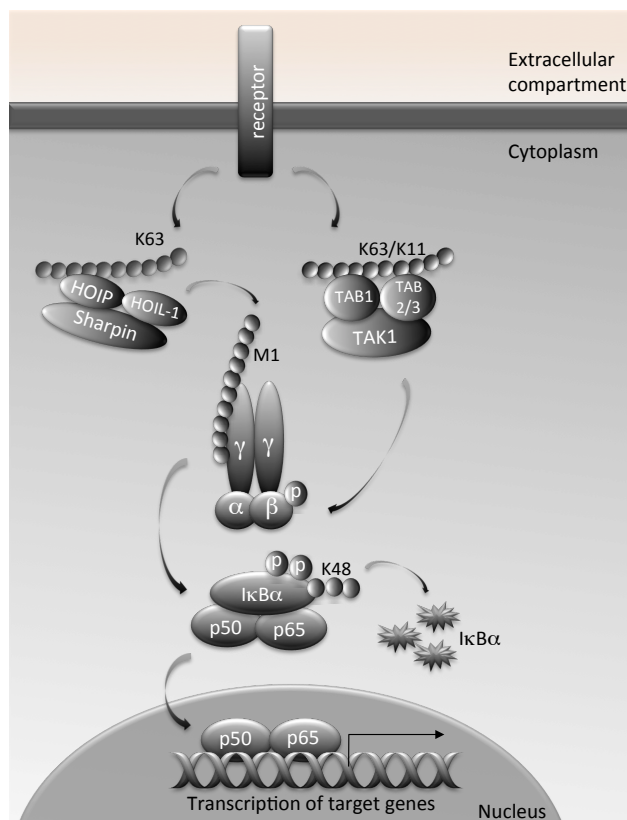


**Figure 2.3: Canonical NF- $\kappa$ B signaling.** Upon receptor stimulation, polyubiquitin chains are generated to serve as platforms for complex assembly for the TAK1 complex as well as the LUBAC complex. TAK1 induces phosphorylation-dependent IKK $\beta$  activation whereas LUBAC attaches linear ubiquitin chains to IKK $\gamma$ . The active IKK complex phosphorylates I $\kappa$ B $\alpha$  followed by K48-linked polyubiquitination and proteasomal degradation of I $\kappa$ B $\alpha$ . The released NF- $\kappa$ B transcription factor translocates into the nucleus to induce transcription of target genes.

Linear ubiquitin chains that are bound by NEMO are generated by the linear ubiquitin assembly complex (LUBAC) (Kirisako et al., 2006). This complex consists of three components: Heme-Oxidized IRP2 ubiquitin ligase 1 (HOIL-1), HOIL-1 interacting protein (HOIP) (the catalytic subunit) and Sharpin (Tokunaga et al., 2011). LUBAC mediates ubiquitination of NEMO with linear ubiquitin chains, which is required for IL-1 $\beta$ , LPS and TNF $\alpha$  induced NF- $\kappa$ B activation (Tokunaga et al., 2011; Emmerich et al., 2013). Ubch5 and Ubch7 are E2 enzymes that support the ubiquitin ligase activity of LUBAC (Gerlach et al., 2011; Ikeda et al., 2011; Tokunaga et al., 2011). In IL-1 $\beta$  stimulated cells, the formation of K63-linked/linear polyubiquitin hybrid chains permits the recruitment of TAK1 and the canonical IKK complex to the same polyubiquitin

chains resulting in the TAK1-catalyzed phosphorylation and activation of the IKK complex (Emmerich et al., 2013).

The active IKK complex catalyzes phosphorylation of two serine residues (Ser32 and Ser36) of  $\text{I}\kappa\text{B}\alpha$ . This phosphorylation in turn leads to K48-linked ubiquitination that targets  $\text{I}\kappa\text{B}\alpha$  for proteasomal degradation. NF- $\kappa\text{B}$  is then released from its inhibitory complex and translocates into the nucleus to bind its target sequences to activate gene transcription.

#### **2.2.2.2 Membrane proximal interactions**

Proinflammatory cytokines initiate a signaling cascade leading to the activation of the IKK complex. Several receptor-induced activation pathways of IKK are described for the Toll-like receptor/Interleukin-1 receptor (TLR/IL-1R) superfamily as well as the tumor necrosis factor receptor (TNFR) superfamily (Napetschnig and Wu, 2013).

##### **2.2.2.2.1 Signaling cascades triggered by the TLR/IL-1R superfamily**

The TLR/IL-1R superfamily belongs to the pattern recognition receptors. Each of the TLRs recognized a specific PAMP (pathogen associated molecular pattern) with their extracellular domain. PAMPs are lipopolysaccharide (LPS) of gram-negative bacteria as well as peptidoglycan and lipoteichoic acid of gram-positive bacteria, RNAs of selected viruses and various forms of stress signals (O'Neill et al., 2013). 13 mammalian TLRs have been identified so far. Their structure consists of three domains: an N-terminal extracellular leucine-rich repeat region to sense extracellular pathogens and signals during tissue injury, a transmembrane domain as well as a C-terminal intracellular Toll/IL-1R (TIR) domain (O'Neill and Bowie, 2007). Each of the different ligands is bound to distinct surfaces of the TLR dimers. Upon sensing these molecules, TLR signaling induces the production of various proinflammatory cytokines including  $\text{TNF}\alpha$ , IL- $1\beta$ , IL-6 and IL-12 as well as the type I interferons  $\text{IFN}\alpha$  and  $\text{IFN}\gamma$ , chemokines, antimicrobial enzymes and other inflammatory mediators (Xie, 2013). These molecules stimulate acute inflammatory responses as well as phagocytosis and autophagy, which present the mechanisms of innate immunity against many pathogens (Into et al., 2012; O'Neill and Bowie, 2007; Sanjuan et al., 2009). Furthermore, TLR signaling serves to prime the adaptive immune response via upregulation of adhesion molecules including ICAM-1 and VCAM and co-stimulatory molecules such as CD40, CD80 and CD86 on antigen presenting cells (Suhir et al., 2010; Kawai et al., 2008). TLRs that sense lipids or proteins are located on the cell membrane and include TLR1, TLR2, TLR4, TLR5, TLR6 and TLR10 (Ostuni et al., 2010). In contrast, TLR3, TLR7, TLR8 and TLR9 recognize microbial and host-derived nucleic acids including double (dsRNA) and single

stranded RNA (ssRNA) as well as CpG DNA and therefore reside in intracellular endosomes (Ostuni et al., 2010; O'Neill et al., 2013). Except TLR3, all TLRs use the MyD88 dependent pathway including TRAF6 to activate NF- $\kappa$ B signaling (O'Neill et al., 2013). An overview of TLR signaling pathways is illustrated in Figure 2.4

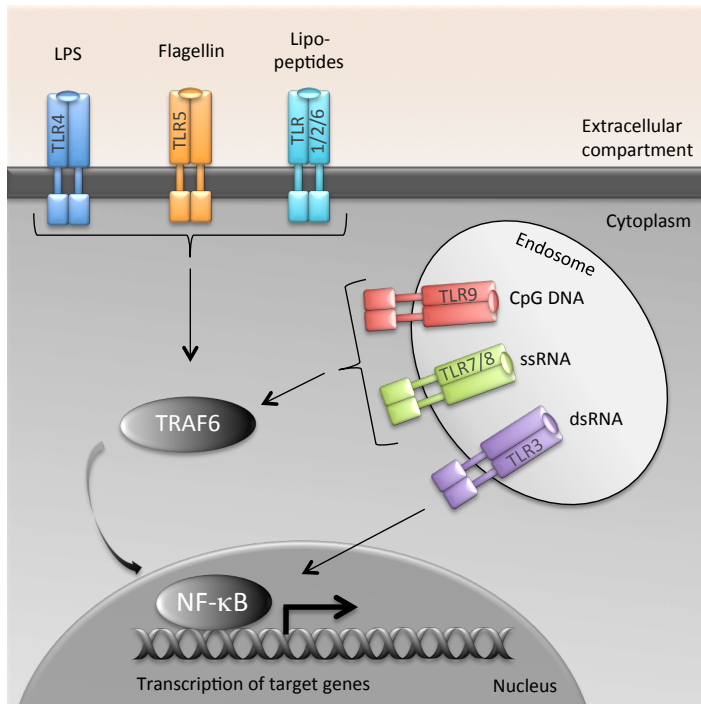


**Figure 2.4: TLR signaling pathways.** Figure adopted from O'Neill et al., 2013. Whereas TLR4, TLR5, TLR1, TLR2 and TLR6 sense their respective ligands at the cell surface, TLR3, TLR7, TLR8 and TLR9 localize in the endosome and recognize microbial and host-derived nucleic acids. After dimerization of the TLRs (except TLR3), MyD88-dependent signaling activates TRAF6 leading to NF- $\kappa$ B activation. TLR3 signals through and MyD88-independent pathway to activate NF- $\kappa$ B.

Receptors of the IL-1R family contain three immunoglobulin-like domains in their extracellular domain that are brought in close proximity upon dimerization (Wang et al., 2010; Thomas et al., 2012). TLRs and IL-1R family members all share a common cytoplasmic TIR domain and consequently involve overlapping components for downstream signaling (Wertz and Dixit, 2012). Upon ligand-induced activation, TLRs and IL-1Rs form dimers for signal progression (Latz et al., 2007; Tsukamoto et al., 2010). Higher-order oligomers of receptors might be required for intracellular signal initiation (Motshwene et al., 2009). It is thought that upon ligand binding to the extracellular domains, the intracellular TIR domains oligomerize creating a platform allowing TIR-domain containing adaptor molecules to nucleate (O'Neill and Bowie, 2007). MyD88 (myeloid differentiation primary-response gene 88) is the primary signaling adaptor protein for IL-1 $\beta$  and TLR signaling (O'Neill and Bowie, 2007). Upon receptor stimulation, several MyD88 proteins oligomerize via their TIR domains at the receptor proximal membrane. They form a platform for other TIR-domain containing adaptor molecules to assemble and oligomerize (O'Neill and Bowie, 2007). MyD88 associates with members of the IL-1R-associated receptor kinases (IRAK) family. MyD88 and IRAK proteins assemble into a large oligomeric

complex termed the Myddosome (Motshwene et al., 2009). Besides MyD88 proteins, this complex consists of IRAK1, IRAK2 and IRAK4 building four layers within the Myddosome. Upon binding of the ligand to the receptor, two top layers of MyD88 are formed and recruit IRAK4 proteins to the complex. After four IRAK4 molecules have assembled the middle layer of the Myddosome, IRAK2 and IRAK1 molecules form the bottom layer of this complex (Figure 2.5) (Lin et al., 2010). The Myddosome serves as a scaffold for phosphorylation of IRAK1 and IRAK2 initiated by IRAK4 to recruit TRAF6 to the membrane (Ye et al., 2002).

TRAF6 is an E3 ubiquitin ligase crucial for TLR and IL-1R induced NF- $\kappa$ B signaling pathway (Wu and Arron, 2003). TRAF6, in conjunction with the E2 complex Ubc13/Uev1a, generates K63-linked polyubiquitin chains required for TRAF6 auto-ubiquitination as well as ubiquitination of substrate proteins including IRAK1 (Conze et al., 2008). These K63-linked polyubiquitin chains provide a platform for the assembly of signaling molecules including the TAK complex and LUBAC (Schmukle and Walczak, 2012). The receptor proximal signaling upon TLR/IL-1R signaling towards NF- $\kappa$ B signaling is depicted in Figure 2.5.

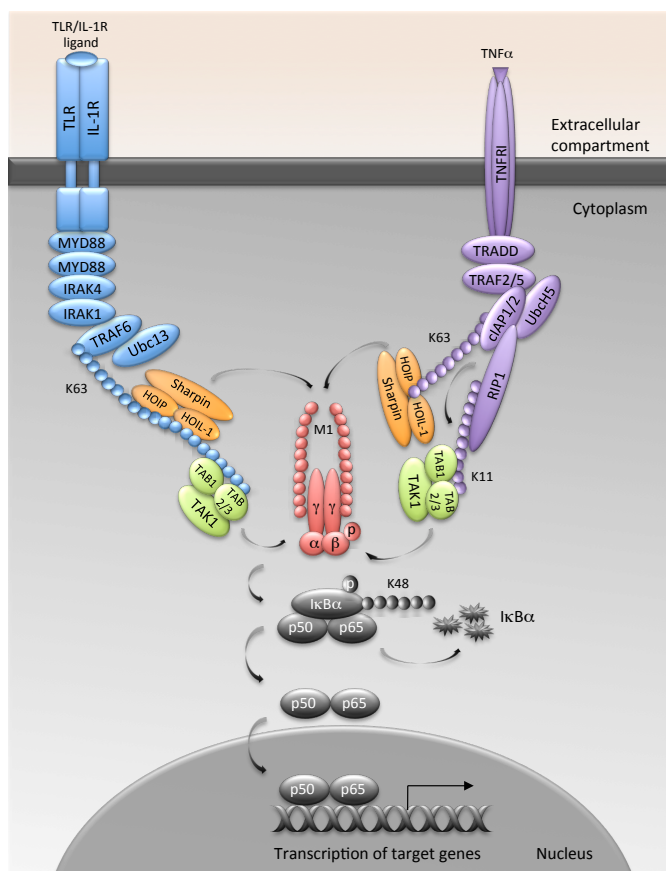


**Figure 2.5: TLR/IL-1R and TNFR induced NF- $\kappa$ B signaling.** Upon receptor stimulation, adaptor proteins are recruited to the receptor proximal membrane to attract E3 ligases for synthesis of polyubiquitin chains. TLR/IL-1R ligand binding induces formation of the Myddosome at the receptor followed by TRAF6 recruitment. Activation of TRAF6 leads to auto-ubiquitination and polyubiquitination of IRAK2. These chains serve as a scaffold for binding of the TAK1 complex and LUBAC. TNF $\alpha$  triggers the assembly of TRAF2/TRAFF5 and cIAP1/2 followed by polyubiquitination of cIAP1/2 and RIP1 to enable TAK1 complex and LUBAC binding for signaling towards NF- $\kappa$ B activation.

#### **2.2.2.2.2 Signaling via the TNF receptor superfamily**

Stimulation of the Tumor Necrosis Factor Receptor (TNFR) superfamily results in either NF- $\kappa$ B activation or apoptosis depending on the proteins that are recruited to the intracellular domain of the TNFRs (Bianchi and Meier, 2009). Upon ligand binding, TNFRs trimerize and TNFR-associated factors (TRAFs) are recruited to the respective receptor either directly or via adaptor proteins. For instance, binding of trimeric TNF $\alpha$  to TNFR1 induces receptor trimerization and subsequently recruitment of the TNFR1-associated death domain proteins (TRADD) to form a platform in order to attract additional signaling mediators. These mediators include the Fas-associated death domain protein (FADD), TRAF2 and the Receptor-Interacting Protein 1 (RIP1). TRAF2 recruits the cellular inhibitor apoptosis proteins 1 and 2 (cIAP1/2) forming an active E3 ligase complex (Mahoney et al., 2008). An overview of TNF $\alpha$  membrane proximal signaling is illustrated in Figure 2.5. It is thought, that cIAP1/2 facilitate K63-linked auto-ubiquitination followed by K63-linked polyubiquitination of TRAF2 and RIP1 (Mahoney et al., 2008). Ubiquitinated RIP1 then might serve as a scaffold for the assembly of the TAK1 complex as well as LUBAC (Haas et al., 2009). LUBAC activity results in linear ubiquitination of RIP1 and NEMO (Gerlach et al., 2011). For optimal IKK activation, the interaction of NEMO with both linear and K63-linked polyubiquitin chains is required (Hadian et al., 2011). Furthermore, K11-linked polyubiquitination of RIP1 mediated by cIAP1 and UbcH5 is reported (Dynek et al., 2010).

#### **2.2.2.3 Regulation of NF- $\kappa$ B by Deubiquitinases**

The removal of polyubiquitin chains by DUBs is necessary to terminate NF- $\kappa$ B activity (Napetschnig and Wu, 2013). Selected DUBs involved in regulating the NF- $\kappa$ B pathway are A20, Cezanne, OTULIN and CYLD (Düwel et al., 2009; Harhaj and Dixit, 2012; Keusekotten et al., 2013). All listed DUBs differ in their temporal activation and ubiquitin linkage specificity ensuring tight regulation of terminating NF- $\kappa$ B activity. Whereas Cezanne prefers K11 linkages to regulate RIP1 ubiquitination (Enesa et al., 2008), OTULIN (OTU DUB with linear linkage specificity) is Met1 specific and is shown to counteract LUBAC-mediated signaling to NF- $\kappa$ B in response to TNF $\alpha$  stimulation (Keusekotten et al., 2013). Several DUBs including A20 and CYLD have been demonstrated to deconjugate K63-linked ubiquitin chains and negatively regulate NF- $\kappa$ B signaling (Wertz et al., 2004; Kovalenko et al., 2003).

A20 (TNFAIP3, tumor necrosis factor alpha induced protein 3) is an ubiquitin-editing enzyme and belongs to the ovarian tumor superfamily of DUBs (Makarova et al., 2000). It mediates deubiquitination of K63-linked polyubiquitin but at the same time is also able to generate K48-linked polyubiquitin chains due to its E3 ligase activity. Both functions are necessary for NF- $\kappa$ B

inhibition (Heyninck and Beyaert, 2005). A20 can deubiquitinate several NF- $\kappa$ B regulatory proteins including TRAF6, RIP1 and NEMO (Boone et al., 2004; Wertz et al., 2004). A20-deficient mice develop severe inflammatory responses in multiple organs due to the enhanced and prolonged activation of NF- $\kappa$ B after stimulation (Lee et al., 2000). A20 is also shown to play a critical role in regulating NF- $\kappa$ B signaling in T cells by counteracting K63-linked polyubiquitination of Malt1 (Düwel et al., 2009). CYLD, as USP deubiquitinase, was originally identified as a tumor suppressor and that mutations in this gene caused familial cylindromatosis, a predisposition of benign tumors of hair follicles (Bignell et al., 2000). CYLD physically interacts with and deubiquitinates NEMO. Furthermore, CYLD downregulates NF- $\kappa$ B signaling by removing attached ubiquitin molecules from TRAF2, TRAF6, TRAF7, RIP1 and NEMO (Trompouki et al., 2003; Kovalenko et al., 2003; Brummelkamp et al., 2003; Yoshida et al., 2005).

### **2.2.3 Noncanonical NF- $\kappa$ B signaling**

As most members of the TNFR family can activate both NF- $\kappa$ B signaling pathways, some primarily activate the noncanonical path including CD40 and BAFF-R on B cells as well as RANK on osteoclasts (Sun, 2012). The noncanonical NF- $\kappa$ B pathway therefore responds to non-inflammatory stimuli and plays a critical role in development and differentiation processes including lymphoid organogenesis and architecture organization, B-cell maturation and survival, maturation of dendritic cells, T-cell differentiation and bone metabolism (Sun, 2012). Compared to the canonical NF- $\kappa$ B signaling, the noncanonical pathway involves slower p100 processing providing a delayed, but long-lasting NF- $\kappa$ B activation (Hoffmann and Baltimore, 2006). Noncanonical NF- $\kappa$ B signaling predominantly targets activation of the RelB/ p52 NF- $\kappa$ B complex and does not depend on IKK $\gamma$  but requires IKK $\alpha$  and NIK (NF- $\kappa$ B inducing kinase) to activate NF- $\kappa$ B signaling (Sun, 2012). A schematic overview of the noncanonical NF- $\kappa$ B signaling pathway is illustrated in Figure 2.2. One essential element in noncanonical NF- $\kappa$ B signaling is the proteasomal processing of p100 to p52 to allow formation of an active NF- $\kappa$ B heterodimer to enter the nucleus and to promote transcription of target genes. This processing is initiated by phosphorylation of IKK $\alpha$ , which is in turn triggered by NIK. Usually, NIK levels in the cytosol are kept low caused by its degradation via the UPS (Vallabhapurapu and Karin, 2009). In unstimulated cells, NIK is constitutively bound to TRAF2 and TRAF3 that are thought to contribute to NIK degradation by generating K63-linked polyubiquitin chains to link cIAP1/2 to NIK (Zarnegar et al., 2008). cIAP1/2 then assemble degradative polyubiquitin chains on NIK

causing its proteasomal degradation. Upon receptor ligation, the cIAP1/2, TRAF2 and TRAF3 proteins are proteasomally degraded leading to NIK stabilization and subsequent phosphorylation and activation of IKK $\alpha$  (Vallabhapurapu et al., 2008). This permits p100 processing and noncanonical NF- $\kappa$ B activation resulting in the upregulation of anti-apoptotic proteins of the Bcl-2 family (such as Bcl-2, Bcl-xl and Mcl-1) to induce cell survival (Wallach and Kovalenko, 2008; Rickert et al., 2011).

#### **2.2.4 NF- $\kappa$ B signaling in diseases**

##### **2.2.4.1 NF- $\kappa$ B signaling in inflammatory disorders and cancer**

NF- $\kappa$ B transcription factors regulate a number of important physiological processes including inflammation and immune response as well as cell growth and survival. In several human diseases such as chronic inflammatory diseases and cancers activation of NF- $\kappa$ B is elevated and contributes to the pathology.

In chronic inflammation, the persistent existence of NF- $\kappa$ B activating stimuli seems to surpass the inhibitory feedback loop leading to an elevated constitutive activation of NF- $\kappa$ B (Hoesel and Schmid, 2013). As a result, chronic inflammation perpetuates and amplifies itself through the diverse autocrine and paracrine loops of cytokines (Makarov, 2001). For example, patients suffering from rheumatoid arthritis (RA), a chronic inflammatory disease leading to joint destruction and disability, exhibit elevated levels of activation of the canonical NF- $\kappa$ B pathway resulting in an inflammatory phenotype marked by excessive cytokine signaling and recruited immune cells in the inflamed pannus (Simmonds and Foxwell, 2008). Furthermore, NF- $\kappa$ B is also shown to have important roles in the pathogenesis of inflammatory bowel disease and chronic obstructive pulmonary disease (Lawrence, 2009).

In cancer, NF- $\kappa$ B is recognized in many steps of cancer initiation and prolongation. NF- $\kappa$ B is constitutively activated in many types of cancer including leukemia, lymphoma, colon cancer, lung cancer and breast cancer (Staudt, 2010). NF- $\kappa$ B activation results in the upregulation of anti-apoptotic genes providing cell survival mechanism leading to cell proliferation and causes pro-tumorigenic functions in cancer cells (Hoesel and Schmid, 2013).



#### **2.2.4.2 NF- $\kappa$ B signaling in metabolic diseases**

Metabolic disorders including obesity, type 2 diabetes and atherosclerosis have been thought as lipid disorders caused by overnutrition. Nowadays, it is known that chronic low-grade inflammation plays a central role in the initiation, propagation and development of metabolic diseases as well (Baker et al., 2011). Consistent with its central role in regulating inflammatory responses, various recent studies revealed the implication of NF- $\kappa$ B in the development of such diseases contributing to the chronic inflammation. Although the exact mechanistic understanding of how inflammatory signaling induces metabolic disorders is not clear yet, recent findings give first insights into this correlation. Upon nutrient excess, resident tissue cells activate NF- $\kappa$ B (Baker et al., 2011). Oxidized lipoproteins in the bloodstream trigger the secretion of specific chemokines by the vascular endothelia and lead to the recruitment of leukocytes to the site of inflammation (Weisberg et al., 2006). Invasion of these leukocytes is mediated by the adhesion molecules ICAM-1 and VCAM induced by NF- $\kappa$ B (Bosanska et al., 2010). Furthermore, hepatocytes as well as adipocytes induce NF- $\kappa$ B in response to overnutrition. TLR4 signaling in adipocytes and macrophages induced by nutritional fatty acids, whose circulating levels are often increased in obesity, causes the activation of inflammatory pathways and plays an important role in obesity-associated insulin resistance as depicted in Figure 2.6 (Shi et al., 2006). TLR4 is found to be upregulated in adipocytes of diet-induced obese mice. Although TLR4-deficient mice have increased obesity, they are partially protected against HFD-induced insulin resistance (Shi et al., 2006). Further research of the inflammatory pathways in obese and diabetic mice confirmed that MyD88 and NF- $\kappa$ B protein levels were elevated in adipose tissue and peripheral blood mononuclear cells (PBMCs) taken from type 2 diabetes mellitus (T2DM) subjects (Creely et al., 2007; Ahmad et al., 2012). Also, the levels of circulating proinflammatory cytokines like TNF $\alpha$  and IL-6 are increased in T2DM subjects as a consequence of elevated NF- $\kappa$ B signaling (Creely et al., 2007; Ahmad et al., 2012). Obesity induced inflammation is mediated, at least in part, by circulating saturated free fatty acids (FFAs) that stimulate intracellular proinflammatory pathways in a TLR4-dependent manner (Heinrichsdorff and Olefsky, 2012).

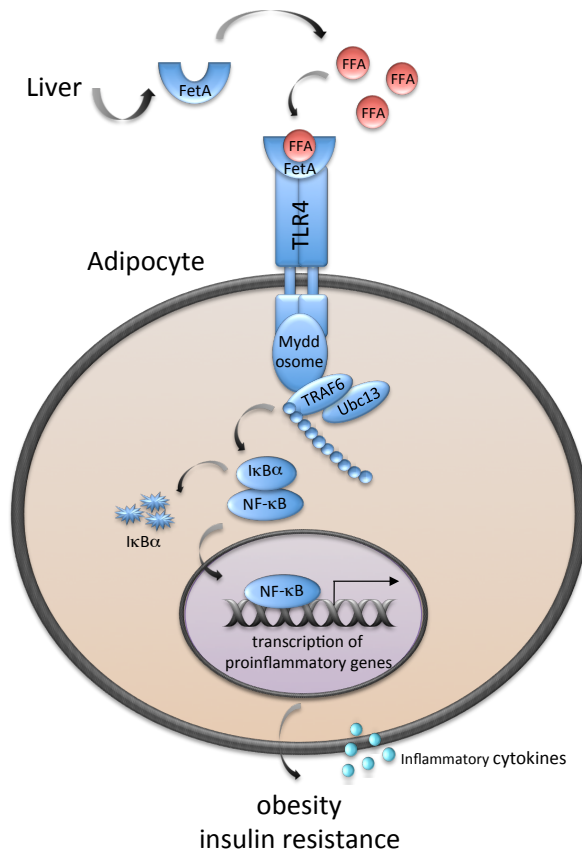


**Figure 2.6: NF-κB and TRAF6 in obesity and insulin resistance** (adopted from Heinrichsdorff and Olefsky, 2012). In obesity, free-fatty-acid (FFA) levels are elevated. FFAs are bound by the liver secretory protein FetuinA (FetA) and present ligands for TLR4. Activated TLR4 signaling results in TRAF6-dependent NF-κB activation and transcription of proinflammatory genes. Constant secretion of inflammatory cytokines causes chronic inflammation leading to worsening of obesity and insulin resistance.

For a long time the connection of FFA and TLR4 has been controversial, but in 2012 Pal et al. identified Fetuin-A as an endogenous ligand for TLR4 that directly links FFA to TLR4 activation (Pal et al., 2012). Fetuin-A (FetA) is a 64kDa glycoprotein that is secreted from the liver and adipose tissue. Knockdown of FetA in mice with insulin resistance caused by a high-fat-diet resulted in decreased TLR4 signaling in adipose tissue (Pal et al., 2012). Administration of FetA caused inflammatory signaling and insulin resistance. Removing either FetA or TLR4 prevented FFA-induced insulin resistance and therefore proves that the FFA-FetA binding to TLR4 stimulates lipid induced insulin resistance (Pal et al., 2012). Elevated circulating FetA levels are detected in obesity and related disorders including type 2 diabetes mellitus and are associated with impaired insulin sensitivity and glucose tolerance (Trepanowski et al., 2014). As NF-κB inflammatory pathways promote metabolic diseases, therapeutic strategies might directly target NF-κB target genes. Therefore, blocking the action of inflammatory mediators is currently an attractive therapeutic approach.

## **2.3 TRAF6 in cellular signaling**

### **2.3.1 The TRAF protein family**

TNFR-associated factor (TRAF) proteins serve as adapter molecules for a variety of cell surface receptors and regulate diverse cellular responses. TRAFs were originally identified as signaling adaptors that directly bind to the cytoplasmic region of receptors of the TNFR superfamily (Inoue et al., 2000). However, over the past decade the number of receptor families that involve TRAFs for signaling has expanded rapidly. These include Toll-like receptors (TLRs), IL-1 receptor family, NOD-like receptors (NLRs), RIG-I-like receptors (RLRs), T cell receptor, IL-17 receptors, IFN receptors and TGF $\beta$  receptors (Xie et al., 2013). The TRAF protein family includes seven members: TRAF1, TRAF2, TRAF3, TRAF4, TRAF5, TRAF6 and TRAF7 (Zotti et al., 2012).

In general, TRAF proteins share a characteristic modular structure of conserved domains to mediate signals from different receptors to various cellular outcomes (Arch et al., 1998). At their C-terminus TRAF proteins possess a TRAF domain that consists of a coiled-coil and the MATH domain. This terminus allows oligomerization of TRAF proteins as well as interaction with receptor proteins and other cytoplasmic factors (Takeuchi et al., 1996). Minor structural differences in this domain among TRAFs define the specificity of each TRAF protein binding to various receptors (Chung et al., 2007; Ely et al., 2007). This defines a main role of TRAFs to serve as adaptor proteins in the assembly of receptor-associated signaling complexes and thereby linking upstream receptors to downstream effector enzymes. Genetically modified murine strains carrying a deletion in the loci encoding for each individual TRAF protein show that each TRAF proteins plays a unique and well defined role in the biology of the cell and the organism (Zotti et al., 2012). Although the N-terminal region of TRAF proteins is less conserved, all TRAFs, except for TRAF1, contain a conserved RING domain connected to a variable number of Zincfinger domains (Ha et al., 2009). The RING domain is found in a large number of E3 ubiquitin ligases and holds the core of the ubiquitin ligase catalytic domain. The RING domains of TRAF3, 6 and 7 are capable of promoting ubiquitination to activate their downstream pathways revealing that TRAFs can facilitate adaptor protein and E3 ubiquitin ligase function (Deng et al., 2000; Bouwmeester et al., 2004; Kayagaki et al., 2007; Alvarez et al., 2010).

In addition to the cytoplasmic domain of receptors, TRAF proteins also interact with various intercellular factors including kinases, regulators of signaling pathways, structural proteins and adaptor molecules to mediate cellular function (Zotti et al., 2012). Whereas TRAF2, TRAF3 and TRAF5 seem to signal within the TNF receptor superfamily, TRAF6 is more pleiotropic in participating in the signal transduction of many receptor systems like IL-1 $\beta$  and LPS signaling as well as in T cell receptor and CD40 signaling (Oeckinghaus et al., 2007; Ye et al., 2002). TRAF-

dependent signaling pathways typically lead to the activation of NF- $\kappa$ B or mitogen-activated protein kinases (MAPKs). Either acting alone or in combination, TRAFs mediate a variety of cellular processes including survival, proliferation, differentiation, activation, cytokine production and autophagy (Xie, 2013). Alterations in TRAFs may contribute to the pathogenesis of human diseases including cancers, autoimmune diseases and immunodeficiencies (Hildebrand et al., 2011; Namjou et al., 2012; Netea et al., 2012).

### 2.3.2 TRAF6

#### 2.3.2.1 Structure of the TRAF6 protein

TRAF6 is a member of the TRAF protein family and functions as an adaptor protein as well as an E3 ubiquitin ligase to mediate cytokine signaling after activation of the transcription factor NF- $\kappa$ B. The TRAF6 coding sequence is located on Chromosome 11p12. Two alternatively spliced transcript variants encoding an identical protein have been reported. The ubiquitously expressed TRAF6 protein exhibits 522 amino acids and a size of 60kDa. TRAF6 is generally located in the cytoplasm but is also found in the nucleus of some aggressive B cell lymphoma as well as in resting and activated T and B cells (Pham et al., 2008). TRAF6 exhibits a RING domain and 4 Zincfingers at its N-terminus whereas the C-terminal TRAF domain contains a Coiled-Coil domain and a conserved MATH domain (Figure 2.7) (Yin et al., 2009).

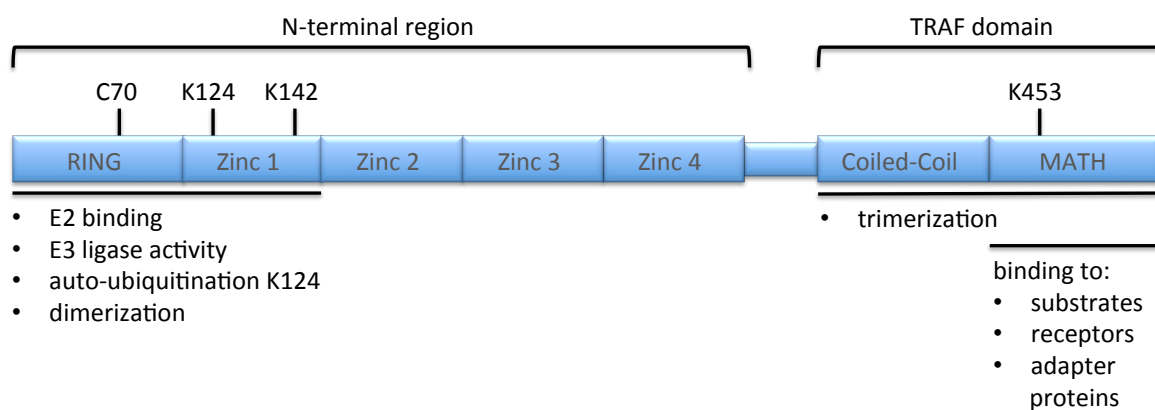


**Figure 2.7: Structure und domain functions of TRAF6.** Schematic illustration of the structure of TRAF6. The N-terminus consists of a RING finger connected to four Zincfinger domains, whereas the C-terminal region (TRAF domain) harbors the Coiled-Coil and the MATH domain. In addition to dimerization, the RING-Zincfinger1 domain mediates binding to E2 enzymes to carry out the E3 ligase activity (via the C70 residue) leading to M63-linked auto-ubiquitination of TRAF6 at K124. TRAF6 can be sumoylated at K124, K142 and K453. The TRAF domain facilitates trimerization and binding to substrates, receptors and adapter proteins.

The TRAF domain forms a mushroom-shaped trimeric structure with the MATH domain as the head for sequence specific interaction with receptors like TLR4 and IL-1R and adaptor proteins including IRAK1 and MyD88 whereas the coiled coil domain presents the stalk for trimerization (Ye et al., 2002). The N-terminal structure of TRAF6 can be described as a golf-club-like formation with the Zincfinger domains forming the shaft and the RING domain building the club head (Yin et al., 2009). The RING domain folds into a canonical cross-brace fold containing an aspartate residue. Stacked aromatic and aliphatic side chains that are conserved among TRAF proteins form the hydrophobic dimer interface whereas the Zincfinger domains structure a canonical  $\beta$ - $\beta$ - $\alpha$ -fold (Yin et al., 2009). The N-terminal region of TRAF6 mediates dimerization (Yin et al., 2009). Furthermore, this domain functions as an E3 ubiquitin ligase for K63-linked polyubiquitination harboring the active cysteine site C70 and is responsible for the interaction with E2 enzymes in order to facilitate ubiquitination (Yin et al., 2009). The alternating dimerization of the N-terminus and trimerization of the C-terminus results in infinite TRAF6 aggregation. These higher-order assemblies are required for TRAF6-mediated polyubiquitination and NF- $\kappa$ B activation (Yin et al., 2009). The TRAF6 protein can be posttranslational modified by SUMO1 at K124, K142 and K453 in the nucleus (Pham et al., 2008) as well as K63-linked poly-ubiquitinated at K124 in the cytoplasm after cell stimulation (Lamothe et al., 2007).

#### **2.3.2.2 Functions of TRAF6 in signaling pathways**

TRAF6 mainly mediates signaling from members of the TLR/IL-1R family (Xie, 2013). By functioning as adaptor protein on the one hand and as E3 ubiquitin ligase on the other hand, this protein serves as a signal transducer in the NF- $\kappa$ B pathway to activate the IKK complex in response to various environmental stimuli including proinflammatory cytokines. In TLR/IL-1R signaling, TRAF6 mediates the MyD88-dependent pathway (all TLRs except TLR3) in order to activate NF- $\kappa$ B signaling (Xie, 2013). In MyD88-dependent signaling, TRAF6, together with the E2 complex Ubc13/Uev1a, mediates the attachment of K63-linked polyubiquitin chains onto substrates (Keating and Bowie, 2009). Besides its requirement in TLR and IL-1R signaling, TRAF6 also is involved in several additional pathways such as TNFR, T cell receptor and IL-17 receptor signaling as well as in DNA damage response (Xie, 2013). The involvement of TRAF6 in various signaling pathways is summarized in Figure 2.8.

TNFR signaling includes CD40 and RANK signaling. Upon CD40 stimulation, TRAF6 and Ubc13 together with many other signaling proteins including TRAF1, TRAF2, TRAF3 and TRAF5 are recruited to the cytoplasmic domain of the receptor inducing the K63-specific ubiquitin ligase

activity of TRAF6 (Xie, 2013). Upon formation of signaling complexes, MEKK1 and TAK1 are phosphorylated and in turn activated to promote MAPK1 and NF- $\kappa$ B signaling to mediate effector functions of CD40 (Bishop et al., 2007). Signaling through Receptor Activator of NF- $\kappa$ B (RANK) is critical for the differentiation and activation of osteoclasts, cells that are responsible for bone resorption. The structural and metabolic integrity of bone is regulated through the dynamic process of bone remodeling mediated by bone resorption through osteoclasts and formation of new bone by osteoblasts (Phan et al., 2004). The interaction of RANK with TRAF6 is required for appropriate formation of cytoskeletal structures and functional resorptive activity of osteoclasts (Armstrong et al., 2002). TRAF6 binds RANK in a unique motif located within the membrane proximal region to induce IKK activation as well as osteoclast differentiation (Darnay et al., 1999; Lamothe et al., 2007).

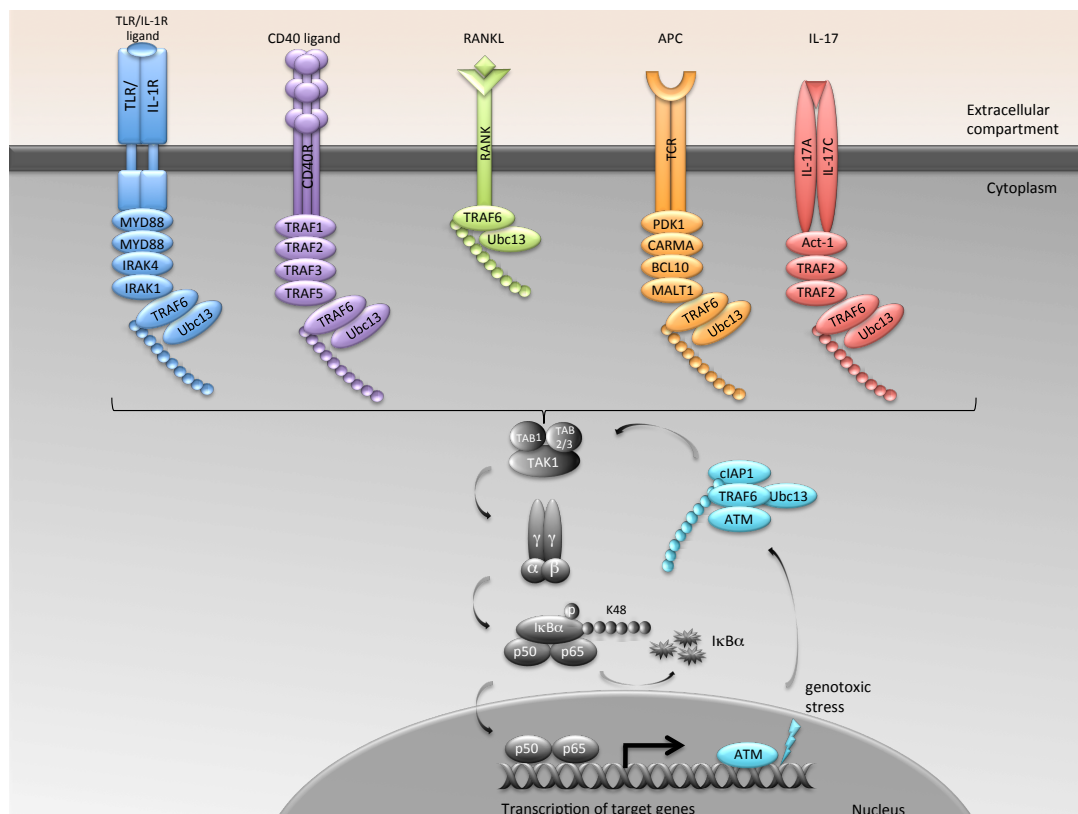


**Figure 2.8: Involvement of TRAF6 in various signaling pathways to activate NF- $\kappa$ B signaling.** Schematic overview of the variety of signaling pathways that are dependent on TRAF6 function to activate NF- $\kappa$ B. Besides TLR/IL-1R signaling, TRAF6 is a critical key part of CD40 signaling along with other TRAF proteins. RANK signaling stimulates NF- $\kappa$ B activation in a TRAF6-dependent manner. Upon T cell stimulation by antigen presenting cells (APC), TRAF6 is recruited to the CARMA1-BCL10-MALT1 complex for signal progress. IL-17 signaling stimulates TRAF proteins to operate together with Act-1 to induce NF- $\kappa$ B activation. Genotoxic stress results in complex formation including cIAP-ATM-TRAF6 to activate NF- $\kappa$ B controlled target gene transcription.

TRAF6 also plays a major role in T cell receptor (TCR) signaling as it is recruited into the CARMA1-BCL10-MALT1 complex via its interaction with the paracaspase MALT1 (Sun et al., 2004; Bidere et al., 2006; Oeckinghaus et al., 2007). TRAF6 activity is required for the K63-linked polyubiquitination of MALT1, which in turn is a prerequisite for signal progression towards NF- $\kappa$ B (Oeckinghaus et al., 2007).

In IL-17 signaling, the heterodimeric IL-17A and IL-17C receptor recruits a novel adaptor protein Act1. Act1 is a E3 ligase that further recruits TRAF6 along with TRAF2 and TRAF5 to the IL-17 receptor complex. In cooperation with the E2 enzyme complex Ubc13/Uev1a, Act1 catalyzes K63-linked polyubiquitination that in turn facilitates ubiquitination of IL-17A to induce NF- $\kappa$ B signaling through TAK1 and IKK activation (Gaffen, 2009; Zepp et al., 2011). IL-17 signaling is responsible in host defense against bacterial, fungal and helminthic parasite infections and is mediated by the T helper cell population Th17 (Chang and Dong, 2011). In DNA damage response, TRAF6 induces NF- $\kappa$ B signaling after activation of the DNA strand break sensor ATM (Ataxia telangiectasia mutated) (Hinz et al., 2010). Upon DNA damage, activated ATM translocates into the cytoplasm to interact with TRAF6 resulting in K63-linked polyubiquitination of TRAF6 followed by recruitment of cIAP1 (Hinz et al., 2010). The ATM-TRAF6-cIAP1 complex then stimulates the phosphorylation of TAK1, followed by cIAP1 catalyzed monoubiquitination of NEMO at Lys285, a prerequisite for genotoxic NF- $\kappa$ B activation and DNA damage response (Hinz et al., 2010).

Engagement of TRAF6 in other signaling pathways upon stimulation of NOD, RIG-I, IFN, TGF- $\beta$ , IL-2 and C-type lectin receptors has been describes as well (Xie, 2013).

### **2.3.2.3 Counteracting TRAF6 activity by DUBs**

TLR and IL-1R induce immune responses that rely on the activity of downstream TRAF6 signaling. Therefore, TRAF6 activation needs to be tightly controlled and is shown to be negatively regulated by several deubiquitinating enzymes including A20, CYLD, USP20 and Cezanne.

A20 is induced in IL-1 $\beta$ /LPS and T cell receptor signaling and was suggested to remove K63-linked polyubiquitin chains from TRAF6 to terminate NF- $\kappa$ B activation (Boone et al., 2004; Heyninck and Beyaert, 1999; Düwel et al., 2009). However, A20-OTU knockin-mice that lack the deubiquitinase domain of A20 do not show signs of inflammation and responded normally to LPS and undergo normal NF- $\kappa$ B activation indicating that the deubiquitinase function of A20 is dispensable for NF- $\kappa$ B signaling (De et al., 2014). It is proposed that A20 rather functions to disrupt the interaction of TRAF6 and Ubc13 than promoting the degradation of TRAF6 and

instead targets Ubc13 with K48-linked polyubiquitin chains for proteasomal degradation (Shembade et al., 2010).

Another cysteine protease DUB that regulates TRAF6 activation is the tumor suppressor Cylindromatosis (CYLD) that directly interacts with TRAF6 after IL-1 $\beta$  stimulation (Kovalenko et al., 2003). CYLD negatively modulates TRAF6-mediated activation of IKK by cleaving off the K63-linked polyubiquitin chains of TRAF6 (Kovalenko et al., 2003). CYLD deficiency in mice does not only cause aberrant immune and inflammatory responses, but also leads to impaired osteoclast differentiation and severe osteoporosis (Jin et al., 2008). CYLD therefore not only regulates TRAF6 activity in IL-1 $\beta$ , but also in RANK signaling by deubiquitinating TRAF6 (Jin et al., 2008).

Additional DUBs controlling TRAF6 activity are the ubiquitin-specific peptidase USP20 and the OTU domain DUB Cezanne (Cellular Zincfinger Anti-NF- $\kappa$ B) (Yasunaga et al., 2012; Luong et al., 2103). While USP20 deubiquitinates TRAF6 in IL-1 $\beta$  induced NF- $\kappa$ B activation, Cezanne suppresses NF- $\kappa$ B signaling in response to hypoxia-reoxygenation by reducing the K63-linked polyubiquitination of TRAF6 (Yasunaga et al., 2012; Luong et al., 2103).

Altogether, considering that TRAF6 is so tightly negatively regulated in a variety of different circumstances and that A20 and CYLD knock out mice develop severe inflammatory syndromes, the negative regulation of TRAF6 signaling is necessary to prevent harmful immune responses and inflammatory diseases.

#### **2.3.2.4 TRAF6 in diseases**

Due to the key role of TRAF6 in innate and adaptive immune response as well as in bone formation and resorption, alterations in TRAF6 expression cause severe consequences. TRAF6 deficient mice exhibit perinatal death with multiple organ abnormalities indicating that TRAF6 is indispensable for early development. The mice die of severe osteopetrosis, splenomegaly and thymic atrophy (Lomaga et al., 1999; Naito et al., 1999). Furthermore, these mice feature systemic inflammation as well as impaired IL-1 $\beta$  and TLR signaling (Zotti et al., 2012).

Overexpression of TRAF6 leads to chronic immune stimulation causing a broad variety of disorders including autoimmune diseases, carcinoma and metabolic diseases. Individual single nucleotide polymorphisms (SNPs) in the TRAF6 gene locus are linked to autoimmune diseases including rheumatoid arthritis and systemic lupus erythematoses (Namjou et al., 2012). Overexpression and amplification of TRAF6 has been reported in several human carcinomas. In colon cancer, TRAF6 is found to be upregulated and to promote proliferation (Sun et al., 2014). Furthermore, amplifications of the TRAF6 sequence have been reported to cause lung cancer as well as osteosarcoma (Starczynowski et al., 2011; Meng et al., 2012). Downregulation of TRAF6



in human lung cancers and osteosarcoma cells results in suppressed NF- $\kappa$ B activation along with diminished tumor formation and invasion suggesting that TRAF6 overexpression may promote the tumorigenesis and invasion of lung cancer and osteosarcoma cells (Starczynowski et al., 2011; Meng et al., 2012).

#### **2.3.2.4.1 TRAF6 in obesity and insulin resistance**

Inflammation displays a major role in the pathogenesis of metabolic disorders associated with obesity. Diet-induced obesity can cause low-level inflammation and insulin resistance involving IL-1 $\beta$  as one of the key inflammatory cytokines (Tack et al., 2012). In monocytes of obese patients TRAF6 levels are increased linking TRAF6 to metabolic disorders (Hulsman et al., 2012). The protein levels of TRAF6, a critical key player in IL-1 $\beta$  induced NF- $\kappa$ B signaling, are increased in adipose tissue samples of obese and type 2 diabetic mice in association with TLR4, MyD88 and NF- $\kappa$ B upregulation (Creely et al., 2007). Gene expression profiles of monocytes of obese subjects revealed elevated levels of TRAF6 (Hulsmans et al., 2012). Further research detected decreased expression of miR-146b-5p in monocytes during obesity. MiR-146b-5p is a microRNA that diminishes the expression of TNF $\alpha$ , IL-1 $\beta$  and IL-6 in monocytes by the targeted repression of IRAK1 and TRAF6 (Hulsmans et al., 2012).

Mice deficient in CD40-TRAF6 signaling exhibit protection against weight gain and insulin resistance in a high-fat-diet model (Chatzigeorgiou et al., 2014). Furthermore, these mice showed a reduction in both adipose tissue inflammation and hepatosteatosis in diabetes-induced-obesity (Chatzigeorgiou et al. 2014). Besides, treatment of mice on high-fat-diet with the small inhibitor SMI 6860766, a CD40-TRAF6 interaction inhibitor, improves glucose tolerance and ameliorates adipose tissue inflammation (Van den Berg et al., 2014).

### **2.4 The TRAF6 - Ubc13 interaction in NF- $\kappa$ B signaling**

#### **2.4.1 The ubiquitin-conjugating enzyme Ubc13**

The Ubc13 protein is encoded by the *UBE2N* gene located on Chromosome 12q22 and composes of 152 amino acids. It is a 17kDa E2 ubiquitin-conjugating enzyme involved in the ubiquitination process. In order to accomplish its function of catalyzing the synthesis of K63-linked polyubiquitin chains it forms a heterodimer with the ubiquitin-conjugating E2 variant Uev1a (McKenna et al., 2003). Uev1a is a UBC-E2 variant that has lost its catalytic cysteine but is still capable of non-covalently binding of ubiquitin (Eddins et al., 2006). The selection of the appropriate lysine used for chain formation requires the recognition of a specific acceptor ubiquitin surface by the E2 donor ubiquitin complex (Berndsen and Wolberger, 2014). To

enable K63-linked specificity, Ubc13 uses the auxiliary subunit Uev1a (Deng et al., 2000). This interaction places the acceptor ubiquitin in a way that the lysine 63 faces the active site of the charged Ubc13. The residues 72-83 of Ubc13 are responsible for the interaction with Uev1a (VanDemark et al., 2001). Proximal to this binding site, the active site cysteine 87 of Ubc13 is located (VanDemark et al., 2001). Together with the respective E3 ubiquitin ligase, for example TRAF6, it mediates K63-linked ubiquitination of the E3 ligase itself as well as of substrates for signal progression (Deng et al., 2000). Ubc13 was first described to regulate TNFR1 signaling as a dominant negative version of Ubc13 blocked TNF $\alpha$  and TRAF2 induced NF- $\kappa$ B signaling (Deng et al., 2000). Ubc13 is also involved in TLR (Akira and Takeda, 2004), IL-1R signaling (Yin et al., 2009) and in B-cell and T-cell-receptor signaling (Yamamoto et al., 2006). Ubc13 genetic ablation studies revealed that homozygous Ubc13 deletion is embryonic lethal (Fukushima et al., 2007; Yamamoto et al., 2006). A hemizygous Ubc13<sup>+/-</sup> mouse strain features impaired TRAF6 ubiquitination and TRAF6-dependent LPS signaling (Fukushima et al., 2007). Conditional Ubc13<sup>-/-</sup> mice generated by Yamamoto et al. showed impaired B cell development as well as reduced B cell and bone marrow macrophage activation in response to LPS and IL-1 $\beta$  stimuli (Yamamoto et al., 2006). Ubc13 is also required for IL-1 $\beta$  induced but not for TNF $\alpha$  induced IKK activation (Xu et al., 2009). Structural studies revealed that TRAF2 and TRAF5, both involved in TNF $\alpha$  signaling, are not capable of interacting with the E2 conjugating enzyme Ubc13 (Yin et al., 2009). Furthermore, TRAF2 and TRAF5 fail to generate polyubiquitin chains in the presence of several tested E2 enzymes (Yin et al., 2009). However, cIAP1 and cIAP2 undergo auto-ubiquitination in the presence of the Ubc13/Uev1a dimer (Yin et al., 2009) and therefore may exhibit the E3 ubiquitin ligases critical for TNF $\alpha$  induced NF- $\kappa$ B signaling. However, it might be possible that other E2 family members, such as UbcH5, which also mediates K63-linked polyubiquitin chain synthesis compensate for Ubc13 in TNF $\alpha$  signaling (Varfolomeev et al., 2008; Xu et al., 2009).

In Ubc13<sup>+/-</sup> mice that were fed a high-fat-diet, lower levels of blood glucose were detected while body weight was not significantly altered (Joo et al., 2013). Reduced insulin secretion coupled with increased insulin sensitivity were obtained indicating that Ubc13 haploinsufficiency improves insulin resistance caused by high-fat-diet (Joo et al., 2013).

### 2.4.2 The direct interaction of TRAF6 and Ubc13

Structural studies demonstrate that Ubc13 is able to directly interact with TRAF6. The Ubc13/Uev1a/TRAF6 complex mediates TRAF6 K63-linked auto-ubiquitination as well as assembly of polyubiquitin chains to activate TAK1 (Lamothe et al., 2007; Yin et al., 2009). While Ubc13 directly interacts with TRAF6, Uev1a provides the linkage specificity (Yin et al., 2009). Already in 2004, Yeast-Two-Hybrid assays revealed that the TRAF6 RING domain interacts with the E2 complex through its direct binding to Ubc13 (Wooff et al., 2004). In 2009, Yin et al. confirmed the necessity of the TRAF6 RING domain for the interaction with Ubc13. Surprisingly, gel filtration chromatography analysis of the complex formation showed that the RING domain alone was not sufficient for Ubc13 interaction. Instead, the RING and Zincfinger1 domain of TRAF6 together mediate complex formation with Ubc13. However, the interaction involves only direct contacts of the RING and the preceding residues to Ubc13 while the Zincfinger1 domain plays a structural role (Yin et al., 2009). In this complex, several residues within the RING domain of TRAF6 form the major contact site with Ubc13: Q54, D57, E69, P21, I72, L74, Met75, A101 and P106. Figure 2.9 presents the ribbon diagram of the TRAF6-Ubc13 complex with the corresponding residues for binding.

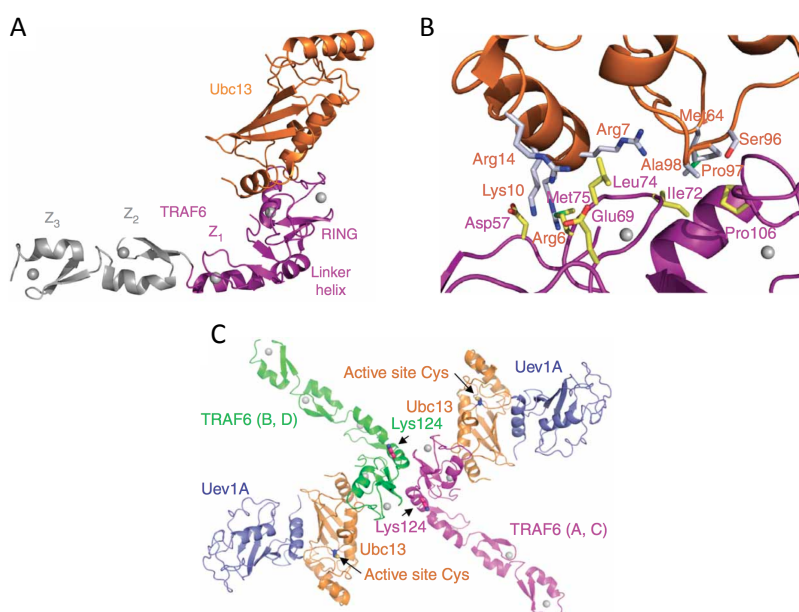


**Figure 2.9: The interaction of TRAF6 and Ubc13 in crystal structures (Yin et al., 2009).** (A) Ribbon diagram of the TRAF6-Ubc13 complex. The RING-Zincfinger1 domain of TRAF6 depicted in magenta facilitates binding of Ubc13 (orange). Thereby, the RING domain mediates direct contacts to Ubc13 whereas the Zincfinger1 (Z1) is critical for maintaining the structure of the RING domain. (B) Detailed illustration of the residues mediating the direct contact of TRAF6 and Ubc13. TRAF6 is shown in magenta, Ubc13 in orange. (C) A dimeric complex of TRAF6-Ubc13-Uev2. The marked Lys124 residues of TRAF6 present the auto-ubiquitination sites. Active site cysteine residues of Ubc13 are shown in orange.

In cells, the interaction of TRAF6 and Ubc13 is critical for both TRAF6 auto-ubiquitination as well as activation of NF- $\kappa$ B upon receptor stimulation such as IL-1 $\beta$  and LPS (Lamothe et al., 2007; Lamothe et al., 2008). Retroviral transfection of TRAF6-deficient MEFs with wildtype TRAF6 rescued auto-ubiquitination as well as NF- $\kappa$ B activation upon stimulation (Yin et al., 2009). In contrast, TRAF6 harboring mutations disrupting the Ubc13 interaction like C70A, D57K, I72D and I74H failed to induce TRAF6 auto-ubiquitination in response to IL-1 $\beta$  stimulation (Yin et al., 2009). Importantly, only TRAF6 wildtype reconstitution led to the activation of the IKK complex whereas the Ubc13-binding mutants did not exhibit IKK activity (Yin et al., 2009). Extended studies revealed that the Zincfinger domains 2-4 of TRAF6 are dispensable for TRAF6 auto-ubiquitination as well as IKK activation and that TRAF6 auto-ubiquitination and Ubc13 binding are dependent on the Zincfinger1 domain and an intact RING domain only (Lamothe et al., 2008). These data support the crucial role of the interaction of the TRAF6 RING-Zincfinger1 (RZ1) domain and Ubc13 in cells not only for TRAF6 auto-ubiquitination but also activation of NF- $\kappa$ B upon stimulation.

In Ubc13, TRAF6 binds the N-terminal helix including the M64 residue displaying one important contact for TRAF6 binding as a M64A mutant did not interact with TRAF6 in Yeast-Two-Hybrid assays (Zheng et al., 2000; Wooff et al., 2004). Other residues involved in TRAF6 binding are R6, R7, K10, R14, as well as S96, P97 and A98 (Yin et al., 2009). However, the impact of TRAF6-binding mutants in Ubc13 on NF- $\kappa$ B activation are not analyzed, yet.

Altogether, the interaction of TRAF6-Ubc13 exhibits several unique features: i) the interaction surface of around 1000 Å<sup>2</sup> is relatively small for protein-protein-binding, ii) residues that are involved in binding are absolutely critical as mutating a single residue leads to the disruption of the complex, iii) the majority of the residue involved in binding are exposed on the interaction surface and are available for hydrophobic interactions, iv) the involved residues are specific for the interaction of TRAF6 and E2 enzymes (Ubc13 and UbcH5), v) the interaction is a transient interaction ( $K_d = 1.6\mu\text{M}$ ) (Yin et al., 2009).

## 2.5 Protein-protein-interactions and the UPS in drug discovery

The identification of small molecules influencing protein function and the process of transforming these molecules into lead series are main goals in modern drug discovery (Bleicher et al., 2003). High-Throughput-Screening (HTS) is a screening of large chemical libraries, mostly performed *in vitro*, to identify hits that are active against biological targets using automation, miniaturized assays and large-scale data analysis (Keseru and Makara, 2006). Up to date, there are 3,000 to 10,000 known disease modifying proteins but only a minor portion of around 400 proteins are explored for therapeutic development (Overington et al., 2006; Jin et al., 2013). The majority of these 400 protein targets fall into a few families including G protein-coupled receptors, nuclear receptors, ion channels or enzymes (for example kinases, proteases, deacetylases) (Makley and Gestwicki, 2013). Many of these targets contain deep grooves that are accessible to bind low molecular weight molecules. In contrast, the modern shift in HTS includes other types of targets like non-enzymes that act as adapter proteins. Similar to enzymes, these adapter molecules regulate a majority of the human proteome and they include proteins involved in organizing signaling pathways, maintaining structural integrity, assembly and disassembly of protein complexes, chaperon function, subcellular transport, transcription, translation and other critical functions (Makley and Gestwicki, 2013). Instead of using enzymatic activity to carry out their biological functions, most adapter proteins involve either transient or stable protein-protein interactions (PPIs). PPIs mediate critical regulatory events in physiology and pathology and therefore may represent important targets for pharmaceutical intervention. Targeting PPIs with small molecules faces two main challenges. First, PPI usually involves a large number of polar and hydrophobic interactions across a large interface of 1,500 - 3,000 Å<sup>2</sup>. Second, the interaction interfaces are usually planar and lack binding pockets (Jin et al., 2014). However, within the interface region not all residues are equally important and it is possible to define hotspots. Hotspots are a small subset of residues of a binding interface that are critical for the interaction. Furthermore, PPIs can be divided into permanent and transient interactions. Transient interactions are easier to target than permanent interactions (Villoutreix et al., 2014).

The ubiquitin system plays an important role in the regulation of most cellular pathways. Its deregulation has been implicated in a wide range of human diseases including cancer, neurodegenerative and immunological disorders as well as viral infections. Therefore, targeting the UPS by small molecules provides an opportunity for the development of therapeutics for the treatment of several diseases. Due to the complexity of the ubiquitination reaction and its outcome, inhibitors targeting the UPS are rather underexplored. However, significant advances

in understanding the molecular nature of the ubiquitination process and its regulation of the cellular signals have been made. Also, improvement of screening methods already led to the discovery of the first compounds targeting the components of the UPS and promises further success. In 2003, the FDA approved the proteasome inhibitor Bortezomib for treatment of hematologic malignancies and thereby became the first drug targeting the UPS in clinics (Kane et al., 2003). Upstream from the proteasome, the UPS provides many additional targets for small molecules such as E3 ubiquitin ligases. In contrast to proteasome, E1 and E2 inhibitors, targeting E3 ligases might specifically impair only a limited set of substrates and might cause fewer toxic side effects. Examples for targeting E3 ligase-protein interactions within the UPS are small molecule inhibitors of the MDM2-p53 PPI. Development of these compounds aims for their administration in cancer therapy to reactivate the p53 tumor suppressor function. Different strategies succeeded in targeting this interaction. The MDM2 inhibitor nutlin interacts with the p53-binding pocket to inhibit p53 degradation whereas the small molecule RITA directly binds p53 to interfere with the p53/MDM2 interaction (Vassilev et al., 2004; Issaeva et al., 2004). RG7112, a derivate of nutlin, is currently undergoing phase I clinical trials (Khoo et al., 2014). Further examples for interfering with PPIs are IAP (inhibitor of apoptosis) inhibitors. IAPs are usually targeted by Smac, a mitochondrial protein and negative regulator of IAPs. It enhances apoptosis by binding to IAPs to prevent their interaction with caspases. The observation that a short IAP-binding motif (IBM) of smac binds IAPs and blocks the interaction of IAPs and caspases led to the development of small molecules that target this IBM of numerous IAPs including XIAP, cIAP1 and cIAP2 (Gyrd-Hansen and Meier, 2010). These compounds induce degradation of IAPs and lead to caspase activation resulting in a decrease viability of cancer cells. The first compound targeting this class of proteins is GDC-0152 and is currently tested in clinical trials (Flygare et al., 2012).

However, no small molecules targeting the interface of an E3 ligase - E2 enzyme are known yet. Due to the unique features of the binding of TRAF6 to Ubc13 (described in 2.4.2) this protein-protein interaction is considered to be druggable. Small molecules targeting this interface would not only abrogate the interaction of TRAF and Ubc13, but would also cause inhibition of the E3 ligase activity of TRAF6 leading to impaired NF- $\kappa$ B signaling in inflammatory diseases and cancer.

### **3 Aim of this thesis**

The E3 ubiquitin ligase TRAF6 is a critical contributor to NF- $\kappa$ B signaling. It is well known to regulate pathways in innate as well as in adaptive immune response. Elevated levels of NF- $\kappa$ B and TRAF6 cause a variety of diseases including autoimmune diseases, carcinomas and metabolic disorders. Therefore, targeting TRAF6 offers a potential novel strategy for therapeutic intervention of multiple diseases. In TRAF6-dependent signaling, TRAF6 interacts with the E2 complex Ubc13/Uev1a to facilitate its auto-ubiquitination and subsequent K63-linked polyubiquitination of substrates to mediate signal transduction towards NF- $\kappa$ B activation. The N-terminal RING-Zincfinger1 domain of TRAF6 is responsible for Ubc13 binding and was therefore selected to be targeted by small molecules. The aim was to establish a suitable a High-Throughput-Screening assay and to perform the HTS campaign. Hits have to be validated and optimized *in vitro* as well as in cell-based assays. After analog screening, the anti-inflammatory potency of the best hit should be analyzed in a high-fat-diet induced obesity mouse model that is marked by glucose intolerance and low-grade chronic inflammation. In 2014, a TRAF6 inhibitor targeting the MATH domain of TRAF6 was shown to improve the chronic inflammation and glucose tolerance in an obese mouse model (Van den Berg et al., 2014). This should enable comparison of the efficiency of the best compound identified in this work in ameliorating the symptoms as well as the effects of targeting the different termini of TRAF6.

## 4 Results

### 4.1 Establishment of a TRAF6-Ubc13 interaction assay for High-Throughput-Screening

#### 4.1.1 Biochemical validation of the TRAF6-Ubc13 interaction

For the identification of small molecules targeting the RING-Zincfinger1 (RZ1) domain of TRAF6 to prevent its binding to Ubc13 as well as its auto-ubiquitination, a suitable *in vitro* High-Throughput-Screening (HTS) setting had to be established. It is proposed that only the N-terminal RZ1 domain of TRAF6 directly interacts with Ubc13 (Wooff et al., 2004; Yin et al., 2009; Lamothe et al., 2008). To confirm these data, a Yeast-Two-Hybrid assay was performed before starting the purification of recombinant proteins. First, selected TRAF6 constructs were cloned into the pGAD vector fusing TRAF6 to the activation domain of the transcription factor GAL4. Ubc13 fulllength was cloned into the pGBD vector marking it with the DNA binding domain of GAL4. Growth of the transformed yeast strain on a selective medium lacking histidine is only obtained after the reconstitution of a functional transcription factor GAL4 upon interaction of TRAF6 and Ubc13. The binding of fulllength TRAF6 to Ubc13 could be confirmed with a fast growing yeast spot (Fig. 4.1). Also, yeast colonies were obtained after transformation of the TRAF6 RZ1 domain and Ubc13. In contrast, yeast colonies carrying single point mutations in the Ubc13 binding motif (C70A, D57K or I72F) within the TRAF6 RZ1 domain did not survive on selective medium. In agreement with these findings, yeast transformed with TRAF6 constructs missing the RZ1 domain but containing the Coiled-Coil or Coiled-Coil and MATH domain did not grow on the selection medium either (Fig. 4.1).

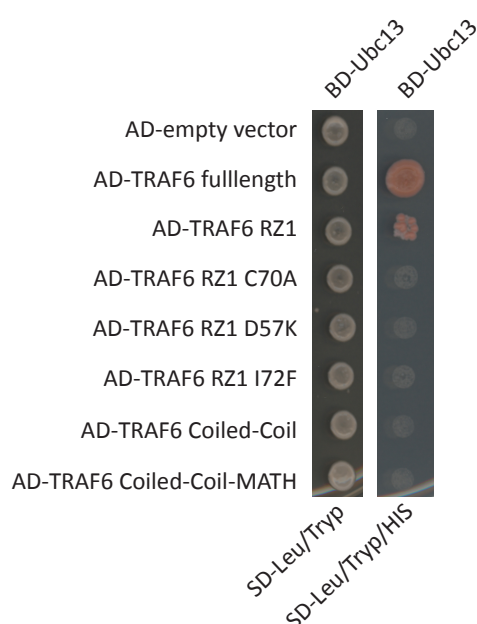


**Figure 4.1: Confirmation of TRAF6 binding to Ubc13 via the N-terminal RING-Zincfinger1 domain.** In a Yeast-Two-Hybrid assay only TRAF6 fulllength and the TRAF6 RING-Zincfinger1 domain interact with Ubc13. Ubc13-binding mutations (C70A, D57K and I72F) or lack of the RING-Zincfinger1 domain do not lead to yeast cell growth.



After confirming that only the RZ1 domain of TRAF6 is required for Ubc13 binding, the TRAF6 RZ1 wildtype as well as the single point mutations (C70A, D57K and I72F) were cloned into the pASK-IBA-3+ vector fusing the protein to a C-terminal StrepII-tag (TRAF6StrepII). Ubc13 and a C-terminal Flag-His-tag were cloned into the pGex-4T1 vector (Ubc13FH). The Coomassie Blue staining of the purified proteins is shown in Figure 4.2A and revealed clean protein solutions. Before establishing an *in vitro* HTS assay with these proteins, a gel-filtration assay was performed with equimolar concentrations of TRAF6 and Ubc13 to confirm binding of the purified proteins. Incubating both proteins caused a peak shift clearly indicating, that TRAF6<sub>WT</sub>StrepII is directly interacting with Ubc13FH (Fig. 4.2B).

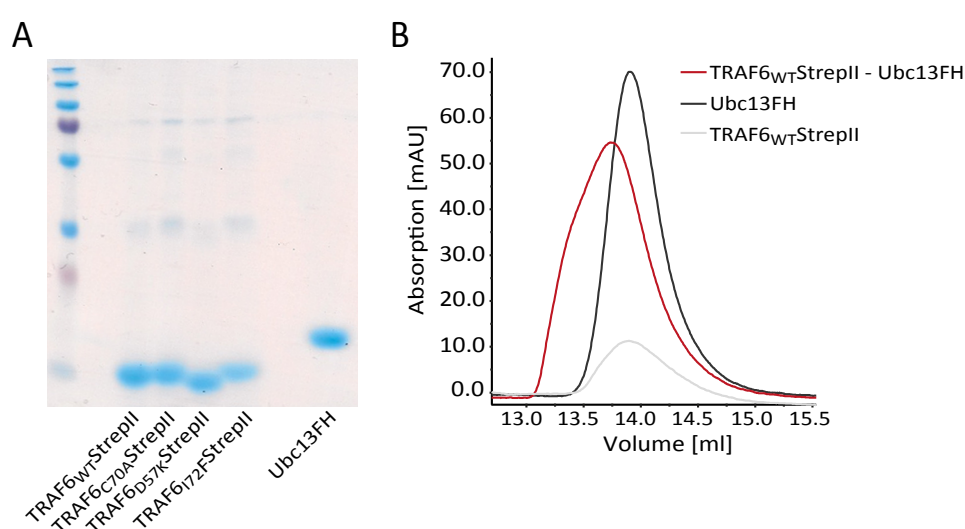


**Figure 4.2: Proof of purity and activity of recombinant purified proteins.** (A)

Recombinant purified proteins appear clean in a Coomassie Blue staining. (B)

Recombinantly purified TRAF6<sub>WT</sub>StrepII and Ubc13FH proteins directly interact in a gel-filtration assay.

#### **4.1.2 Establishment of the ALPHAScreen TRAF6-Ubc13 binding assay for HTS**

For establishing a suitable *in vitro* HTS system the ALPHAScreen system (Amplified Luminescence Proximity Homogeneous Assay) provided by Perkin Elmer was used. For the establishment of a functional ALPHAScreen system Strep-Tactin Donor beads binding to TRAF6StrepII and Nickel Chelate Acceptor beads targeting Ubc13FH were applied to the reaction mix. The first step in establishing this assay was to determine optimal protein concentrations. Cross-titrations of TRAF6<sub>WT</sub>StrepII-Ubc13FH and TRAF6<sub>C70A</sub>StrepII-Ubc13FH to define the best conditions for a suitable screening were performed (Fig. 4.3A and data not shown). The optimal protein amounts were set to a concentration that still was in the linear range but also provided feasible production of protein amounts. Accordingly, the ideal protein concentration of TRAF6StrepII was 100nM, whereas for Ubc13FH 75nM was assessed (Fig. 4.3A). Under these conditions the signal units for TRAF6<sub>WT</sub>StrepII-Ubc13FH interaction still

remained in the upper range of the linear scale, whereas the TRAF6<sub>C70A</sub>StreptII-Ubc13FH assay exhibited only background signals (Fig. 4.3A). Next, the amount of Donor and Acceptor beads was titrated to yield a high ratio of TRAF6<sub>WT</sub> to TRAF6<sub>mutant</sub>. Out of 7 tested concentrations (20 - 2 µg/mL) 4 µg/mL beads still revealed a ratio of TRAF6<sub>WT</sub> to TRAF6<sub>mutant</sub> with more than 100 fold induction (Fig. 4.3B) and therefore was determined to be sufficient for the screening assay. In a mutant screen with the screening conditions defined thus far, TRAF6<sub>D57K</sub>StreptII was the best control mutant with a 193 fold ratio compared to the wildtype TRAF6<sub>WT</sub>StreptII (Fig. 4.3C). Hence, the TRAF6<sub>D57K</sub>StreptII protein was selected as a reference for the intensity of maximum inhibition during screening procedure. Including the TRAF6<sub>D57K</sub>StreptII mutant in every performed screen was necessary to determine the highest level of inhibition as the signal units did vary from assay to assay depending on the efficacy of the bead batches (Figures 4.3A and 4.3B).

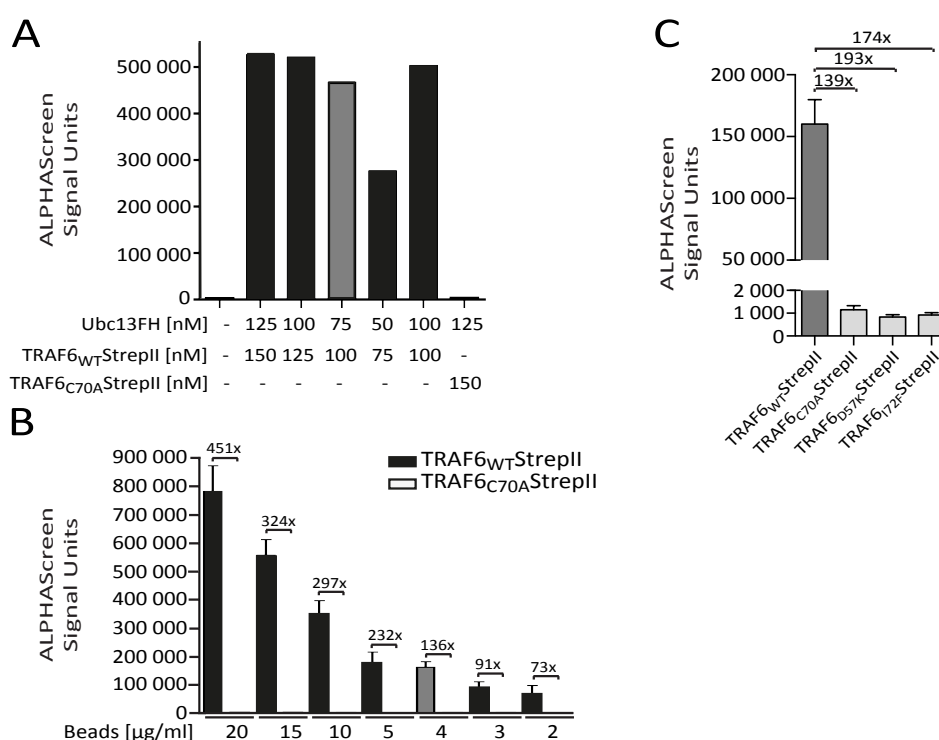


**Figure 4.3: Benchtop establishment of the ALPHAScreen assay.** (A) Cross-titrations of protein amounts revealed 100nM TRAF6StreptII and 75nM Ubc13FH as the optimal protein concentration combination. (B) Cross-titrations of bead amounts illustrated 4 µg/mL of Donor and Acceptor beads as the most reasonable concentration. (C) TRAF6 mutant screen highlighted TRAF6<sub>D57K</sub> as the best mutant. Mean and standard deviation are depicted.

For the final settings presented in Figure 4.4A, all conditions were tested in the presence of 0.5% DMSO that was used for dissolving the compounds. TRAF6<sub>WT</sub>StreptII and Ubc13FH incubated with Donor and Acceptor beads featured high signal units, which were abrogated

when replacing TRAF6<sub>WT</sub> by the TRAF6<sub>D57K</sub> mutant (Fig. 4.4A). Background signals were also obtained in the absence of one of the two beads as well as beads without any protein (Fig. 4.4A). This confirmed that the interaction of TRAF6<sub>WT</sub>StreptII and Ubc13FH is highly specific as well as direct and that the requirements for converting this benchtop assay in an automated HTS assay are met.

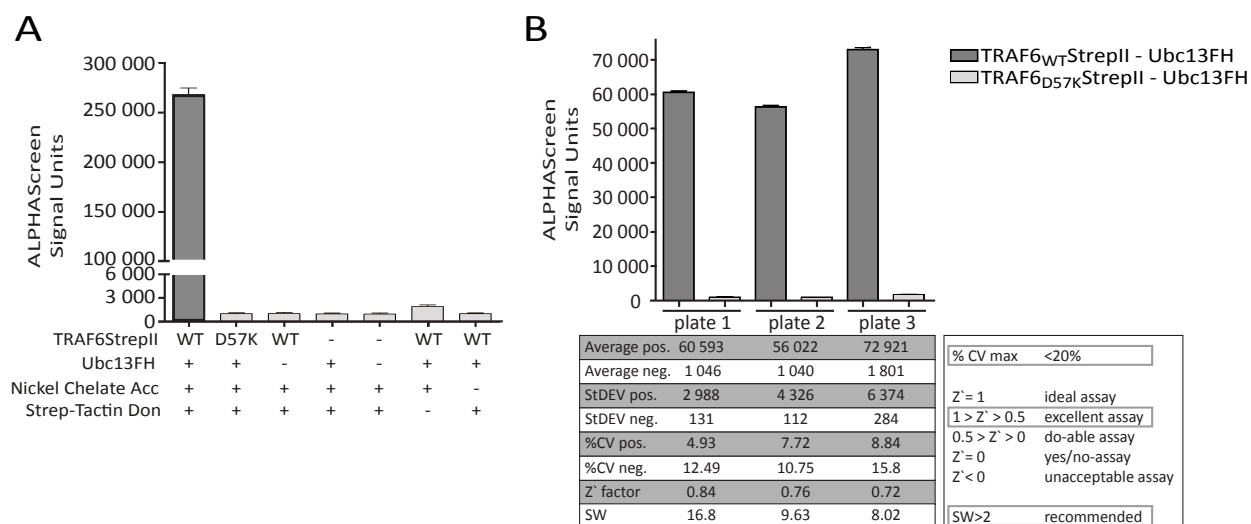


**Figure 4.4: Converting the ALPHAScreen method from a benchtop into an automated assay.** (A) Established ALPHAScreen conditions for benchtop use including all controls confirm a specific assay for High-Throughput-Screening. (B) Calculated statistical computations of an inter-plate test in automated ALPHAScreen settings revealing excellent assay conditions for High-Throughput-Screening. Mean and standard deviation are depicted.

For the automation of the ALPHAScreen assay both protein solutions as well as the beads were pipetted automatically. To imitate compound transfer, DMSO was applied to the solutions automatically as well. In Figure 4.4B, results of an inter-plate test of an automated screen are listed. In order to determine the quality, several statistical parameters were calculated: the average of the positive and negative controls as well the standard deviations (StDEV), coefficient of variation (CV), the Z' factor and the signal window (SW) (for a detailed description of the parameters see 7.2.3.10). All CV values for the positive as well as the negative controls did not exceed 20% and therefore referred to an optimal assay (Fig. 4.4B). The calculated Z' factors reaching from 0.72 to 0.84 displayed values for an excellent assay (Zhang et al., 1999). Furthermore, all plates met the criterion of a recommended SW higher than 2. The required acceptance criteria of CV < 20%, Z' factor > 0.5 and SW > 2 (Iversen et al., 2012) plus the DMSO compatibility were all met and therefore, the established ALPHAScreen assay settings qualified as an appropriate HTS assay.

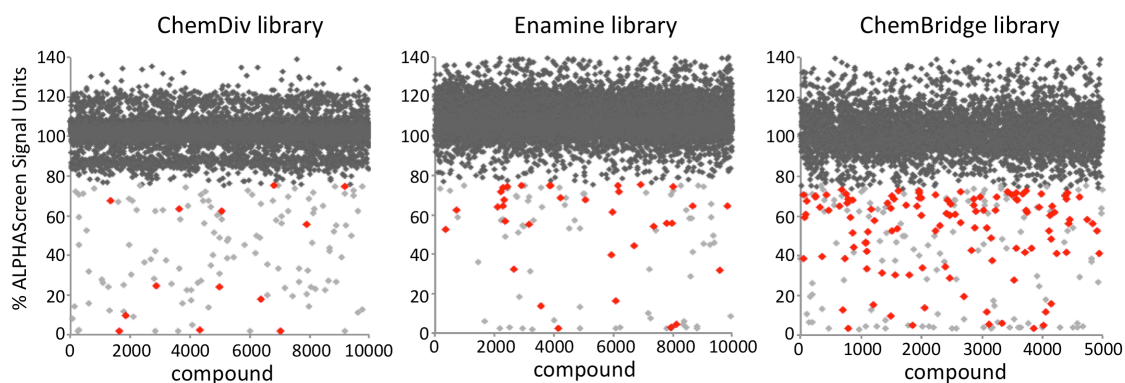
## 4.2 HTS, Hit identification and Hit verification

### 4.2.1 HTS – Hit identification

For the identification of small molecules impairing the TRAF6-Ubc13 interaction, three in-house chemical diverse libraries were available: ChemDIV (10,000 compounds), Enamine (10,000 compounds) and ChemBridge (5,000 compounds). In the screening process each compound was screened with a final concentration of 10 $\mu$ M. All 80 screening plates met the criteria for the Z' factor (between 0.5 and 0.9; data not shown). For the CV, only 7 out of 80 plates showed a value slightly higher than 20% whereas 73 plates met the criteria for CV < 20% (data not shown). The results for all three library screenings are summarized in Figure 4.5A. In dark grey compounds not affecting the TRAF6-Ubc13 interaction in this ALPHAScreen assay are displayed. Small molecules interfering with the ALPHAScreen technology are shown in light grey. Compounds specifically inhibiting TRAF6-Ubc13 binding are presented in red. Figure 4.5B presents the scheme of selecting hit compounds out of the performed HTS. In total 520 out of 25,000 tested compounds showed an inhibition of TRAF6-Ubc13 binding with more than 25% at 10 $\mu$ M compound concentration. This corresponds to a primary hit rate of 2.08%. These 520 compounds were analyzed being for frequent hitters. Frequent hitters are compounds acting by non-specific mechanisms and either interfere with the ALPHAScreen chemistry or prevent the binding of Nickel Chelate beads to the His-tag moiety of the proteins (Schorpp et al., 2014). In parallel with the TRAF6-Ubc13 screen, 3 additional HTS campaigns were performed using the ALPHAScreen technology as well but involving different tag-combinations (GST-His, His-Myc and Biotin-His). Several compounds appeared to inhibit all analyzed protein-protein interactions and were identified as frequent hitters (Schorpp et al., 2014). Altogether 137 compounds referred to frequent hitters at a 10 $\mu$ M concentration and therefore were eliminated from the hit list. Furthermore, in parallel with the TRAF6-Ubc13 screen another HTS campaign involving GST-OTUB1-Ubc13FH was conducted. OTUB1 is a deubiquinating enzyme targeting an interface of Ubc13 that overlaps with the TRAF6 binding site (Wiener et al., 2012). In order to identify compounds specifically targeting TRAF6 rather than Ubc13, the screenings of TRAF6<sub>WT</sub>StreptII-Ubc13FH and GST-OTUB1-Ubc13FH were compared for compounds impairing both interactions at a concentration of 10 $\mu$ M. In the end, 205 small molecules hitting both assay had to be eliminated referring to 178 compounds remaining for hit picking (Fig. 4.5B). This led to a hit rate of 0,712% out of 25,000 screened compounds that specifically inhibit the TRAF6-Ubc13 interaction and thereby most likely target TRAF6.

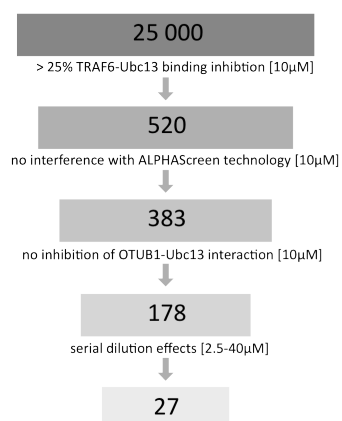
Summarizing the HTS campaign, out of 25,000 compounds 178 hit molecules were obtain after exclusion of frequent hitters and small molecules most likely targeting Ubc13FH.

A



- Compounds with no effect
- Compounds interfering with ALPHAScreen technology
- Specific hits

B



C

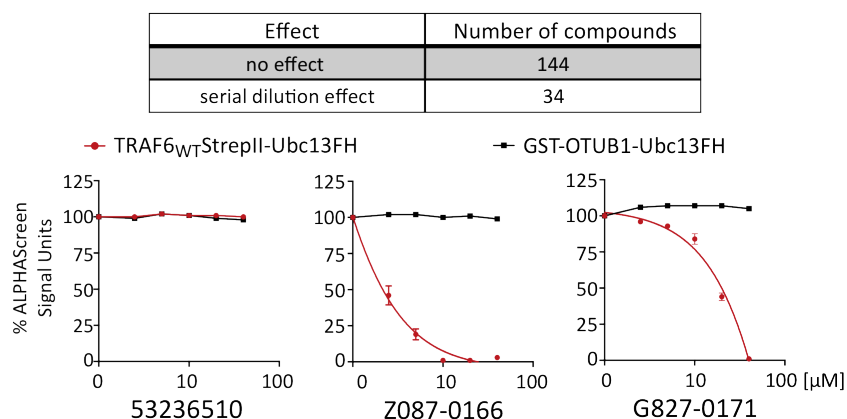


**Figure 4.5: High-Throughput-Screening campaign and subsequent hit verification.** (A) Overview of the activity of compounds of three in-house small molecule libraries. In red, all specific hits are displayed. Specific hits are classified as molecules that do not interfere with the ALPHAScreen technology (frequent hitters and His frequent hitters are excluded) and do not target Ubc13. (B) Scheme for selecting compounds including the compound numbers as well as the conditions for exclusion. (C) Summary of biochemical hit verification assay of 178 primary hit compounds and exemplary data for each type of possible effects. The majority of the retested compounds show no effect (53236510). 34 compounds demonstrate a specific serial dilution effect with either strong (Z087-0166) or weak (G827-0171) inhibitory potential. Mean and standard deviation are shown.

#### 4.2.2 HTS – Hit verification

Next, a hit picking campaign was completed to verify the 178 small molecules out of the HTS campaign for specific and dose-dependent effects. Therefore, five-point serial dilutions of the 178 small molecules ranging from 2.5µM to 40µM final compound concentration were prepared. These dilutions were applied to the TRAF6<sub>WT</sub>StrepII-Ubc13FH ALPHAScreen assay and in parallel to the GST-OTUB1-Ubc13FH ALPHAScreen assay. In Figure 4.5C, a summary of the

results is illustrated. All in all, 144 compounds did not show inhibitory effects in both tested assays implying their false positive nature in the initial HTS campaign. One example for false positive hits (compound 53236510) is displayed in the first diagram of Figure 4.5C. 34 compounds demonstrated inhibitory serial dilution effects on TRAF6<sub>WT</sub>StrepII-Ubc13FH interaction, but at the same time did not affect the binding of GST-OTUB1 to Ubc13FH in ALPHAScreen assay. However, not all compounds reached an IC<sub>50</sub> value below 40µM (Figure 4.6A). Exemplary, the second and the third diagram in Figure 4.5C present two out of these 34 compounds with a strong (Z087-0166) or a moderate (G827-0171) inhibitory effect.

The results obtained from the HTS campaign and the hit verification demonstrate that 34 out of 25,000 small molecules exhibited a specific and dose-dependent inhibition of the TRAF6<sub>WT</sub>StrepII-Ubc13FH interaction.

### **4.3 Biochemical and cell-based Hit validation**

In order to validate the 34 verified hits, all compounds were reordered from the corresponding companies. Unfortunately, only 27 compounds were available by that time. Thus, biochemical as well as cell-based assays were performed with the 27 reordered compound to verify their inhibitory potential.

#### **4.3.1 Biochemical hit validation**

In order to prove the specificity of the 27 selected compounds in binding to TRAF6, ALPHAScreen assays including the protein-protein interactions of TRAF6StrepII-Ubc13FH, GST-OTUB1-Ubc13FH and GST-RNF8-Ubc13FH were conducted in parallel. RNF8 (RING finger 8) is an E3 ubiquitin ligase carrying a RING-motif responsible for the interaction to Ubc13 and is involved in DNA damage response (Campbell et al., 2012). Since the RING domains of TRAF6 and RNF8 display a significantly structural similarity (supplement 10.11), this interaction was included in the hit validation process to exclude general RING domain binding compounds. Serial dilution experiments were performed assaying all three different ALPHAScreen assays in parallel. Out of the 27 reordered small molecules only compound 20 did not affect TRAF6Strep-Ubc13FH binding (Figure 4.6A and B). All other molecules showed reduced TRAF6-Ubc13 interaction. In total, 13 out of 27 compounds showed strong effects (IC<sub>50</sub> < 10µM) on TRAF6-Ubc13 binding while not impairing either OTUB1-Ubc13 or RNF8-Ubc13 interaction. Exemplary, compound 18 is shown in Figure 4.6B. Graphs of all 27 compounds are shown in the supplement 10.1-4. In a range of an IC<sub>50</sub> between 11µM and 50µM eight small molecules inhibited the binding of TRAF6 to Ubc13 but at the same time did not affect OTUB1-Ubc13 or

RNF8-Ubc13 interaction. Finally, five compounds only had little effects on TRAF6-Ubc13 binding ( $IC_{50}$  from 51 to  $100\mu M$ ). In some cases  $IC_{50}$  values of the primary hit compounds and the reordered compounds differed pointing out the batch-to-batch variability (Figure 4.6A). Hence, in biochemical hit validation experiments, only one compound (C20) did not display an inhibitory potential. All other compounds still revealed specific impairment of TRAF6-Ubc13 binding without affecting OTUB1-Ubc13 or RNF8-Ubc13 interaction.

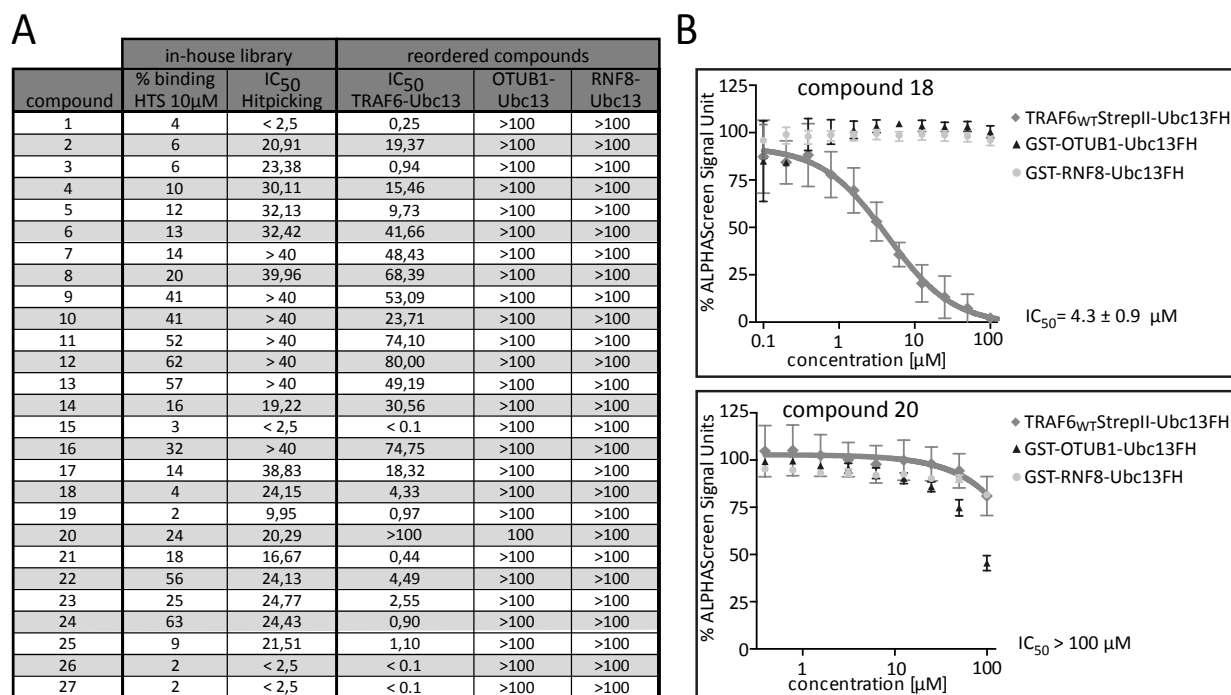


**Figure 4.6: Biochemical hit validation of 27 reordered compounds using the ALPHAScreen system.** (A) Summary of the analyzed hit compounds in ALPHAScreen assays in the High-Throughput-Screening, hit verification and hit validation experiments with reordered compounds. Except compound 20, all compounds specifically reduced the interaction of TRAF6-Ubc13. (B) Exemplary data of two reordered compounds in titration assays in the hit validation process. Compound 18 impairs TRAF6-Ubc13 binding specifically whereas compound 20 does not. Mean and standard deviation are depicted.

#### 4.3.2 Cell-based hit validation

For accomplishing the validation of the 27 hits in cells, cell toxicity of each compound was analyzed in a CellTiter-Blue viability assay which is a homogeneous and fluorometric method to estimate the number of viable cells in a multiwell plate format. This approach is based on the ability of living cells to convert the redox dye resazurin into resofurin, a fluorescent end product. The fluorescence signal is proportional to the number of viable cells. The compounds were applied to human hepatoma cells (HepG2) and to mouse embryonic fibroblasts (MEF). HepG2 are often used as standard cells in testing cytotoxicity of small molecules as drugs are

primarily metabolized in the liver. Administering the cytotoxicity of the compounds in MEF cells was required because following analyses were conducted in these cells. A summary of all compounds in HepG2 and MEF cells at a concentration of 50 $\mu$ M, which will be the highest working concentration in later experiments, is presented in Figure 4.7A. A compound was considered to be non-cell toxic when the cell viability obtained after 24hours of compound treatment was still higher than 75%. Only compounds C5, C11, C20 and C24 showed less than 75% viable cells in both cell lines although C5, C11 and C24 almost reached the 75% cell viability limit (Fig. 4.7A). C20, however, exhibited the most prominent cytotoxicity with less than 40% of living cells in both cell lines and therefore is indeed considered to be cell toxic. Compounds C8, C19 and C22 decreased cell viability under 75% only in HepG2 cells, but remained non-cell toxic in MEF cells. Compound C10 and C4 are the only molecules, which displayed a higher toxicity on MEF cells compared to HepG2. This observation needs to be considered for hit validation in the following cell-based assays in MEF cells.

Next, the compounds were analyzed for their effects on NF- $\kappa$ B activation in Electrophoretic Mobility Shift Assay (EMSA). Compounds were tested in IL-1 $\beta$  and TNF $\alpha$  stimulation experiments to determine selectivity of the compounds. The TRAF6 dependency of IL-1 $\beta$  induced NF- $\kappa$ B signaling was verified in TRAF6<sup>-/-</sup> MEF cells that were not able to activate NF- $\kappa$ B signaling (Lamothe et al., 2008 and Figure 4.7B). NF- $\kappa$ B activation upon TNF $\alpha$  stimulation was not impaired in these cells (Yamamoto et al., 2006 and Figure 4.7B). In the first round of experiments, MEF cells were treated with 30 $\mu$ M and 50 $\mu$ M compound for six hours, subsequently stimulated with IL-1 $\beta$ , lysed and then analyzed in EMSA. In the second round, compounds were tested after IL-1 $\beta$  and TNF $\alpha$  stimulation side by side. Figure 4.7C represents one experiment of the second round. For the exact quantification of NF- $\kappa$ B activation after stimulation, the levels of NF- $\kappa$ B were normalized to Oct1 amounts, which are commonly used as a loading control for EMSA. NF- $\kappa$ B activation was then quantified using the LabImage1D software to compare the efficiencies of the tested compounds. Compound C26 did not show an effect. Compound C22 showed an IL-1 $\beta$  specific, but very mild effect on NF- $\kappa$ B activation whereas C24 and C25 led to a stronger IL-1 $\beta$  specific impaired NF- $\kappa$ B signaling compared to TNF $\alpha$ . Compounds C23 and C27 exhibited strong effects after IL-1 $\beta$  stimulation but reduced TNF $\alpha$  induced NF- $\kappa$ B activation to the same extent (Figure 4.7C). Figure 4.7D summarizes the quantifications for each compound at a concentration of 50 $\mu$ M after IL-1 $\beta$  as well as TNF $\alpha$  stimulation.



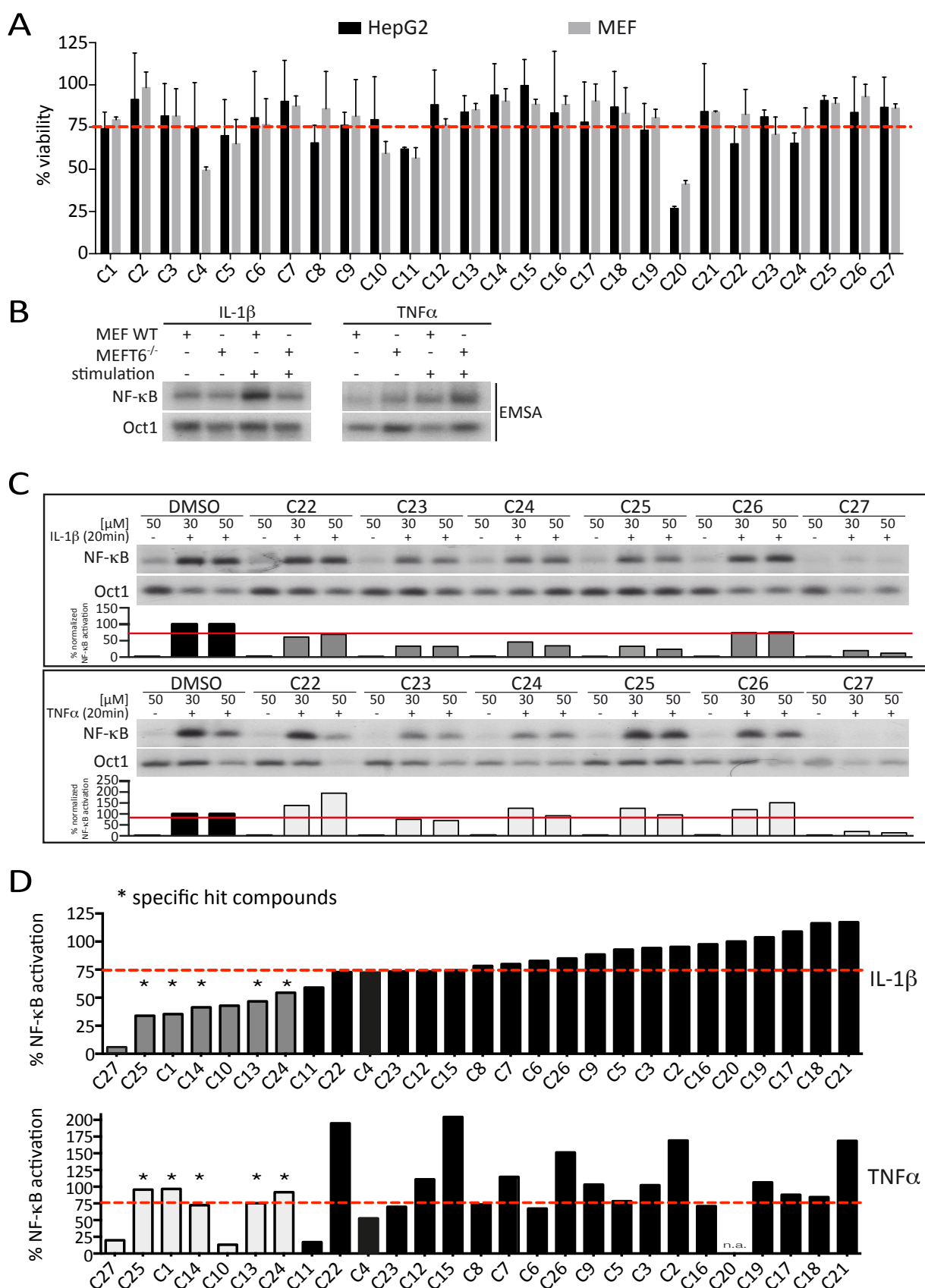


**Figure 4.7: Cytotoxicity assays and cell-based hit validation of 27 compounds using EMSA technology.** (A) CellTiter-Blue assays of 27 compounds for cell toxicity tests in HepG2 and MEF cells after 24 hours of compound treatment. C20 is cell toxic in HepG2 as well as in MEF cells. Compounds C4, C5, C10, C11 and C24 display a slight

reduction in cell viability whereas all other compounds show no cell toxic effects. Mean and standard deviation are depicted. (B) EMSA experiments upon IL-1 $\beta$  and TNF $\alpha$  stimulation experiments in wildtype MEF and TRAF6<sup>-/-</sup> MEF cells revealed the TRAF6-dependency of IL-1 $\beta$  induced NF- $\kappa$ B activation whereas TNF $\alpha$  signaling does not rely on TRAF6. (C) Exemplary data for the quantification of EMSA experiments derived from compound treated cells (50 $\mu$ M) after IL-1 $\beta$  and TNF $\alpha$  stimulation. C23 and C27 treatment cause a strong reduction in NF- $\kappa$ B activation after IL-1 $\beta$  and TNF $\alpha$  stimulation. C25 reduces NF- $\kappa$ B activation selectively after IL-1 $\beta$  stimulation whereas C26 does not show inhibitory potential. (D) Summary of quantified NF- $\kappa$ B activation for 27 compounds out of the EMSA experiments at a concentration of 50 $\mu$ M. IL-1 $\beta$  data were generated out of two experiments; TNF $\alpha$  stimulation experiments were performed only once. C25, C1, C13, C14 and C24 are the only compounds that showed an IL-1 $\beta$  selective inhibition of NF- $\kappa$ B activation.

Small molecules were considered to be a specific hit compound by meeting the following two criteria: i) NF- $\kappa$ B activation after IL-1 $\beta$  stimulation was reduced in both test rounds by more than 25% at 50 $\mu$ M compound concentration (quantification of each single experiment is depicted in supplement 10.5) and ii) TNF $\alpha$  induced NF- $\kappa$ B activation must not be reduced by more than 25% at a concentration of 50 $\mu$ M. Whereas 6 compounds did not impair NF- $\kappa$ B activation, 19 compounds reduced activation of NF- $\kappa$ B after IL-1 $\beta$  stimulation in at least one round. 8 out of these 19 molecules decreased IL-1 $\beta$  induced NF- $\kappa$ B activation in both test rounds (C1, C4, C10, C13, C14, C24, C25 and C27). Nevertheless, C4, C10 and C27 did not meet the second criteria of not inhibiting TNF $\alpha$  induced NF- $\kappa$ B activation by more than 25%. Furthermore, it cannot be excluded that C4 and C10 diminished NF- $\kappa$ B activation due to their slightly cytotoxic effects obtained in MEF cells in CellTiter-Blue assays (Figure 4.7A). In the end, 5 out of 27 tested compounds met the criteria for presenting selective hit compounds in these hit validation settings: C1, C13, C14, C24, C25 whereas C25 was the most effective compound after IL-1 $\beta$  stimulation while not impairing TNF $\alpha$  induced NF- $\kappa$ B activation.

#### **4.4 Validation of C27 in biochemical and cell-based assays**

C27 is a compound from the ChemDIV library and its chemical structure is depicted in Figure 4.8A. It meets the Lipinski's rule of five (Figure 4.8B) and therefore is considered to be a drug-like and potentially orally available compound (Lesson, 2012). The criteria for the Lipinski's rule of five are depicted in 7.1.13. C27 showed a strong effect in specifically impairing the TRAF6-Ubc13 interaction *in vitro* in ALPHAScreen assays as well as decreasing activation of NF- $\kappa$ B after IL-1 $\beta$  stimulation in MEF cells. Treatment of MEF cells with C27 showed that it also interferes with TNF $\alpha$  induced NF- $\kappa$ B activation. Although this compound did not display pathway selectivity, it was the strongest acting compound in NF- $\kappa$ B activation experiments. To further

examine the effectiveness and selectivity of this small molecule, biochemical as well as cell-based studies were performed.

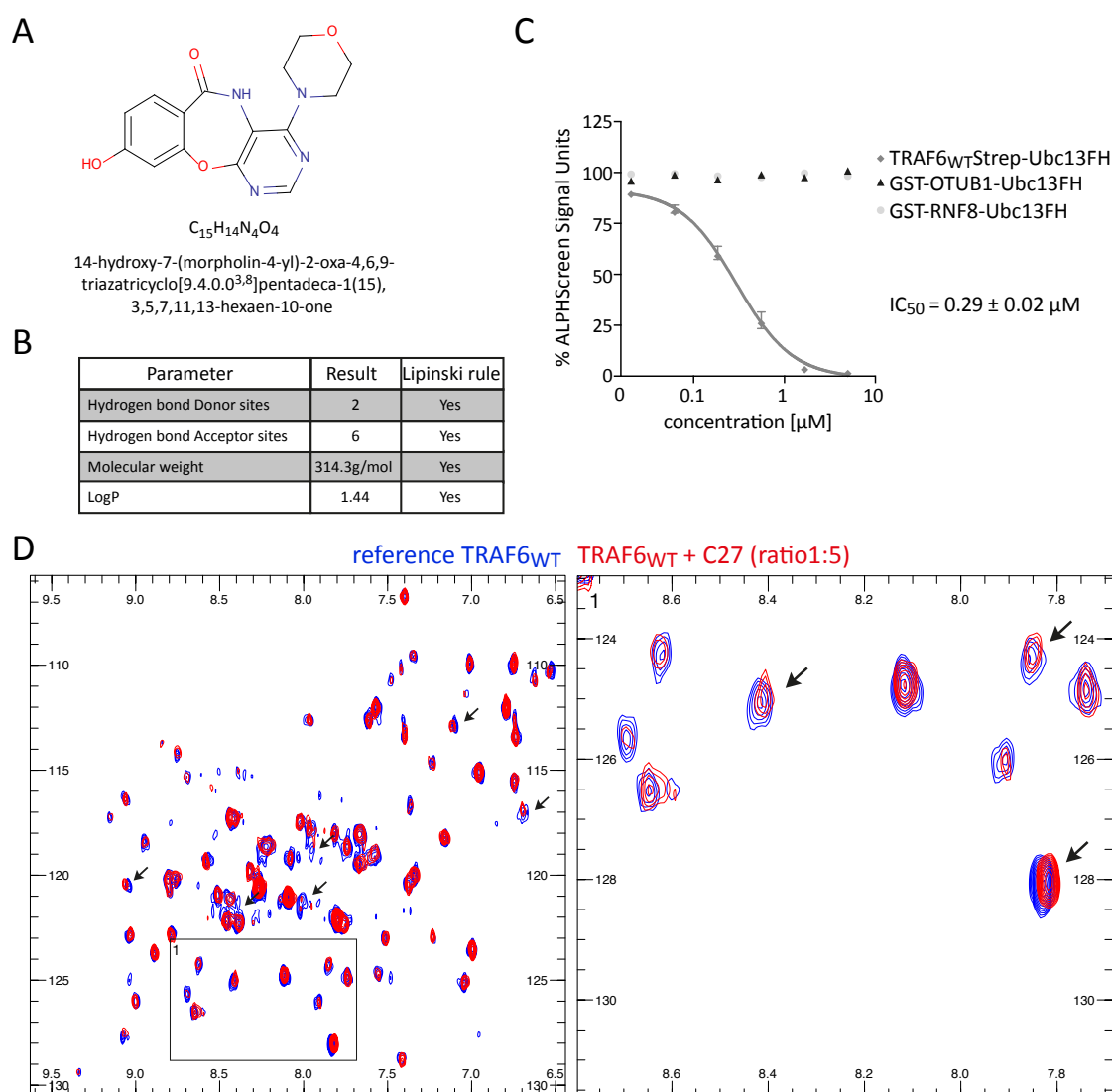


**Figure 4.8: Biochemical validation of C27.** (A) Compound structure, chemical formula and name of C27. (B) Molecular properties of C27 that meet the criteria of the Lipinski's rule of five. (C) ALPHAScreen assays testing increasing concentrations of C27. C27 impairs TRAF6<sub>WT</sub>StrepII-Ubc13FH interaction dose-dependently while binding of GST-OTUB1 and GST-RNF8 to Ubc13FH remain unaffected. Mean and standard deviation are shown. (D) NMR studies of TRAF6<sub>WT</sub> and C27 revealing that C27 directly targets TRAF6 (NMR experiments were performed by Dr. Grzegorz Popowicz from the Institute of Structural Biology at the Helmholtz Zentrum München).

#### 4.4.1 Biochemical validation of C27

To specify the IC<sub>50</sub> for C27, dose-response ALPHAScreen assays in a lower range were performed (0.02 - 10μM). C27 showed a strong inhibitory effect on TRAF6<sub>WT</sub>StrepII-Ubc13FH interaction with an IC<sub>50</sub> of 0.29μM ± 0.02μM while GST-OTUB1 and GST-RNF8 binding to Ubc13FH remained unaffected indicating that C27 is specifically targeting TRAF6 RZ1 *in vitro*

(Figure 4.8C). To confirm the direct binding of C27 to TRAF6,  $^{15}\text{N}$ -labeled TRAF6<sub>WT</sub> protein without carrying tags was recombinantly purified and analyzed in nuclear magnetic resonance (NMR) experiments. NMR experiments were performed by Dr. Grzegorz Popowicz at the Institute of Structural Biology at the Helmholtz Zentrum München. NMR spectra of TRAF6<sub>WT</sub> only (blue) and TRAF6<sub>WT</sub> incubated with C27 (red) at a ratio of 1:5 are depicted in Figure 4.8D. Multiple peaks were shifting or disappearing upon C27 treatment indicating that C27 directly targets the TRAF6 RZ1 domain. Arrows highlight peaks that are strongly affected by C27. As C27 directly targets the RING-Zincfinger1 domain of TRAF6, further investigations of C27 were carried out in cell-based assays.

#### **4.4.2 Cell-based validation of C27**

Before investigating the influence of C27 in NF- $\kappa$ B signaling after various stimuli, a more precise cell toxicity study was performed. Besides CellTiter-Blue experiments, Hoechst33342 and Mitotracker stainings in living cells were conducted. Hoechst33342 is a cell-permeable blue fluorescent dye that intercalates into DNA and is used to determine the nucleus area in this experiment. Mitotracker is a red fluorescent dye that incorporates into mitochondria of living cells and is used to analyze the mitochondrial mass. In CellTiter-Blue experiments, C27 was well tolerated in HepG2 and MEF cells up to the tested concentration of 100 $\mu\text{M}$  (Figure 4.9A). Moreover, in both cell lines the nucleus area and the overall mitochondrial mass were not markedly altered (Figure 4.9A).

To verify the EMSA data from the hit validation assays, time-dependent experiments in MEF cells were conducted to analyze the phosphorylation status of I $\kappa$ B $\alpha$ , its degradation and the resulting NF- $\kappa$ B DNA binding after various stimuli. In previous EMSA experiments NF- $\kappa$ B activation was drastically reduced to 10% when treating cells with 30 $\mu\text{M}$  C27 (Figure 4.7D and supplement 10.5). Therefore, time-dependent experiments were performed with applying only 5 $\mu\text{M}$  C27 to the cells. After DMSO or compound treatment for six hours, cells were stimulated with IL-1 $\beta$ , LPS or TNF $\alpha$  for the indicated time points (Figure 4.9B). In IL-1 $\beta$  stimulation experiments, the induced phosphorylation of I $\kappa$ B $\alpha$  was delayed after C27 treatment and consistent with that degradation of I $\kappa$ B $\alpha$  was reduced after 20 min stimulation as well. In line with this, NF- $\kappa$ B activation was diminished for all indicated time points compared to the DMSO treated cells. These data indicate that 5 $\mu\text{M}$  C27 were still sufficient to impair NF- $\kappa$ B activation.

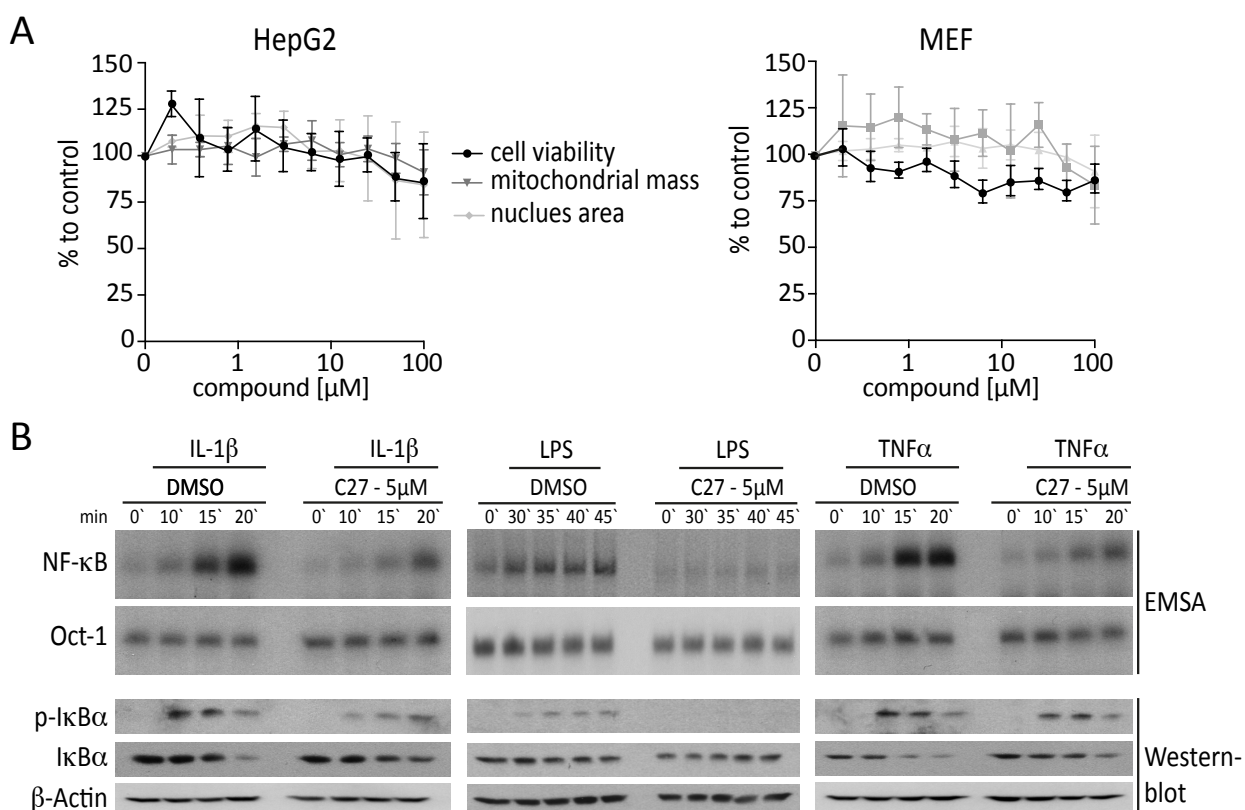


**Figure 4.9: Cytotoxicity tests and cell-based verification of C27 after IL-1 $\beta$ , LPS and TNF $\alpha$  stimulation in EMSA experiments.** (A) Cytotoxicity tests of C27 in HepG2 and MEF cells. C27 is well tolerated by HepG2 and MEF cells. Means and standard deviation are depicted. (B) Time-dependent NF- $\kappa$ B EMSA and Western Blot data of MEF cells treated with 5 $\mu$ M C27 and stimulation with IL-1 $\beta$ , LPS or TNF $\alpha$ . C27 impairs activation of NF- $\kappa$ B in all three signaling pathways.

As expected, 5 $\mu$ M of compound 27 inhibited LPS induced NF- $\kappa$ B activation resulting from diminished phosphorylation of I $\kappa$ B $\alpha$  as well. It appears that C27 influenced LPS signaling stronger than IL-1 $\beta$  signaling in EMSA experiments but this might result from a weaker induction of NF- $\kappa$ B activation upon LPS stimulation that is also visible in the degradation of I $\kappa$ B $\alpha$ . Upon TNF $\alpha$  stimulation, phosphorylation and degradation of I $\kappa$ B $\alpha$  as well as activation of NF- $\kappa$ B were reduced similar to IL-1 $\beta$  (Figure 4.9B).

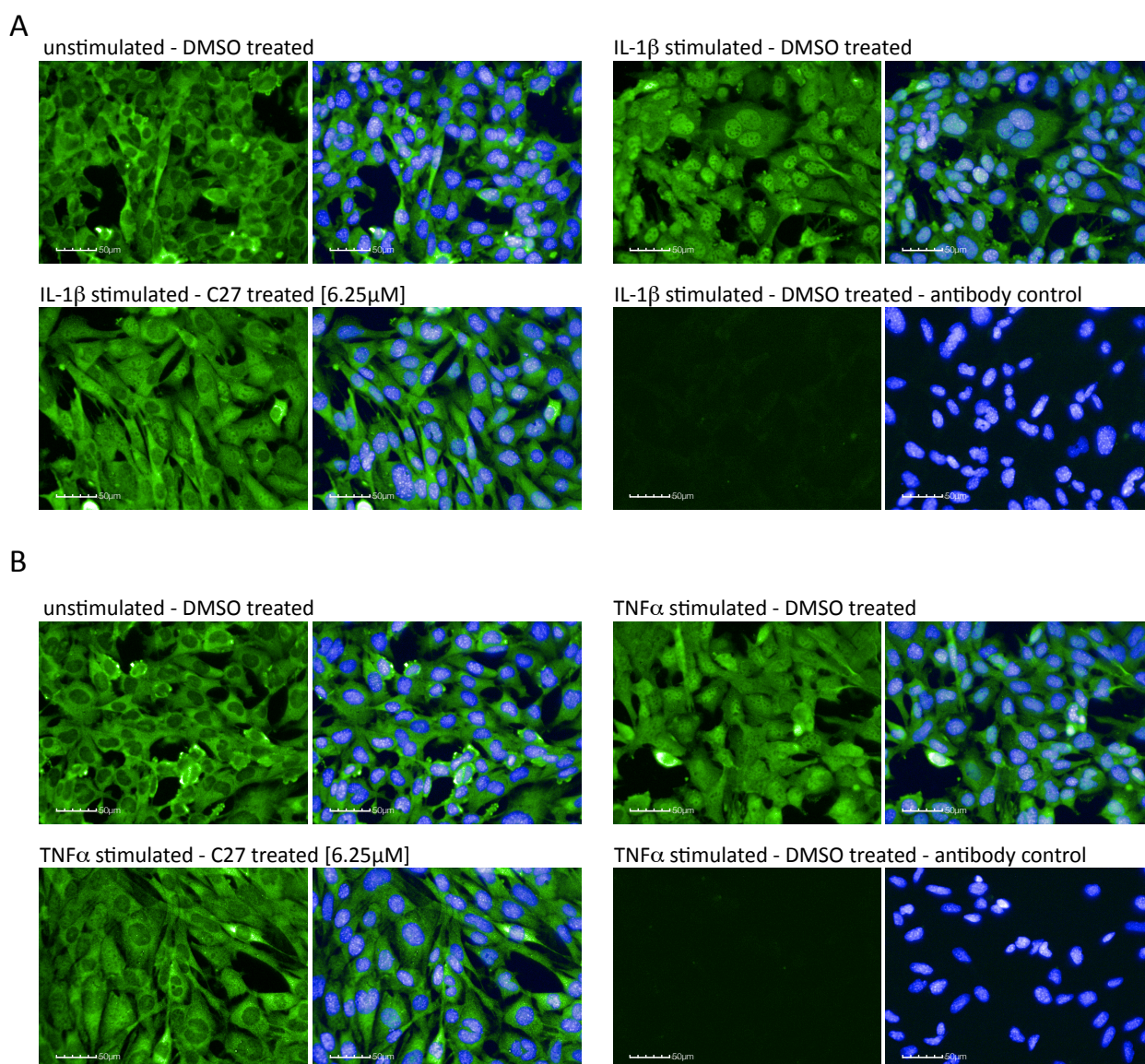


**Figure 4.10: Cell-based verification of C27 after IL-1 $\beta$  and TNF $\alpha$  stimulation in MEF cells in p65 translocation experiments.** Upon IL-1 $\beta$  or TNF $\alpha$  stimulation (20min), p65 translocates into the nucleus. At a concentration of 6.25 $\mu$ M, C27 impairs nuclear translocation of p65 after IL-1 $\beta$  (A) and TNF $\alpha$  (B) stimulation.

To further analyze the inhibitory potential of C27 in a second assay, nuclear translocation of the p65 subunit of NF- $\kappa$ B upon IL-1 $\beta$  and TNF $\alpha$  stimulation was analyzed in MEF cells. After treatment of the cells with 6.25 $\mu$ M C27, cells were stimulated with the respective cytokine, fixed and stained for p65 immunofluorescence experiments. Representative images are depicted in 4.10. Upon stimulation with either IL-1 $\beta$  or TNF $\alpha$ , p65 translocated from the cytoplasm into the nucleus. However, IL-1 $\beta$  stimulation led to a stronger accumulation of p65 in the nucleus compared to TNF $\alpha$ . C27 treatment reduced p65 nuclear translocation after IL-1 $\beta$  and TNF $\alpha$  stimulation.



In a third assay, expression of NF- $\kappa$ B dependent target genes was analyzed by quantitative realtime polymerase chain reaction (qPCR) after IL-1 $\beta$ , LPS and TNF $\alpha$  stimulation. Similar to the EMSA experiments, MEF cells were compound treated and stimulated. After extraction of RNA from the cell lysates and reverse transcription into complementary DNA (cDNA), the cDNA was used as the template for qPCR to analyze the expression of selected NF- $\kappa$ B dependent target genes. mRNA levels of A20 were found to be upregulated by IL-1 $\beta$ , TNF $\alpha$  and LPS (Figure 4.11). The expression of mRNA coding for ICAM-1 was only induced after IL-1 $\beta$  and TNF $\alpha$  stimulation (Figures 4.11A and B). Treatment of MEF cells with C27 caused a significant reduction in mRNA expression for ICAM-1 and A20 in a dose-dependent manner in all three tested stimulation experiments whereas an overall higher influence on ICAM-1 levels was observed (Figure 4.11). Taken together, the results of the EMSA, p65 translocation and qPCR studies imply that C27 indeed causes a significant reduction of NF- $\kappa$ B signaling, but does not differentially affect IL-1 $\beta$ /LPS and TNF $\alpha$  induced NF- $\kappa$ B activation.

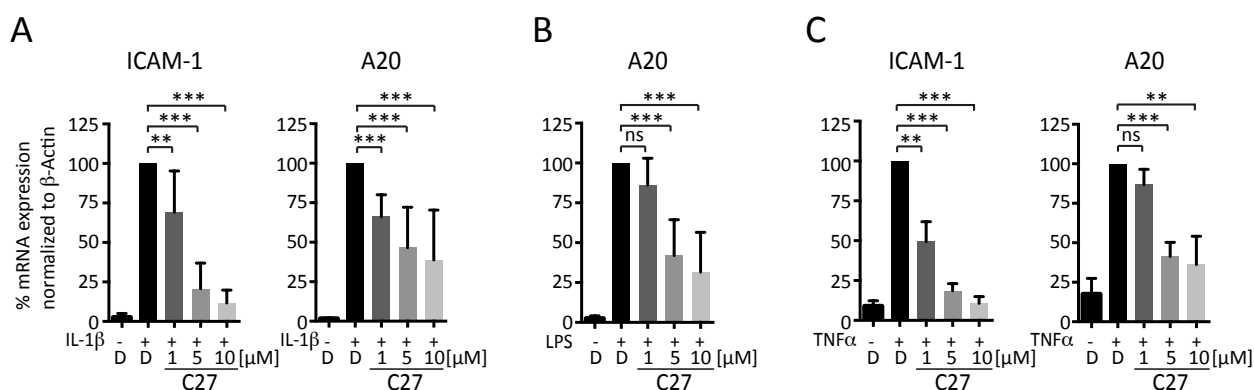


**Figure 4.11: Cell-based verification of C27 after IL-1 $\beta$ , LPS and TNF $\alpha$  stimulation in MEF cells in qPCR experiments.** Quantitative realtime PCR studies after IL-1 $\beta$  (60min) (A), LPS (75min) (B) or TNF $\alpha$  (60min) (C) stimulation reveal dose-dependent effects of C27 in NF- $\kappa$ B target gene expression. Specificity for IL-1 $\beta$  and LPS over TNF $\alpha$  signaling was not obtained. Means and standard deviation are shown. Significances are calculated using Student's t-test (p-value < 0.01).

Since C27 displayed such a strong biochemical and cellular effect, further research was done analyzing the mode of action of this compound. The influence of the compound on NF- $\kappa$ B signaling after IL-1 $\beta$  stimulus was investigated in more detail. First, the endogenous auto-ubiquitination of TRAF6 that is a prerequisite for NF- $\kappa$ B activation after IL-1 $\beta$  stimulation was examined (Lamothe et al., 2007). For that, MEF cells were treated with increasing amounts of C27. Upon stimulation, TRAF6 was immunoprecipitated from the cell lysates and analyzed for ubiquitination (Figure 4.12A). Applying 10 $\mu$ M and 15 $\mu$ M C27 to MEF cells led to mild reduction

of TRAF6 auto-ubiquitination (Figure 4.12A). Surprisingly, 5 $\mu$ M of C27 did not affect TRAF6 auto-ubiquitination. It appears that the amount of compound to interfere with NF- $\kappa$ B signaling was assay-type-dependent. Due to the need of different well formats, the ratio of cells to compound varied among the assays.

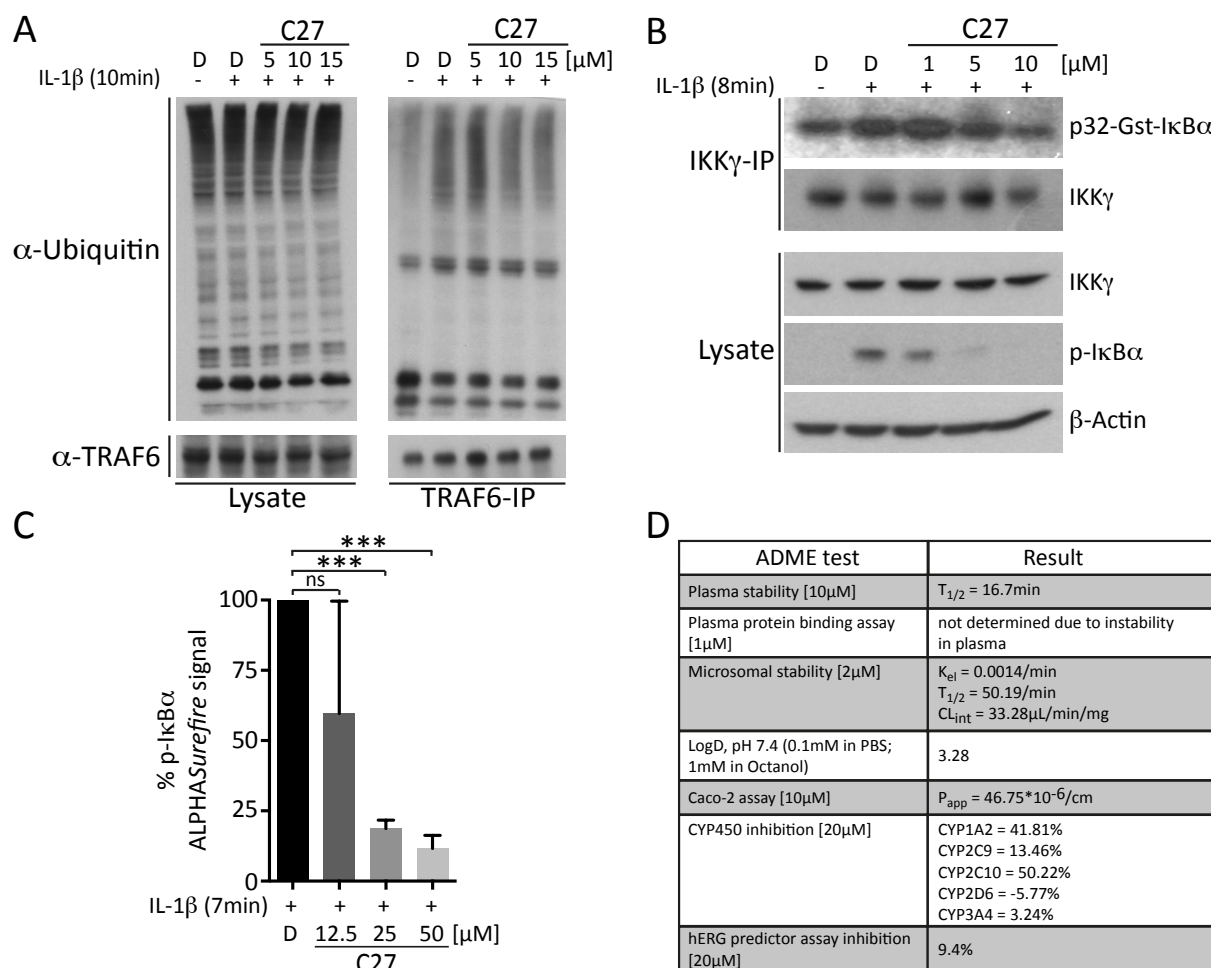


**Figure 4.12: Determining the mode of action of C27 in IL-1 $\beta$  signaling in MEF cells.** (A) IL-1 $\beta$  induced TRAF6 auto-ubiquitination is reduced by pre-treatment of cells with various concentrations of C27. (B) The activity of the IKK complex after IL-1 $\beta$  stimulation is dose dependently decreased by C27. (C) p-I $\kappa$ B $\alpha$  ALPHASurefire experiments reveal an inhibitory effect by increasing amounts of C27. Mean and standard deviations are depicted. Statistical significance is verified using Student's t-test (p-value < 0.01). (D) ADME studies were performed by Bienta, ENAMINE Ltd. and determine instability of C27 in plasma.

Next, the activity of the IKK complex was analyzed to determine the mechanism of action of C27 in cells. Again, MEF cells were pre-treated with C27, stimulated and lysed. Immunoprecipitated NEMO was incubated with recombinantly purified GST-I $\kappa$ B $\alpha$  and <sup>32</sup>Phosphorus (<sup>32</sup>P). The kinase activity was analyzed by SDS-PAGE followed by autoradiography and Western Blot. While 1 $\mu$ M C27 did not show any effect on phosphorylation of GST-I $\kappa$ B $\alpha$ ,



5 $\mu$ M and 10 $\mu$ M reduced the kinase activity dose-dependently (Figure 4.12B). An inhibitory effect was also observed in the phosphorylation levels of I $\kappa$ B $\alpha$  in the lysate fraction that was comparable for the phosphorylation status of I $\kappa$ B $\alpha$  in EMSA experiments (Figure 4.9B). To further confirm these results, p-I $\kappa$ B $\alpha$  ALPHASurefire experiments were performed. ALPHASurefire is an ALPHAScreen-based technology using Donor and Acceptor beads to detect protein phosphorylation from cell lysates. Dose-dependent reduction of the levels of phosphorylation of I $\kappa$ B $\alpha$  after compound treatment and IL-1 $\beta$  stimulation again proved the inhibitory effect of C27 (Figure 4.12C). Taking these results together, C27 shows a strong effect on IKK complex activity, phosphorylation of I $\kappa$ B $\alpha$  and NF- $\kappa$ B activation. Contrary, TRAF6 auto-ubiquitination is very mildly affected and is unlikely to cause such a strong impact on downstream signaling events. Data obtained so far indicate that C27 interferes with NF- $\kappa$ B signaling upstream of the IKK complex or targets the components of the IKK complex to diminish its activity.

To further characterize the behavior of C27, absorption-distribution-metabolism-excretion (ADME) studies were performed to define pharmacokinetics and pharmacodynamics of C27. Results are depicted in Figure 4.12D. Plasma stability assays revealed C27 as an instable compound with a half-life of 16.7 min. Whether C27 is degraded or structurally modified by plasma enzymes remains unclear up to this point. Due to the instability of C27 in plasma, plasma protein binding tests could not be performed successfully. The metabolic stability of C27 was assessed in mouse hepatic microsomes revealing a elimination constant  $k_{el}$ = 0.0014/min, a half-life of  $T_{1/2}$ = 50.19 min and an intrinsic clearance of  $Cl_{int}$ = 33.28  $\mu$ L/min/mg. Additionally, the distribution coefficient (LogD) is determined to measure the balance of lipophilicity and hydrophilicity. The LogD of C27 was calculated to 3.28 and is considered to be in the optimal range (for LogP, see 4.8B). The Caco-2 (human colon adenocarcinoma cell) assay was used to evaluate the permeability of C27 that was assessed to 46.75 \* 10<sup>-6</sup>cm/s providing a good oral absorption (Lau et al., 2004). In Cytochrom (CYP) P450 inhibition assays, C27 inhibited only two out of five tested CYP enzymes. No significant binding of C25 to hERG was observed in the hERG (human Ether-a-go-go related gene) predictor assay.

Taking all results together, C27 is a very active compound inhibiting NF- $\kappa$ B signaling. However, no pathway selectivity is observed as IL-1 $\beta$ , LPS and TNF $\alpha$  induced NF- $\kappa$ B activation was impaired to the same extent. Furthermore, plasma stability assays revealed that C27 is highly instable in plasma environment and therefore would not be available for its activity in the plasma.

## 4.5 Validation of C25 in biochemical and cell-based experiments

In the cellular verification of the 27 hit compounds, C25 demonstrated very strong and specific effects not only *in vitro* (Figure 4.4A) but also in first cell-based assays (Figure 4.7A). The chemical structure of C25 is presented in Figure 4.13A. It fulfills all four criteria of the Lipinski's rule of five and therefore is referred to be a drug-like small molecule (Figure 4.13B).

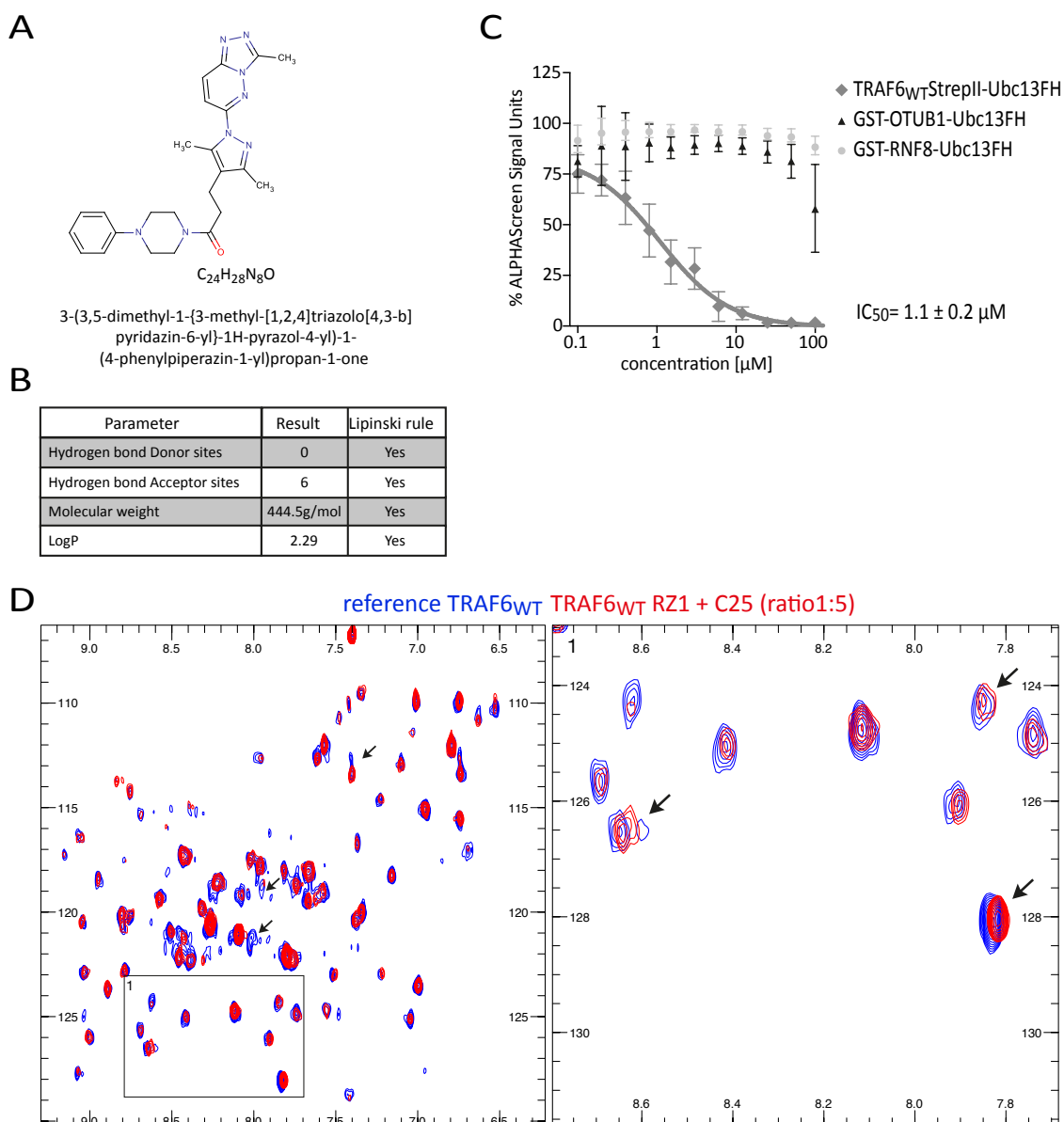


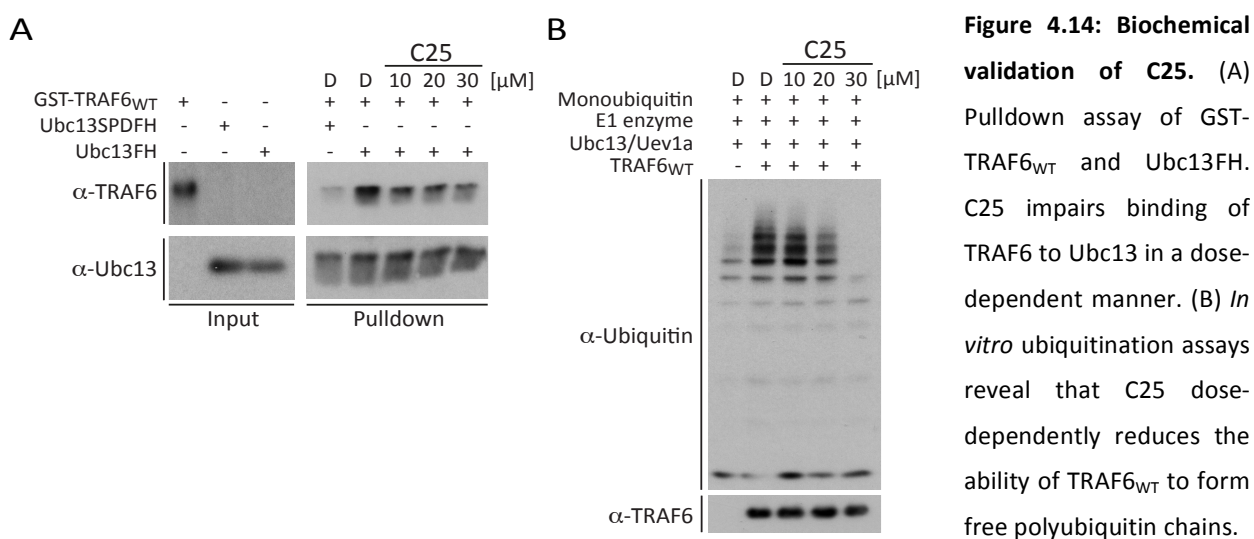
**Figure 4.13: Biochemical validation of C25.** (A) Compound structure, chemical formula and name of C25. (B) Parameters of the Lipinski's rule of five for C25 revealed a drug-like small molecule. (C) ALPHA Screen assays analyzing increasing concentrations of C25. C25 impairs TRAF6<sub>WT</sub>StrepII-Ubc13FH interaction dose-dependently while binding of GST-OTUB1 and GST-RNF8 to Ubc13FH remain unaffected. Mean and standard deviation are depicted. (D) NMR studies of TRAF6<sub>WT</sub> and C25. C25 directly binds TRAF6<sub>WT</sub> (NMR experiments were performed by Dr. Grzegorz Popowicz from the Institute of Structural Biology at the Helmholtz Zentrum München).

#### 4.5.1 Biochemical analysis of C25

In the initial ALPHA Screen testing of reordered C25, a specific inhibition of TRAF6<sub>WT</sub>StreptII binding to Ubc13FH in a dose-dependent manner (Figure 4.13C) was observed. IC<sub>50</sub> calculations revealed a value in the very low micro molar range ( $1.1 \pm 0.2 \mu\text{M}$ ). Besides, the interactions of GST-OTUB1-Ubc13FH and GST-RNF8-Ubc13FH remained mainly unaffected, but a slight reduction of the GST-OTUB1-Ubc13FH binding at 100  $\mu\text{M}$  C25 was observed (Figure 4.13C). These data imply that C25 is a specifically acting compound up to 100  $\mu\text{M}$  *in vitro* and targets TRAF6<sub>WT</sub>StreptII rather than Ubc13FH. To further confirm this assumption, untagged TRAF6<sub>WT</sub> was analyzed in NMR after C25 treatment in a 1:5 ratio. Indeed, C25 directly targets TRAF6<sub>WT</sub> as several peaks are shifting and disappearing as marked with arrows in Figure 4.13D. This indicates a direct binding of the compound to TRAF6<sub>WT</sub>. Compared to the NMR spectra of C27 (Fig. 4.8D) treated TRAF6<sub>WT</sub>, the same residues are targeted suggesting that both compounds despite their structural heterogeneity bind similar amino acids within TRAF6.

To verify whether targeting TRAF6 by C25 indeed influences the binding of TRAF6 to Ubc13 and subsequently its E3 ligase activity, additional *in vitro* experiments were performed. First, the interaction of recombinant purified GST-TRAF6<sub>WT</sub> and Ubc13FH was analyzed in pulldown assays. The usage of GST-TRAF6<sub>WT</sub> was chosen to further ensure that C25 does not affect the StreptII-tag of TRAF6<sub>WT</sub> in the initial ALPHA Screen experiments. GST-TRAF6<sub>WT</sub> was pre-incubated with DMSO or compound followed by adding Ubc13FH. After immunoprecipitation of Ubc13FH, binding of GST-TRAF6<sub>WT</sub> to Ubc13FH was analyzed via Western Blot. As a control, the Ubc13-SPD mutant, a triplemutant that is not able to bind TRAF6, was included and revealed the specificity of this pulldown assay. Increasing amounts of C25 (10, 20 and 30  $\mu\text{M}$ ) led to a dose-dependent reduction in binding of GST-TRAF6<sub>WT</sub> to Ubc13FH (Figure 4.14A). Compared to the ALPHA Screen, higher concentrations of C25 were required in this assay due to a more than five fold higher input of proteins. Second, the impact of an impaired TRAF6-Ubc13 binding on E3 ligase activity was analyzed in a functional *in vitro* ubiquitination assay. This method is based on the ability of the TRAF6-Ubc13 complex to assemble free polyubiquitin chains. Untagged TRAF6<sub>WT</sub> was pre-incubated with DMSO or compound and applied to the reaction mix including E1 enzyme, the Ubc13/Uev1a complex, monoubiquitin and ATP for the assembly of free ubiquitin chains. The formation of polyubiquitin chains were subsequently analyzed in Western Blot experiments. Adding TRAF6<sub>WT</sub> led to the formation of free polyubiquitin chains under DMSO conditions meaning that the purified protein is active in this experimental setup. Pre-incubation of TRAF6 protein with increasing concentrations of C25 (10, 20 and 30  $\mu\text{M}$ ) led to a

dose-dependent loss of polyubiquitin assembly indicating that targeting the RZ1 domain of TRAF6 indeed leads to a reduction of E3 ubiquitin ligase activity (Fig. 4.14B).



Taken together, the completed *in vitro* assays gave rising evidence that C25 specifically targets the RZ1 domain of TRAF6 and that this binding negatively affects both the interaction to Ubc13 and the E3 ligase activity of TRAF6. Next, the verification of this effectiveness needed to be confirmed in cell-based assays.

#### 4.5.2 Verification of C25 in cell-based assays

Initial EMSA experiments revealed a moderate inhibition of IL-1 $\beta$  induced NF- $\kappa$ B activation by C25 while TNF $\alpha$  mediated NF- $\kappa$ B activation remained unaffected (Figures 4.7C and 4.7D). First, cytotoxicity studies were carried out in more detail. CellTiter-Blue as well as Hoechst3342 and Mitotracker stainings were performed in both HepG2 and MEF cells. CellTiter-Blue stainings demonstrated no substantial decrease in cell viability up to 50 $\mu$ M C25 in HepG2 and MEF cells (Fig. 4.15A). Mitochondrial mass as well as nuclear area experiments did not exhibit any effects in both cell lines up to 100 $\mu$ M C25 implying that C25 is non toxic to cells (Fig. 4.15A).

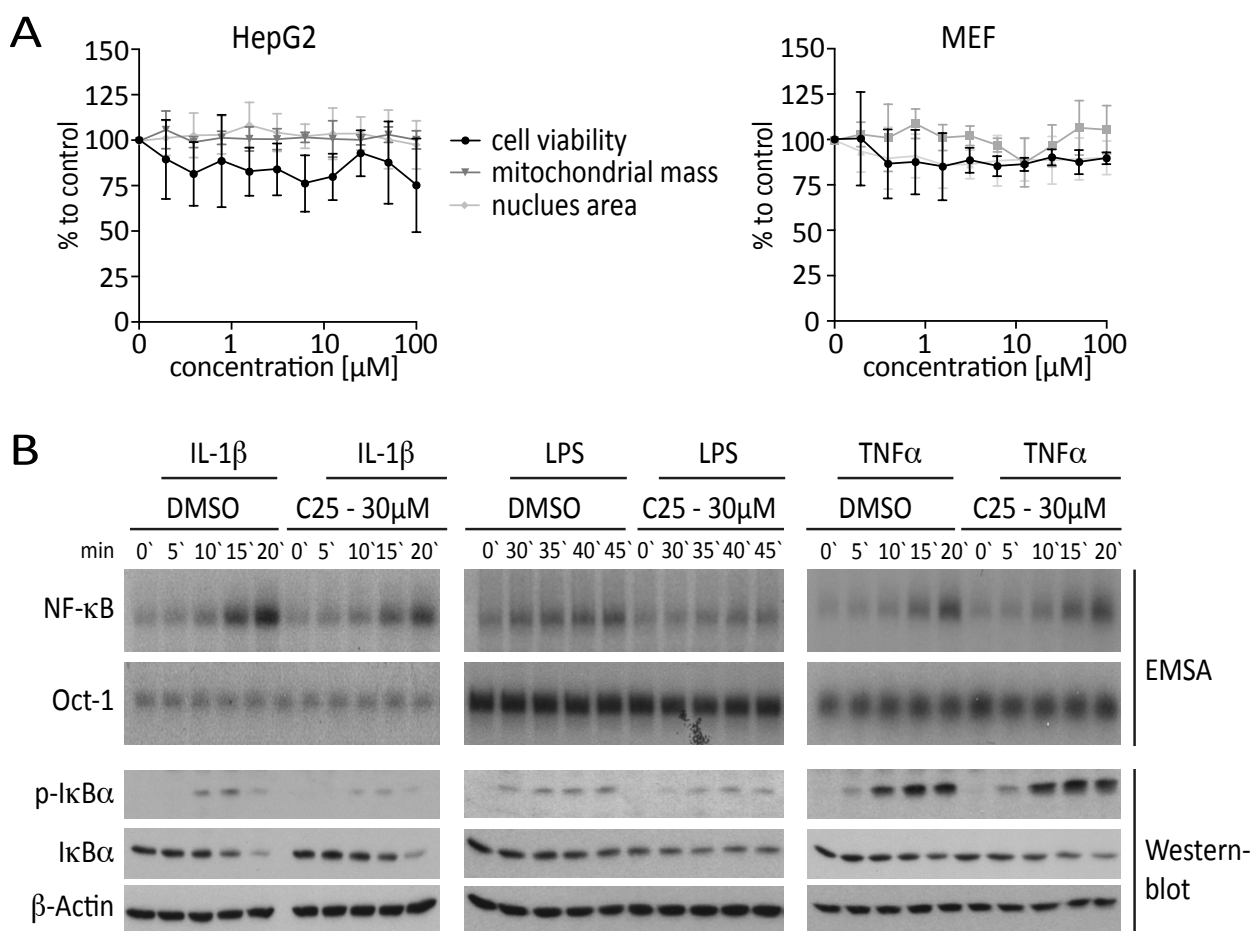


**Figure 4.15: Cytotoxicity assays and cell-based verification of C25 after IL-1 $\beta$ , LPS and TNF $\alpha$  stimulation in EMSA experiments.** (A) Cytotoxicity tests of C25 in HepG2 and MEF cells. C25 is well tolerated by HepG2 cells up to 50 $\mu$ M compound. MEF cells remain viable up to 100 $\mu$ M compound. Means and standard deviations are shown. (B) Time-dependent experiments of MEF cells treated with 30 $\mu$ M C25 and stimulation with IL-1 $\beta$ , LPS or TNF $\alpha$  analyzed in EMSA and Western Blot experiments. While C25 treatment does impair phosphorylation and degradation of I $\kappa$ B $\alpha$  as well as NF- $\kappa$ B activation after IL-1 $\beta$  and LPS stimulation, TNF $\alpha$  signaling remains unaffected.

Next, C25 treated MEF cells were analyzed in EMSA after IL-1 $\beta$ , LPS and TNF $\alpha$  stimulation for the indicated time points (Fig. 4.15B). Since IL-1 $\beta$  and LPS use similar adaptor proteins, kinases and ligases including TRAF6 after receptor stimulation, C25 is expected to reduce NF- $\kappa$ B activation in both pathways (Wertz and Dixit, 2010). Due to the fact, that TNF $\alpha$  signaling is independent of TRAF6, this pathway should not be affected by C25 (Figure 4.7B). Treatment of MEF cells with 30 $\mu$ M C25 led to a moderate reduction of NF- $\kappa$ B activation, as well as phosphorylation and subsequent degradation of I $\kappa$ B $\alpha$  after IL-1 $\beta$  stimulation (Fig. 4.15B) proving previous findings out of the initial EMSA experiments (Fig. 4.7D and supplement 10.5). LPS mediated NF- $\kappa$ B activation and phosphorylation of I $\kappa$ B $\alpha$  was decreased in a similar manner

(Fig. 4.15B). In contrast, C25 treatment did not affect TNF $\alpha$  induced activation of NF- $\kappa$ B nor phosphorylation and degradation of I $\kappa$ B $\alpha$  (Fig. 4.15B). To further define the influence of C25 on NF- $\kappa$ B signaling, MEF cells were treated with 25 $\mu$ M C25 and analyzed in p65 translocation experiments. Upon IL-1 $\beta$  stimulation, C25 led to a mild effect in retaining p65 in the cytoplasm (Figure 4.16A). After TNF $\alpha$  stimulation nuclear translocation of p65 was not as strong as IL-1 $\beta$  induced translocation of p65. However, C25 treatment did not impair p65 translocation (Figure 4.16B)

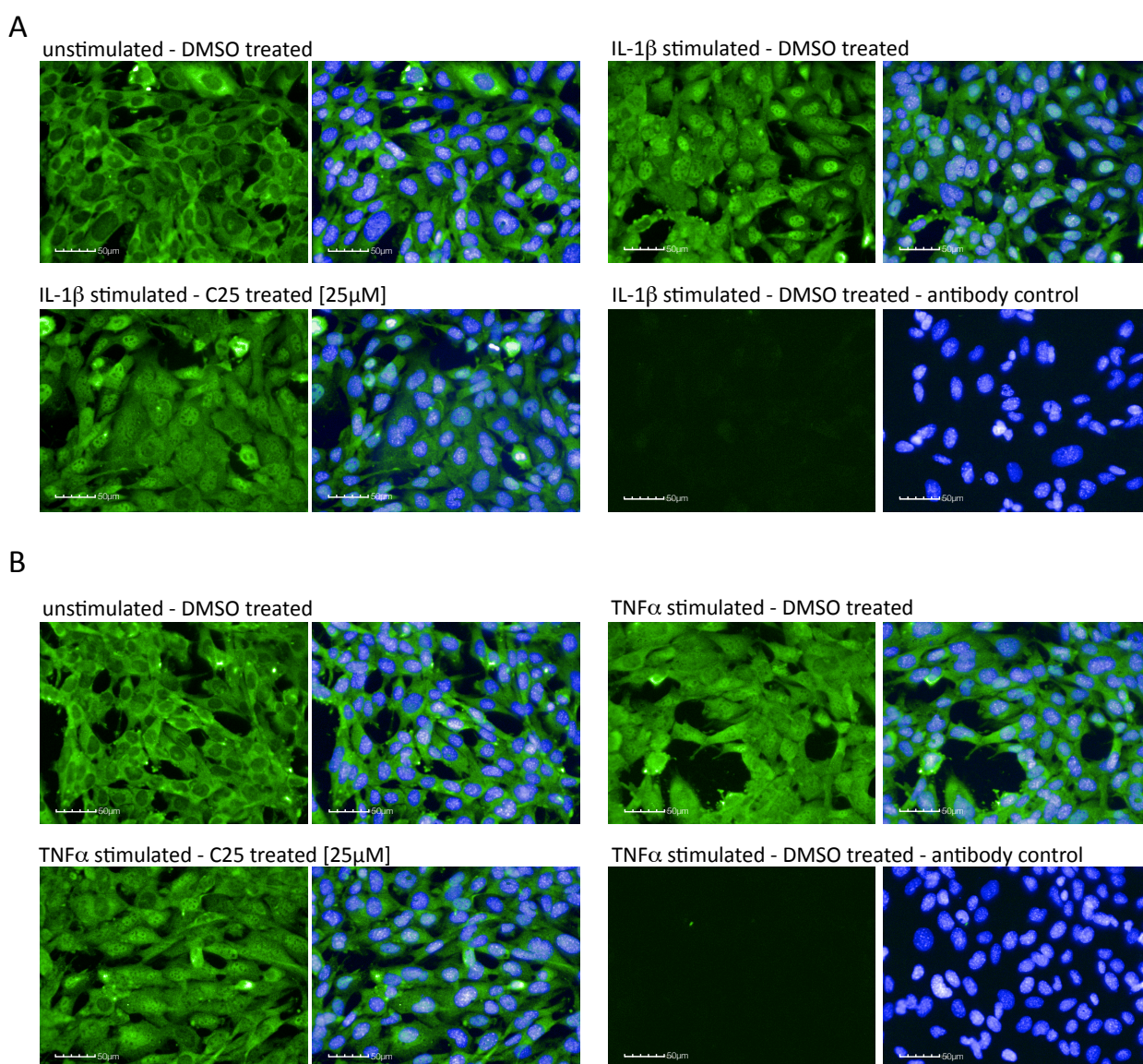


**Figure 4.16: Cell-based verification of C25 after IL-1 $\beta$  and TNF $\alpha$  stimulation in p65 translocation assays in MEF cells.** Upon C25 treatment, p65 translocation induced by IL-1 $\beta$  stimulation is mildly affected (A), whereas TNF $\alpha$ -induced p65 translocation is not altered (B).



To further specify the mechanism of action of C25 a more detailed investigation of NF- $\kappa$ B signaling after IL-1 $\beta$  stimulation was carried out. First, the observed decrease in phosphorylation levels of I $\kappa$ B $\alpha$  in the time-dependent experiments after IL-1 $\beta$  stimulation was confirmed in p-I $\kappa$ B $\alpha$  ALPHASurefire experiments (Fig. 4.17A). Although treatment with C25 led to a significantly dose-dependent decline of p-I $\kappa$ B $\alpha$  after IL-1 $\beta$  stimulation (Fig. 4.17A), the influence of C25 was weaker compared to the time-dependent data in Figure 4.15B due to an altered ratio of cells to compounds in different well formats. Furthermore, the levels of TNF $\alpha$  induced p-I $\kappa$ B $\alpha$  were determined using the ALPHASurefire method. These experiments showed almost no impact of C25 in TNF $\alpha$  signaling towards activation of NF- $\kappa$ B (Fig. 4.17A). Second, mRNA levels of selected IL-1 $\beta$  induced target genes (ICAM-1 and A20) were determined by qPCR and are presented in Figure 4.17B. Here, pre-treatment of cells with C25 led to a very mild, but not significant effect on target gene expression.

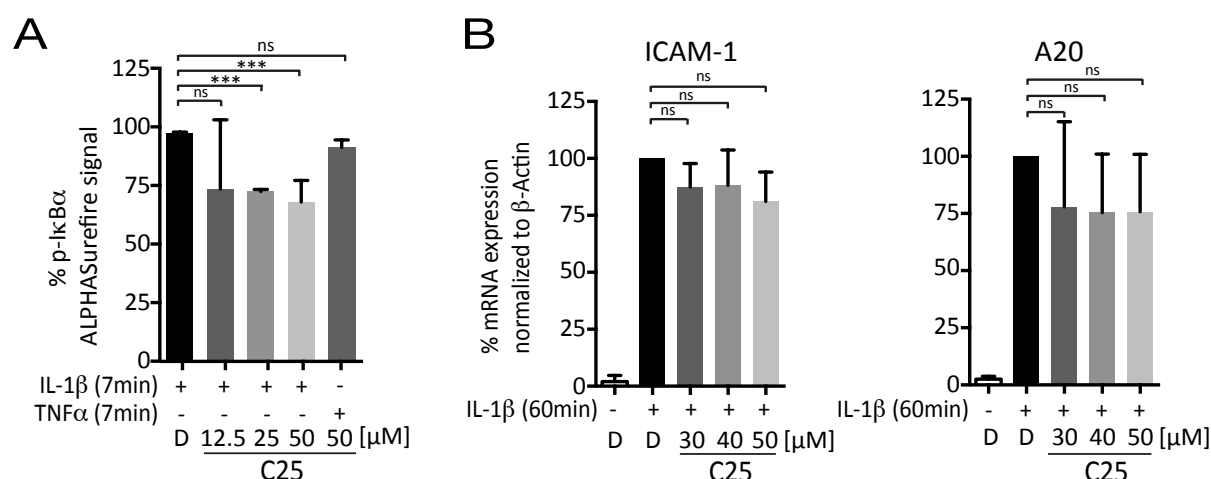


**Figure 4.17: Verification of C25 in ALPHASurefire and qPCR experiments in MEF cells in IL-1 $\beta$  induced NF- $\kappa$ B activation.** (A) p-I $\kappa$ B $\alpha$  ALPHASurefire experiments reveal a mild significant inhibitory effect by increasing amounts of C25 after IL-1 $\beta$  stimulation. Phosphorylation levels of I $\kappa$ B $\alpha$  in TNF $\alpha$  signaling are not significantly affected. (B) qPCR studies show very mild effects of C25 in IL-1 $\beta$  induced NF- $\kappa$ B signaling. Means and standard deviations are depicted. Statistical analyses are performed using Student's T-test (p-value < 0.01).

Summarizing the biochemical data, *in vitro* C25 is a highly active and specifically acting compound that directly targets TRAF6 causing impaired binding to Ubc13 as well as reducing E3 ligase activity. However, this strong efficacy could not be confirmed in cell-based assays. C25 only causes mild effects on phosphorylation and degradation of I $\kappa$ B $\alpha$ , NF- $\kappa$ B activation and target gene expression in IL-1 $\beta$  signaling. Nevertheless, C25 appears to act pathway specific as TNF $\alpha$  signaling is not influenced in all analyzed methods. Therefore, C25 can be considered to

be a promising small molecule for further improvement by performing structure activity relationship (SAR) screening.

## **4.6 Hit optimization**

The stage of hit optimization is characterized by chemical modification of the compound to obtain analogs with improved potency *in vitro* and in cells. With the medical advice of Dr. Manfred Rösner, 47 analogs of C25 were defined for testing. Three residues (R1, R2 and R3 in Figure 4.18A) of C25 were selected to be subjects of variation.

### **4.6.1 Biochemical Structural activity relationships of C25**

First, the 47 analogs were analyzed in triplicates for inhibitory function in all three available ALPHAScreen settings in a seven-point titration curve (0.07 - 50 $\mu$ M). Out of these 47 analogs, three compounds (C25-0167, C25-0189 and C25-0140) showed a slightly stronger or comparable effect to C25 while binding of GST-OTUB1 or GST-RNF8 to Ubc13FH was not affected (Figure 4.18B). Exact inhibition curve data and chemical structures of these compounds are illustrated in Figure 4.19. The IC<sub>50</sub> values were not significantly optimized and inhibition curves did rather overlay with C25 than improve. Furthermore, ten analogs revealed IC<sub>50</sub> values from 3 $\mu$ M to 10 $\mu$ M for TRAF6<sub>WT</sub>StreptII-Ubc13FH binding (Figure 4.18B and supplement 10.6-9). Only one of these, C25-212, had an impact on GST-RNF8 and GST-OTUB1 interaction to Ubc13FH as well, but to a lesser extent (Figure 4.18B and data not shown). 14 tested analogs did inhibit the TRAF6<sub>WT</sub>StreptII-Ubc13FH interaction in an IC<sub>50</sub> range from 10 $\mu$ M to 50 $\mu$ M while no influence on GST-OTUB1-Ubc13FH and GST-RNF8-Ubc13FH binding was observed. For 20 tested analogs no inhibitory potential could be detected (Figure 4.18B). It appears that at least one of the aromatic structures at either R1 or R2 is required to target TRAF6 preventing its binding to Ubc13. Removing the triazolring at R3 leads to a complete loss of the inhibitory potential implying that the compounds target TRAF6 with an aromatic residue at either R1 or R2 and a heterocyclic structure at R3. In addition, when deleting one of the two aromatic structures at R1 or R2 or overcoming the planarity of C25, a trend towards improved solubility was recognized. Concluding the analog screening, out of 47 tested compounds, three compounds showed a slightly enhancement in inhibiting TRAF6-Ubc13 *in vitro* but at the same time did not influence the binding of GST-OTUB to Ubc13FH. These compounds were subsequently verified in cell-based assays.



Chemical structure of a pyrazole-pyridine derivative. The structure shows a pyridine ring connected at its 2-position to the 1-position of a pyrazole ring. The pyrazole ring has methyl groups at the 3 and 5 positions and a side chain at the 4-position. The side chain consists of a methylene group, a carbonyl group, and a substituent R1-R2. A substituent R3 is attached to the 3-position of the pyridine ring.

	Solubility	R1	R2	R3	TRAF6-Ubc13 IC50 [μM]	OTUB1-Ubc13 IC50 [μM]	RNF8-Ubc13 IC50 [μM]
C25	-	Phenyl	Piperazin	CH3	2,8	> 50	> 50
C25-0167	+	3-MeO-phenyl	Piperazin	CH3	1,5	> 50	> 50
C25-0189	-	2-Pyridyl	Piperazin	CH3	2,6	> 50	> 50
C25-0140	+	Benzyl	Piperidin	CH3	2,6	> 50	> 50
C25-0196	-	4-F-phenyl	Piperazin	CH3	3,0	> 50	> 50
C25-0058	-	4-F-phenyl	Piperazin	H	3,3	> 50	> 50
C25-0174	-	--	Pyrrolidino	CH3	3,4	> 50	> 50
C25-0209	-	4-MeO-phenyl	Piperazin	CH3	4,5	> 50	> 50
C25-0029	-	3-MeO-phenyl	Piperazin	H	4,6	> 50	> 50
C25-0071	-	4-MeO-phenyl	Piperazin	H	5,4	> 50	> 50
C25-0033	+	Phenyl	Piperazin	H	6,0	> 50	> 50
C25-0266	+	3-Cl-benzyl	--	CH3	6,7	> 50	> 50
C25-0051	+	2-Pyridyl	Piperazin	H	9,5	> 50	> 50
C25-0212	+	5-Me-2-furylmethyl	--	CH3	9,5	~50	~50
C25-0211	-	2-F-phenyl	Piperazin	CH3	10,4	> 50	> 50
C25-0172	+	Phenyl-(CH2)3-	--	CH3	11,4	> 50	> 50
C25-0002	+	Benzyl	Piperidin	H	12,5	> 50	> 50
C25-0175	-	2,5-diMe-phenyl	Piperazin	CH3	20,5	> 50	> 50
C25-0253	+	4-Cl-benzyl	--	CH3	21,2	> 50	> 50
C25-0198	+	3-Indolylmethyl	--	CH3	23,7	> 50	> 50
C25-0269	+	2-Thienylmethyl	--	CH3	24,6	> 50	> 50
C25-0224	+	Benzyl	--	CH3	26,5	> 50	> 50
C25-0034	+	Phenyl-(CH2)3-	--	H	32,4	> 50	> 50
C25-0208	+	Ethyl	Piperazin	CH3	34,0	> 50	> 50
C25-0031	+	4-Me	Piperidino	H	39,4	> 50	> 50
C25-0036	+	--	Pyrrolidino	H	40,0	> 50	> 50
C25-0254	+	2-F-benzyl	--	CH3	40,4	> 50	> 50
C25-0265	+	2-Furylmethylthioethyl	--	CH3	42,7	> 50	> 50
C25-0095	+	2-Pyrimidinyl	Piperazin	H	> 50	> 50	> 50
C25-0142	+	3-Pyridyl	--	CH3	> 50	> 50	> 50
C25-0166	+	2-MeO-phenyl	Piperazin	CH3	> 50	> 50	> 50
C25-0218	+	Morpholinoethyl	--	CH3	> 50	> 50	> 50
C25-0227	+	4-Acetamidophenyl	--	CH3	> 50	> 50	> 50
C25-0149	+	2,4-DiF-phenyl	--	CH3	> 50	> 50	> 50
C25-0155	+	3-Ethoxycarbonyl-phenyl	--	CH3	> 50	> 50	> 50
C25-0159	+	3-F-phenyl	--	CH3	> 50	> 50	> 50
C25-0183	+	3-Methylbutyl	--	CH3	> 50	> 50	> 50
C25-0214	+	4-CF3O-phenyl	--	CH3	> 50	> 50	> 50
C25-0223	+	4-Acetyl-phenyl	--	CH3	> 50	> 50	> 50
C25-0144	+	3-MeO-phenyl	--	CH3	> 50	> 50	> 50
C25-0275	+	--	2-Furylethyl	CH3	> 50	> 50	> 50
C25-0028	+	2-MeO-phenyl	Piperazin	H	> 50	> 50	> 50
C25-0024	+	2-Furylmethyl	--	H	> 50	> 50	> 50
C25-0054	+	4-Fluorobenzyl	--	H	> 50	> 50	> 50
C25-0083	+	Benzyl	4-Piperidinyl	H	> 50	> 50	> 50
C25-0643	+	Phenyl	Piperazin	4-F-phenyl	> 50	> 50	> 50
C25-1379	+	4-F-phenyl	Piperazin	Phenyl	> 50	> 50	> 50
C25-0089	+	4-Acetamidophenyl	--	H	> 50	> 50	> 50

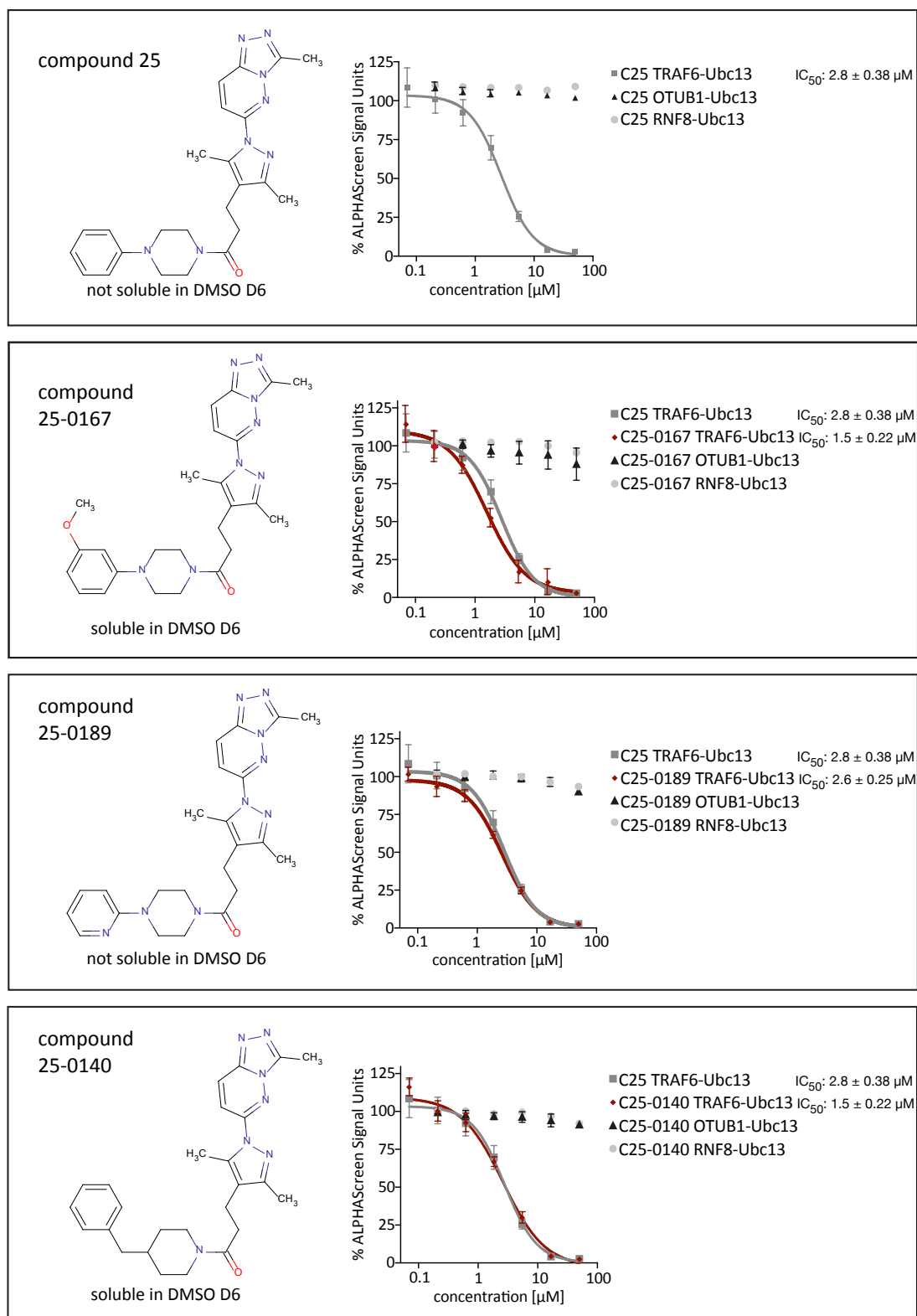


**Figure 4.19: Biochemical analog screening using the ALPHAScreen technology.** Chemical structures, solubility and titration curves in TRAF6<sub>WT</sub>StreptII-Ubc13FH ALPHAScreen experiments of the three best hits out of the analog screening: C25-0167, C25-0189 and C25-0140. Dose-dependent effects of all compounds on TRAF6<sub>WT</sub>StreptII-Ubc13FH interaction are observed. Importantly, the binding of GST-OTUB1 and GST-RNF8 to Ubc13FH remain unaffected. Mean and standard deviation are shown.

#### **4.6.2 Verification of the three best analogs of C25 in cell-based assays**

The three compounds C25-0167, C25-0189 and C25-0140 exhibiting comparable *in vitro* efficacies to C25 were tested in cell-based assays for their inhibitory potential on NF- $\kappa$ B activation. Initially, these compounds were examined for cytotoxicity in HepG2 and MEF cells using the CellTiter-Blue technology. Whereas HepG2 cells exhibited slight sensitivity to the compounds C25-0140 and C25-0167, all tested compounds were well tolerated by MEF cells (Figure 4.20A). Next, EMSA experiments with 20 $\mu$ M and 30 $\mu$ M compound and IL-1 $\beta$  stimulation were performed. Results are presented in Figure 4.20B and revealed C25-0140 as the compound with the strongest inhibitory effect. To further prove this observation, the levels of p-I $\kappa$ B $\alpha$  in ALPHASurefire experiments after IL-1 $\beta$  stimulation were analyzed. In this experiment, all three investigated compounds showed improved efficacy compared to C25. Again, C25-0140 demonstrated the best inhibitory potential with dose-dependent inhibition using 25 $\mu$ M and 50 $\mu$ M compound concentration whereas C25-0167 and C25-0189 did not (Figure 4.20C). As depicted in Figure 4.18B, C25 and C25-0189 were not well dissolved in DMSO while C25-0140 and C25-0167 were completely soluble in DMSO. The improved potency of C25-0140 in MEF cells might arise from the better solubility in contrast to C25. For pathway specificity tests, p-I $\kappa$ B $\alpha$  ALPHASurefire experiments were accomplished after treatment of MEF cells with 50 $\mu$ M of each compound and subsequent TNF $\alpha$  stimulation. Data in Figure 4.20D show that compounds that are less effective in IL-1 $\beta$  signaling (C25, C25-0167 and C25-0189) did almost not influence TNF $\alpha$  stimulated phosphorylation of I $\kappa$ B $\alpha$ . However, C25-0140 did impact p-I $\kappa$ B $\alpha$  after TNF $\alpha$  stimulation to the same extent as in IL-1 $\beta$  signaling (Fig. 4.20C and D).

To summarize the analog screening, three out of 47 tested compounds showed comparable *in vitro* activity to the hit compound C25: C25-0140, C25-0167 and C25-0189. Out of these three compounds C25-0140 demonstrated the strongest inhibitory potential in IL-1 $\beta$  signaling. However, this effect is also given after TNF $\alpha$  stimulation suggesting no pathway specificity. Nevertheless, due to the improved potency of C25-0140, this compound was subject for further investigation due to the involvement of both IL-1 $\beta$  and TNF $\alpha$  signaling in most chronic inflammatory diseases.

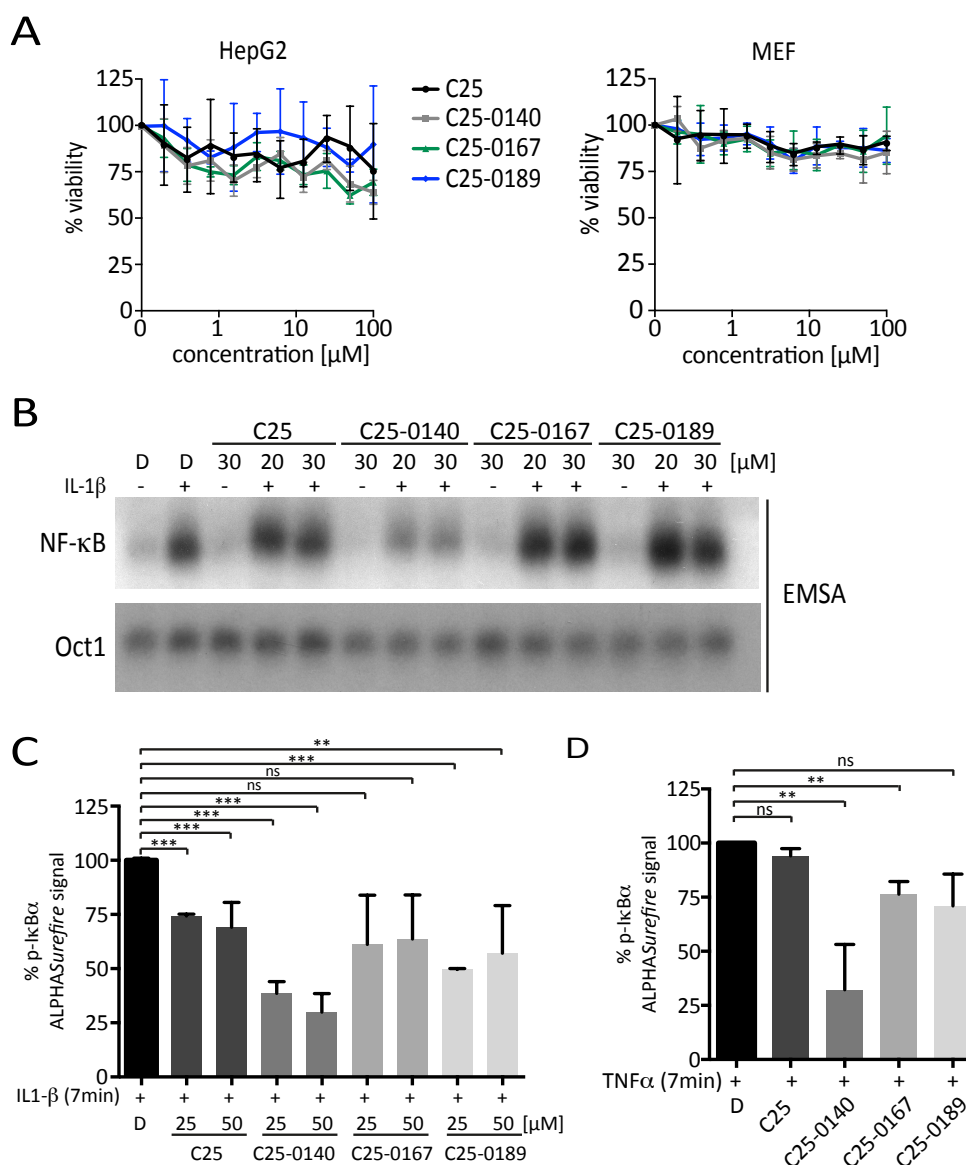


**Figure 4.20: Verification of the best three analogs of C25 in cell-based assays in MEF cells.** (A) Cytotoxicity studies of C25, C25-0140, C25-0167 and C25-0189 in CellTiter-Blue experiments. (B) EMSA studies of C25, C25-0140, C25-0167 and C25-0189 after IL-1 $\beta$  stimulation. C25-0140 shows the strongest inhibitory potential. (C) p-I $\kappa$ B $\alpha$  ALPHASurefire experiments confirm C25-0140 as the most inhibitory compound after IL-1 $\beta$  stimulation. (D) p-I $\kappa$ B $\alpha$  ALPHASurefire experiments after TNF $\alpha$  stimulation of compound-treated MEF cells [50 $\mu$ M] show no pathway specificity of C25-0140. Means and standard deviations are shown. Statistical significances are determined using Student's t-test ( $p$ -value < 0.01).

#### 4.7 In-depth analysis of C25-0140

Out of the analog screening, C25-0140 appeared to be the strongest inhibitory compound in cells. To verify these data, *in vitro* as well as cell-based assays were carried out. Compared to C25, the Phenyl-residue at R1 is replaced by a Benzyl-group in C25-0140 and R2 is changed to a Piperidin. With modifying these two groups the planar structure of C25 is overcome and the solubility of this compound in DMSO was remarkably improved. The chemical structure,

formula and name of C25-0140 are depicted in Figure 4.21A. The parameters for analyzing the criteria of the Lipinski's rule are depicted in Figure 4.21B and describe C25-0140 as a drug-like and potential orally available compound.

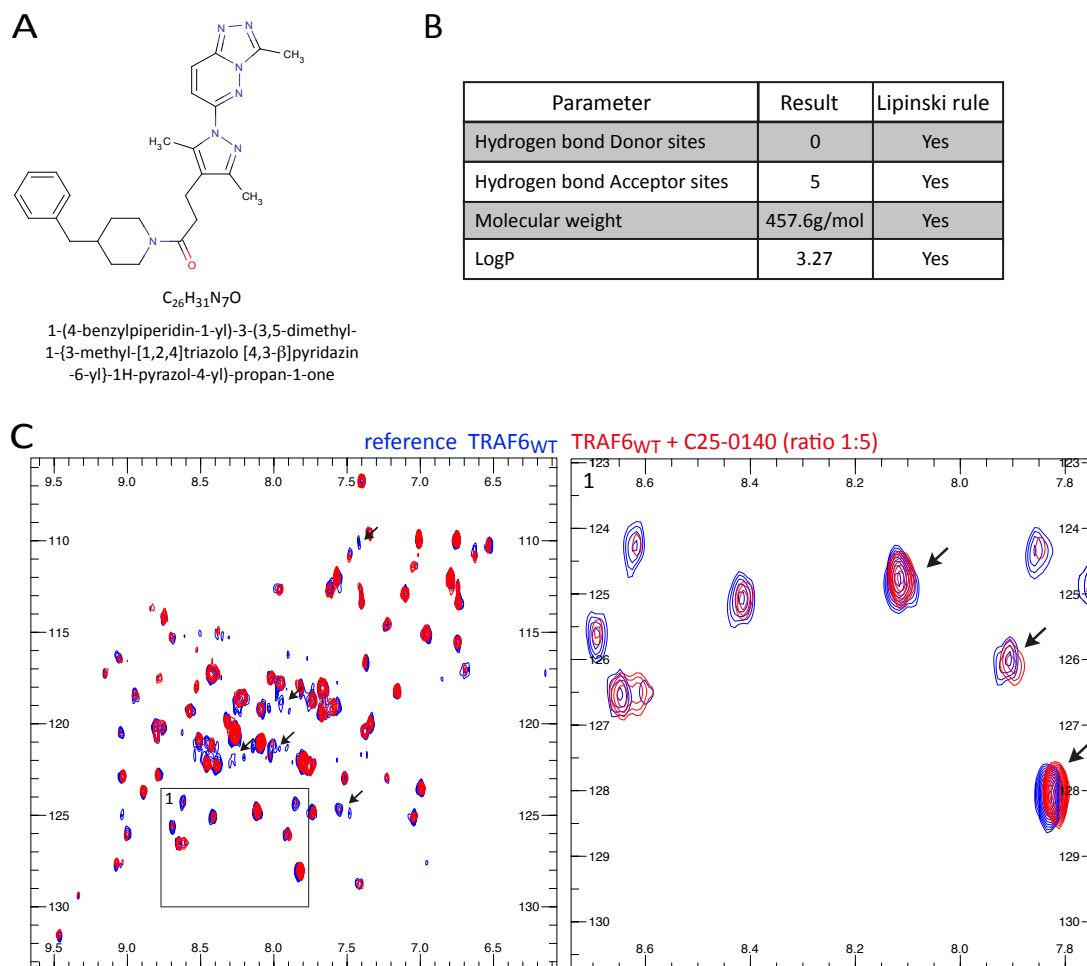


**Figure 4.21: Biochemical validation of C25-0140.** (A) Compound structure, chemical formula and name of C25-0140. (B) Chemical parameters of C25-0140 meet the Lipinski's rule of five and determine C25-0140 as a drugable compound. (D) NMR studies of TRAF6<sub>WT</sub> and C25-0140 reveal a direct binding of the compound to TRAF6 (NMR experiments were performed by Dr. Grzegorz Popowicz from the Institute of Structural Biology at the Helmholtz Zentrum München).

#### 4.7.1 Biochemical studies of C25-0140

In the analog screening described in section 4.6, C25-0140 was analyzed for affecting TRAF6<sub>WT</sub>StreptII-Ubc13FH binding as well as the interactions of GST-OTUB1-Ubc13FH and GST-RNF8-Ubc13FH. Dose-response curves are presented in Figure 4.19. The binding of TRAF6 to Ubc13 was impaired in a similar manner as C25. Still, the interaction of Ubc13 to OTUB1 and RNF8 was not altered at all under these conditions. To verify a direct binding of C25-0140 to TRAF6 RZ1 NMR studies were carried out as already described in section 4.4.1. The results are

displayed in Figure 4.21C. Similar to C25, multiple peaks did shift or disappear after adding compound C25-0140. Thereby, C25-0140 shows a similar pattern of peaks changing compared to C25 (Figure 4.13C).

The direct binding of C25-0140 to TRAF6 RZ1 was further analyzed by pulldown assays. Pre-incubation of GST-TRAF6<sub>WT</sub> with increasing amounts of C25-0140 (10, 20 and 30  $\mu$ M) led to a slight reduction in binding to Ubc13FH (Figure 4.22A). Next, the effect of an impaired TRAF6-Ubc13 binding was determined in a functional *in vitro* ubiquitination assay. Targeting untagged TRAF6<sub>WT</sub> with increasing compound concentrations of C25-0140 led to a decreased formation of polyubiquitin chains to the levels of the Ubc13 binding deficient mutant TRAF6<sub>D57K</sub> (Fig. 4.22B). In comparison to C25 (Fig. 4.14B), C25-0140 is slightly more active at a concentration of 20  $\mu$ M. The discrepancy of the efficiency of C25-0140 between pulldown assays and ubiquitination assay is due to the higher concentration of proteins that is required for pulldown assays. To conclude, *in vitro* data showed that C25-0140 does not demonstrate a significant improvement in its inhibitory potential and thereby is comparable to C25.

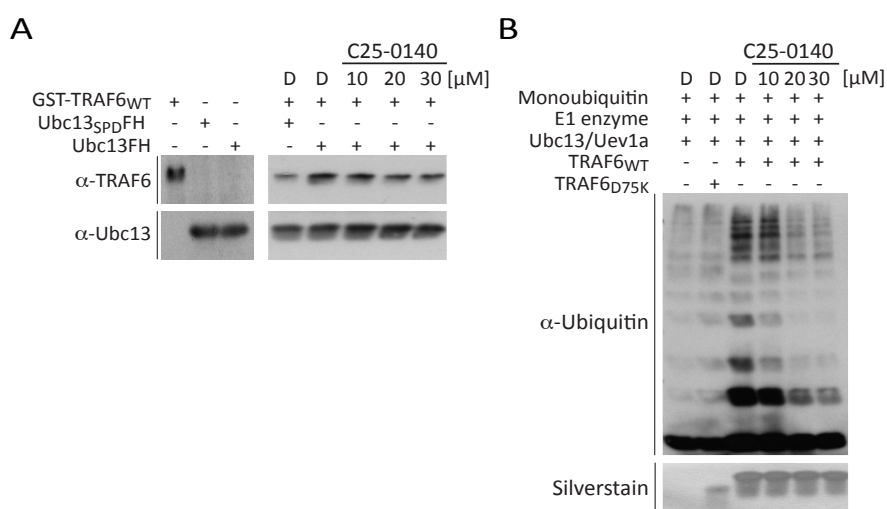


**Figure 4.22: Biochemical validation of C25-0140.** (A) *In vitro* pulldown assay of GST-TRAF6<sub>WT</sub> and Ubc13FH. C25-0140 reduces TRAF6 binding to Ubc13 dose-dependently. (B) Pre-incubation of TRAF6<sub>WT</sub> with C25-0140 leads to a dose-dependent decrease in assembling free polyubiquitin chains in *in vitro* ubiquitination assays.

#### 4.7.2 Investigation of C25-0140 in cell-based assays

Although C25-0140 did not show improved efficiency in inhibiting the TRAF6-Ubc13 interaction *in vitro*, EMSA and ALPHASurefire experiments revealed an elevated inhibitory potency of C25-0140 (Fig. 4.20A). However, this observation applies to both IL-1 $\beta$  and TNF $\alpha$  signaling towards NF- $\kappa$ B. For further investigation, detailed cytotoxic analysis was performed in HepG2 as well as in MEF cells first. CellTiter-Blue experiments in HepG2 cells seemed to be slightly influenced by C25-0140 although this effect did not show any dose-dependency. Whereas the mitochondrial

mass detected by Mitotracker staining remained unaffected, the nucleus area estimated from the Hoechst 33342 staining did decrease at 100 $\mu$ M compound concentration in the HepG2 cell line (Figure 4.23A). In MEF cells, CellTiter-Blue assays did not show any influence of C25-0140 on cell viability (Fig. 4.23A). This was also true for the nucleus area (Fig. 4.23A). However, the mitochondrial mass was increased by approximately 25% starting at a concentration of 50 $\mu$ M C25-0140 (Fig. 4.23A).

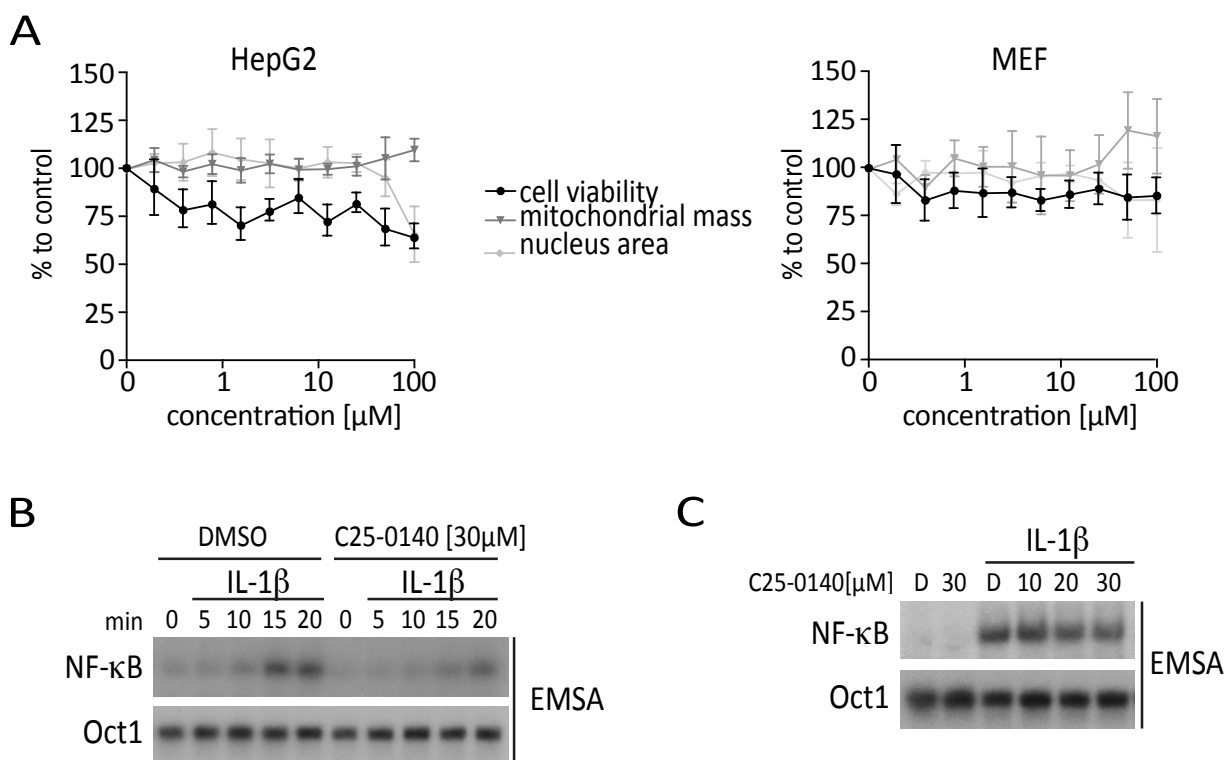


**Figure 4.23: Cytotoxicity tests and cell-based verification of C25-0140 in EMSA experiments.** (A) Cytotoxicity tests of C25-0140 in HepG2 and MEF cells revealing that MEF cells tolerate C25-0140 better than HepG2 cells (B) C25-0140 treated MEF cells show a delayed and reduced activation of NF- $\kappa$ B after IL-1 $\beta$  stimulation (C) C25-0140 causes dose-dependent decrease of NF- $\kappa$ B activation after both IL-1 $\beta$ .

Next, the influence of C25-0140 on NF- $\kappa$ B activation after IL-1 $\beta$  was analyzed in time- and dose-dependent EMSA experiments. Treatment of cells with 30 $\mu$ M C25-0140 led to a reduced and delayed activation of NF- $\kappa$ B in IL-1 $\beta$  stimulation experiments (Fig. 4.23B). Pre-treatment of MEF cells with increasing amounts of C25-0140 (10-30 $\mu$ M) led to a dose-dependent reduction of NF- $\kappa$ B activation (Fig. 4.23C). In p65 translocation experiments, cells were pre-treated with 12.5 $\mu$ M C25-0140. Compound treatment reduced IL-1 $\beta$  and TNF $\alpha$  induced nuclear translocation of p65 as shown in Figure 4.24.



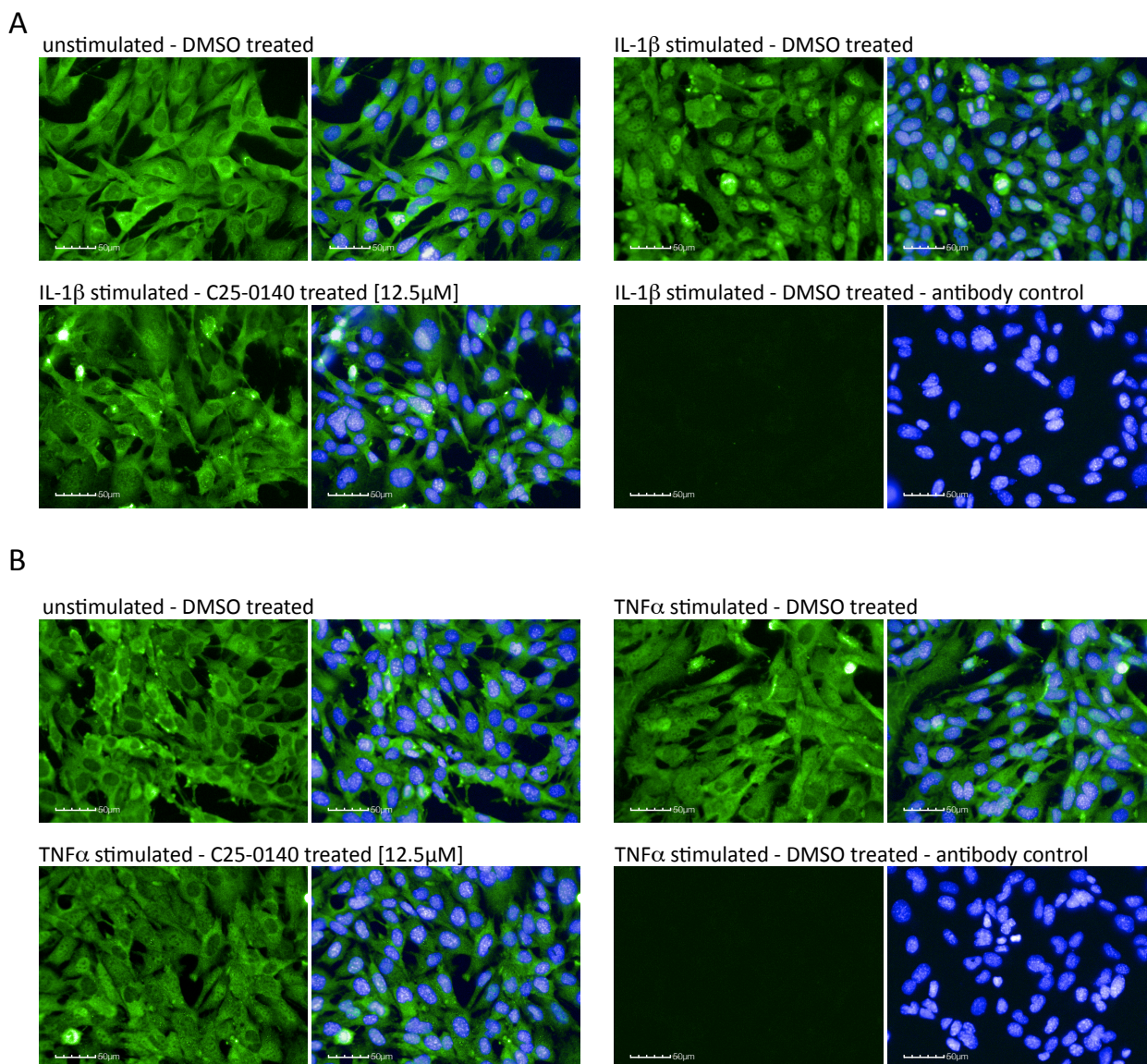


**Figure 4.24: Verification of the inhibitory potential of C25-0140 in p65 translocation assays.** MEF cells were pre-treated with 12.5 $\mu$ M C25-0140 and stimulated with either IL-1 $\beta$  (A) or TNF $\alpha$  (B) for 20 min. C25-0140 reduced nuclear translocation of p65 in both stimulation experiments.

To further analyze the pathway specificity of C25-0140, target gene expression experiments were performed using qPCR. In order to compare the efficiency of the compound to all three signaling pathways (IL-1 $\beta$ , LPS and TNF $\alpha$ ), the same target genes were chosen for all stimulation experiments. However, only A20 was found to be induced by all of the stimulants. ICAM-1 gene expression was only regulated by IL-1 $\beta$  and TNF $\alpha$  stimulation. Instead, IL-6 expression was analyzed in the case of LPS stimulation. For A20, only a mild, but dose-dependent reduction of mRNA expression was obtained for all three stimulants up to 20 $\mu$ M C25-0140 treatment (Fig. 4.25). However, LPS-induced upregulation of A20 could not significantly be impaired by C25-0140 (Fig. 5.23B). Compared to A20, ICAM-1 was stronger affected after IL-1 $\beta$  and TNF $\alpha$



stimulation with a slightly higher impact on TNF $\alpha$  signaling. Also, IL-6 mRNA induction after LPS stimulation was diminished dose-dependently and to a higher extent than A20. In general, compared to the effects of C25 in qPCR experiments (Fig. 4.17B) a clearly higher inhibitory potential was accomplished with C25-0140.

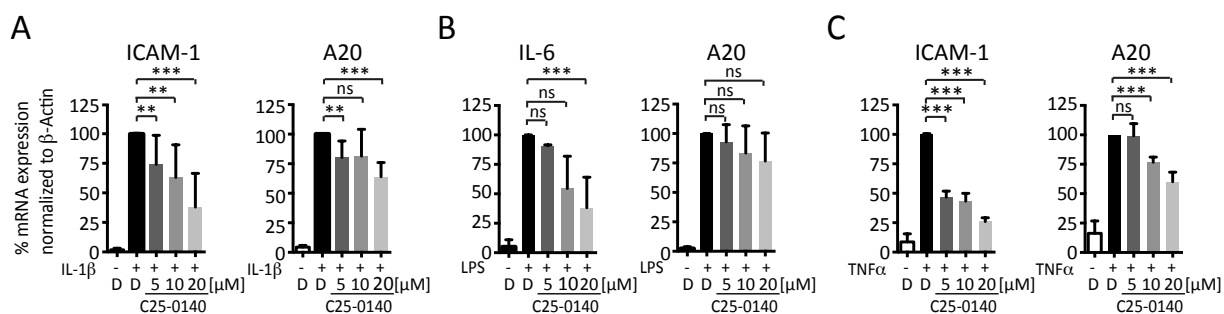


**Figure 4.25: Investigation of C25-0140 in NF- $\kappa$ B target gene expression in qPCR experiments.** qPCR studies after IL-1 $\beta$  (60 min) (A), LPS (75 min) (B) or TNF $\alpha$  (60 min) (C) stimulation lead to a moderate reduction of target gene expression but no pathway selectivity is obtained. Mean and standard deviation are depicted. Statistical significances are calculated using Student's t-test ( $p$ -value < 0.01).

To conclude the EMSA and qPCR experiments, C25-0140 clearly shows an appropriate inhibitory effect on NF- $\kappa$ B activation. However, this influence appears to not be pathway specific as all the tested signaling pathways IL-1 $\beta$ , LPS and TNF $\alpha$  were affected.

To further characterize the mechanism of action of C25-0140, additional experiments upstream of NF- $\kappa$ B activation and target gene expression were performed after IL-1 $\beta$  stimulation. First, endogenous TRAF6 auto-ubiquitination after stimulation was examined using increasing concentrations of C25-0140 (10, 20 and 30  $\mu$ M). Already at a concentration of 10  $\mu$ M C25-0140, TRAF6 ubiquitination was diminished compared to DMSO treated cells (Fig. 4.26A). Stronger effects were achieved with higher concentrations and were even completely abrogated with 30  $\mu$ M C25-0140 (Fig. 4.26A). Second, the phosphorylation of I $\kappa$ B $\alpha$  in ALPHASurefire experiments after IL-1 $\beta$  stimulation was diminished in a dose-dependent manner (Fig. 4.26B) and was markedly improved compared to C25 (Fig 4.17A). Last, the activity of the IKK complex after IL-1 $\beta$  stimulation was analyzed. Pre-treatment of MEF cells with increasing concentrations of C25-0140 led to a decrease in phosphorylation of recombinant GST-I $\kappa$ B $\alpha$  by the immunoprecipitated IKK complex comparable to the unstimulated control (Fig 4.26C). This observation is also true for p-I $\kappa$ B $\alpha$  levels in the lysate samples that are strongly reduced after compound treatment (Fig. 4.26C).

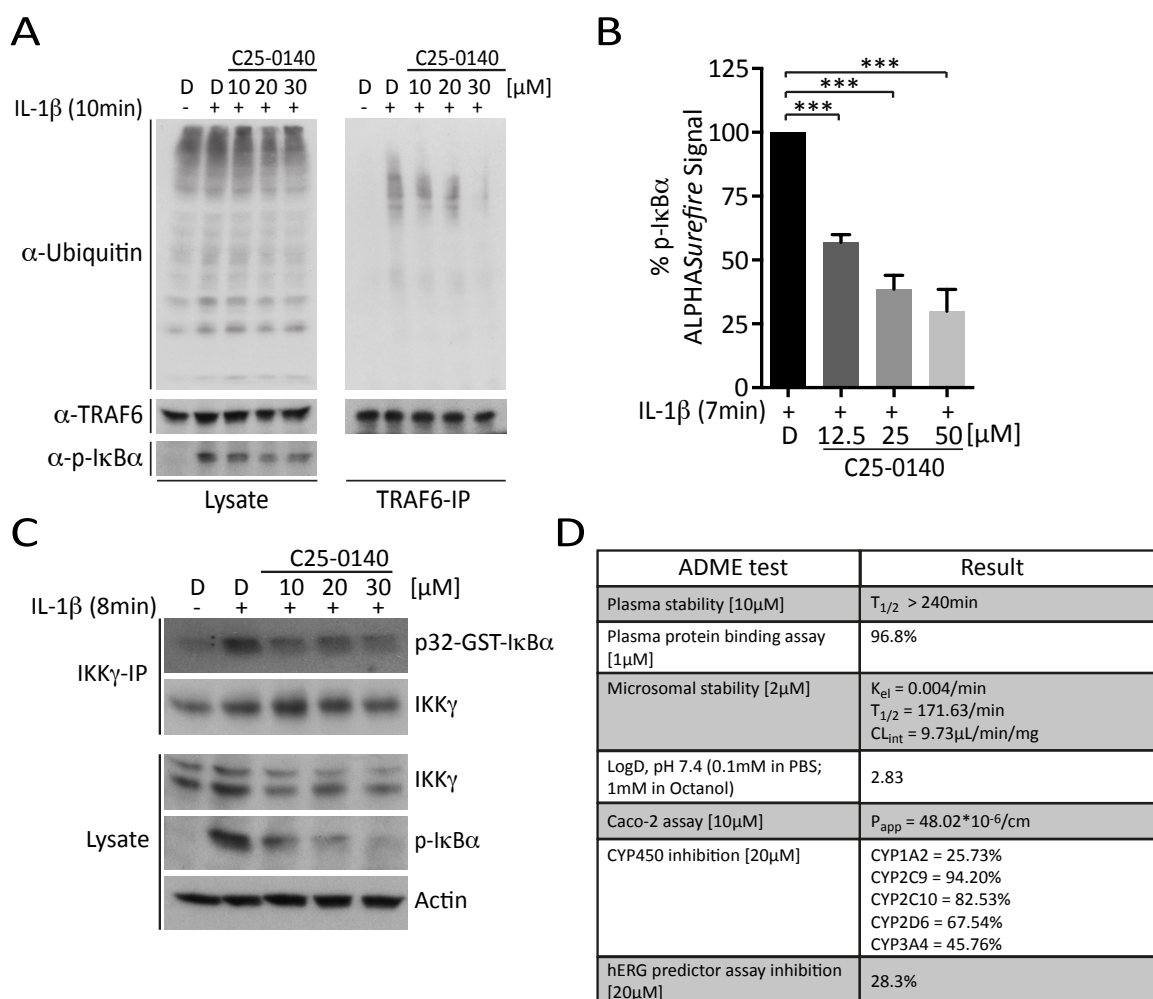


**Figure 4.26: C25-0140 impairs IL-1 $\beta$  stimulated NF- $\kappa$ B signaling upstream of NF- $\kappa$ B activation in MEF cells.** (A) Pre-treatment of MEF cells with C25-0140 leads to a dose-dependent reduction of IL-1 $\beta$  induced TRAF6 auto-ubiquitination. (B) p-I $\kappa$ B $\alpha$  ALPHASurefire experiments reveal an inhibitory effect by increasing amounts of C25-0140 after IL-1 $\beta$  stimulation. Mean and standard deviation are shown. Statistical significances are calculated using Student's t-test ( $p$ -value < 0.01). (C) C25-0140 decreases the activity of the IKK complex in a dose-dependent manner. (D) ADME studies of C25-0140 carried out by Bienta, ENAMINE Ltd. Except CYP450 inhibition, C25-0140 exhibits good parameter.

Summarizing the assays analyzing the impacts of C25-0140 upstream of NF- $\kappa$ B activation, C25-0140 targets TRAF6 auto-ubiquitination which leads to impaired activity of the IKK assay and reduced p-I $\kappa$ B $\alpha$  levels causing a diminished NF- $\kappa$ B activation and target gene expression.

For further analysis of C25-0140, ADME studies were performed. An overview of the experiments, tested concentrations as well as the results is given in Figure 4.26D. Plasma stability assays did not observe any degradation of C25-0140 in over 240 minutes in a mouse plasma environment referring to highly stable compound. However, the compound was 96.8% bound by plasma proteins. The microsomal stability assay revealed a metabolic stability of C25-

0140 with an elimination constant  $k_{el}$  = 0.004/min, a half life of  $T_{1/2}$  = 171.63 minutes and an intrinsic clearance  $Cl_{int}$  = 9.73 $\mu$ L/min/mg. The distribution coefficient (LogD) was estimated to 2.83, which is considered to be in an optimal range (for LogP, see 4.21B). In the caco-2 assay, the permeability coefficient was calculated to 48.02\*10<sup>-6</sup>/cm/s referring to an optimal permeability of C25-0140 (Huang et al., 2009). In the CYP450 inhibition assay, C25-0140 shows inhibition of all tested CYP450 subsets to a different extent. In the hERG predictor assay C25-0140 inhibited 28.3% of tracer binding at a concentration of 50 $\mu$ M and with this relates to a modest inhibition. Thus, except its activity on CYPs, C25-0140 is a compound with overall good ADME parameters.

After testing the behavior of C25-0140 in ADME studies, this compound was analyzed in a low-grade chronic inflammation mouse model to test its pharmacological potency.

#### **4.7.3 Analysis of the effect of C25-0140 in an obese mouse model**

Chronic inflammation is widely observed in obesity. In obese mouse models, a high-fat-diet (HFD) increases NF- $\kappa$ B activation (Carlsen et al., 2009) and leads to upregulation of inflammatory genes like TNF $\alpha$ , IL-1 $\beta$  and IL-6 in the epidermal white adipose tissue (eWAT) (Makki et al., 2013). Furthermore, mice that are mutated in CD40-TRAF6 signaling show milder body weight gain, lower fat mass as well as improved insulin sensitivity and reduced inflammation in adipose tissue in HFD experiments compared to CD40 wildtype mice (Chatzigeorgiou et al., 2014). As C25-0140 exhibits the potential to significantly inhibit TRAF6 induced NF- $\kappa$ B activation *in vitro* and in MEF cells, obese mice were chosen to analyze the effect of TRAF6-Ubc13 inhibition in a mouse model. The small molecule SMI 6860766 targets the MATH domain of TRAF6 and was analyzed also in a HFD obese mouse model (Van Den Berg et al., 2014). This allowed comparison of both compounds in affecting the chronic inflammation as well as the glucose intolerance. In cooperation with the Institute for Diabetes and Obesity (IDO) 16 mice were set on a HFD for at least 12 months gaining obesity and Type II Diabetes Mellitus associated with insulin resistance. Reaching a body weight of at least 40g (average body weight = 55g), these mice were divided into two groups and treated with either control solution or C25-0140 every 24 hours with a dose of 14 $\mu$ mol/kg (=6.4mg/kg) intra peritoneal for 20 days. Every day before injection, the body weight of the mice and their food intake were monitored. The results of these measurements are summarized in Figure 4.27A and 4.27B. Whereas the control treated mice constantly gained body weight under HFD conditions, C25-0140 treated individuals did hardly increase their body weight over the 20 test days (Figure 4.27A). Importantly, food intake did not differ between the two groups over the entire

treatment period (Figure 4.27B). Given these observations and the evidence, that mice with a mutated CD40-TRAF6 signaling show improved insulin sensitivity, a glucose tolerance test (GTT) was performed on day 18. A GTT is conducted to investigate the clearance of the glucose out of the blood. Therefore, glucose was applied to the mice two hours after administration of C25-0140. Blood samples were taken before, 15 min, 30 min, 60 min and 120 min after glucose administration and the amount of glucose was measured using commercial available test strips. Data out of the GTT are presented in Figure 4.27C. After applying glucose to the mice, blood glucose levels increased within 15 min. Afterwards, glucose is constantly cleared out of the body. However, no significant alteration in glucose clearance between the control and C25-0140 treated mice was obtained in either blood glucose levels or area under the curve calculations (Figure 4.27C).

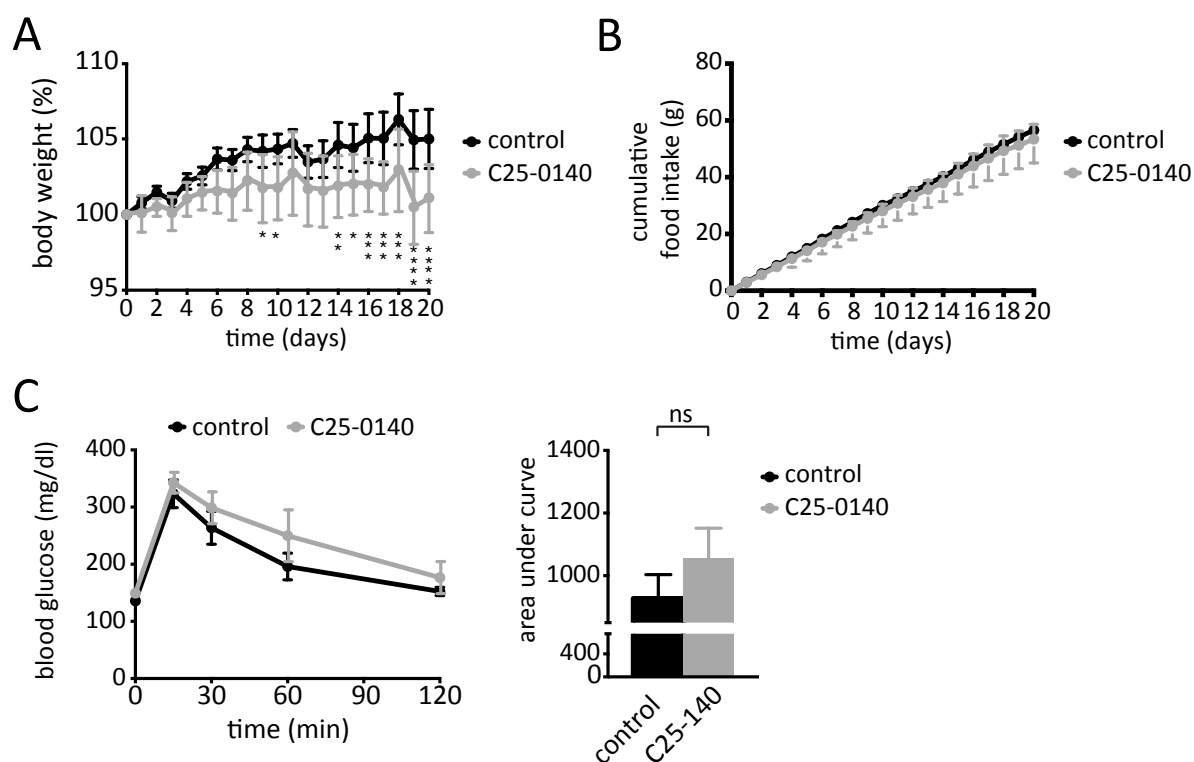


**Figure 4.27: C25-0140 affects body weight gain in high-fat-diet experiments while food intake and glucose intolerance remains unchanged.** (A) C25-0140 treated mice show milder body weight gain than control mice in high fat diet studies.  $n=8$  in each group (B) Food intake remains unaffected in both groups.  $n=8$  in each group (C) C25-0140 does not alter clearance of blood glucose in a glucose tolerance test.  $n=8$  in each group. Mean and standard deviations are depicted. Statistical significances are determined by two-way Anova test (body weight) and Student's t-test (GTT) ( $p$ -value  $< 0.01$ ). These experiments were conducted in collaboration with members of the Institute of Diabetes and Obesity at the Helmholtz Zentrum München.

To further analyze the mechanism behind the stop of gaining weight during C25-0140 treatment, all mice were sacrificed on day 20 two hours after compound administration. Epidermal white adipose tissue was removed from the body and frozen in liquid nitrogen. For evaluation of the inflammatory status of the treated mice, protein and RNA was isolated from the white adipose tissue. First, the protein levels of phosphorylated I $\kappa$ B $\alpha$  and total I $\kappa$ B $\alpha$  were determined using the ALPHASurefire assays. The ratio of p-I $\kappa$ B $\alpha$  to I $\kappa$ B $\alpha$  of all eight mice per group are illustrated in Figure 4.28A. Treatment of obese mice with C25-0140 led to a decreased ratio of p-I $\kappa$ B $\alpha$  to I $\kappa$ B $\alpha$  implying that less I $\kappa$ B $\alpha$  is phosphorylated and at the same time the degradation of I $\kappa$ B $\alpha$  is impaired. Although these results were not significant after the Student's t-test, this is a first hint of reduced inflammation in the white adipose tissue after C25-0140 treatment. Next, RNA was isolated from five mice, reversely transcribed into cDNA and analyzed in qPCR experiments for the expression of several inflammatory marker and NF- $\kappa$ B target genes. The levels of target gene expression were related to the housekeeping gene  $\beta$ -Actin. IL-1 $\beta$ , IL-2 and TNF $\alpha$  gene expression were investigated as primary examples for proinflammatory cytokines and are depicted in Figure 4.28B. The gene expression of all three cytokines is downregulated with IL-1 $\beta$  and IL-2 mRNA exhibiting the strongest effect while TNF $\alpha$  is only mildly impaired. The decrease in IL-1 $\beta$  mRNA expression was the only significant data set. For further NF- $\kappa$ B target gene studies ICAM-1, A20, VCAM-1 and I $\kappa$ B $\alpha$  were selected and results are illustrated in Figure 4.28C. Whereas ICAM-1 and A20 mRNA levels were diminished to a lesser extent, VCAM and I $\kappa$ B $\alpha$  gene expressions were affected stronger. Although, only for VCAM a significant reduction was obtained, the downregulation of all investigated target genes hints at an anti-inflammatory potential of C25-0140 in white adipose tissue.

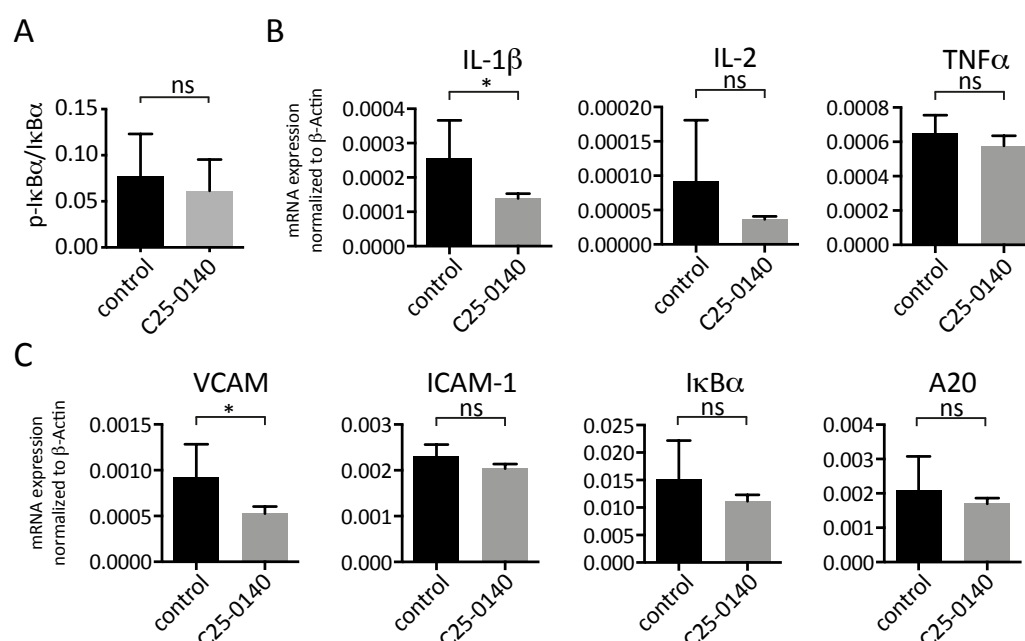


**Figure 4.28: C25-0140 reduces inflammation of epidermal white adipose tissue of obese mice mildly.** (A) The ratio of p-IκBα/IκBα protein levels is reduced after C25-0140 treatment. n= 8 in each group (B) mRNA levels of the proinflammatory cytokines IL-2, IL-1β and TNFα are decreased in C25-0140 treated mice. n= 5 in each group (C) C25-0140 administration leads to diminished NF-κB target genes expression. n= 5 in each group. Mean and standard deviation are depicted. Statistical significances are calculated using Student's t-test (p-value < 0.1).

Summarizing all data testing C25-0140 in an obese and diabetic mouse model, treatment with this small molecule leads to a milder weight gain of mice set on a high-fat-diet compared to control mice. More importantly, this observation was not due to reduced food intake. However, clearance of the blood glucose was not significantly changed. In contrast, protein and RNA data performed from the white adipose tissue of C25-0140 treated mice revealed a slight improvement of the inflammatory status. Further analysis will be necessary to unravel the mechanism of C25-0140 to cause the observed effect on body weight.

## **5 Discussion**

The E3 ubiquitin ligase TRAF6 is well known to regulate signaling in innate and adaptive immune response (Kobayashi et al., 2004). Upon stimulation, TRAF6 interacts with the E2 complex Ubc13/Uev1a to facilitate auto-ubiquitination and subsequent K63-linked polyubiquitination of substrates to mediate signal transduction towards NF- $\kappa$ B activation (Lamothe et al., 2007). The N-terminal RING-Zincfinger1 (RZ1) domain of TRAF6 is responsible for Ubc13 binding (Yin et al., 2009) and was therefore selected to be targeted by small molecules. For the identification of compounds specifically binding to the TRAF6 RZ1 domain and thereby preventing the interaction to Ubc13, 25,000 small molecules were analyzed in a High-Throughput-Screening (HTS) campaign using the ALPHAScreen technology. Out of this screening, 27 hit compounds were further investigated *in vitro* as well as in cell-based experiments. The most promising hits were investigated in more detail. C27 is a strong inhibitor of the TRAF6-Ubc13 interaction leading to a highly impaired NF- $\kappa$ B activation. However, this effect is not selective for IL-1 $\beta$ /LPS signaling as TNF $\alpha$  signaling is affected to the same extent as well. In contrast, C25 showed a more pathway specific but less effective inhibition of NF- $\kappa$ B activation upon IL-1 $\beta$  and LPS compared to TNF $\alpha$  stimulation. To further improve the efficacy of this compound, analog screening was performed revealing C25-0140 as a stronger inhibitor of NF- $\kappa$ B. However, in cells this impact also affects IL-1 $\beta$ /LPS as well as TNF $\alpha$  signaling to the same extent although in ALPHAScreen assays this small molecule acts very selective for only targeting TRAF6 *in vitro*. Nevertheless, this small molecule was investigated in a low-grade chronic inflammation obesity mouse model to prove its anti-inflammatory potential. Upon compound treatment, these mice did not gain weight while on a high-fat-diet compared to control mice. A mild inhibitory effect on inflammation, but no improvement of glucose clearance out of the blood was observed.

### **5.1 Targeting the TRAF6-Ubc13 interaction: a novel approach for interfering with E3 ligase activity by protein-protein-interaction inhibition**

Functional genomic studies predict that approximately 3,000 disease modifying proteins exist (Russ and Lampel, 2005). However, up to date around 400 of these proteins are targeted for therapeutic intervention mainly belonging to the families of G protein-coupled receptors, enzymes, ion channels, protein kinases and others (Russ and Lampel, 2005). Although protein-protein-interactions (PPIs) are vital to most biological processes and are critical in regulating physiology and pathology, they remain rather underexplored in the field of drug discovery.

Reasons for that might be the large interaction surface area involved in protein-protein-binding ( $1,500 - 3,000\text{\AA}^2$ ) and the lack of deep pockets for small molecule binding (Jin et al., 2014). Nevertheless, with rising advancements in establishing new assay technologies it is much easier to determine binding energetics at the macromolecular interface and hotspot residues and inhibitors of protein-protein-interactions are likely to present the next generation of highly innovative drugs providing specificity and selectivity (Buckley and Crews, 2014). Published small molecules targeting protein-protein interactions bind with drug-like potencies to hotspots on the contact surface of the target protein. Hotspots are a small subset of residues of a binding interface that are involved in the interaction. The discovered small molecules interact with much higher efficiencies than the contact atoms of the natural protein partner (Wells and McClendon, 2007).

Alterations in the function of components of the ubiquitin proteasome system (UPS) are associated with a variety of disease states including oncogenesis, inflammation and metabolic dysfunction (Guèdat and Colland, 2007). The involvement of many components of the UPS implies that there exists a large number of potential target sites for pharmacological interference in the ubiquitin regulatory machinery (Guèdat and Colland, 2007). Within the UPS, E3 ligases represent an attractive drug target. Each E3 ligase binds and ubiquitinates a limited set of substrates and is therefore involved in only a few selected regulatory pathways (Goldenberg et al., 2005). Hence, inhibition of a particular E3 is expected to affect only a defined number of pathways that are regulated by this enzyme. Furthermore, specifically targeting a limited group of substrates might lead to fewer toxic side effects and to a more suitable targeted therapy (Landré et al., 2014). With the selectivity of ubiquitination provided by the E3 ligases, the specificity issues observed with proteasome or E1 and E2 inhibitors could therefore be overcome. As proteasome activity is essential for the survival of any cell, proteasome inhibition targets an essential cell function (Guèdat and Colland, 2007). Bortezomib, a proteasome inhibitor approved by the Food and Drug Administration (FDA), is clinically effective in treating multiple myeloma and relapsed mantle cell lymphoma (Skaar et al., 2014). Besides its clinical success, numerous side effects have been reported and multiple myelomas evolving Bortezomib resistance have been observed (Skaar et al., 2014). Like inhibition of the proteasome, targeting an E1 enzyme not only impairs degradation of all proteins that are targeted for destruction by the UPS, but also all pathways that require ubiquitination for a regulatory, non-proteolytic role (Landré et al., 2014). The compound MLN4924 targets the nucleotide-binding site of the E1 enzyme NAE (NEDD8 activating enzyme) and indirectly affects the UPS as NEDDylation is essential for the activation of the SCF-Cullin-containing E3 complex (Soucy et al., 2009).



Substrates of the SCF-complex including p27, HIF1 $\alpha$  and I $\kappa$ B play fundamental roles in cancer development. Upon SCF-complex inhibition by MLN4924 these substrates accumulate and lead to cell cycle arrest, senescence and apoptosis (Soucy et al., 2009). This small molecule is currently being tested in phase I/II clinical trials for treatment of hematologic and non-hematologic malignancies (Landré et al., 2014). However, E1 inhibitors need to be further investigated focusing on specificity and cell pharmacology due to the fact that targeting the E1 machinery might affect multiple pathways. It cannot be excluded that many of these pathways could be critical for the function of vital cells (Guèdat and Colland, 2007).

E2 enzymes are shown to play a role in determination of the type of the polyubiquitin chain linkage. E2 enzymes bind E1, E3 and ubiquitin, and can be targeted at different interaction surfaces. An inhibitor of the Ubc13/Uev1a complex blocks the formation of the E2-ubiquitin thioester conjugate preventing the synthesis of K63-linked polyubiquitin chains that results in impaired NF- $\kappa$ B activation followed by reduced proliferation and viability of cancer cells (Pulvino et al., 2012). Each E2 can associate and cooperate with a specific set of E3s. Thus, a more selective approach for small molecule inhibition might be to interfere with this E2-E3 interaction (Landré et al., 2014). In this thesis, a novel approach was taken to specifically target the E2-E3 interaction of TRAF6 and Ubc13 to selectively interfere with TRAF6-dependent downstream signaling. Since most of the E3 ligases bind several E2 enzymes, in the case of TRAF6 Ubc13 and UbcH5 (Yin et al., 2009), it was aimed at targeting the interaction site at the E3 ligase (Landré et al., 2014). TRAF6 can be targeted at either the N-terminal RING-Zincfinger1 or the C-terminal MATH domain. Whereas the MATH domain mediates adaptor protein functions and binding of substrate proteins, the N-terminal RZ1 domain provides interaction to E2 enzymes and E3 ligase activity. Inhibitors (6877002 and its analog 6860776) targeting the MATH domain of TRAF6 are already described and are shown to impair LPS induced NF- $\kappa$ B activation as well as to improve glucose tolerance in obesity by reducing the accumulation of immune cells in adipose tissue and turning the immune response towards an anti-inflammatory profile (Chatzigeorgiou et al., 2014). In general, E3 inhibitors in PPIs that have been reported so far target the binding of the E3 ligase to its substrate or disrupt interaction of proteins within E3 multiprotein complexes (Skaar et al., 2014).

Therefore, a novel approach is targeting the N-terminal RING Zincfinger1 domain of TRAF6 to prevent its binding to E2 enzymes and to impair the E3 ligase function at the same time. The TRAF6-Ubc13 interaction displays several advantages for small molecule interference. As most of the E2-E3 interactions, the binding of TRAF6 to Ubc13 is transient and competes with the binding of E1 to E2 (Berndsen and Wolberger, 2014). A dissociation constant in the low

micromole range ( $K_d=1.6\mu\text{M}$ ) is described for TRAF6-Ubc13 (Yin et al., 2009), suggesting that a disruption of this complex by a small molecule is feasible. Importantly, the relatively small interaction surface of only  $1000\text{ \AA}^2$  and the surface exposure of several critical residues involved in binding of the RZ1 domain to Ubc13 suggests that there are several options for the docking of a small molecule to prevent this interaction. Indeed, 27 compounds were identified and verified as the first small molecule inhibitors that interfere with the interaction of TRAF6-Ubc13 in *in vitro* binding assays. For the tested compounds, it was also shown that disruption of Ubc13 binding severely impaired E3 ligase function, demonstrating that the E2-E3 interface represents a powerful strategy to target E3 ligase activity. Further, the inhibitors act specific, because none of the compounds interfered with the interaction of the related RING E3 ligase RNF8 and Ubc13. This is important as it provides a proof of concept that selective inhibition of E2-E3 interactions represents a feasible strategy to target E3 ligase function. The identified compounds display diverse molecular structures and contain different scaffolds suggesting that selectivity in targeting the RZ1 domain in TRAF6 can be achieved with diverse chemical moieties. Despite the considerable heterogeneity of the compounds, all 27 identified molecules harbor at least three aromatic structures including at least one heterocycle containing nitrogen or oxygen atoms suggesting that these structures are preferably to target the N-terminal domain of TRAF6. The small molecules might either directly bind to the TRAF6-E2 interface to compete for Ubc13 association or they might change the structural conformation of TRAF6 RZ1 and thereby indirectly abrogate binding of Ubc13. The identification of a large number of compounds that specifically target the TRAF6-Ubc13 interaction clearly proves that it is indeed possible to target the E2-E3 interaction surface and prevent binding of E2 enzymes to E3 ligases resulting in impaired E3 ligase activity. Also, these small molecules indicate that targeting of such a relatively short and low affinity binding E2-E3 surface might overcome several obstacles that are associated with PPI inhibition often including the large interaction surface area and the lack of deep pockets.

As already mentioned, a different strategy to interfere with TRAF6 adaptor protein function is to target the C-terminal MATH instead of the RING-Zincfinger1 domain to prevent protein-protein-interaction. One recent approach was to impair TRAF6-CD40 signaling that involves the binding of the TRAF6 MATH domain to the cytosolic domain of the CD40 receptor (Chatzigeorgiou et al., 2014). In a screening cascade, 800 out of 400,000 compounds were identified by computational approaches by applying ADME/toxicity filters (using the Lipinski's rule of 5) as well as performing rigid and flexible docking (Chatzigeorgiou et al., 2014). The 800 top-scoring compounds were analyzed in a NF- $\kappa$ B reporter gene assay in the RAW 264.7 cell line revealing 51 compounds that

reduced NF- $\kappa$ B activation by at least 50% at 10 $\mu$ M. Analog screening of the initial best compound 6877002 revealed six bioactive analogs that all inhibited NF- $\kappa$ B activation in RAW 264.7 cells dose-dependently as well as suppression of CD40-induced expression of IL-1 $\beta$  and IL-6 in primary macrophages (Chatzigeorgiou et al., 2014). In a LPS-stimulated NF- $\kappa$ B reporter gene assay IC<sub>50</sub> values were determined for these compounds. The initial small molecule 6877002 reduced NF- $\kappa$ B activation with IC<sub>50</sub> = 15.9 $\mu$ M whereas the analog 6860776 exhibited an IC<sub>50</sub> = 0.3 $\mu$ M (Chatzigeorgiou et al., 2014). Compared to that, compounds identified in this thesis demonstrated higher IC<sub>50</sub> values in cells. C25 displayed IC<sub>50</sub> values above 50 $\mu$ M in p-I $\kappa$ B $\alpha$  ALPHASurefire and qPCR experiments while the analog C25-0140 showed IC<sub>50</sub> values between 10 $\mu$ M and 20 $\mu$ M dependent on IL-1 $\beta$ , LPS or TNF $\alpha$  stimulation (Figures 4.17, 4.20 and 4.25). This indicates that the compounds efficiency needs to be further improved. However, it is not possible to judge the specificity of the compounds 6877002 and 6860776, because analyses of pathways that do not require TRAF6 for signaling have not been performed. Furthermore, the disruption of the TRAF6-CD40 complex was not shown *in vitro* and therefore it is not possible to correlate cell data with the suggested *in vitro* effects of the compounds. The common structure of 6877002 and the analogs consists of two Ring structures with different substituents connected by the same linker (Chatzigeorgiou et al., 2014). Compared to that, C27 contains four heterocyclic structures (Figure 4.8), while C25 and C25-0140 consist of five different aromatic structures as well as multiple substituents and thus, provide more contact residues for targeting amino acids (Figure 4.19).

Altogether, it is possible to identify TRAF6 interacting compounds using different strategies involving computational approaches as well as *in vitro* and cell-based experiments. Thereby, TRAF6 can be targeted at the N-terminal RZ1 domain or the C-terminal MATH domain. Interfering with these binding interfaces leads to impaired of NF- $\kappa$ B signaling in both cases.

## **5.2 Identification and verification of TRAF6-Ubc13 inhibitors *in vitro***

### **5.2.1 High-Throughput assays for screening of selective TRAF6-Ubc13 inhibitors**

For the identification of small molecules targeting the RZ1 domain of TRAF6 to prevent binding to Ubc13, a HTS campaign was conducted. The ALPHAScreen technology was preferred as this technology demonstrates several advantages for a HTS assay. First, it is a homogeneous assay that allows measuring by mix and read only. Second, it is a proximity assay with a broad energy transfer distance of around 200nm between donor and acceptor beads. Third, it displays very high sensitivity and very low background levels resulting in a high signal/background ratio. Upon excitation one donor bead can generate up to 60,000 singlet oxygen molecules per second

resulting in high signal amplification. The ALPHAScreen technology can therefore be used for low to high affinity binding interactions (pM to mM). The high sensitivity allows minimizing the assay volume making it very cost effective. Last, the donor and acceptor beads exhibit a strong resistance to DMSO (up to 20% in Ungermannova et al., 2013) as well as the stable signal up to six hours (Ungermannova et al., 2013). However, due to its complex chemistry, one of the disadvantages of this assay is the high rate of false positive hits interfering in binding interactions by either forming aggregates or impairing assay signaling. Light scattering is produced by insoluble compound aggregates that are misfolded upon dilution in aqueous buffers. Small molecules impeding with the ALPHAScreen technology are referred to frequent hitters (Schorpp et al., 2014) and could be either singlet oxygen quencher, color quencher (also known as inner filters) or acceptor bead competitors, which is more commonly for the Nickel Chelate Acceptor beads (Perkin Elmer, TruHitsKit). These ALPHAScreen frequent hitter (ALPHAScreen-FH) molecules need to be extracted from the hit list by counter screens, the pan-assay-interference-compounds (PAINS) filters (Baell and Holloway, 2010) or additional filters including His-frequent hitters (Schorpp et al., 2014) or the TruHits Kit provided by Perkin Elmer. Frequent hitter detection and the TruHits kit was chosen here as a strategy to eliminate false positive hits. Filters to identify ALPHAScreen-His-FH were developed based on the data originated from four robust ALPHAScreen assays that involved His-tagged proteins and Nickel Chelate beads and were performed at the Assay Development and Screening (ADSP) platform at the Helmholtz Zentrum München. Out of 25,000 screened molecules, 60 compounds were identified as ALPHAScreen-FHs and 77 small molecules were determined as ALPHAScreen-His-FHs (Schorpp et al., 2014). The analysis of the initial screening data using PAINS filters identified the majority of the ALPHAScreen-FHs (52 out of 60), whereas only two out of 77 ALPHAScreen-His-FHs were discovered. The design of the PAINS filters resulted from frequent hitters that initially hit six ALPHAScreen assays, but also interfered with other technologies (Baell and Holloway, 2010). The PAINS filter did not recognize eight compounds. These small molecules predominantly comprised fused aromatic systems or quinone moieties in their structures and are assumed to quench excitation/emitted radiation or singlet oxygen. Six additional filters for ALPHAScreen-FHs were developed because of the structural diversity of these compounds (Schorpp et al., 2014). For the ALPHAScreen-His-FHs, new filters needed to be developed as only two out of 77 small molecules were identified by the PAINS filters. 18 of the 77 compounds comprise a common molecular fragment (Figure 5.1A). This molecular structure is known to form bifurcated hydrogen bonds with XH-donating groups (X=N, O) (Slepukhin et al., 2013; Salmina et al., 2011) and to cause coordination complexes with metal ions (Kaim, 2002). Due to

the good NH-donor properties of the imidazole rings of the His-residues of tagged proteins, the molecular fragment is assumed to form bifurcated hydrogen-bond complexes with the His-tag and to prevent immobilization of the proteins on the bead surface (Figure 5.1B). The same compounds may act as chelating agents as well and absorb on the bead surface (Figure 5.1C). In both cases, the generation of an ALPHAScreen signal is disrupted. The remaining 59 ALPHAScreen-His-FHs are mostly known chelating agents such as 8-hydroxyquinolines (Albrecht et al., 2008), picolylamines (Chen et al., 2011; Bratsos et al., 2011) and pyridines (Constable et al., 1998) and are known to bind zinc (II) metalloproteins (Agrawal et al., 2010). Therefore, 19 additional filters were developed to identify ALPHAScreen-His-FHs (Schorpp et al., 2014). All newly developed filters are available at the OCHEM website (<http://ochem.eu/alters>) and can be freely accessed by users to filter results of their HTS campaigns. In conclusion, the utilization of different filters allowed the elimination of many false positive hit compounds. In this work, out of 520 primary hit compounds 137 small molecules were identified as frequent hitters and were excluded from the hit list. 383 compounds remained for further investigation. Although chemoinformatic filters are necessary to predict frequent hitters, it cannot replace *in vitro* counter screening assays completely.

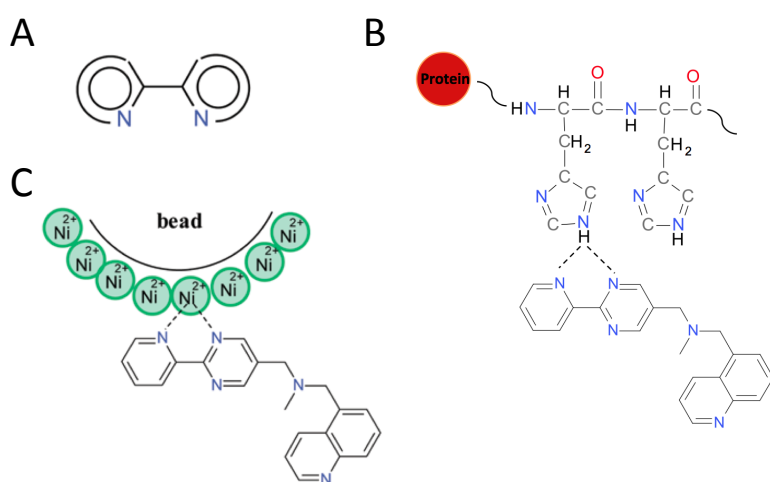


**Figure 5.1. Potential mechanism of action of the identified ALPHAScreen-His-Frequent Hitters (FH).** Dashed lines depict interactions. Figures from Schorpp et al., 2014. (A) 18 ALPHAScreen-His-FHs share this common molecular fragment. (B) Hypothetical hydrogen bonds that are formed between the molecular fragment and the His-tag of the protein. (C) Hypothetical chelate complex formation by the molecular fragment and the Ni<sup>2+</sup>-ions of the acceptor bead surface.

In order to obtain compounds that specifically target the TRAF6 RING-Zincfinger1 domain, the primary hit compounds were tested to impact the interaction of OTUB1 and Ubc13 in ALPHAScreen experiments. Superposition of the structure of Ubc13 bound to TRAF6 showed that the binding site for the DUB OTUB1 overlaps with the E3 RING binding site (Wiener et al., 2012). Out of 383 tested molecules, 205 affected the OTUB1-Ubc13 interaction as well. These 205 compounds were assumed to target Ubc13 and were excluded from the hit list. Serial dilution experiments using the ALPHAScreen technology further excluded 151 compounds

without concentration-dependent effects. To further ensure that the 27 hit compounds specifically target TRAF6 instead of general RING domains, the effect of these compound on the interaction of the E3 RING ligase RNF8 and Ubc13 were analyzed as the RING domains of TRAF6 and RNF8 exhibit significantly similar structures (Figure 5.2B and supplement 10.11). None of the 27 tested compounds impaired the interaction of RNF8 to Ubc13 proving that these compounds specifically inhibit the TRAF6-Ubc13 interaction *in vitro*. The ALPHAScreen technology with all the advantages mentioned above displays an excellent tool in High-Throughput-Screening not only as a primary screening assay but also for counter screening assays to achieve specificity of the analyzed small molecules.

### **5.2.2 Low-Throughput assays for verifying selected TRAF6-Ubc13 inhibitors**

The High-Throughput assays allowed reducing the number of putative candidates to a number that could be confirmed in secondary Low-Throughput assays. First, a pulldown assay was established to test the compounds in a secondary assay that is different from the ALPHAScreen technology and involves a different tag combination as well. A pulldown assay is used to determine interactions between molecules in solution via immobilization of the bait protein to beads and incubation with the interaction partner. After washing, the complex is eluted from the beads and analyzed in SDS-Page and Western Blot. Only a limited number of small molecules could be validated. Both compounds, C25 and C25-0140, reduced the binding of TRAF6 to Ubc13 dose-dependently in pulldown assays (Figures 4.14 and 4.22). Second, in order to confirm the binding of the compounds to the TRAF6 RZ1 domain, NMR experiments were established to verify that the compounds are indeed binding to TRAF6. The NMR technology uses magnetic properties of certain atomic nuclei and not only allows the verification of a direct binding between two interaction partners but is also used to determine the amino acids that are involve in binding. For this, untagged TRAF6 was measured in NMR experiments after compound treatment. The compounds C27, C25 and C25-0140 caused shifting or disappearing of peaks of the TRAF6 spectrum indicating that these small molecules are directly binding to the TRAF6 RZ1 domain (Figure 4.8, 4.13 and 4.21).

In addition, a number of assays were considered or conducted to study the effects of the inhibitors including time resolved Förster resonance energy transfer (TR-FRET), DELFIA (Dissociation-Enhanced Lanthanide Fluorescence Immunoassay) and MST (Microscale Thermophoresis) but for good reasons these analyses were not prioritized or did not lead to reliable assays. TR-FRET is a proximity-based assay build on the energy transfer between two fluorophores. The distance allowing energy transfer between the fluorophores has a maximum

of 10nm, which is close to the distance of large molecules (as antibody or hemoglobin) (Glickmann et al., 2002). The structural analysis of the TRAF6-Ubc13 interface (Yin et al., 2009) suggested that the terminal tags are too distant for an energy transfer in TR-FRET and therefore this technique was not proceeded. Nevertheless, TR-FRET assays were established to monitor assembly of polyubiquitin chains using tagged ubiquitin moieties (Hong et al., 2003) and hence it may be interesting to establish TR-FRET as a secondary assay to analyze TRAF6 activity in response to compound inhibition. The DELFIA system provides an ELISA-based assay and works in a static environment with proteins immobilized to a plate instead of proteins in solution. It was established for analyzing other low affinity PPIs like the interaction of ubiquitin chains to the ubiquitin binding domain of NEMO (Hadian et al., 2011). However, a specific interaction of TRAF6 and Ubc13 in DELFIA assays could not be confirmed. Potentially, the immobile environment in the plate bound format does not allow detection of this interaction. Alternatively, the required extensive washing steps might interfere with the transient TRAF6-Ubc13 interaction. Finally, MST uses the motion of molecules in microscopic temperature gradients and can be used to detect binding of proteins or small molecules to fluorescently labeled proteins (Jerabek-Willemsen et al., 2011). However, a specific binding of Ubc13 to fluorescently labeled TRAF6 could not be detected, putatively because the labeling might involve amino acids that are critical for binding or due to potential oligomerization of the complex. Therefore, these approaches were not further pursued and NMR and pulldown studies to detect binding of compounds to TRAF6 in Low-Throughput assays were preferred instead.

### **5.3 Verification of the newly identified TRAF6-Ubc13 inhibitors in cell-based assays**

To directly analyze the effects of the compounds identified *in vitro*, it was aimed to establish a reliable interaction assay between TRAF6 and Ubc13 in cells. However, neither the endogenous interaction after IL-1 $\beta$  stimulation as published in Shembade et al. in 2010 could be confirmed nor could co-immunoprecipitation studies and FRET experiments after overexpression of the proteins in Hek293 and MEF cells reveal a stable binding of TRAF6 and Ubc13 (data not shown). Most of the E2-E3 interactions including TRAF6 and Ubc13 are transient and also display dissociation constants in the low micromole range (Berndsen and Wolberger, 2014). In cells, this interaction is stimulation dependent and does not occur in unstimulated cells and is difficult to detect reliably (Shembade et al., 2010). Therefore, determining the influence of the compounds on NF- $\kappa$ B activation as a functional readout for an active TRAF6-Ubc13 complex was preferred. For the verification of the hit compounds in cell-based assays, the Electrophoretic-Mobility-Shift-Assay (EMSA) was selected to analyze the activation of NF- $\kappa$ B. The EMSA technology has many

advantages like exhibiting robustness as well as high sensitivity and at the same time no signal amplification due to the use of radioisotope-labeled nucleic acids (Hellmann and Fried, 2007). Because of the high sensitivity, this assay permits working with crude cell extracts and only low concentrations of protein and nucleic acids are required (Hellmann and Fried, 2007). In EMSA experiments, the effects of the compounds on NF- $\kappa$ B activation were analyzed after IL-1 $\beta$  and TNF $\alpha$  stimulation. This emerged as an optimal opportunity to determine the impact of the small molecules on NF- $\kappa$ B signaling in a fast and highly sensitive manner. At an early stage, these data allowed to focus on inhibitors that were also active in a cellular context. The results then served as a starting point to further test the best hits in assays downstream and upstream of NF- $\kappa$ B DNA-binding activity.

Based on EMSA analyses two initial hits (C27 and C25) were chosen for further evaluation that included NF- $\kappa$ B induced target gene expression, nuclear translocation of NF- $\kappa$ B dimers, the phosphorylation and degradation of I $\kappa$ B $\alpha$ , activation of the IKK complex as well as auto-ubiquitination of TRAF6. All experiments were performed after stimulation with the respective cytokine and on endogenous level to avoid unspecific effects due to overexpression of proteins. Downstream of NF- $\kappa$ B activation, target genes were analyzed in qPCR experiments and revealed dose-dependent inhibition of ICAM-1 and A20 after compound treatment with C27 and C25-0140 and stimulation of IL-1 $\beta$ , TNF $\alpha$  and LPS. Upstream of NF- $\kappa$ B DNA-binding, translocation activity of the NF- $\kappa$ B dimer was analyzed in a p65 translocation assay via immunofluorescence. Phosphorylation of I $\kappa$ B $\alpha$  was determined in two independent assays: Western Blot and ALPHASurefire experiments. Degradation of I $\kappa$ B $\alpha$  was detected in Western Blot and the activity of the IKK complex investigated in a kinase assay. All performed experiments showed dose-dependent effects of the compounds. Thereby, C27 and C25-0140 affected inhibition of NF- $\kappa$ B activation stronger than C25, but did not act pathway specific. In a functional assay the E3 ligase activity of TRAF6 was verified by detecting the auto-ubiquitination of TRAF6 upon IL-1 $\beta$  stimulation. TRAF6 only exhibits E3 ligase activity upon binding to Ubc13. Therefore, inhibition of the activity of TRAF6 concludes an impaired interaction of TRAF6 and Ubc13. Upon compound treatment with C27 or C25-0140, endogenous TRAF6 ubiquitination was diminished in both cases leading to the conclusion that the TRAF6-Ubc13 interaction in cells indeed might be affected.

The verification of the compounds effects in cells involved a variety of diverse assay technologies including EMSA, qPCR, Western Blot, Kinase assay, ALPHASurefire and immunoprecipitation experiments. This is an important criterion during hit verification in cell-based assays and to exclude the possibility of assay-related effects after compound treatment.



Inhibitory effects in all performed assays strongly support the negative regulatory impact of the tested compounds on multiple levels of the NF- $\kappa$ B signaling cascade.

#### **5.4 Selectivity of compounds targeting the RING-Zincfinger1 domain of TRAF6**

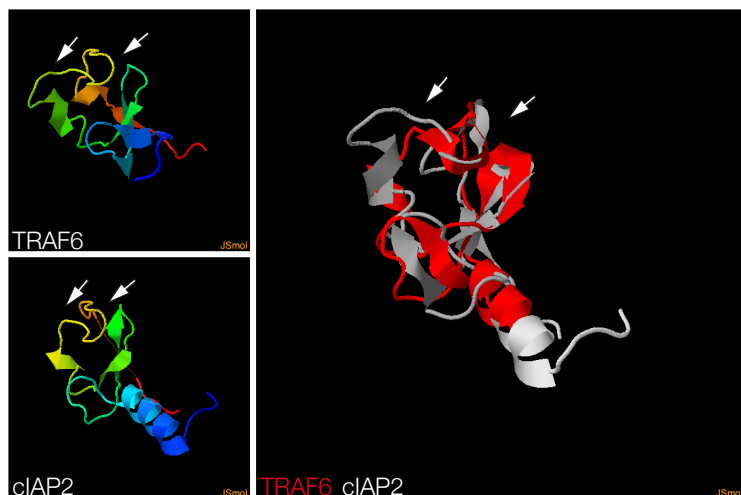
Out of the HTS campaign and a secondary optimization three compounds (C27, C25 and C25-0140) were identified as inhibitors selectively targeting the TRAF6-Ubc13 binding *in vitro*. However, in cell-based assays only C25 showed pathway selectivity towards IL-1 $\beta$ /LPS signaling whereas C27 and C25-0140 inhibited activation of NF- $\kappa$ B to a stronger extent but not selectively. Selectivity was determined via analysis of NF- $\kappa$ B activation after IL-1 $\beta$ , LPS and TNF $\alpha$  stimulation. Whereas IL-1 $\beta$  and LPS stimulation induce TRAF6-dependent signaling, TNF $\alpha$  leads to NF- $\kappa$ B activation independent of TRAF6. C25 is a small molecule exhibiting only mild impacts on NF- $\kappa$ B activation after IL-1 $\beta$  and LPS stimulation. However, TNF $\alpha$  induced NF- $\kappa$ B activation is not affected. In contrast, compounds like C27 and C25-0140 strongly affecting TRAF6-dependent NF- $\kappa$ B activation by IL-1 $\beta$  and LPS also reduced TNF $\alpha$  induced NF- $\kappa$ B activation to the same extent. An influence of TRAF6 in TNF $\alpha$  induced NF- $\kappa$ B signaling is very unlikely, because TRAF6<sup>-/-</sup> MEF cells exhibit no altered NF- $\kappa$ B activation upon TNF $\alpha$  stimulation (Figure 4.7B). Two possible scenarios may explain the non-selective inhibition of the stronger acting compounds in cells: first, other RING domains of proteins containing this structure are targeted as well or second, the compounds bind to additional proteins within the NF- $\kappa$ B signaling pathway that are different from RING containing proteins.

A first explanation for the non-pathway selective effects of C27 and C25-0140 could be that RING domains of other members of the TRAF protein family members or additional E3 ubiquitin ligases harboring a RING domain might be targeted as well. Five E3 ligases containing a RING motif are involved in TNF $\alpha$  induced NF- $\kappa$ B activation to modify the components of the TNFR signaling complex with non-degrading, regulatory K63-linked polyubiquitin chains: the RING domain-containing molecules TRAF2, cIAP1 and cIAP2 and the RBR (RING1-BetweenRING-RING2) E3 ligases HOIL-1 and HOIP of the LUBAC complex (Wajant and Scheurich, 2011). All RING E3 ligases contain a Zincfinger type RING domain with 40-60 residues presenting a Cys-X<sub>2</sub>-Cys-X<sub>9-39</sub>-Cys-X<sub>1-3</sub>-His-X<sub>2-3</sub>-Cys-X<sub>2</sub>-Cys-X<sub>4-48</sub>-Cys-X<sub>2</sub>-Cys motif (where X can be any amino acid; histidines and cysteines are sometimes exchanged) (Budhidarmo et al., 2012). All RING E3 ligases coordinate two zinc ions in a cross brace arrangement. The core of the RING domain displays two  $\beta$ -strands ( $\beta$ A and  $\beta$ B), one  $\alpha$ -helix ( $\alpha$ A) and two loops (loop1 and loop2) that surround the first and second zinc coordination sites and contact the E2 enzyme (Budhidarmo et al., 2012). However,

TRAF2 might be excluded from the list of potentially targeted proteins, because the RING domain of TRAF2 is not required for TNF $\alpha$  induced IKK/NF- $\kappa$ B signaling (Zhang et al., 2010). The RING E3 ubiquitin ligases cIAP1 and cIAP2 contain a RING motif as well and are essential for TNF $\alpha$  induced NF- $\kappa$ B signaling (Mahoney et al., 2008). According to the similar structure of RING E3 ligases, the possibility arises that the compounds C27 and C25-0140 might target cIAP1 and cIAP2 for inhibition resulting in impaired TNF $\alpha$  induced NF- $\kappa$ B activation as well. To test this hypothesis a structural alignment using the FATCAT software (flexible structure alignment by chaining aligned fragment pairs allowing twists) was conducted. For cIAP1, no crystal structure of the RING domain is available, but the RING domain of cIAP2 (PDB: 3eb5) is annotated in the Protein Data Bank (PDB) and was structural aligned to the RING domain of TRAF6 (PDB: 2jmd) as illustrated in Figure 5.2A. Between the two proteins, out of 62 compared positions 55 were equivalent even without a twist (supplement 10.10). A p-value of 0.0138 confirms the significant similarity between both domains (supplement 10.10). In the structural alignment the similarity of the  $\beta$ -strands,  $\alpha$ -helices and the loops are visible. The interaction surface to Ubc13 is indicated by the arrows in Figure 5.2A.

In the hit verification process of compounds specifically targeting the RZ1 domain of TRAF6, the RING E3 ligase RNF8 was included in the screening procedure. The structures of the RING domains of TRAF6 and RNF8 also exhibit a significant similarity (p-value = 0.000204) and 59 equivalent positions out of 62 compared residues without a twist (Figure 5.2B and supplement 10.11). Compounds targeting general RING domains would interfere in both assays, TRAF6-Ubc13 and RNF8-Ubc13. However, none of the 27 hit compounds that interrupted TRAF6-Ubc13 binding inhibited the RNF8-Ubc13 interaction indicating that the identified compounds indeed target only the TRAF6-Ubc13 interaction surface. In NMR experiments, C27, C25 and C25-0140 caused shifting of the same peaks within the TRAF6 proteins suggesting that the multiple heterocyclic structures, that have all three compounds in common, target identical residues within the RZ1 domain of TRAF6.

A



B

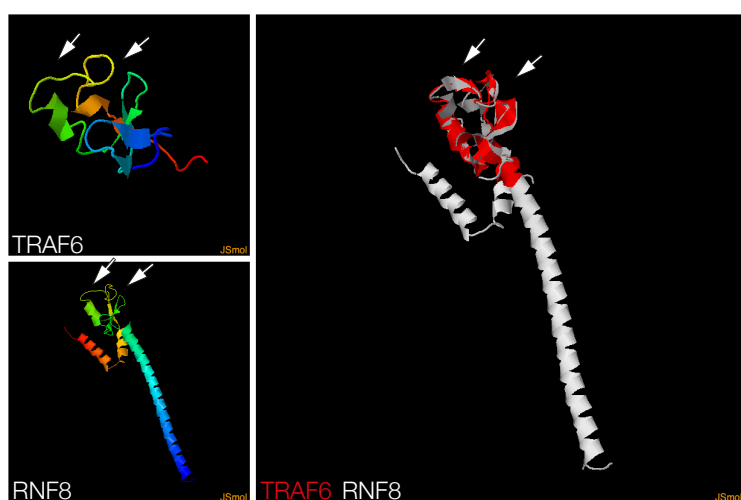


**Figure 5.2: Comparison of RING containing E3 ubiquitin ligases cIAP2 and RNF8 with the TRAF6 RING domain.** Structural alignments were performed using the FATCAT software provided by the Godzik's lab. The interaction surface to Ubc13 is indicated by arrows. (A) Structural alignment of the RING domains of TRAF6 (PDB: 2jmd) and cIAP2 (PDB: 3eb5). The RING domains are structurally significantly similar. (B) Structural alignment of the RING domains of TRAF6 (PDB: 2jmd) and RNF8 (PDB: 4yac) revealed structural similarity between both domains.

Due to the fact that the compounds affect the RZ1 domain of TRAF6, but not the RING domain of RNF8, it is most likely that the Zincfinger1 domain of TRAF6 is targeted because RNF8 does not contain such a Zincfinger motif. The Zincfinger1 domain of TRAF6 is not directly involved in the Ubc13 interaction but plays a critical role in maintaining the structural conformation of the RING domain to allow binding to Ubc13. Without the Zincfinger1 motif, TRAF6 auto-ubiquitination as well as interaction to Ubc13 is impaired (Lamothe et al., 2008). Targeting the Zincfinger1 domain of TRAF6 might cause conformational changes within the RING domain in a way that the interaction surface is no longer available for Ubc13 binding. As a consequence, it is unlikely that RING domains of additional E3 ligases or other proteins containing RING domains are targeted by the compounds C27, C25 and C25-0140. However, it cannot be excluded that Zincfinger domains of other proteins are targeted including the two Zincfinger motifs within the RBR domain of the E3 ligase HOIP, which is a unique feature of HOIP (Stieglitz et al., 2013; Spratt et al., 2014).

A second explanation for the non-selective effects of the compounds C27 and C25-0140 could be that the compounds target additional protein domains different from TRAF6 within the NF- $\kappa$ B signaling in cells. Due to the fact that IL-1 $\beta$ , LPS and TNF $\alpha$  induced NF- $\kappa$ B activation are reduced to the same extent, it might be conceivable that signaling components are targeted that are used by all three receptor signaling pathways. Upon IL-1 $\beta$ , LPS and TNF $\alpha$  stimulation, reduced phosphorylation and degradation of I $\kappa$ B $\alpha$  was detected after compound treatment. Effects of the compounds in I $\kappa$ B $\alpha$  signaling, nuclear translocation of the NF- $\kappa$ B dimers, its DNA-binding activity as well as transcriptional regulation of target genes can therefore be excluded. Signaling components acting upstream of the phosphorylation of I $\kappa$ B $\alpha$  might be targeted instead. Upon IL-1 $\beta$  stimulation, the activity of the IKK complex was diminished after compound treatment. This implies that the activity of the IKK complex itself is impaired or that signaling events upstream of the IKK complex activation are targeted. This would include the activity of either the LUBAC complex or the TAB/TAK1 complex. Furthermore, it cannot be excluded that the activity of E1 enzymes or E2 complexes within the ubiquitination process are impaired as well. Replacing TRAF6 with the E3 ligase RNF8 in *in vitro* ubiquitination assays could help to analyze the influence on E1 and E2 enzymes.

Altogether, it can be clearly stated that the identified compounds directly target the RZ1 domain of TRAF6 but that other protein domains within the NF- $\kappa$ B signaling cascade might be subjects to compound binding as well.

### **5.5. Targeting the RING-Zincfinger1 domain of TRAF6**

An intact RING-Zincfinger1 domain of TRAF6 is required for the interaction with the E2 enzyme complex Ubc13/Uev1a, its K63-linked auto-ubiquitination and the ability to activate IKK and NF- $\kappa$ B upon stimulation (Lamothe et al., 2008). In order to prevent TRAF6-dependent NF- $\kappa$ B activation multiple possibilities in targeting the TRAF6 RZ1 domain are given. First, the lysine residue 124 (K124) is the critical ubiquitin acceptor site residue that is responsible for TRAF6-auto-ubiquitination. Mutation of this site abrogated TRAF6-mediated NEMO ubiquitination, TAK1 and IKK activity as well as NF- $\kappa$ B activation upon stimulation (Lamothe et al., 2007). However, this mutant is still able to interact with Ubc13 and to form TRAF6 dimers (Yin et al., 2009). Second, the interaction to Ubc13 requires an intact RING-Zincfinger1 domain. Single point mutations within the RING domain including D75K, C70A, I72F abolished the interaction to Ubc13 (Yin et al., 2009). Although the Zincfinger1 domain of TRAF6 is not directly involved in Ubc13 binding, it plays a critical structural role in holding the RING domain in place for binding to Ubc13 (Yin et al., 2009). Third, TRAF6 dimerization is required for the higher-order oligomerization of

TRAF6 to mediate IL-1 $\beta$  induced IKK activation and I $\kappa$ B $\alpha$  phosphorylation (Yin et al., 2009). The TRAF6 dimerization mutants Q82A, R88A, F118A, N121A and E126Q within the RING domain caused a significant reduction of TRAF6 dependent NF- $\kappa$ B activation (Yin et al., 2009; Megas et al., 2011). The TRAF6 dimerization interface lies apart from the Ubc13 interaction site and TRAF6 dimerization mutants were still able to interact with Ubc13 (Yin et al., 2009).

Altogether, it is possible to target multiple residues within the TRAF6 RZ1 domain to prevent NF- $\kappa$ B activation: a) the ubiquitin acceptor side residue K124; b) the Ubc13-interacting residues including D57, C70 and I72; c) the residues of the Zincfinger1 domain of TRAF6 that might cause conformational changes within the RING domain; d) the residues responsible for TRAF6 dimerization including Q82, R88 and F118. All possibilities are depicted in Figure 5.3.

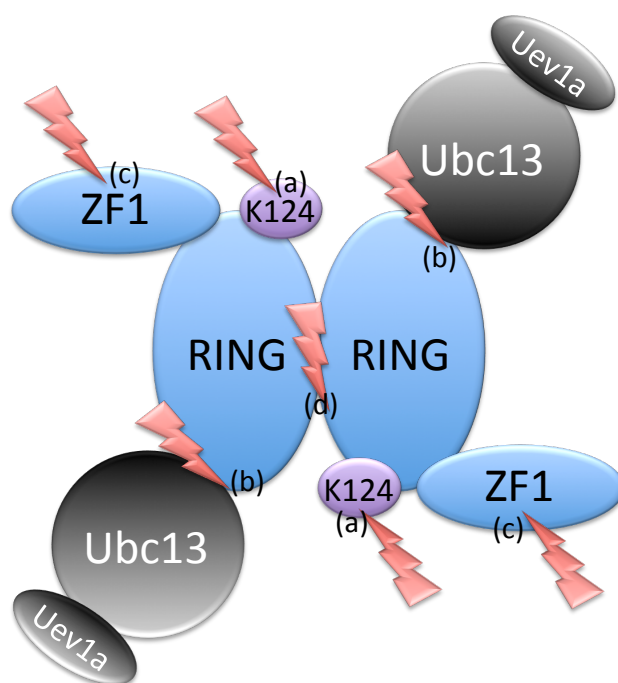


**Figure 5.3. 4 different possibilities to target the RING-Zincfinger1 domain of TRAF6 (blue) to interfere with NF- $\kappa$ B signaling.** Targeting the Lysine 124 residue (K124 in purple) (a) covers the ubiquitin acceptor side for TRAF6 auto-ubiquitination. Binding to the Ubc13-interacting residues (b) prevents interaction to the E2 complex Ubc13/Uev1a. (c) Targeting residues of the Zincfinger1 (ZF1) domain of TRAF6 might cause conformational changes of the RING domain. (d) Binding to the residues that are responsible for TRAF6 dimerization abolished higher-order oligomerization for signal progression.

The compounds C27, C25 and C25-0140 directly bind the TRAF6 RING-Zincfinger1 domain in NMR experiments. Due to a missing assignment of the NMR data of TRAF6, it is not yet possible to define the residues that are targeted by the compounds. Targeting the K124 residue as well as interfering with the dimerization residues by the compounds can be excluded due to the fact that all compounds interrupt the TRAF6-Ubc13 interaction whereas the K124 mutant and the TRAF6 dimerization mutants still exhibit TRAF6-Ubc13 binding. However, one possibility would be that residues within the RING domain that are responsible for Ubc13 binding are targeted resulting in impaired binding to Ubc13. Another option would be that the compounds bind apart from the RING domain in the Zincfinger1 domain leading to a change in structural conformation

of the RING domain and thereby preventing binding to Ubc13. NMR assignments or crystallography will help to identify the exact residues that are targeted by the compounds.

### **5.6 Targeting the TRAF6-Ubc13 interaction for therapeutic intervention**

The interaction of TRAF6-Ubc13 is involved in a variety of signaling pathways like IL-1 $\beta$  and LPS signaling leading to the activation of NF- $\kappa$ B. Retroviral transfection of TRAF6-deficient MEF cell with wildtype TRAF6 rescued TRAF6 auto-ubiquitination as well as signaling towards NF- $\kappa$ B activation whereas the Ubc13 binding mutants could not (Yin et al., 2009). Upregulation of TRAF6-dependent pathways including IL-1 $\beta$  and LPS signaling are a main cause for autoimmune diseases and chronic inflammation. Targeting this binding and therefore abrogating NF- $\kappa$ B mediated inflammation could help to relieve the clinical symptoms.

#### **5.6.1 Targeting TRAF6 in Obesity**

Obesity induced inflammation is an important contributor to the induction of insulin resistance. Free fatty acids are bound by the liver secretory protein FetuinA and target the TLR2/4 receptors leading to chronic inflammatory signaling involving TRAF6 in obesity and diabetes (Pal et al., 2012; Yin et al., 2014). Mice deficient in CD40-TRAF6 signaling did not gain body weight compared to control mice in HFD experiments and showed reduced basal glucose levels as well as improved insulin sensitivity (Chatzigeorgiou et al., 2014). Targeting the MATH domain of TRAF6 with the compound SMI 6860766 to prevent the CD40-TRAF6 interaction did not lead to improved body weight, but to an ameliorated glucose tolerance test although basal levels of glucose and insulin in plasma did not differ among compound and control treated mice. A reduced leukocyte count in the adipose tissues of these individuals led to improved inflammation as well (Van den Berg et al., 2014). As the SMI 6860766 inhibitor was the first small molecule that targets TRAF6 and was tested in a mouse model, C25-0140 was also analyzed in a diet-induced obesity (DIO) mouse model. This not only enabled comparison of the efficiency of the compound identified in this work, but also led to the analysis of the differential effects when targeting the MATH domain or the RING-Zincfinger1 domain of TRAF6. When testing C25-0140 in the DIO mouse model, a significant improvement in body weight was observed. Whereas the gene expression of pro-inflammatory cytokines and NF- $\kappa$ B target genes tend to be reduced, glucose clearance out of the blood could not be improved.

Differences in the mouse studies between testing SMI 6860766 and C25-0140 were bodyweight and time period of the HFD before starting the studies as well as the treatment period. SMI 6860766 treated mice were fed with a HFD for 12 weeks only until reaching an average body

weight of around 33g (Van den Berg et al., 2014). Compared to that, mice that received C25-0140 were set on a HFD for at least one year and exhibited an average bodyweight of 55g. Mice were SMI 6860766 treated for six weeks with a concentration of 10 $\mu$ mol/kg compared to 20 days treatment with 14 $\mu$ mol/kg C25-0140. The application of compounds for 20 days is a standard protocol at the Institute of Diabetes and Obesity at the Helmholtz Zentrum München. The standard protocol for glucose tolerance tests differed between the two groups as well. While SMI 6860766 treated mice were starved for 12 hours and injected with 1mg glucose per gram bodyweight, mice receiving C25-0140 were starved for 6 hours only and then challenged with 1.5mg glucose per gram bodyweight. Comparing the two mouse studies, mice in C25-0140 testing displayed a higher bodyweight and received HFD for a longer period assuming that clinical symptoms like glucose intolerance as well as the grade of chronic inflammation were more elevated in these mice. Therefore, the initial clinical conditions for C25-0140 treatment were severe compared to the SMI 6860766 treatment study. This could be one possible explanation for the only slight improvement of the inflammatory status upon C25-0140 treatment. Also, parameters for pharmacodynamics and pharmacokinetics of 6860766 are not published and toxicokinetics of the compounds cannot be compared. Although the daily applied dose of C25-0140 was higher, these mice were only treated for half of the period of SMI 6860766 treatment. A longer treatment period might have demonstrated a stronger effect of C25-0140 regarding the chronic inflammation. However, Van den Berg et al. obtained enhanced glucose tolerance already after three weeks of SMI 6860766 treatment (Van den Berg et al., 2014). C25-0140 did not ameliorate the glucose clearance out of the blood after 20 days of treatment. Although inflammation parameters in both studies were improved, targeting the RZ1 domain of TRAF6 instead of the MATH domain does not enhance glucose tolerance, but reduces bodyweight instead.

The differential effects obtained upon SMI 6860776 and C25-0140 treatment might also be caused by the distinct mode of action of both compounds. SMI 6860776 targets the C-terminal MATH domain and causes disruption of the interaction to receptors, adaptor proteins and substrates as well as impaired trimerization of the TRAF6 molecules. In contrast, C25-0140 binds to the N-terminal RZ1 domain to prevent interaction to Ubc13, E3 ligase activity and dimerization of TRAF6. Interfering with the functions carried out by the C-terminal domain of TRAF6 might exert different effects than inhibition of the RZ1 domain. This might also be reflected in insulin downstream signaling. Activated insulin-like growth factor-1 (IGF-1) receptor may directly engage TRAF6 activation as ubiquitination of TRAF6 as well as its interaction with the IGF-1 receptor was induced after IGF-1 stimulation (Yang et al., 2009). TRAF6 was found to be a direct E3 ligase for

Akt to mediate Akt ubiquitination, membrane recruitment, phosphorylation at Threonine 308 and enhancing its activity towards GSK3 $\beta$  (Glycogen Synthase Kinase 3 $\beta$ ) upon IGF-1 stimulation leading to the suppression of gluconeogenesis (Yang et al., 2009). Further research of Cheng et al. in 2013 on sensitizing insulin signaling in hepatocytes revealed that TRAF6 is responsible for the K63-linked polyubiquitination of APPL1 (adaptor protein, phosphotyrosine interaction, PH (pleckstrin homology) domain and leucine zipper containing 1) at Lysine 160 upon insulin stimulation (Cheng et al., 2013). Hepatic overexpression of APPL1 enhanced insulin induced phosphorylation of Akt and its downstream substrate GSK3 $\beta$  resulting in a significant reduction of plasma glucose and insulin levels in HFD mice. Such effects were not observed in mice with hepatic overexpression of the APPL1 K160R mutant. Hepatocytes with reduced TRAF6 expression showed impairment in APPL1 ubiquitination, its membrane recruitment as well as phosphorylation of Akt and its downstream substrate GSK3 $\beta$ . As a result, insulin was not able to suppress glucose production anymore due to an increase in mRNA and protein expression of the gluconeogenic genes phosphoenolpyruvate-carboxykinase (PEPCK) and glucose-6-phosphatase (G6Pase) (Cheng et al., 2013). The authors proclaim that TRAF6 is an obligatory signaling component that mediates insulin actions in hepatocytes by promoting ubiquitin dependent membrane targeting of the APPL1-Akt complex. Thereby, suppression of TRAF6 abolishes the insulin sensitizing actions of APPL1. The described insulin sensitizing process strongly depends on the E3 ligase activity of TRAF6. No function of the MATH domain of TRAF6 is described in this signaling so far. Targeting the RZ1 domain of TRAF6 would lead to an abrogation of insulin induced signaling and worsening of the glucose tolerance. This might explain why treatment of obese mice with C25-0140 does not improve glucose clearance out of the blood.



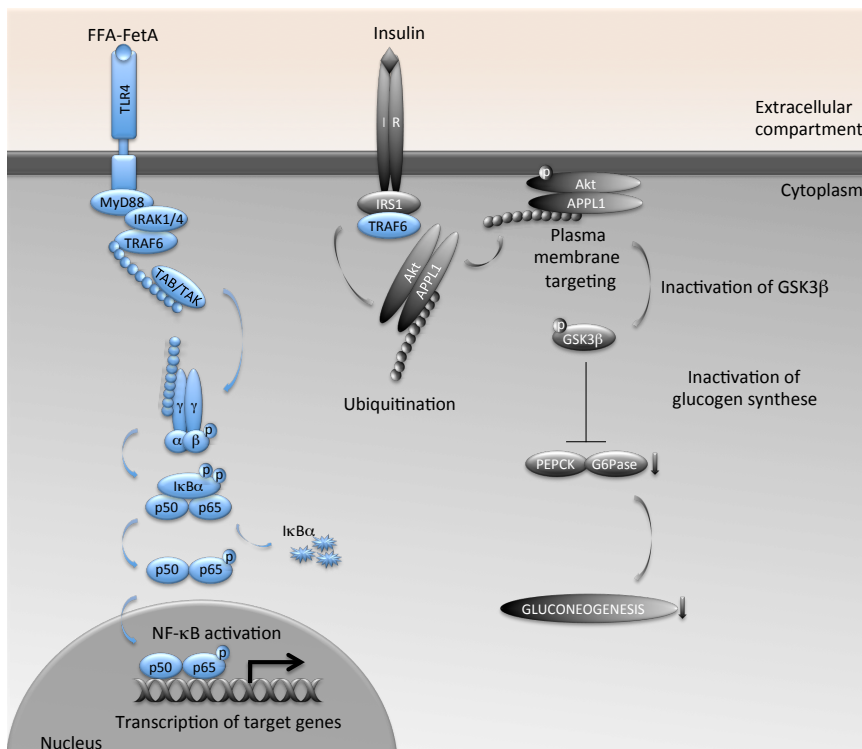


**Figure 5.4: The dual functions of TRAF6 in diet-induced obesity.**

TRAF6 is a major key player in maintaining inflammation of obesity through its involvement in TLR4 signaling leading to elevated NF- $\kappa$ B signaling. Additionally, TRAF6 is required for the insulin sensitizing actions by activating the APPL1-Akt axis after insulin stimulation in order to abrogate gluconeogenesis and initiating glucose uptake and storage.

In general, it appears that the RZ1 domain of TRAF6 plays a dual role in diet-induced obesity. Figure 5.4 illustrates both functions. First, due to its recruitment to the TLR2/4 receptor complex triggered by the free fatty acid – FetuinA ligand, it plays an important role in causing chronic inflammation in diabetic and obese individuals. Here, inhibiting TRAF6 might lead to the desirable effect of lowering inflammation. However, as a second function of the RZ1 domain, TRAF6 is also known as an important key mediator in insulin sensitizing to enhance the suppression of gluconeogenesis via the APPL1-Akt-GSK3 $\beta$  axis. Impairing TRAF6 activity in insulin signaling would induce increased insulin insensitivity and reduced glucose clearance out of the blood.

Surprisingly, Kwon et al. found that IL-13, an anti-inflammatory cytokine, is induced in adipose tissue of obese humans and HFD-mice. Pro-inflammatory cytokines like IL-1 $\beta$  and TNF $\alpha$  mediate IL-13 production in adipocytes in an IKK $\beta$  dependent manner. Adipocyte-specific IKK $\beta$  deletion diminished IL-13 expression and enhanced the production of inflammatory cytokines and infiltration of pro-inflammatory immune cells in adipose tissue resulting in a worsening of the insulin resistant state. The authors proclaim that although IKK $\beta$  activates the expression of pro-inflammatory cytokine, it also induces the production of the anti-inflammatory IL-13 in adipocytes, which counteracts adipose tissue inflammation and insulin resistance. With targeting TRAF6, the activity of IKK $\beta$  might be impaired and therefore IL-13 production together with its anti-inflammatory and glucose lowering effect might be worsened as well. Apparently, the anti-

inflammatory action of IL-13 but not the improvement of glucose clearance could be compensated when inhibiting TRAF6 RZ1.

Considering all the multiple effects of TRAF6 in inflammation and insulin signaling, targeting the RZ1 domain of TRAF6 in diet-induced obesity appears to be a double-edged sword as inflammation will be ameliorated whereas insulin resistance might not be improved. Therefore, further research will be necessary to evaluate the feasibility of targeting TRAF6 RZ1 for the treatment of obesity.

### **5.6.2 Targeting TRAF6 in rheumatoid arthritis**

Single nucleotide polymorphisms (SNPs) studies have linked TRAF6 to autoimmune diseases such as rheumatoid arthritis (RA) (Namjou et al., 2012). RA is a common autoimmune disease associated with systemic inflammation that causes swelling and deformation of the joints including destruction of bones and cartilage. Arthritis in RA develops in four steps. In the induction phase injuries, infections or exposures to toxic substances (smoking) activate the inflammatory cascade leading to infiltration of monocytes/macrophages into the synovium and secretion of pro-inflammatory cytokines like IL-1 $\beta$ , TNF $\alpha$ , IL-17 and IL-10 (Kirkham et al., 2006). The inflammation phase is characterized by presenting the selfantigens and subsequent polyclonal activation of T cells and B cells. Next, the cartilage autoantigens, which are normally not accessible to the immune system, become exposed by damage introducing the self-perpetuation phase. In the last phase, the destruction phase, synovial fibroblasts and osteoclasts are activated by proinflammatory cytokines such as TNF $\alpha$  and IL-6 causing destruction of bone and cartilage. TRAF6 levels were shown to be elevated in the synovium and correlated with synovitis severity leading to the hypothesis that synovial TRAF6 is involved in the pathogenesis of synovial inflammation and osteoclast differentiation (Zhu et al., 2012). Indeed, the RING-Zincfinger1 domain of TRAF6 is integrated into several signaling pathways in RA: i) IL-1 $\beta$  and TLR signaling in immune cells like macrophages, ii) in T cells signaling via the T cell receptor complex, iii) in B cell signaling after CD40 stimulation, iv) IL-17 signaling in immune cells, epithelial cells and fibroblast (Xie, 2013) and v) osteoclast differentiation (Lamothe et al., 2007). Therefore, targeting TRAF6 in RA would not only affect the systemic inflammation but also the destruction of the bones and cartilage. Current therapies against TNF $\alpha$ , IL-1 $\beta$  and IL-6 in addition to T cell and B cell inhibitors have indeed resulted in favorable clinical outcomes in patients with RA (Scheinecker et al., 2008), but ameliorate the systemic inflammation only and do not target the destruction of the bones and cartilage by osteoclasts. A recent study investigating Vitisin A, a resveratrol tetramer found in *Vitis thunbergii*, led to inhibition of osteoclast differentiation and

bone resorption by preventing RANKL induced TRAF6 ubiquitination and TRAF6-TAK1 formation (Chiou et al., 2014). Targeting the TRAF6 ubiquitination appears to be sufficient to impair the destruction process of bones and cartilage in RA. C25-0140 is shown to directly bind TRAF6 and to prevent endogenous TRAF6 auto-ubiquitination in MEF cells after IL-1 $\beta$  stimulation (Figure 4.26). Therefore, targeting TRAF6 with C25-0140 in RA and other autoimmune disorders would specifically interfere with IL-1 $\beta$ , T cell and B cell signaling as well as osteoclast differentiation.

### **5.6.3 Targeting TRAF6 in cancer**

A detailed analysis of lung cancer cell lines and primary tumors identified an amplification of the TRAF6 gene at chromosome 11p13 (Starczynowski et al., 2011). Concomitant with this finding, TRAF6 mRNA was overexpressed in lung cancers. Inhibition of TRAF6 in human lung cancer cell lines led to a reduction in NF- $\kappa$ B activation, cell growth and tumor formation (Starczynowski et al., 2011). Increased levels of TRAF6 expression in human lung adenocarcinoma cells could be confirmed by Zhong et al. in 2012. In osteosarcoma patient samples, TRAF6 mRNA as well as proteins levels were elevated compared to normal bone tissue (Meng et al., 2012). The same group revealed a shift towards G1 phase in cell cycle progression in TRAF6 deficient cells leaving less cells in S and G2 phase (Meng et al., 2012). In addition, they found decreased cell invasion ability and increased apoptotic cell number in TRAF6 depleted cells. These results suggest that TRAF6 might be involved in invasion and metastasis of osteosarcoma. At the same time this implies that a downregulation of TRAF6 might inhibit the proliferation of cancer cells leading to cell cycle arrest in G1 phase. To further unravel the role of TRAF6 in cancer, Sun et al. found that TRAF6 upregulates the expression of the hypoxia-inducible factor (HIF)-1 $\alpha$  independently of oxygen. HIF-1 $\alpha$  protein but not mRNA levels were affected. They found that TRAF6 mediates K63-linked polyubiquitination of HIF-1 $\alpha$  after binding to the protein to promote tumor growth and angiogenesis (Sun et al., 2013). Just recently, the same group detected TRAF6 upregulated in colon cancer in correlation with the tumor grade (Sun et al., 2014). Different from other reports knockdown of TRAF6 did not reduce the survival of colon cancer cells but rather sensitized the cancer cells to the treatment with the conventional anti-cancer drugs 5-fluorouracil and etoposide (Sun et al., 2014).

An increased sensitivity to anti-cancer drugs of cells lacking TRAF6 might also be related to the involvement of TRAF6 in DNA damage response (Hinz et al., 2010). After genotoxic stress, ATM is required for the activation of TRAF6 E3 ubiquitin ligase activity resulting in Ubc13 dependent K63-linked polyubiquitination and cIAP1 recruitment. The ATM-TRAF6-cIAP1 complex mediates TAB2-dependent TAK1 phosphorylation leading to IKK $\gamma$  monoubiquitination at K285 followed by

NF- $\kappa$ B activation (Hinz et al., 2010). Upon DNA damage, the E3 ligase activity of TRAF6 is required not only to promote TRAF-mediated polyubiquitination in conjunction with Ubc13, but also to catalyze the monoubiquitination of IKK $\gamma$  (Hinz et al., 2010). As C25-0140 directly interferes with the TRAF6 E3 ligase activity in MEF cells upon IL-1 $\beta$  stimulation, inhibitory effects on NF- $\kappa$ B activation and cancer cell proliferation upon genotoxic stress are anticipated. As mentioned, TRAF6 protein levels are upregulated in various cancer samples and were associated with invasion and metastasis of the tumors as well as increasing the sensitivity to anti-cancer treatment. Targeting the RING-Zincfinger1 domain of TRAF6 might not only impair NF- $\kappa$ B signaling induced by anti-cancer drugs, but would also hold these cells back in G1 phase to stop cancer proliferation and increase the sensitivity against anti-cancer drug treatment. Therefore, interfering with TRAF6 N-terminal dependent signaling during cancer treatment might be promising.

Elevated NF- $\kappa$ B activation in cancer cells provide a survival mechanism by upregulating anti-apoptotic genes resulting in drug and treatment resistance. For example, the induction of NF- $\kappa$ B activation by radiotherapy induced DNA damage response is one of the main causes for cancer cells to evade this therapy (Kozakai et al., 2012). These resistances might be mediated through by the ATM-TRAF6-cIAP1 axis. A combination of NF- $\kappa$ B inactivation and radiotherapy could facilitate the overcome of radio-resistant responses and may become a new therapeutic option for treating cancer as it could be already proved for prostate cancer (Kozakai et al., 2012). Further combination studies of chemotherapeutic reagents (glucocorticoid Dexamethason) and NF- $\kappa$ B targeting drugs (proteasome inhibitor Bortezomib) confirmed the increased cytotoxicity in multiple myeloma cells (Salem et al., 2013). Although inhibiting NF- $\kappa$ B during cancer treatment so far appears to be successful, cancer cells acquire resistance to the drug (for example Bortezomib) limiting its efficacy (Lü and Wang, 2013). Therefore, the need for drugs affecting new targets like TRAF6 within NF- $\kappa$ B signaling is given. Activation of NF- $\kappa$ B upon genotoxic stress depends on the E3 ligase activity of TRAF6 (Hinz et al., 2010). C25-0140 directly targets the RZ1 domain of TRAF6 and caused impaired NF- $\kappa$ B activation. Treatment with C25-0140 would probably reduce NF- $\kappa$ B activation accompanied with induced cell death of cancer cells. This strategy could help to develop new NF- $\kappa$ B inhibitors and to counteract the problems drug resistance.

## 6 Outlook

All investigated compounds directly target the RING-Zincfinger1 domain of the E3 ligase TRAF6. In stimulation experiments, the compounds C27 and C25-0140 cause a non-pathway selective inhibition of NF- $\kappa$ B activation. Further experiments upstream of the phosphorylation of I $\kappa$ B $\alpha$  in IL1- $\beta$ /LPS and TNF $\alpha$  induced signaling will be necessary to identify additional targets of the compounds C27 and C25-0140. For example, chemical proteomics approaches might identify further proteins that are bound by these compounds. This will help to define the mode of action of these compounds and will be basis for further research to unravel the strong inhibitory effects towards NF- $\kappa$ B signaling.

Although the interaction of TRAF6-Ubc13 displays several advantages for targeting a protein-protein-interaction, it appears to be difficult to target this binding specifically. Therefore, another important focus will be to improve the selectivity and efficacy of C25-0140. Crystallography studies or NMR assignments need to be performed to define the exact residues that are targeted by the compounds. This will be basis for further analog design to increase specificity and reduce potential side effects as well as to improve the efficacy of the compounds. Crystallography experiments have been initiated already and growth of crystals is obtained but need to be further improved.

In the diet induced obesity mouse study, C25-0140 reduced body weight gain but no improvement in glucose tolerance. It will be necessary to identify the mechanism behind the effect on weight gain upon compound treatment. First experiments could be expression profiling of genes involved in fatty acid or carbohydrate metabolism. It will also be interesting to further analyze the differential effects of the N-terminal and C-terminal domains of TRAF6 in obesity.

TRAF6 is upregulated in diseases that exhibit chronic NF- $\kappa$ B signaling including autoimmune diseases and various cancers. Inhibition of the TRAF6 auto-ubiquitination is shown to reduce NF- $\kappa$ B activation as well as osteoclast differentiation and bone resorption activity (Chiou et al., 2014). A mouse model for RA will therefore be considered for testing C25-0140 (or improved chemical analogs) to relieve the clinical symptoms of this autoimmune disease. In a cancer mouse model like osteosarcoma, C25-0140 should be analyzed as well as it might sensitize cancer cells to chemotherapeutic induced apoptosis. Also, a combinatorial therapy of C25-0140 and other inhibitors of NF- $\kappa$ B for potential synergistic effects should be taken into account.

## 7. Material and Methods

### 7.1 Material

#### 7.1.1 Instruments and Equipment

Instrument / Equipment	Company
Agarose gel chambers	Neolab, Munich
Amersham Hyperfilm ECL	GE Healthcare, Munich
Amicons cut off 3kD; 5mL, 15mL,	Millipore, Schwabach
ÄKTA purifier	GE Healthcare, Munich
Bacteria culture flasks	Schott, Zwiesel
Bacteria incubators	Sartorius, Göttingen; Memmert, Schwabach
Centrifuges	
Beckmann Avanti J-26 XP (rotors: JA-10; JA 25.5; JS5.3)	Beckmann Coulter, Krefeld
Cooling centrifuge cell culture 5810R	Eppendorf, Hamburg
Cooling lab centrifuge 5417R	Eppendorf, Hamburg
Centrifuge bottles 500mL, 50mL	Beckmann Coulter, Krefeld
Cell counting chambers	Neolab, Munich
Cell culture flasks/dishes	BD, Heidelberg; Nunc
Cell scraper	Sarstedt, Newton in USA
CO <sub>2</sub> incubator	Binder, Tuttlingen
Cover foil qPCR	4titude, Berlin
Cover foil 384-well opti and proxiplates	LVL Technologies, Crailsheim
Cryo vials	Greiner, Frickenhausen
Cuvettes	Brand, Wertheim
Cyclone 3G working station	Perkin Elmer, Wiesbaden
Developer Optimax typ TR	MS Laboratory instruments, Wiesloch
EMSA gel chamber	Roth, Karlsruhe
Envision plate reader	Perkin Elmer, Wiesbaden
Eppendorf tubes 1.5mL, 2mL	Eppendorf, Hamburg
Falcon tubes 15mL, 50mL	Neolab, Munich
FlexDrop	Perkin Elmer, Wiesbaden

Fridge and freezers (-20°, -80°C)	Liebherr, Ochsenhausen
Fuji medical x-ray film	Kisker Biotech, Steinfurt
Glass bottle 1L, 500mL, 250mL	Schott, Zwiesel
Gel dryer	Biorad, Hercules, USA
HiTrap Desalting column 5mL	GE Healthcare, Munich
Light Cycler 480	Roche Diagnostics, Mannheim
Light Cycler 96 well plates	4titude, Berlin
Magnetic stirrer	IKA Labortechnik, Staufen
Microwave	SHARP, Hamburg
Nanodrop	Thermo Scientific, Rockford in USA
Operetta	Perkin Elmer, Wiesbaden
Pipettes (5000µL, 1000µL, 200µL, 100µL, 20µL, 10µL, 2.5µL)	Eppendorf, Hamburg
Pipette tips	Eppendorf, Hamburg
Plastic pipettes (50mL, 25mL, 10mL, 5mL, 2mL)	Greiner Bio-one, Kremsmünster in Austria
Petri dishes	Greiner Bio-one, Kremsmünster in Austria
pH meter	Hanna Instruments, Ann Arbor in USA
Photometer	Eppendorf, Hamburg
RNAse-free tips	StarLab, Hamburg
Rotator	Neolab, Munich
Power supply	Consort, Turnhout in Belgium
PVDF-membran	Millipore, Schwabach
Scalpel	B. Braun, Melsungen
Sciclone G3	Perkin Elmer, Wiesbaden
SDS-PAGE gel chamber	PHASE, Lübeck
Semi-dry blotter	Roth, Karlsruhe
Sonifier U9200S	Hielscher Ultrasonics, Teltow
Superdex 75 100/300GL	GE Healthcare, Munich
Superdex 75 HiLoad 16/600	GE Healthcare, Munich
StrepTrap HP column 1mL	GE Healthcare, Munich
Syringe 26G	B. Braun, Melsungen
Tissue culture hoods	Nunc - Thermo Scientific, Rockford, USA

Thermocycler	Eppendorf, Hamburg
Ultrasonic bath SONOREX RK 103	Bandelin, Berlin
UV-table	Herolab, Wiesloch
Vortexer	Scientific industries, Bohemia in USA
Whatman paper	Whatman, Dassel
Water-jet vacuum pump	Schott, Zwiesel
384 opti plates	Perkin Elmer, Wiesbaden
384 proxi plates	Perkin Elmer, Wiesbaden
Greiner 384 µclear plates	Sigma-Aldrich, Taufkirchen

### 7.1.2 Chemicals

Acrylamid/Bisacrylamid	Roth, Karlsruhe
Adenosin-tri-phosphate, ATP	Sigma-Aldrich, Taufkirchen
[ <sup>32</sup> P]-α-ATP, 10mCi/mL	Perkin Elmer, Wiesbaden
[ <sup>32</sup> P]- γ-ATP, 10mCi/mL	Perkin Elmer, Wiesbaden
Agarose	Biozym, Hessisch Oldendorf
Amino acids for <i>S. cerevisiae</i> plates (Try, His, Leu, Phe, Glu, Asp, Val, Thr, Ser)	Roth, Karlsruhe
Ammonium persulfate, APS	BioRad, Munich
Ampicillin	Roth, Karlsruhe
Ammonium chloride	Roth, Karlsruhe
Ammonium – N15 chloride	Sigma-Aldrich, Taufkirchen
Anhydrotetracycline ATC	IBA, Goettingen
Antibiotics (eukaryotic cell culture)	Life Technologies, Darmstadt
β-Glycerophosphate	Sigma-Aldrich, Taufkirchen
Biotin	Sigma-Aldrich, Taufkirchen
Bovine Serum Albumin (BSA)	Sigma-Aldrich, Taufkirchen
Bovine Serum Albumin (BSA)	PAA, Pasching in Austria
Bovine Serum Albumin (BSA) 10mg/mL	New England Biolab, Frankfurt
Boric acid	Roth, Karlsruhe
Bradford reagent	BioRad, Munich



Calciumchloride-Dihydrate	Roth, Karlsruhe
Chloramphenicol	Roth, Karlsruhe
Cobalt(II)Chloride-Hexahydrate	Roth, Karlsruhe
Coomassie Brilliant Blue R250	Roth, Karlsruhe
Copper(II)Chloride-Dihydrate	Roth, Karlsruhe
Creatine phosphate	Sigma-Aldrich, Taufkirchen
Dulbecco's Modified Eagle Medium (DMEM)	Life Technologies, Darmstadt
Dimethylsulfoxid DMSO D6	Sigma-Aldrich, Taufkirchen
dNTPs	Fermentas, St. Leon-Roth
Dithiothreitol DTT	Sigma-Aldrich, Taufkirchen
Ethylenediaminetetraacetic acid EDTA	Roth, Karlsruhe
Ethanol p.a.	Merck, Darmstadt
Ethidiumbromide	Roth, Karlsruhe
Fetal calf serum (FCS)	Life Technologies, Darmstadt
Ficoll 400	Roth, Karlsruhe
Glucose $\alpha$ -Monohydrat	Roth, Karlsruhe
Glutathione, reduced	Sigma-Aldrich, Taufkirchen
Glutathione Sepharose 4B	VWR, Darmstadt
Glutathione Sepharose 4 fast flow	VWR, Darmstadt
Glycerin	Roth, Karlsruhe
HEPES	Roth, Karlsruhe
Hoechst33342	Life Technologies, Darmstadt
Human TNF $\alpha$	Biomol, Hamburg
IRAK1/4 inhibitor I5409	Sigma-Aldrich, Taufkirchen
Isopropyl- $\beta$ -D-thiogalactoside (IPTG)	Fermentas, St. Leon-Roth
Isopropanol p.a.	Merck, Darmstadt
LB-agar	Roth, Karlsruhe
LB-medium	Roth, Karlsruhe
Lipopolysaccharide	Sigma-Aldrich, Taufkirchen
Lithiumacetate	Roth, Karlsruhe
Magnesium chloride	Roth, Karlsruhe
Magnesiumsulfate Heptahydrate	Sigma-Aldrich, Taufkirchen

Mangan(II)Chloride-Tetrahydrate	Roth, Karlsruhe
Mitotracker Deep Red FM	Life Technologies, Darmstadt
Murine IL-1 $\beta$	Pepro-Tech, Hamburg
NP-40 (Nonidet P40 Substitute)	Sigma-Aldrich, Taufkirchen
Penicillin Streptomycin	Life Technologies, Darmstadt
Phosphate buffered saline PBS 10x	Applichem, Darmstadt
Potassium chloride	Roth, Karlsruhe
Potassium hydrogen phosphate (KH <sub>2</sub> PO <sub>4</sub> )	Roth, Karlsruhe
Poly-(d(I-C))	Roche Diagnostics, Mannheim
Protease/Phosphatase-inhibitor RocheComplete	Roche Diagnostics, Mannheim
Prestained Protein Marker (Page Ruler)	Fermentas, St. Leon-Roth
Protein-G-Sepharose 4 fast flow	GE Healthcare, Munich
Roswell Park Memorial Institute RPMI	Life Technologies, Darmstadt
Roti-load 4xSDS loading buffer	Roth, Karlsruhe
Rotisolon B	Roth, Karlsruhe
SOC outgrowth medium	New England Biolabs, Frankfurt
Sodium citrate	Roth, Karlsruhe
Sodium chloride NaCl	Roth, Karlsruhe
Disodium phosphate (Na <sub>2</sub> HPO <sub>4</sub> -Dihydrate)	Roth, Karlsruhe
Sodium dodecyl sulfate SDS	Roth, Karlsruhe
Sodium fluoride NaF	Sigma-Aldrich, Taufkirchen
Sodium hydroxide NaOH	Roth, Karlsruhe
Sodium (meta) vanadate	Sigma-Aldrich, Taufkirchen
Strep Elution buffer	IBA, Goettingen
Tetramethylethylenediamine TEMED	BioRad, Munich
Thrombin protease	GE Healthcare, Munich
Thiamine Hydrochloride	Sigma-Aldrich, Taufkirchen
Tris	Roth, Karlsruhe
Triton-X100	Roth, Karlsruhe

Trypsin/EDTA	Life technologies, Darmstadt
Tween-20	Roth, Karlsruhe
Tween-80	Sigma-Aldrich, Taufkirchen
Yeast nitrogen base (Difco)	Roth, Karlsruhe
Zinc chloride ZnCl <sub>2</sub>	Sigma-Aldrich, Taufkirchen
2-log DNA ladder	New England Biolabs, Frankfurt

### 7.1.3 Antibodies

Primary Antibody	Dilution in Western Blot	Company
β-Actin I-19	1:1 000	Santa Cruz, Heidelberg
Flag M2	immunoprecipitation	Sigma, Taufkirchen
IκBα C21	1:1 000	Santa Cruz, Heidelberg
p-IκBα Ser32/36 5A5	1:1 000	Cell Signaling, Leiden in Belgium
IKKγ FL419	immunoprecipitation	Santa Cruz, Heidelberg
IKKγ 1.T.26	1:500	Santa Cruz, Heidelberg
p65 C-20	immunofluorescence 1:250	Santa Cruz, Heidelberg
TRAF6 EP591Y	1:2 000	Abcam, Cambridge in England
Ubc13 4919	1:1 000	Cell Signaling
Ubiquitin P4D1	1:1 000	Santa Cruz, Heidelberg
Secondary antibody	Dilution in Western Blot	Company
Anti-Goat	1:7 500	Dianova, Hamburg
Anti-Mouse	1:7 500	Dianova, Hamburg
Anti-Rabbit	1:7 500	Dianova, Hamburg
Anti-Rat	1:7 500	Dianova, Hamburg
Fluorescein Goat Anti Rabbit	1:400	Life Technologies, Darmstadt

### 7.1.4 Enzymes and Kits

Enzyme / Kit	Company
Alkaline Phosphatase CIP	New England Biolabs, Frankfurt
ALPHAScreen Protein A IgG Kit	Perkin Elmer, Wiesbaden

Bradford reagent	BioRad, Munich
CellTiter-Blue Kit	Promega, Mannheim
Expand-High-Fidelity Kit	Roche Diagnostics, Mannheim
Gel extraction Kit	Qiagen, Hilden
Glutathione ALPHA Donor beads	Perkin Elmer, Wiesbaden
Klenow fragment 5,000U/mL	Fermentas, St. Leon-Roth
LumiGlo reagent 20x	Cell signaling, Frankfurt
KAPA SYBR Fast qPCR Kit (optimized for LC480)	VWR, Darmstadt
Nickel-Chelate ALPHA Acceptor beads	Perkin Elmer, Wiesbaden
Nucleo Spin Plasmid Kit	Macherey-Nagel, Düren
p-I $\kappa$ B $\alpha$ (Ser32/36) ALPHASurefire Kit	Perkin Elmer, Wiesbaden
QiaQuick Nucleotide removal kit	Qiagen, Hilden
Silver Stain Kit	Pierce, Rockford in USA
Rapid DNA ligation Kit	Roche Diagnostics, Mannheim
RNeasy Kit	Qiagen, Hilden
RQ1 RNase-free DNaseI	Promega, Mannheim
Shredder Kit	Qiagen, Hilden
SuperScript III First Strand cDNA Synthesis System for RT-PCR	Life Technologies, Darmstadt
Strep-Tactin <sup>®</sup> ALPHA Donor bead	Perkin Elmer, Wiesbaden
Total I $\kappa$ B $\alpha$ ALPHASurefire Kit	Perkin Elmer, Wiesbaden
TRIzol <sup>®</sup> reagent	Life Technologies, Darmstadt
Restriction endonucleases (BamHI, EcoRI, NcoI, NotI, PstI, SacII)	New England Biolabs, Frankfurt

### 7.1.5 Bacteria strains

BL21 Codon Plus(DE3) RIPL

strain for protein production from Agilent Technologies, Waldbronn

TOP10 E.coli

(F-mcrA ( $\Delta$  mrr-hsdRMS-mcrBC)  $\Phi$ 80lacZ  $\Delta$ M15  $\Delta$ lacX74 nupG recA1 araD139  $\Delta$ (ara-leu)7697 galE15 galK16 rpsL (strR)end A1 $\lambda$ -); Research Unit Cellular Signal Integration, Prof. Krappmann, Helmholtz Zentrum München

**7.1.6 Eukaryotic cell lines**

MEF	Mouse Embryonic fibroblast cells
MEF TRAF6 <sup>-/-</sup>	TRAF6 knockout MEF cells, obtained from Claus Scheidereit at the Max-Delbrück-Centrum, Berlin
HeLa	Henriette Lacks cells, derived from cervical cancer
HepG2	human liver carcinoma cell line

**7.1.7 Mouse strains**

C57BL/6 J	a laboratory mice strain, mice were fed an high-fat-diet to generate diet-induced obesity mice
-----------	--

**7.1.8 Recombinant proteins**

Recombinant protein	Company
E1-activating enzyme (UBC1)	Boston Biochem, Chambridge in USA
E2-conjugating enzyme complex (rhHis6-Ubc13/Uev1a)	Boston Biochem, Chambridge in USA
GST-IκBα (AA 1-73)	Affinity-purified from E.coli from Krappmann Group
Inorganic pyrophosphatase E.coli	RayBiotech, Norcross in USA
Creatine phosphokinase	Sigma-Aldrich, Taufkirchen
Human recombinant Ubiquitin	Boston Biochem, Cambridge in USA

**7.1.9 Vectors and generated plasmids**

Empty vector	Description
pASK-IBA3plus	Bacterial protein expression vector tagging the protein with a C-terminal StrepII-tag; restriction sites NcoI and SacII were used for cloning; vector provided by IBA GmbH, Göttingen
pGex 4T1	Bacterial vector for expression of GST-fusion proteins with thrombin site; DNA sequences were introduced via the restriction sites BamHI and NotI; empty vector from GE Healthcare, Munich
pGAD-C(x)	Yeast-two-hybrid “prey” vector for fusing a gene

	to the GAL4 activation domain, EcoRI and PstI restriction sites were used for cloning
pGBD-C(x)	Yeast-two-hybrid “bait” vector for fusing a gene to the GAL4 binding domain; for cloning, EcoRI and PstI restriction sites were used
<b>Generated plasmids</b>	
TRAF6 <sub>WT</sub> StreptII	in pASK-IBA 3 plus vector
TRAF6 <sub>C70A</sub> StreptII	in pASK-IBA 3 plus vector
TRAF6 <sub>D57K</sub> StreptII	in pASK-IBA 3 plus vector
TRAF6 <sub>I72F</sub> StreptII	in pASK-IBA 3 plus vector
GST-TRAF6 <sub>WT</sub>	in pGex 4T1 vector
Ubc13FlagHis	in pGex 4T1 vector, generated by Dr. Kenji Schorpp
GST-OTUB1	in pGex 4T1 vector, generated by Dr. Kenji Schorpp
GST-RNF8	in pGex 4T1 vector, generated by Elisabeth Weber
TRAF6 fulllength	in pGAD-C1 vector
TRAF6 RING-Zincfinger1 (RZ1) WT	in pGAD-C1 vector
TRAF6 RZ1 C70A	in pGAD-C1 vector
TRAF6 RZ1 D57K	in pGAD-C1 vector
TRAF6 RZ1 I72F	in pGAD-C1 vector
TRAF6 Coiled Coil	in pGAD-C1 vector
TRAF6 Coiled-Coil – MATH	in pGAD-C1 vector
Ubc13 fulllength	in pGBD-C1 vector

#### 7.1.10 Oligonucleotides

qPCR oligonucleotides	Sequence
A20 for	5' GCT CAA CTG GTG TCG TGA AG 3'
A20 rev	5' ATG AGG CAG TTT CCA TCA CC 3'
β-Actin for	5' CCT CTA TGC CAA CAC AGT GC 3'

$\beta$ -Actin rev	5' GTA CTC CTG CTT GCT GAT CC 3'
ICAM-1 for	5' CGC TCA GAA GAA CCA CCT TC 3'
ICAM-1 rev	5' GGA GAC GCA GAG GAC CTT AAC 3'
I $\kappa$ B $\alpha$ for	5' TTG CTG AGG CAC TTC TGA AAG 3'
I $\kappa$ B $\alpha$ rev	5' TCT GCG TCA AGA CTG CTA CAC T 3'
IL-1 $\beta$ for	5' TCA GCA CCT CAC AAG CAG AG 3'
IL-1 $\beta$ rev	5' GCC CAT ACT TTA GGA AGA CAC G 3'
IL-2 for	5' GAG TGC CAA TTC GAT GAT GAG 3'
IL-2 rev	5' AGG GCT TGT TGA GAT GAT GC 3'
IL-6 for	5' ACC ACG GCC TTC CCT ACT TC 3'
IL-6 rev	5' CTC ATT TCC ACG ATT TCC CAG 3'
TNF $\alpha$ for	5' CCA CCA TCA AGG ACT CAA ATG 3'
TNF $\alpha$ rev	5' GAG ACA GAG GCA ACC TGA CC 3'
VCAM for	5' CCC CTC ATT CCT TAC CAC CC 3'
VCAM rev	5' AGT TGG GGA TTC GGT TGT TCT 3'
EMSA oligonucleotides	
NF- $\kappa$ B	5' GAT CCA GGG CTG GGG ATT CCC CAT CTC CAC AGG 3' 5' GAT CCC TGT GGA GAT GGG GAA TCC CCA GCC CTG 3'
Oct-1	5' GAT CTG TCG AAT GCA AAT CAC TAG AA 3' 5' GAT CTT CTA GTG ATT TGC ATT CGA CA 3'

#### 7.1.11 Buffers

Buffer	Composition
ALPHAScreen buffer	1xPBS; 0.5% BSA, 0.01% Tween-20
Blocking buffer	3% BSA (PAA) in PBS-Tween20 (0.1%)
10x Blotting buffer	48mM Tris; 39mM Glycine; 0.037% SDS; 20% Methanol
CoIP-wash buffer	150mM NaCl; 25mM Hepes (pH 7.5); 0.2% NP-40; 1mM Glycerol
CoIP-lysis buffer	CoIP-wash buffer; 10mM NaF; 8mM $\beta$ -Glycerophosphat; 1mM DTT; 300 $\mu$ M Sodium-vanadate; complete protease inhibitor

1% SDS-CoIP-lysis buffer	CoIP-lysis buffer; 1% SDS
EMSA-annealing buffer	50mM Tris-HCl, pH 8; 70mM NaCl; 5mM dNTP-A;
EMSA-2xshift buffer	40mM HEPES pH7.9; 120mM KCl; 8% Ficoll;
High-salt-lysis buffer	20mM HEPES PH7.9; 350mM NaCl; 1mM MgCl <sub>2</sub> ; 0.5mM EDTA; 0.1mM EGTA; 20% Glycerol; 1% NP-40; 10mM NaF; 8mM $\beta$ -Glycerophosphate; 1mM DTT; 300 $\mu$ M Sodium-vanadate; Complete protease inhibitor
Kinase buffer	20 $\mu$ M HEPES pH7.9; 10mM MgCl <sub>2</sub> ; 20 $\mu$ M ATP; 20mM $\beta$ -Glycerophosphat; 200 $\mu$ M Sodium-Vanadate; 1mM DTT
10x K63 assay buffer	250nM Tris-HCl pH 7.6; 25mM MgCl <sub>2</sub> ; 50mM creatine phosphate; 3U/mL inorganic pyrophosphatase; 3U/mL creatine phosphokinase
<sup>15</sup> N-labeled M9 mineral medium	1x <sup>15</sup> N-labeled M9 salt solution; 0.40% Glucose; 1mM MgCl <sub>2</sub> ; 0.3mM CaCl <sub>2</sub> ; 1 $\mu$ g/mL Biotin; 1 $\mu$ g/mL Thiamine, 1x Trace element solution
<sup>15</sup> N-labeled M9 salt solution (10x)	337mM Na <sub>2</sub> HPO <sub>4</sub> *2H <sub>2</sub> O; 220mM KH <sub>2</sub> PO <sub>4</sub> ; 85.5mM NaCl; 935 <sup>15</sup> NH <sub>4</sub> Cl
GST-Wash buffer	1xPBS; 400mM NaCl; 1mM DTT
Pulldown buffer	1xPBS; 5% Glycerin; 1% Triton-X100
PEG medium for <i>S. cerevisiae</i>	100mM Lithiumacetate; 10mM Tris-HCl, pH 8.0; 1mM EDTA, pH 8.0; 40% (w/v) PEG-3350
RIPA buffer	150mM NaCl; 1% NP-40; 0.5% Sodium-deoxycholate; 0.1% SDS; 50mM Tris-HCl pH 8.0; Complete protease inhibitor
<i>S. cerevisiae</i> plates	0.67% yeast nitrogen base (Difco); 0.2% drop out amino acid mix, 2% glucose; 2% agar Drop out amino acid mix: 20mg Try, His; 30mg Leu; 50mg Phe; 100mg Glu, Asp; 150mg Val; 200mg Thr; 400mg Ser;
10x SDS buffer	250mM Tris; 2M Glycine; 1% SDS
Separation gel buffer (5x)	1.88mM Tris-HCl (pH 8.8)



Separation gel	375mM Tris-HCl pH 8.8; 10-12.5% Acrylamide; 0.1% SDS; 0.075% APS; 0.05% TEMED
Stacking gel buffer (4x)	0.5M Tris-HCl pH 6.8
Stacking gel	125mM Tris-HCl pH 6.8; 5% Acrylamide; 0.1% SDS, 0.1% APS; 0.1% TEMED
TRAF6-wash buffer	100mM Tris-HCl pH8.0; 20mM NaCl
Stripping buffer	200mM Glycine; 0.1% SDS; 1% Tween-20; pH 2.2
20x TBE buffer	1M Tris; 1M Boric Acid; 20mM EDTA; pH 8.3
Trace Element solution (100x)	13.4mM EDTA; 3.1mM FeCl <sub>3</sub> *6H <sub>2</sub> O; 0.62mM ZnCl <sub>2</sub> ; 76μM CuCl <sub>2</sub> *2xH <sub>2</sub> O; 42μM CoCl <sub>2</sub> *6xH <sub>2</sub> O; 162μM H <sub>3</sub> BO <sub>3</sub> ; 8.1μM MnCl <sub>2</sub> *4H <sub>2</sub> O;
TRAF6 storage buffer	20mM Tris-HCl pH 8.0; 20mM NaCl; 100μM ZnCl <sub>2</sub> ; 5ml DTT
TRAF6 desalting buffer	2mM Tris-HCl pH 8.0; 20mM NaCl; 100μM ZnCl <sub>2</sub> ; 1mM DTT

### 7.1.12 Software

Software	Company
Adobe software CS5	Adobe Systems incorporated, San Jose` in USA
CLC sequence viewer	Qiagen, Hilden
Gene construction kit	Textco BioSoftware, Raleigh in USA
Harmony	Perkin Elmer,
LabImage 1D	Kapelan, Leipzig
Microsoft office 2011	Microsoft, Redmond in USA
Nanodrop 2000 Software	Thermo Scientific, Rockford in USA
PRISM 6	GraphPad Software, La Jolla in USA

### 7.1.13 Screening libraries and small molecules

For High-Throughput-Screening, a chemoinformatic expert at the Helmholtz Zentrum München designed three diversity libraries. Selection criteria for each compound were:

- i) a molecular weight less than 600g/mol,
- ii) suitable logS/logP values for good solubility,
- iii) meeting the criteria of the Lipinski's rule of five,

- a. not more than five hydrogen bond donors
- b. not more than 10 hydrogen bond acceptors
- c. the molecular weight should not exceed 500g/mol
- d. LogP value is less than five
- iv) over 90% purity,
- v) pass the filters to exclude compounds
  - a. that exhibit reactive, unstable and toxic chemical groups,
  - b. which chemotypes cause acute or chronic toxicity
  - c. that are trivial compounds and already present in commercial available libraries

The goal was to have diverse chemical structures within one library and among the three libraries. Three in-house libraries were designed considering the listed criteria and ordered at the respective company: ChemDIV (10,000 compounds), Enamine (10,000 small molecules) and ChemBridge (5,000 compounds).

For reordering the hit compounds, compounds were reordered from the respective companies:

Compound number	Library
Compounds 1-11	ChemBridge
Compounds 12-19	ENAMINE
Compounds 20-27	ChemDIV

Compounds were reordered at a powder stock and were dissolved to a concentration of 20mM in DMSO D6. If necessary, the compound solution was ultrasonic-treated for 30 seconds. Aliquots were frozen at -20°C.

ADME studies for C27 and C25-0140 were conducted by Bienta, ENAMINE Ltd.

## 7.2 Methods

### 7.2.1 Molecular biological methods

#### 7.2.1.1 Polymerase chain reaction (PCR)

For cloning genes into various vectors, the DNA sequences of TRAF6, Ubc13, OTUB1 and RNF8 were amplified from complementary DNA (cDNA) (synthesis see 7.2.1.8) using Polymerase chain reaction (PCR). Therefore, PCR was performed using the *Expand High Fidelity* Kit (Roche) including:

- 5µL 10x Expand High Fidelity buffer
- 1µL dNTPs (10mM each)
- 1µL of forward and reverse primer (20µM each)
- 100ng cDNA
- 1µL DNA polymerase (Expand High Fidelity Mix)
- ad 50µL H<sub>2</sub>O

The following PCR-program was set up:

Step	Temperature	Time	Cycles
Initial denaturation	95°C	5min	1
Denaturation	95°C	30sec	30
Annealing	65°C	30sec	30
Elongation	72°C	30sec-3mins (30sec per 500basepairs)	30
Final elongation	72°C	7mins	1
Cooling	4°C	∞	1

**Table 7.1:** PCR-program to generate PCR amplicates for cloning

For mutagenesis, primer carrying the mutation were applied to the PCR mix and thereby introduced the mutation to the new PCR product.

#### 7.2.1.2 Agarose Gel Electrophoresis and DNA extraction from gel

For the separation of linearized DNA, samples (PCR product or restriction digest probes) were mixed with 6x loading dye and loaded on an agarose gel (1.5% agarose dissolved in 1xTBE and 0.2µg/mL Ethidiumbromide). For size control, the 2-Log DNA ladder was loaded as well. Gels were run in 1xTBE buffer applying 8 V/cm gel. PCR fragments stained with Ethidiumbromide were visualized by UV-excitation and cut out with a scalpel. The extraction of the DNA from the gel was performed according to the Qiagen *Gel Extraction* Kit protocol and eluted in 50µL autoclaved H<sub>2</sub>O. The purified DNA was further used for restriction digest followed by ligation.

### **7.2.1.3 Restriction digest**

PCR products as well as plasmids were digested using restriction enzymes and buffers from New England Biolabs. After 2 hours at the appropriate incubation temperature, 1µL CIP was added to the vector samples for 30 min at 37°C to dephosphorylate the vector ends to prevent re-ligation. Samples were separated by agarose gel electrophoresis and purified from the gel.

### **7.2.1.4 Ligation**

The purified and restricted DNA samples were ligated using the *Rapid DNA Ligation Kit* following the manufacturer's protocol. A ratio of vector: insert = 1:3 was chosen for optimal ligation results.

### **7.2.1.5 Transformation of bacteria cells**

For transformation, the entire ligation mix or up to 500ng plasmid were added to the respective bacteria strain and incubated on ice for 30mins. Heat-shock was performed at 42°C for 45 seconds followed by cooling the cells on ice for 2 minutes. After adding 800µL SOC-medium to the cells, the suspension was incubated at 37°C for 1 hour at 900rpm. Subsequently, the bacteria were plated on LB-agar plates containing the respective antibiotics and incubated for 18 hours at 37°C.

### **7.2.1.6 Plasmid preparation**

For analytical plasmids preparation, a single bacteria colony was inoculated in 5mL LB-medium containing the respective antibiotics and grown for 16 hours at 37°C and 180rpm. Plasmid DNA was isolated following the *NucleoSpin Plasmid Kit*.

### **7.2.1.7 RNA extraction**

To obtain cDNA as a template for cloning,  $1 \times 10^6$  HeLa cells were pelleted and subsequently lysed according to the *Qiashredder* protocol. For quantitative Realtime PCR experiments, all cells of one sample were lysed. RNA was isolated according to the manufacturer's protocol of the Qiagen *RNeasy Kit*. The isolation of RNA from epidermal white adipose tissue from DIO mice was performed using TRIzol® Reagent according to manufacturer's instruction. To clear the isolated RNA from genomic DNA, samples (up to 5µg RNA) were treated with *DNaseI* (Promega) for 30 minutes at 37°C. This reaction was inactivated at 65°C for 15 minutes. The RNA probes were stored at -80°C.

### 7.2.1.8 cDNA synthesis and Quantitative Realtime PCR

For the reverse transcription of RNA into cDNA, the DNaseI digested RNA samples were processed using the *SuperScript III First Strand cDNA Synthesis System* following the manufacturer's protocol. Thereby, random hexamers provided in the kit were used for reverse transcription. cDNA samples were stored at -20°C. In order to quantify the amount of cDNA in the samples, the LightCycler480 (LC480) system and the *KAPA SYBR FAST qPCR Kit* were used. Thereby, each primer pair was designed for sequence specific amplification of a single target gene. For each primer pair the following reaction mix was prepared per sample and pipetted in a 96-well plate:

- 1µL of each primer (20µM)
- 10µL 2x KAPA SYBRGreen master mix
- 6µL H<sub>2</sub>O
- 2µL cDNA

After sealing and centrifuging the plate at 200xg, the PCR was performed using the LC480 system with the following program:

Step	Temperature	Time	Cycles
Initial denaturation	95°C	10min	1
Denaturation	95°C	10sec	35
Annealing	60°C	10sec	35
Elongation	72°C	10sec	35
Generation of melting curves	65-95°C	15sec	1

**Table 7.2:** PCR-program to generate PCR amplificates for qualitative realtime PCR

Melting curves were analyzed to ensure amplification of only one specific PCR product. For determining the amount of mRNA transcripts in the initial sample, the house keeping gene  $\beta$ -Actin was included to normalize the samples. For the relative quantification, the  $\Delta\Delta C_p$  method first described by Pfaffl (Pfaffl, 2001) was applied. The  $C_p$  value of the target was related to the  $C_p$  value of the house keeping gene. For amplification efficiencies, a value of 2 was applied. DMSO-treated samples were normalized to 1 and compound-treated samples were referred to these samples. qPCR experiments were performed at least three times and are depicted as mean  $\pm$  standard deviation of the mean. For statistical analysis the two-tailed Unpaired t-test was applied and statistical significance was determined by a p-value < 0.05/p-value < 0.1. \* = p-value < 0.05; \*\* = p-value < 0.01; \*\*\* = p-value < 0.001

## 7.2.2 Cell biological methods

### 7.2.2.1 Cultivation of eukaryotic cells

For cultivation of eukaryotic cells, cells were grown in medium containing 10% fetal bovine serum and 1% antibiotics. MEF and HeLa cells were cultured in Dulbecco's Modified Eagle Medium (DMEM) whereas HepG2 cells were grown in Roswell Park Memorial Institute (RPMI) medium. All cell lines are adherent cells and were therefore grown in cell culture flasks to ensure attachment of the cells. Upon 90% cell density, cells were splitted. Thereby, the medium was removed, cells were washed with PBS and detached with trypsin/EDTA. To inactivate the trypsin, cells were suspended in a five-time excess of culture medium, diluted as required and seeded in the cell culture flask.

### 7.2.2.2 Compound treatment and stimulation of MEF cells

For compound treatment, MEF cells were seeded the day before treatment. Depending on the assay that was performed after compound treatment, cell number and well-format differed. An overview is given in the following table:

Assay	Number of cells	Well-format	Volume [mL]
EMSA / quantitative RT-PCR	$1.2 \cdot 10^5$	6	3
ALPHASurefire	$1 \cdot 10^4$	96	0.25
Endogenous TRAF6 ubiquitination	$2.5 \cdot 10^6$	15cm dish	30
IKK kinase assay	$5.5 \cdot 10^5$	10cm dish	15
p65 translocation assay	$3 \cdot 10^3$	384	0.1

**Table 7.3:** Overview of number of seeded cell, well-format and volume depending on the performed assay

The cells were treated with the respective amount of compound and stocked up with DMSO to ensure equivalent DMSO concentrations in all samples. After six hours of incubation, cells were stimulated. Depending on the assay, different stimulation amounts and time points were required as shown in the following table:

Assay	Amount [ng/mL]	Volume [mL]	Time [min]
<b>EMSA</b>			
IL-1 $\beta$	1	2	20
TNF $\alpha$	10	2	20
LPS	5000	2	30
<b>quantitative RT-PCR</b>			
IL-1 $\beta$	1	2	60
TNF $\alpha$	10	2	60
LPS	5000	2	75
<b>ALPHASurefire</b>	1	0.1	7
<b>Endogenous TRAF6 ubiquitination</b>	3.5	20	10
<b>IKK kinase assay</b>	1	10	8
<b>p65 translocation assay</b>			
IL-1 $\beta$	1	0.1	20
TNF $\alpha$	10	0.1	20

**Table 7.4:** Various stimulation procedures depending on the performed assay

After stimulation, cells were put on ice, medium was removed and cells were washed with ice-cold PBS. After completely removing the PBS, cells were disrupted with the respective lysis buffer.

### 7.2.2.3 Toxicity assays

For CellTiter-Blue stainings as well double-staining of Hoechst33342 and Mitotracker, MEF ( $1.2 \cdot 10^3$ /well) and HepG2 ( $4 \cdot 10^3$  cells/well) cells were seeded in two  $\mu$ clear 384 well plates in 100  $\mu$ L medium. After 18 hours of incubation, compounds were transferred to the cells using the Sciclone G3 automation system. After 24 hours, stainings were performed. For CellTiter-Blue stainings, 10  $\mu$ L of the CellTiter-Blue reagent was added to cells in 50  $\mu$ L medium. After 40 minutes, the fluorescence ( $560_{\text{Ex}}/590_{\text{EM}}$ ) was recorded using the Envision plate reader. Thereby, metabolically active cells are capable of converting the non-fluorescent dye Resazurin into the fluorescent Resorufin. For double staining of Hoechst33342 and Mitotracker, both dyes were diluted in medium (final concentrations: Hoechst33342 = 0.5  $\mu$ g/mL; Mitotracker = 0.12  $\mu$ M). 25  $\mu$ L of the medium containing the dyes were applied to the compound-treated cells in 50  $\mu$ L medium. After 45 minutes incubation at 37°C, the stainings were imaged and evaluated in the Operetta system using the Harmony software. Hoechst33342 is a cell-permeable blue fluorescent dye staining nuclear acids and is used for determination of the nucleus area in this experiment. A decrease in nucleus area is indicative for condensed and fragmented apoptotic

nuclei as the apoptotic process causes nuclear condensation and DNA fragmentation (Hua and Xu, 2000). Mitotracker is a red fluorescent dye that incorporates into mitochondria of living cells and is used to analyze the mitochondrial mass in this experiment. Depending on the compound targeting the mitochondria, the mitochondrial mass could either be reduced or increased.

#### **7.2.2.4 Storage of eukaryotic cells**

For long-time storage in liquid nitrogen, cells were detached from the cell culture flask as described in 7.2.2.1.  $1 \times 10^6$  cells were pelleted, resuspended in 1mL storage medium containing 20% FBS, 1% penicillin-streptomycin and 10% DMSO and transferred into a cryo vial. The vial was stored over night at  $-80^{\circ}\text{C}$  in a freezing container and then transferred into liquid nitrogen.

#### **7.2.2.5 p65 translocation assay**

In order to analyze nuclear translocation of p65 after compound treatment, MEF cells were seeded in  $\mu$ clear plates, treated and stimulated as described in 7.2.2.2. Cells were washed with PBS and fixed with 2% PFA for 30 min. After washing with PBS, cells were permeabilized by adding 0.2% Triton-X100 in PBS for 30 min and subsequently washed three times in PBS. The primary antibody p65 (C-20) was 1:250 diluted in 2% BSA and 0.1% Triton-X100 in PBS and incubated for two hours. After washing for three times in PBS, the fluorescently labeled secondary antibody was diluted (1:400) in 2% BSA and 0.1% Triton-X100 in PBS and incubated in subdued light for one hour. The cells were washed three times in PBS and stained with Hoechst33342 (1:10,000 in PBS) for 5 min. After washing the cells with PBS, images were

#### **7.2.2.6 Yeast-Two-Hybrid- (Y2H) assay**

In order to test the interaction of TRAF6 and Ubc13, various constructs were cloned in pGAD-C(x) and pGBD-C(x) vectors using the EcoRI and PstI restriction sites for the performance of an Y2H-assay. For transforming yeast cells, 1 $\mu$ L of a plasmid was added to a 10 $\mu$ L yeast aliquot. Subsequently, 360 $\mu$ L of PEG medium were added to the yeast cells. After incubation for 30 minutes at room temperature, 40 $\mu$ L of DMSO was added to the cells and heat shock was performed for 15 minutes at  $42^{\circ}\text{C}$ . Cells were centrifuged at 200xg for five minutes at room temperature and the pellet resuspended in 100 $\mu$ L and plated on *S. cerevisiae* (SC) selection plates lacking Leucin and Tryptophan. Yeast cells were grown for three days at  $30^{\circ}\text{C}$ . For spotting the yeast colonies, several yeast colonies were resuspended in 1mL autoclaved water. Optical dense ( $\text{OD}_{600}$ ) was measured from a 1:10 dilution. After adjusting an  $\text{OD}_{600}=1$ , 5 $\mu$ L were



spotted on a SC-Leu/Trp/His plate and grown for three days at 30°C. A grown spot revealed an interaction of TRAF6 and Ubc13.

### **7.2.3 Biochemical and immunological methods**

#### **7.2.3.1 Recombinant protein purification**

##### **7.2.3.1.1 Purification of TRAF6StrepII**

The cDNA sequences of the RING-Zincfinger1 domain of wildtype TRAF6 and Ubc13 binding mutants (C70A, D57K and I72F) were cloned into the pASK-IBA3+ vector via the restriction sites SacII and NcoI. This marks TRAF6 RING-Zincfinger1 proteins with a C-terminal StrepII-tag. For protein purification, the plasmids were transformed into BL21 codon plus RIPL cells and spread on a LB-agar plate containing the antibiotics Ampicillin and Chloramphenicol. Bacteria cells were grown for 18 hours at 37°C. One colony was transferred into 5mL LB-medium containing Ampicillin and Chloramphenicol and incubated at 37°C for 18 hours. 350µL of the bacteria suspension were further expanded in 20mL LB-medium with Ampicillin and Chloramphenicol. For protein purification, the 20mL bacteria suspension was added to 1L LB-medium containing both antibiotics. Protein production was induced at an OD<sub>600</sub>= 0.6-0.8 by adding 200µg anhydrotetracycline, 0.5mM Isopropyl-β-D-thiogalactopyranosid (IPTG) and 100µM ZnCl<sub>2</sub>. Cells were incubated at 18°C for 16 hours. Afterwards, cells were centrifuged at 2,600xg for 20minutes at 4°C. The pellet was resuspended in 10ml TRAF6-washbuffer including 1 pill of protease inhibitor Complete mini. The suspension was sonified (8x30seconds) and subsequently centrifuged at 53,000xg for 2x30minutes. For the purification of the StrepII-tagged proteins, the protein solution was applied to StrepTrap columns using the ÄKTA purifier. After washing, the StrepII-protein was eluted from the column using the Strep-elution buffer containing desthiobiotin. The eluted protein was concentrated using Amicons (cut off 3kDa) down to 1mL. Using the ÄKTA purifier and a HiTrap Desalting 5ml column, the protein was desalted and exchanged to storage buffer. The protein was concentrated in Amicons up to 2µg/µL and stored in small aliquots at -80°C.

##### **7.2.3.1.2 Purification of untagged TRAF6 protein**

The cDNA sequences of the TRAF6 RING-Zincfinger1 domain wildtype and D57K mutant were cloned into the pGex 4T1 vector via the BamHI and NotI restriction sites. This marks the TRAF6 protein with a N-terminal GST-tag. For the purification of the <sup>15</sup>N -labeled TRAF6, the bacteria suspension was grown as described in 7.2.3.1.1 in 1L <sup>15</sup>N medium. For purifying unlabeled

TRAF6, the  $^{15}\text{NH}_4$  was replaced with regular  $\text{NH}_4$ . For protein production, 1mM IPTG and 100 $\mu\text{M}$   $\text{ZnCl}_2$  was added at an  $\text{OD}_{600}$  = 0.6-0.7. After 16 hours at 18°C, the cells were centrifuged and the pellet resuspended in 10ml TRAF6-washbuffer including 1 Complete mini pill. After sonification (8x30seconds) and centrifugation (2x30minutes at 53,000xg), the protein suspension was incubated with 1mL pre-washed Glutathione Sepharose 4 fast flow beads for 2 hours at 4°C. Subsequently, beads were washed with 100mL Strep-washbuffer and then incubated with 50Units Thrombin in 2mL washbuffer for 3 hours at roomtemperature to cut off the GST-tag from TRAF7. The TRAF6 protein was eluted in 5mL washbuffer and again incubated with 1mL Glutathione Sepharose 4 fast flow beads for 1 hour at 4°C. Afterwards, the solution was centrifugated for 5minutes at 200xg and the supernatant transferred into an Amicon for concentration followed by centrifugation at 20,000xg for 30minutes. The supernatant was then applied to a HiLoad Superdex75 column using the ÄKTA purifier for separating the untagged TRAF6 protein from uncleaved protein as well as buffer exchange in desalting buffer. After concentration in an Amicon column to 2 $\mu\text{g}/\mu\text{L}$ , the protein aliquots were stored at -80°C.

#### **7.2.3.1.3 Purification of Ubc13FH**

The cDNA sequence for Ubc13 fulllength and the Ubc13SPD mutant and the Flag-His-tag were cloned into the pgex 4T1 vector using the restriction sites BamHI and NotI. This cloning was performed by Dr. Kenji Schorpp. Bacteria transformed with the plasmid were grown up to 1L LB-medium as described in 7.2.3.1.1. Upon reaching an  $\text{OD}_{600}$  = 0.6-0.8, protein production was induced by adding 1mM IPTG. After 18 hours at 21°C, cells were harvested and the pellet resuspended in GST-washbuffer containing 1 Complete mini pill. After sonification (12x30seconds) and centrifugation (2x30minutes), the protein solution was incubated with 1mL pre-washed Glutathione Sepharose 4 fast flow beads for 2 hours at 4°C. After washing the beads with 100mL GST-washbuffer, the beads were incubated with 50Units Thrombin in 2mL washbuffer over night. The Ubc13 protein was eluted in 5mL washbuffer and incubated with 1mL Glutathione Sepharose 4 fast flow beads for 1 hours at 4°C. After centrifugation at 200xg for 2minutes, the supernatant was concentrated to 1ml and centrifuged at 20,000xg for 30minutes. The protein was applied to Superdex75 column using the ÄKTA purifier to desalted the Ubc13FH protein in PBS and to clear it from uncleaved protein. The protein again was concentrated and aliquots were stored at -80°C.

#### **7.2.3.1.4 Purification of GST-tagged TRAF6, OTUB1 and RNF8 proteins**

The cDNA sequences of TRAF6<sub>WT</sub> (RING-Zincfinger1), OTUB1 (fulllength) and RNF8 (RING domain) were cloned into the pGex 4T1 vector via the BamHI and NotI restriction sites. Cloning of the OTUB1 and RNF8 constructs was conducted by Dr. Kenji Schorpp. Bacteria solutions were grown up to 1L LB-medium as described in 7.2.3.1.1. Protein production was induced by adding 1mM IPTG (and 100µM ZnCl<sub>2</sub> in case of TRAF6<sub>WT</sub>) at an OD<sub>600</sub>= 0.6-0.7. Processing of bacteria cells was performed as described in 7.2.3.1.3. Thereby, TRAF6<sub>WT</sub> was resuspended in Strep-washbuffer and sonified for 8x30 seconds. After incubating the beads and protein solution, the beads were washed with the respective washbuffer. The GST-proteins were eluted with 5mL 50mM Glutathione and concentrated in Amicons to 1mL volume. The eluted proteins were desalted using HiTrap Desalting columns and the ÄKTA purifier system. While GST-OTUB1 and GST-RNF8 were desalted in PBS, GST-TRAF6<sub>WT</sub> was desalted in TRAF6 storage buffer. After concentration, the aliquots were stored at -80°C.

#### **7.2.3.2 Sodium-Dodecyl-Sulfate-Polyacrylamid-Gelectrophoresis (SDS-PAGE)**

For analytical separation of proteins, a discontinuous SDS-PAGE under reducing conditions was performed. Thereby, the pore size of the separation gel (10 or 12.5%) was determined by different amounts of acrylamid. For polymerization of the separation buffer, the crosslinker APS (ammonium persulfate) and radical starter TEMED (tetramethylethylendiamin) were added. While polymerizing, the gel was covered with isopropanol. After polymerization and removal of the isopropanol, the 5% stacking gel was added. After loading the samples, 120V was applied to the gel in 1x SDS electrophoresis buffer for 90 minutes. For size control, the protein marker PageRuler Plus Prestained Protein Ladder was loaded on the gel as well.

#### **7.2.3.3 Coomassie and Silverstain**

In order to check the purity of recombinant proteins, the proteins were loaded on a SDS-gel (separation gel: 12.5%). After SDS-PAGE, the gel was washed in bidest H<sub>2</sub>O. For Coomassie blue staining, the Coomassie blue solution was added to the gel and incubated for 18 hours at room temperature to allow staining of the protein. Thereby, the sulfonic acid groups of the dye bind to the positive protein amine groups. The stained gel was washed in bidest H<sub>2</sub>O to visualize the proteins. In case, the Coomassie blue staining was not sensitive enough to detect the proteins, a Silverstaining was performed using *the Pierce Silver Stain Kit* according to manufacturer's instructions.

#### **7.2.3.4 Western Blot and Immunodetection**

To visualize protein after SDS-PAGE by immuno-detection, the separated proteins were transferred to a PVDF-membrane via semi-dry-blotting. Thereby, PVDF membranes were activated in methanol and together with the SDS-gel placed in the blotting apparatus between whatman papers that were soaked in blotting buffer. The protein transfer occurred at 80mA per gel for 60 - 90 minutes. Subsequently, the membrane was blocked with 3% BSA in PBS-Tween20 (PBS-T) for 60 minutes to cover unspecific binding sites. After washing the membrane in PBS-T (3x10 minutes), the specific primary antibody, diluted in 1.5% BSA, was added to the membrane and incubated over night at 4°C. Afterwards, the membrane was washed in PBS-T and the horseradish-peroxidase conjugated secondary antibody, diluted in 0.75% BSA, was applied to the membrane for one hour at room temperature. The membrane was washed in PBS-T and Enhanced chemiluminescence (ECL) substrate was added. The horseradish-peroxidase produces chemiluminescence that is detected by exposure to x-ray films for various time points and developed. To detect another protein on the same membrane, the membrane was incubated with stripping buffer for 60 minutes, afterwards washed in PBS-T and blocked with 3% BSA before adding the next primary antibody.

#### **7.2.3.5 Gel-filtration assay**

The direct interaction of the recombinantly purified proteins TRAF6<sub>WT</sub>StrepII and Ubc13FH was verified by gel-filtration assays. First, 50µg of TRAF6<sub>WT</sub>StrepII protein was applied to the Superdex 75 100/300GL column in PBS to obtain the absorption spectra ( $A_{280}$ ) for TRAF6 alone. Next, equimolar amounts of Ubc13FH (60µg) in PBS were loaded to obtain the absorption spectra of Ubc13FH. For the interaction study, equimolar amounts of both proteins were pre-incubated in PBS for 30 minutes at room temperature followed by absorption spectra analysis.

#### **7.2.3.6 In vitro Ubiquitination assay**

The ability of TRAF6 to form K63-linked polyubiquitin chains in conjunction with Ubc13 is analyzed after compound treatment. Therefore, untagged TRAF6<sub>WT</sub> and TRAF6<sub>D57K</sub> were recombinantly purified. 0.125µM TRAF6 protein were pre-incubated with DMSO/compound in a total volume of 100µL in K63 assay buffer for 30 minutes at room temperature. An aliquot of input samples were transferred to a new tube and denaturated by adding 4x SDS loading buffer and heating the samples (95°C). A master mix containing 0.01µM E1-activating enzyme (UBE1), 0.2µM E2-conjugating enzyme complex (Ubc13/Uev1a), 1mM ZnCl<sub>2</sub>, 2mM ATP und 4µM monoubiquitin was added to the protein and the reaction mixture was incubated for 120

minutes at 37°C. The reaction was stopped by adding 4xSDS loading buffer and heating up the samples to 95°C for 5 minutes. The input sample were loaded on a 12.5% SDS gel and stained with the *Pierce Silver Stain* Kit. The ubiquitination samples were loaded on a 10% SDS gel, blotted and stained for Ubiquitin and TRAF6 in Western Blot analysis.

#### **7.2.3.7 Pulldown assay**

To analyze the effect of the compounds on the GST-TRAF6<sub>WT</sub> - Ubc13FH interaction, 500ng GST-TRAF6<sub>WT</sub> protein was incubated with the respective amounts of compound in pulldown buffer for 30 minutes at room temperature followed by addition of 1µg Ubc13FH for 2 hours at 4°C. Next, Ubc13FH was immunoprecipitated by adding 1µL Flag M2 antibody for 2 hours at 4°C. After incubation with 10µL pre-washed Protein-G-Sepharose beads for 2 hours, the beads were washed eight times with pulldown buffer. The proteins were eluted by adding 2x SDS loading buffer and heating of the samples (95°C). Samples were loaded on a 12.5% gel and stained for TRAF6 and Ubc13 in Western Blot experiments.

#### **7.2.3.8 Saturation-Transfer-Difference-Nuclear-Magnetic-Resonance (STD-NMR)**

STD-NMR was performed by Dr. Grzegorz Popowicz from the Institute of Structural Biology, Helmholtz Zentrum München. For protein-base experiments <sup>15</sup>N-labeled and untagged TRAF6 RING-Zincfinger1 protein was recombinantly purified as described in 7.2.3.1.2 in a minimal media with <sup>15</sup>N-Ammoniumchloride as a sole nitrogen source and concentrated to c= 120µM. Protein and compound were incubated at a ratio of 1:5 in a 3mm NMR tube for 10 minutes before the spectra acquisition. To observe chemical shift perturbations upon the compound addition, two dimensional SOFAST-HMQC spectra were acquired. All measurements were performed using Bruker Avance 600 MHz spectrometer.

#### **7.2.3.9 ALPHAScreen assay**

The ALPHAScreen technology was chosen for High-Throughput-Screening of the TRAF6<sub>WT</sub>StreptII-Ubc13FH interaction. This method is a bead-based assay technology for studying biomolecular interactions in a microplate format. The system requires two bead types binding to either of the proteins: Donor and Acceptor bead. Upon illumination at 680nm the Donor bead releases a singlet oxygen by converting ambient oxygen through its photosensitizer phthalocyanine. If an Acceptor bead is in close proximity, the energy is transferred from the singlet oxygen to thioxene derivatives within the Acceptor beads emitting a light signal at 520-620nm.

Conducting a benchtop ALPHAScreen experiment starts with adding the protein that is targeted by Donor beads to the 384-well-opti-plate (concentrations and volumes as indicated below) and is followed by mixing in Ubc13FH. After one hour of incubation at room temperature, 10µL of both Donor and Acceptor beads were added to the reaction mix in subdued light followed by one of incubation und subsequently read-out at the Envision plate reader.

Protein	Concentration [nM]	Volume [µL]	Beads required	Bead amount [µg]
<b>TRAF6StrepII</b>	100nM	30	StrepTactin Donor	4
<b>Ubc13FH</b>	75nM	10	Nickel-Chelate Acceptor	4

Protein	Concentration [nM]	Volume [µL]	Beads required	Bead amount [µg]
<b>GST-OTUB1</b>	30nM	30	Glutathione Donor	3
<b>GST-RNF8</b>	30nM	30	Glutathione Donor	3
<b>Ubc13FH</b>	20nM	10	Nickel-Chelate Acceptor	3

**Table 7.5:** Experimental set-up of the different combinations of ALPHAScreen assays

### 7.2.3.10 High-Throughput-Screening

In order to identify small molecules that specifically target the RING-Zincfinger1 domain of TRAF6 to prevent its binding to Ubc13 a total of 25,000 compounds were screened. Thereby, three in-house libraries were available for HTS. In the initial HTS campaign, a compound concentration of 10µM was tested. Therefore, the compound plates from the different libraries were prediluted in ALPHAScreen buffer to 60µM and a volume of 0.6µL of the compound was transferred to the assay plate during the HTS campaign.

For performance of an automated ALPHAScreen assay, the TRAF6 protein (concentration and volume as indicated in 7.2.3.9) was applied to the 384-well-opti-plates involving the FlexDrop system and is followed by transfer of the compound via the Sciclone G3 transfer station. After adding Ubc13FH with the FlexDrop and incubation for one hour at room temperature, both beads were mixed in using the FlexDrop as well but in subdued light. Read-out of the plates occurred after another hour of incubation at room temperature. Statistical parameters including the Coefficient of Variation, Z' factor and Signal Window were calculated to determine the quality of the HTS campaign. In order to determine the quality of a HTS campaign, several statistical parameters were calculated: the average of the positive and negative controls as well the standard deviations, coefficient of variation, the Z' factor and the Signal window. The coefficient of variation (CV) gives the standard deviation as a percentage of the mean of a data

set and should not exceed 20% for an optimal assay (Lilly et al., 2007). The Z' factor compares the mean of the positive signal to the mean of the negative control and will have a high value when further apart. Z' factors between a value of 0.5 and 1 indicate for an excellent assay (Zhang et al., 1999). The signal window (SW) provides the degree of separation of the signals between positive and negative controls and should exceed a value of 2 (Sittampalam et al., 1997).

To evaluate the efficiency of the compounds, ALPHAScreen units of compound-treated samples were calculated to DMSO treated samples. Thereby, the TRAF6<sub>D57K</sub> mutant served as the control for maximum inhibition and was included in every plate of the screening. Compounds that inhibited TRAF6<sub>WT</sub>StrepII-Ubc13FH by more than 25% were considered to be active (n=500). After elimination of frequent hitters and His-hitters (Schorpp et al., 2014) as well as small molecules interfering with the GST-OTUB1-Ubc13FH interaction, 178 compounds were defined as primary hits and were subsequently tested in nine-point serial dilution assays (2.5-40µM) in TRAF6<sub>WT</sub>StrepII-Ubc13FH, GST-OTUB1-Ubc13FH and GST-RNF8-Ubc13FH ALPHAScreen experiments. Only compounds with serial dilution effects on TRAF6<sub>WT</sub>StrepII-Ubc13FH, but no effects on GST-OTUB1-Ubc13FH and GST-RNF8-Ubc13FH were taken for further research (n=32).

#### **7.2.3.11 Electro-Mobility-Shift-Assay (EMSA)**

In order to analyze the effects of the compounds on activation of NF-κB, MEF cells were seeded, treated and stimulated as described in 7.2.2.2. 70µL of High-Salt-Lysis-Buffer was added to the cells and cells were scraped from the plate. The solution was incubated at 4°C for 30 minutes rotating to allow lysis of the cells. After centrifuging the lysates for 40 minutes at 20,000xg and 4°C, the supernatant was transferred into a new tube and samples were stored at -80°C.

For preparation of the radioactive NF-κB and Oct-1 probes, the oligonucleotides were labeled with <sup>32</sup>P-α-dATP. 5µg of each Oligonucleotide was annealed in 50µL annealing buffer for 10 minutes at 90°C and cooled down over night in the thermocycler. For radioactive labeling of the oligonucleotides, the following reaction was prepared:

Annealed Oligonucleotide	1µL (= 400ng)
10x Kleenow buffer	2.5µL
dNTPs-A (5mM each)	1.8µL
<sup>32</sup> P-α-dATP	3µL
DNA Polymerase I (Kleenow)	1µL

H <sub>2</sub> O	ad 25μL
------------------	---------

The reaction mix was incubated at 37°C for 30 minutes and subsequently purified using the *QiaQuick Nucleotide Removal Kit*. The labeled probes were stored at -20°C.

For the shift reaction the following reaction mix was prepared:

2x shift buffer	10μL
BSA (10μg/μL)	1μL
DTT (100mM)	1μL
Poly d(I-C) 2μg/μL	1μL
Lysate	4μg
Radioactive labeled probe	10,000-20,000 counts per minute
H <sub>2</sub> O	ad 20μL

The mix was incubated at room temperature for 30 minutes and then loaded on a native polyacrylamide gel (5%). The samples were separated at 26mA per gel in 1x TBE running buffer. Subsequently, the gel was dried on whatman paper in vacuum for one hour. Radioactivity was determined via exposure to an x-ray film at -80°C and developing the film.

In order to quantify the radioactive intensity, the x-ray film for the NF-κB as well as Oct-1 activation were digitalized by scanning. Using the LabImage1D software, the intensity of the radioactive bands was quantified. Therefore, one area covering the radioactive band (NF-κB as well as Oct-1) and another area for the background was defined. Intensity and size of the defined areas were calculated. To calculate the intensity of a single band, the intensity of each area was normalized to its size. Next, the intensity of the background was subtracted from the intensity of the band. After that, the normalized NF-κB intensity was related to the normalized Oct-1 intensity for the final NF-κB activation. DMSO-treated samples were set to 100% and compound-treated probes were related to that.

#### **7.2.3.12 Immunoprecipitation of TRAF6 for endogenous ubiquitination**

Cells were seeded, compound treated and stimulated with IL-1β as indicated in 7.2.2.2. For cell lysis, 500μL Co-IP lysis buffer containing 1% SDS was applied to the cells. Subsequently, cells were scraped from the plate and the cells were disrupted by repeatedly passing the solution through a syringe (26G). After incubation of the lysate at 4°C for 30 minutes rotating, the solution was centrifuged for 30 minutes at 4°C and 20,000xg. The supernatant was transferred to a new tube and lysate samples were taken. Afterwards, the samples were diluted to 0.1% SDS and incubated with 5μL TRAF6 antibody EP591Y for two hours at 4°C. 20μL pre-washed Protein-G-Sepharose beads were added and the reaction mix further incubated over night at



4°C. Beads were washed three times in Co-IP buffer and the protein was eluted using 2x SDS loading buffer and heating up the sample. The proteins were separated by SDS-PAGE (10% separation gel) and stained for Ubiquitin and TRAF6 in Western Blot analysis.

#### **7.2.3.13 IKK kinase assay**

MEF cells were seeded, compound treated and stimulated with IL-1 $\beta$  as depicted in 7.2.2.2. Cells were lysed in 500 $\mu$ L CoIP lysis buffer, incubated at 4°C for 30 minutes and centrifuged at 4°C and 20,000xg for 30 minutes. After taking input samples, the supernatant was then mixed with 6 $\mu$ L IKK $\gamma$  antibody FL-419 and incubated for two hours at 4°C. After adding 20 $\mu$ L pre-washed Protein-G-Sepharose beads, the sample was incubated over night at 4°C. The beads were washed three times with CoIP buffer followed by one washing step in kinase buffer. The beads were incubated with 20 $\mu$ L kinase buffer, 1.5mg GST-I $\kappa$ B $\alpha$  (1-53) and 0.5 $\mu$ L  $^{32}$ P- $\gamma$ -ATP for 30 minutes at 37°C. The reaction was stopped by adding 10 $\mu$ L of 4x SDS loading buffer and proteins were separated by SDS-Page (12.5 % separation gel) and analyzed by autoradiography as well as Western Blot.

#### **7.2.3.14 ALPHASurefire**

ALPHASurefire is a bead-based ALPHA technology provided by Perkin Elmer to analyze protein levels of phosphorylated cellular proteins. The phosphorylated protein is detected by using 2 antibodies: one targets the specific phospho-epitope of the protein, while the other one is directed against a non-phospho-epitope at the distal end of this protein. The antibodies are then selectively bound by either Donor or Acceptor beads analog to the ALPHAScreen system. Upon phosphorylation both beads are brought together generating a signal. In order to detect protein levels of p-I $\kappa$ B $\alpha$  (Ser32/36) as well as total I $\kappa$ B $\alpha$ , MEF cells were seeded, compound treated and stimulated as described in 7.2.2.2. The protein levels were analyzed using the ALPHASurefire kits following manufacturer's instruction. The general 2-plate protocol was performed. Therefore, the lysates were transferred from the 96-well assay plate to a 384 well-plate before adding the Acceptor mix. Experiments were performed at least three times and are depicted as mean  $\pm$  standard deviation of the mean. For statistical analysis, the Unpaired t-test was applied and statistical significance was determined by a p-value < 0.05. \* = p-value < 0.05; \*\* = p-value < 0.01; \*\*\* = p-value < 0.001

### **7.2.4 Diet-Induced-Obesity (DIO) mouse study**

#### **7.2.4.1 Treatment of DIO-mice**

Observation of mice, compound-treatment and measurements were carried out by members of the Institute of Diabetes, Helmholtz Zentrum München. Mice were fed a high-fat-diet until they reached a body weight of at least 40g and developed diabetes-induced-obesity. The mice were separated in control group and a group for C25-0140 injection. Mice were treated every day with 14µmol/kg (=7.4mg/kg) C25-0140 intra peritoneal for a period of 20 days. Thereby, C25-0140 was dissolved in 2.9% DMSO, 1.5% Tween-80 and 1xPBS. Every day before injection, the body weight and food intake were measured. On day 20, mice were sacrificed two hours after compound injection and epidermal white adipose tissue from both body sites was removed, frozen in liquid nitrogen and stored at -80°C. To determine the statistical significance of the loss of bodyweight in the DIO-mouse-study, a two-way-Anova test was applied.

#### **7.2.4.2 Glucose Tolerance Test (GTT)**

On day 18, a GTT was performed. Therefore, mice were starved for six hours and two hours after compound injection challenged with 1.5g glucose per kg body weight. Before, 15, 30, 60 and 120 minutes after glucose injection, blood glucose levels were measured using Freestyle Life Test strips. For statistical analysis, the Unpaired t-test was applied and statistical significance was determined by a p-value < 0.05.

#### **7.2.4.3 Isolation of protein from epidermal white adipose tissue of DIO mice**

A small piece of the epidermal white adipose tissue (ewat) was lysed in 200µL RIPA-buffer containing protease-phosphatase-inhibitors and incubated at 4°C rotating for two hours. The solution was then centrifuged at 20,000xg for 30 minutes and the soluble fraction containing the proteins was transferred into a new tube. This step was repeated until the protein fraction was completely free of fat. The protein concentration was determined using the Bradford assay. For ALPHASurefire experiments, 4mg protein of each sample were analyzed.

## 8 References

- Agrawal, A., S. L. Johnson, J. A. Jacobsen, M. T. Miller, L. H. Chen, M. Pellecchia and S. M. Cohen (2010). "Chelator Fragment Libraries for Targeting Metalloproteinases." *Chem Med Chem* 5(2): 195–199.
- Ahmad, R., A. Al-Mass, V. Atizado, A. Al-Hubail, F. Al-Ghimlas, M. Al-Arouj, A. Bennakhi, S. Dermime and K. Behbehani (2012). "Elevated expression of the toll like receptors 2 and 4 in obese individuals: its significance for obesity-induced inflammation." *J Inflamm (Lond)* 9(1): 48.
- Akira, S. and K. Takeda (2004). "Toll-like receptor signalling." *Nat Rev Immunol* 4(7): 499-511.
- Albrecht, M., M. Fiege, O. Osetska (2008). "8-Hydroxyquinolines in Metallosupramolecular Chemistry." *Coord Chem Rev* 252 (8): 812–824.
- Alvarez, S. E., K. B. Harikumar, N. C. Hait, J. Allegood, G. M. Strub, E. Y. Kim, M. Maceyka, H. Jiang, C. Luo, T. Kordula, S. Milstien and S. Spiegel (2010). "Sphingosine-1-phosphate is a missing cofactor for the E3 ubiquitin ligase TRAF2." *Nature* 465(7301): 1084-1088.
- Arch, R. H., R. W. Gedrich and C. B. Thompson (1998). "Tumor necrosis factor receptor-associated factors (TRAFs)--a family of adapter proteins that regulates life and death." *Genes Dev* 12(18): 2821-2830.
- Armstrong, A. P., M. E. Tometsko, M. Glaccum, C. L. Sutherland, D. Cosman and W. C. Dougall (2002). "A RANK/TRAF6-dependent signal transduction pathway is essential for osteoclast cytoskeletal organization and resorptive function." *J Biol Chem* 277(46): 44347-44356.
- Baell, J. B. and G. A. Holloway (2010). "New substructure filters for removal of pan assay interference compounds (PAINS) from screening libraries and for their exclusion in bioassays." *J Med Chem* 53(7): 2719-2740.
- Baker, R. G., M. S. Hayden and S. Ghosh (2011). "NF-kappaB, inflammation, and metabolic disease." *Cell Metab* 13(1): 11-22.
- Basseres, D. S. and A. S. Baldwin (2006). "Nuclear factor-kappaB and inhibitor of kappaB kinase pathways in oncogenic initiation and progression." *Oncogene* 25(51): 6817-6830.
- Berndsen, C. E. and C. Wolberger (2014). "New insights into ubiquitin E3 ligase mechanism." *Nat Struct Mol Biol* 21(4): 301-307.
- Bianchi, K. and P. Meier (2009). "A tangled web of ubiquitin chains: breaking news in TNF-R1 signaling." *Mol Cell* 36(5): 736-742.
- Bignell, G. R., W. Warren, S. Seal, M. Takahashi, E. Rapley, R. Barfoot, H. Green, C. Brown, P. J. Biggs, S. R. Lakhani, C. Jones, J. Hansen, E. Blair, B. Hofmann, R. Siebert, G. Turner, D. G. Evans, C. Schrandt-Stumpel, F. A. Beemer, A. van Den Ouweland, D. Halley, B. Delpech, M. G. Cleveland, I. Leigh, J. Leisti and S. Rasmussen (2000). "Identification of the familial cylindromatosis tumour-suppressor gene." *Nat Genet* 25(2): 160-165.
- Bishop, G. A., C. R. Moore, P. Xie, L. L. Stunz and Z. J. Kraus (2007). "TRAF proteins in CD40 signaling." *Adv Exp Med Biol* 597: 131-151.

- Boone, D. L., E. E. Turer, E. G. Lee, R. C. Ahmad, M. T. Wheeler, C. Tsui, P. Hurley, M. Chien, S. Chai, O. Hitotsumatsu, E. McNally, C. Pickart and A. Ma (2004). "The ubiquitin-modifying enzyme A20 is required for termination of Toll-like receptor responses." *Nat Immunol* 5(10): 1052-1060.
- Bosanska, L., D. Michalsky, Z. Lacinova, I. Dostalova, M. Bartlova, D. Haluzikova, M. Matoulek, M. Kasalicky and M. Haluzik (2010). "The influence of obesity and different fat depots on adipose tissue gene expression and protein levels of cell adhesion molecules." *Physiol Res* 59(1): 79-88.
- Bouwmeester, T., A. Bauch, H. Ruffner, P. O. Angrand, G. Bergamini, K. Croughton, C. Cruciat, D. Eberhard, J. Gagneur, S. Ghidelli, C. Hopf, B. Huhse, R. Mangano, A. M. Michon, M. Schirle, J. Schlegl, M. Schwab, M. A. Stein, A. Bauer, G. Casari, G. Drewes, A. C. Gavin, D. B. Jackson, G. Joberty, G. Neubauer, J. Rick, B. Kuster and G. Superti-Furga (2004). "A physical and functional map of the human TNF-alpha/NF-kappa B signal transduction pathway." *Nat Cell Biol* 6(2): 97-105.
- Bratsos, I., D. Urankar, E. Zangrando, P. Genova-Kalou, J. Kosmrlj, E. Alessio and I. Turel (2011). "1-(2-Picolyl)- Substituted 1,2,3-Triazole as Novel Chelating Ligand for the Preparation of Ruthenium Complexes with Potential Anticancer Activity." *Dalton Trans* 40: 5188–5199.
- Bremm, A., S. M. Freund and D. Komander (2010). "Lys11-linked ubiquitin chains adopt compact conformations and are preferentially hydrolyzed by the deubiquitinase Cezanne." *Nat Struct Mol Biol* 17(8): 939-947.
- Brummelkamp, T. R., S. M. Nijman, A. M. Dirac and R. Bernards (2003). "Loss of the cylindromatosis tumour suppressor inhibits apoptosis by activating NF-kappaB." *Nature* 424(6950): 797-801.
- Buckley, D. L. and Crews, C. M. (2014). „Small-Molecule Control of Intracellular Proteins of the Ubiquitin Proteasome System." *Angew Chem* 53(9): 2312-2330.
- Budhidarmo, R., Y. Nakatani and C. L. Day (2012). "RINGS hold the key to ubiquitin transfer." *Trends Biochem Sci* 37(2): 58-65.
- Campbell, S. J., R. A. Edwards, C. C. Leung, D. Neculai, C. D. Hodge, S. Dhe-Paganon and J. N. Glover (2012). "Molecular insights into the function of RING finger (RNF)-containing proteins hRNF8 and hRNF168 in Ubc13/Mms2-dependent ubiquitylation." *J Biol Chem* 287(28): 23900-23910.
- Carlsen, H., F. Haugen, S. Zadelaar, R. Kleemann, T. Kooistra, C. A. Drevon and R. Blomhoff (2009). "Diet-induced obesity increases NF-kappaB signaling in reporter mice." *Genes Nutr* 4(3): 215-222.
- Chang, S. H. and C. Dong (2011). "Signaling of interleukin-17 family cytokines in immunity and inflammation." *Cell Signal* 23(7): 1069-1075.
- Chatzigeorgiou, A., T. Seijkens, B. Zarzycka, D. Engel, M. Poggi, S. van den Berg, S. van den Berg, O. Soehnlein, H. Winkels, L. Beckers, D. Lievens, A. Driessen, P. Kusters, E. Biessen, R. Garcia-Martin, A. Klotzsche-von Ameln, M. Gijbels, R. Noelle, L. Boon, T. Hackeng, K. M. Schulte, A. Xu, G. Vriend, S. Nabuurs, K. J. Chung, K. Willems van Dijk, P. C. Rensen, N. Gerdes, M. de Winther, N. L. Block, A. V. Schally, C. Weber, S. R. Bornstein, G. Nicolaes, T. Chavakis and E. Lutgens (2014). "Blocking CD40-TRAF6 signaling is a therapeutic target in obesity-associated insulin resistance." *Proc Natl Acad Sci U S A* 111(7): 2686-2691.
- Chen, M., X. Lv, Y. Liu, Y. Zhao, J. Liu, P. Wang and W. Guo (2011). "An 2-(2'-Aminophenyl) Benzoxazole-Based OFF-ON Fluorescent Chemosensor for Zn<sup>2+</sup> in Aqueous Solution." *Org Biomol Chem* 9: 2345–2349.

- Chen, F. E. and G. Ghosh (1999). "Regulation of DNA binding by Rel/NF-kappaB transcription factors: structural views." *Oncogene* 18(49): 6845-6852.
- Chen, Z. J. (2005). "Ubiquitin signalling in the NF-kappaB pathway." *Nat Cell Biol* 7(8): 758-765.
- Cheng, K. K., M. A. Iglesias, K. S. Lam, Y. Wang, G. Sweeney, W. Zhu, P. M. Vanhoutte, E. W. Kraegen and A. Xu (2009). "APPL1 potentiates insulin-mediated inhibition of hepatic glucose production and alleviates diabetes via Akt activation in mice." *Cell Metab* 9(5): 417-427.
- Chiou, W. F., Y. L. Huang and Y. W. Liu (2014). "(+)-Vitisin A inhibits osteoclast differentiation by preventing TRAF6 ubiquitination and TRAF6-TAK1 formation to suppress NFATc1 activation." *PLoS One* 9(2): e89159.
- Chung, J. Y., M. Lu, Q. Yin, S. C. Lin and H. Wu (2007). "Molecular basis for the unique specificity of TRAF6." *Adv Exp Med Biol* 597: 122-130.
- Clague, M. J., I. Barsukov, J. M. Coulson, H. Liu, D. J. Rigden and S. Urbe (2013). "Deubiquitylases from genes to organism." *Physiol Rev* 93(3): 1289-1315.
- Clague, M. J., J. M. Coulson and S. Urbe (2012). "Cellular functions of the DUBs." *J Cell Sci* 125(Pt 2): 277-286.
- Clark, K., S. Nanda and P. Cohen (2013). "Molecular control of the NEMO family of ubiquitin-binding proteins." *Nat Rev Mol Cell Biol* 14(10): 673-685.
- Constable, C.E., D. Morris, S. Carr (1998). "Functionalised 3,3[Prime or Minute]-Bipyridines—A New Class of Dinucleating Ligands." *N J Chem* 22: 287–294.
- Conze, D. B., C. J. Wu, J. A. Thomas, A. Landstrom and J. D. Ashwell (2008). "Lys63-linked polyubiquitination of IRAK-1 is required for interleukin-1 receptor- and toll-like receptor-mediated NF-kappaB activation." *Mol Cell Biol* 28(10): 3538-3547.
- Creely, S. J., P. G. McTernan, C. M. Kusminski, M. Fisher f, N. F. Da Silva, M. Khanolkar, M. Evans, A. L. Harte and S. Kumar (2007). "Lipopolysaccharide activates an innate immune system response in human adipose tissue in obesity and type 2 diabetes." *Am J Physiol Endocrinol Metab* 292(3): E740-747.
- Darnay, B. G., J. Ni, P. A. Moore and B. B. Aggarwal (1999). "Activation of NF-kappaB by RANK requires tumor necrosis factor receptor-associated factor (TRAF) 6 and NF-kappaB-inducing kinase. Identification of a novel TRAF6 interaction motif." *J Biol Chem* 274(12): 7724-7731.
- De, A., T. Dainichi, C. V. Rathinam and S. Ghosh (2014). "The deubiquitinase activity of A20 is dispensable for NF-kappaB signaling." *EMBO Rep* 15(7): 775-783.
- Deng, L., C. Wang, E. Spencer, L. Yang, A. Braun, J. You, C. Slaughter, C. Pickart and Z. J. Chen (2000). "Activation of the IkappaB kinase complex by TRAF6 requires a dimeric ubiquitin-conjugating enzyme complex and a unique polyubiquitin chain." *Cell* 103(2): 351-361.
- Deshaies, R. J. and C. A. Joazeiro (2009). "RING domain E3 ubiquitin ligases." *Annu Rev Biochem* 78: 399-434.

- Düwel, M., V. Welteke, A. Oeckinghaus, M. Baens, B. Kloo, U. Ferch, B. G. Darnay, J. Ruland, P. Marynen and D. Krappmann (2009). "A20 negatively regulates T cell receptor signaling to NF-kappaB by cleaving Malt1 ubiquitin chains." *J Immunol* 182(12): 7718-7728.
- Dynek, J. N., T. Goncharov, E. C. Dueber, A. V. Fedorova, A. Izrael-Tomasevic, L. Phu, E. Helgason, W. J. Fairbrother, K. Deshayes, D. S. Kirkpatrick and D. Vucic (2010). "c-IAP1 and UbcH5 promote K11-linked polyubiquitination of RIP1 in TNF signalling." *EMBO J* 29(24): 4198-4209.
- Eddins, M. J., C. M. Carlile, K. M. Gomez, C. M. Pickart and C. Wolberger (2006). "Mms2-Ubc13 covalently bound to ubiquitin reveals the structural basis of linkage-specific polyubiquitin chain formation." *Nat Struct Mol Biol* 13(10): 915-920.
- Edelmann, M. J., A. Iphofer, M. Akutsu, M. Altun, K. di Gleria, H. B. Kramer, E. Fiebigler, S. Dhe-Paganon and B. M. Kessler (2009). "Structural basis and specificity of human otubain 1-mediated deubiquitination." *Biochem J* 418(2): 379-390.
- Eletr, Z. M., D. T. Huang, D. M. Duda, B. A. Schulman and B. Kuhlman (2005). "E2 conjugating enzymes must disengage from their E1 enzymes before E3-dependent ubiquitin and ubiquitin-like transfer." *Nat Struct Mol Biol* 12(10): 933-934.
- Ely, K. R., R. Kodandapani and S. Wu (2007). "Protein-protein interactions in TRAF3." *Adv Exp Med Biol* 597: 114-121.
- Emmerich, C. H., A. Ordureau, S. Strickson, J. S. Arthur, P. G. Pedrioli, D. Komander and P. Cohen (2013). "Activation of the canonical IKK complex by K63/M1-linked hybrid ubiquitin chains." *Proc Natl Acad Sci USA* 110(38): 15247-15252.
- Enesa, K., M. Zakkar, H. Chaudhury, A. Luong le, L. Rawlinson, J. C. Mason, D. O. Haskard, J. L. Dean and P. C. Evans (2008). "NF-kappaB suppression by the deubiquitinating enzyme Cezanne: a novel negative feedback loop in pro-inflammatory signaling." *J Biol Chem* 283(11): 7036-7045.
- Faesen, A. C., M. P. Luna-Vargas, P. P. Geurink, M. Clerici, R. Merckx, W. J. van Dijk, D. S. Hameed, F. El Oualid, H. Ovaas and T. K. Sixma (2011). "The differential modulation of USP activity by internal regulatory domains, interactors and eight ubiquitin chain types." *Chem Biol* 18(12): 1550-1561.
- Ferrao, R., J. Li, E. Bergamin and H. Wu (2012). "Structural insights into the assembly of large oligomeric signalosomes in the Toll-like receptor-interleukin-1 receptor superfamily." *Sci Signal* 5(226): re3.
- Finley, D. (2009). "Recognition and processing of ubiquitin-protein conjugates by the proteasome." *Annu Rev Biochem* 78: 477-513.
- Flygare, J. A., M. Beresini, N. Budha, H. Chan, I. T. Chan, S. Cheeti, F. Cohen, K. Deshayes, K. Doerner, S. G. Eckhardt, L. O. Elliott, B. Feng, M. C. Franklin, S. F. Reisner, L. Gazzard, J. Halladay, S. G. Hymowitz, H. La, P. LoRusso, B. Maurer, L. Murray, E. Plise, C. Quan, J. P. Stephan, S. G. Young, J. Tom, V. Tsui, J. Um, E. Varfolomeev, D. Vucic, A. J. Wagner, H. J. Wallweber, L. Wang, J. Ware, Z. Wen, H. Wong, J. M. Wong, M. Wong, S. Wong, R. Yu, K. Zobel and W. J. Fairbrother (2012). "Discovery of a potent small-molecule antagonist of inhibitor of apoptosis (IAP) proteins and clinical candidate for the treatment of cancer (GDC-0152)." *J Med Chem* 55(9): 4101-4113.
- Fukushima, T., S. Matsuzawa, C. L. Kress, J. M. Bruey, M. Krajewska, S. Lefebvre, J. M. Zapata, Z. Ronai and J. C. Reed (2007). "Ubiquitin-conjugating enzyme Ubc13 is a critical component of TNF receptor-

associated factor (TRAF)-mediated inflammatory responses." *Proc Natl Acad Sci USA* 104(15): 6371-6376.

Gaffen, S. L. (2009). "Structure and signalling in the IL-17 receptor family." *Nat Rev Immunol* 9(8): 556-567.

Gerlach, B., S. M. Cordier, A. C. Schmukle, C. H. Emmerich, E. Rieser, T. L. Haas, A. I. Webb, J. A. Rickard, H. Anderton, W. W. Wong, U. Nachbur, L. Gangoda, U. Warnken, A. W. Purcell, J. Silke and H. Walczak (2011). "Linear ubiquitination prevents inflammation and regulates immune signalling." *Nature* 471(7340): 591-596.

Gilmore, T. D. (2006). "Introduction to NF-kappaB: players, pathways, perspectives." *Oncogene* 25(51): 6680-6684.

Glickman, J. F., X. Wu, R. Mercuri, C. Illy, B. R. Bowen, Y. He and M. Sills (2002). "A comparison of ALPHAScreen, TR-FRET, and TRF as assay methods for FXR nuclear receptors." *J Biomol Screen* 7(1): 3-10.

Goldenberg, S. J., J. G. Marblestone, M. R. Mattern and B. Nicholson (2010). "Strategies for the identification of ubiquitin ligase inhibitors." *Biochem Soc Trans* 38(Pt 1): 132-136.

Guédat, P. and F. Colland (2007). "Patented small molecule inhibitors in the ubiquitin proteasome system." *BMC Biochem* 8 Suppl 1: S14.

Gyrd-Hansen, M. and P. Meier (2010). "IAPs: from caspase inhibitors to modulators of NF-kappaB, inflammation and cancer." *Nat Rev Cancer* 10(8): 561-574.

Ha, H., D. Han and Y. Choi (2009). "TRAF-mediated TNFR-family signaling." *Curr Protoc Immunol* Chapter 11: Unit11 19D.

Haas, T. L., C. H. Emmerich, B. Gerlach, A. C. Schmukle, S. M. Cordier, E. Rieser, R. Feltham, J. Vince, U. Warnken, T. Wenger, R. Koschny, D. Komander, J. Silke and H. Walczak (2009). "Recruitment of the linear ubiquitin chain assembly complex stabilizes the TNF-R1 signaling complex and is required for TNF-mediated gene induction." *Mol Cell* 36(5): 831-844.

Hadian, K., R. A. Griesbach, S. Dornauer, T. M. Wanger, D. Nagel, M. Metlitzky, W. Beisker, M. Schmidt-Suprian and D. Krappmann (2011). "NF-kappaB essential modulator (NEMO) interaction with linear and lys-63 ubiquitin chains contributes to NF-kappaB activation." *J Biol Chem* 286(29): 26107-26117.

Haglund, K. and I. Dikic (2005). "Ubiquitylation and cell signaling." *EMBO J* 24(19): 3353-3359.

Harhaj, E. W. and V. M. Dixit (2012). "Regulation of NF-kappaB by deubiquitinases." *Immunol Rev* 246(1): 107-124.

Hatakeyama, S., M. Yada, M. Matsumoto, N. Ishida and K. I. Nakayama (2001). "U box proteins as a new family of ubiquitin-protein ligases." *J Biol Chem* 276(35): 33111-33120.

Heinrichsdorff, J. and J. M. Olefsky (2012). "Fetuin-A: the missing link in lipid-induced inflammation." *Nat Med* 18(8): 1182-1183.

Hellman, L. M. and M. G. Fried (2007). "Electrophoretic mobility shift assay (EMSA) for detecting protein-nucleic acid interactions." *Nat Protoc* 2(8): 1849-1861.

- Heyninck, K. and R. Beyaert (2005). "A20 inhibits NF-kappaB activation by dual ubiquitin-editing functions." *Trends Biochem Sci* 30(1): 1-4.
- Hildebrand, J. M., Z. Yi, C. M. Buchta, J. Poovassery, L. L. Stunz and G. A. Bishop (2011). "Roles of tumor necrosis factor receptor associated factor 3 (TRAF3) and TRAF5 in immune cell functions." *Immunol Rev* 244(1): 55-74.
- Hinz, M., M. Stilmann, S. C. Arslan, K. K. Khanna, G. Dittmar and C. Scheidereit (2010). "A cytoplasmic ATM-TRAF6-clAP1 module links nuclear DNA damage signaling to ubiquitin-mediated NF-kappaB activation." *Mol Cell* 40(1): 63-74.
- Hoesel, B. and J. A. Schmid (2013). "The complexity of NF-kappaB signaling in inflammation and cancer." *Mol Cancer* 12: 86.
- Hoffmann, A. and D. Baltimore (2006). "Circuitry of nuclear factor kappaB signaling." *Immunol Rev* 210: 171-186.
- Hoffmann, A., G. Natoli and G. Ghosh (2006). "Transcriptional regulation via the NF-kappaB signaling module." *Oncogene* 25(51): 6706-6716.
- Hong, C. A., E. Swearingen, R. Mallari, X. Gao, Z. Cao, A. North, S. W. Young and S. G. Huang (2003). "Development of a high throughput time-resolved fluorescence resonance energy transfer assay for TRAF6 ubiquitin polymerization." *Assay Drug Dev Technol* 1(1 Pt 2): 175-180.
- Huang, L., E. Kinnucan, G. Wang, S. Beaudenon, P. M. Howley, J. M. Huibregtse and N. P. Pavletich (1999). "Structure of an E6AP-UbcH7 complex: insights into ubiquitination by the E2-E3 enzyme cascade." *Science* 286(5443): 1321-1326.
- Husnjak, K. and I. Dikic (2012). "Ubiquitin-binding proteins: decoders of ubiquitin-mediated cellular functions." *Annu Rev Biochem* 81: 291-322.
- Huxford, T. and G. Ghosh (2009). "A structural guide to proteins of the NF-kappaB signaling module." *Cold Spring Harb Perspect Biol* 1(3): a000075.
- Ikeda, F., Y. L. Deribe, S. S. Skanland, B. Stieglitz, C. Grabbe, M. Franz-Wachtel, S. J. van Wijk, P. Goswami, V. Nagy, J. Terzic, F. Tokunaga, A. Androulidaki, T. Nakagawa, M. Pasparakis, K. Iwai, J. P. Sundberg, L. Schaefer, K. Rittinger, B. Macek and I. Dikic (2011). "SHARPIN forms a linear ubiquitin ligase complex regulating NF-kappaB activity and apoptosis." *Nature* 471(7340): 637-641.
- Inoue, J., T. Ishida, N. Tsukamoto, N. Kobayashi, A. Naito, S. Azuma and T. Yamamoto (2000). "Tumor necrosis factor receptor-associated factor (TRAF) family: adapter proteins that mediate cytokine signaling." *Exp Cell Res* 254(1): 14-24.
- Into, T., M. Inomata, E. Takayama and T. Takigawa (2012). "Autophagy in regulation of Toll-like receptor signaling." *Cell Signal* 24(6): 1150-1162.
- Issaeva, N., P. Bozko, M. Enge, M. Protopopova, L. G. Verhoef, M. Masucci, A. Pramanik and G. Selivanova (2004). "Small molecule RITA binds to p53, blocks p53-HDM-2 interaction and activates p53 function in tumors." *Nat Med* 10(12): 1321-1328.



- Iversen, P. W., B. Beck, Y. F. Chen, W. Dere, V. Devanarayan, B. J. Eastwood, M. W. Farmen, S. J. Iturria, C. Montrose, R. A. Moore, J. R. Weidner and G. S. Sittampalam (2004). HTS Assay Validation. *Assay Guidance Manual* Bethesda (MD).
- Jerabek-Willemsen, M., C. J. Wienken, D. Braun, P. Baaske and S. Duhr (2011). "Molecular interaction studies using microscale thermophoresis." *Assay Drug Dev Technol* 9(4): 342-353.
- Jin, L., W. Wang and G. Fang (2014). "Targeting protein-protein interaction by small molecules." *Annu Rev Pharmacol Toxicol* 54: 435-456.
- Jin, L., A. Williamson, S. Banerjee, I. Philipp and M. Rape (2008). "Mechanism of ubiquitin-chain formation by the human anaphase-promoting complex." *Cell* 133(4): 653-665.
- Jin, W., M. Chang, E. M. Paul, G. Babu, A. J. Lee, W. Reiley, A. Wright, M. Zhang, J. You and S. C. Sun (2008). "Deubiquitinating enzyme CYLD negatively regulates RANK signaling and osteoclastogenesis in mice." *J Clin Invest* 118(5): 1858-1866.
- Johnson, E. S., P. C. Ma, I. M. Ota and A. Varshavsky (1995). "A proteolytic pathway that recognizes ubiquitin as a degradation signal." *J Biol Chem* 270(29): 17442-17456.
- Joo, E., S. I. Matsuzawa, J. C. Reed, T. Hayashi, K. Tsuda and N. Inagaki (2013). "Ubc13 haploinsufficiency protects against high-fat diet-induced insulin resistance via TRAF- mediated inflammatory responses." Posterabstract number 865 at the EASD virtual meeting, Barcelona 2013
- Kaim, W. (2002). "The Coordination Chemistry of 1,2,4,5-Tetrazines." *Coord Chem Rev* 230 (1): 127–139.
- Kane, R. C., P. F. Bross, A. T. Farrell and R. Pazdur (2003). "Velcade: U.S. FDA approval for the treatment of multiple myeloma progressing on prior therapy." *Oncologist* 8(6): 508-513.
- Karin, M. (1999). "How NF-kappaB is activated: the role of the IkappaB kinase (IKK) complex." *Oncogene* 18(49): 6867-6874.
- Kawai, T. and S. Akira (2008). "Toll-like receptor and RIG-I-like receptor signaling." *Ann N Y Acad Sci* 1143: 1-20.
- Kayagaki, N., Q. Phung, S. Chan, R. Chaudhari, C. Quan, K. M. O'Rourke, M. Eby, E. Pietras, G. Cheng, J. F. Bazan, Z. Zhang, D. Arnott and V. M. Dixit (2007). "DUBA: a deubiquitinase that regulates type I interferon production." *Science* 318(5856): 1628-1632.
- Keating, S. E. and A. G. Bowie (2009). "Role of non-degradative ubiquitination in interleukin-1 and toll-like receptor signaling." *J Biol Chem* 284(13): 8211-8215.
- Kee, Y. and J. M. Huibregtse (2007). "Regulation of catalytic activities of HECT ubiquitin ligases." *Biochem Biophys Res Commun* 354(2): 329-333.
- Kershaw, E. E. and J. S. Flier (2004). "Adipose tissue as an endocrine organ." *J Clin Endocrinol Metab* 89(6): 2548-2556.
- Keseru, G. M. and G. M. Makara (2006). "Hit discovery and hit-to-lead approaches." *Drug Discov Today* 11(15-16): 741-748.

- Keusekotten, K., P. R. Elliott, L. Glockner, B. K. Fiol, R. B. Damgaard, Y. Kulathu, T. Wauer, M. K. Hospenthal, M. Gyrd-Hansen, D. Krappmann, K. Hofmann and D. Komander (2013). "OTULIN antagonizes LUBAC signaling by specifically hydrolyzing Met1-linked polyubiquitin." *Cell* 153(6): 1312-1326.
- Khoo, K. H., C. S. Verma and D. P. Lane (2014). "Drugging the p53 pathway: understanding the route to clinical efficacy." *Nat Rev Drug Discov* 13(3): 217-236.
- Kim, H. T., K. P. Kim, F. Lledias, A. F. Kisselev, K. M. Scaglione, D. Skowyra, S. P. Gygi and A. L. Goldberg (2007). "Certain pairs of ubiquitin-conjugating enzymes (E2s) and ubiquitin-protein ligases (E3s) synthesize nondegradable forked ubiquitin chains containing all possible isopeptide linkages." *J Biol Chem* 282(24): 17375-17386.
- Kirisako, T., K. Kamei, S. Murata, M. Kato, H. Fukumoto, M. Kanie, S. Sano, F. Tokunaga, K. Tanaka and K. Iwai (2006). "A ubiquitin ligase complex assembles linear polyubiquitin chains." *EMBO J* 25(20): 4877-4887.
- Kirkham, B. W., M. N. Lassere, J. P. Edmonds, K. M. Juhasz, P. A. Bird, C. S. Lee, R. Shnier and I. J. Portek (2006). "Synovial membrane cytokine expression is predictive of joint damage progression in rheumatoid arthritis: a two-year prospective study (the DAMAGE study cohort)." *Arthritis Rheum* 54(4): 1122-1131.
- Kishimoto, K., K. Matsumoto and J. Ninomiya-Tsuji (2000). "TAK1 mitogen-activated protein kinase kinase is activated by autophosphorylation within its activation loop." *J Biol Chem* 275(10): 7359-7364.
- Kobayashi, T., M. C. Walsh and Y. Choi (2004). "The role of TRAF6 in signal transduction and the immune response." *Microbes Infect* 6(14): 1333-1338.
- Komander, D. and M. Rape (2012). "The ubiquitin code." *Annu Rev Biochem* 81: 203-229.
- Kovalenko, A., C. Chable-Bessia, G. Cantarella, A. Israel, D. Wallach and G. Courtois (2003). "The tumour suppressor CYLD negatively regulates NF-kappaB signalling by deubiquitination." *Nature* 424(6950): 801-805.
- Kozakai, N., E. Kikuchi, M. Hasegawa, E. Suzuki, H. Ide, A. Miyajima, Y. Horiguchi, J. Nakashima, K. Umezawa, N. Shigematsu and M. Oya (2012). "Enhancement of radiosensitivity by a unique novel NF-kappaB inhibitor, DHMEQ, in prostate cancer." *Br J Cancer* 107(4): 652-657.
- Kulathu, Y. and D. Komander (2012). "Atypical ubiquitylation - the unexplored world of polyubiquitin beyond Lys48 and Lys63 linkages." *Nat Rev Mol Cell Biol* 13(8): 508-523.
- Kwon, H., S. Laurent, Y. Tang, H. Zong, P. Vemulapalli and J. E. Pessin (2014). "Adipocyte-specific IKKbeta signaling suppresses adipose tissue inflammation through an IL-13-dependent paracrine feedback pathway." *Cell Rep* 9(5): 1574-1583.
- Lamothe, B., A. Besse, A. D. Campos, W. K. Webster, H. Wu and B. G. Darnay (2007). "Site-specific Lys-63-linked tumor necrosis factor receptor-associated factor 6 auto-ubiquitination is a critical determinant of I kappa B kinase activation." *J Biol Chem* 282(6): 4102-4112.

- Lamothe, B., A. D. Campos, W. K. Webster, A. Gopinathan, L. Hur and B. G. Darnay (2008). "The RING domain and first zinc finger of TRAF6 coordinate signaling by interleukin-1, lipopolysaccharide, and RANKL." *J Biol Chem* 283(36): 24871-24880.
- Landré, V., B. Rotblat, S. Melino, F. Bernassola and G. Melino (2014). "Screening for E3-ubiquitin ligase inhibitors: challenges and opportunities." *Oncotarget* 5(18): 7988-8013.
- Landstrom, M. (2010). "The TAK1-TRAF6 signalling pathway." *Int J Biochem Cell Biol* 42(5): 585-589.
- Latz, E., A. Verma, A. Visintin, M. Gong, C. M. Sirois, D. C. Klein, B. G. Monks, C. J. McKnight, M. S. Lamphier, W. P. Duprex, T. Espevik and D. T. Golenbock (2007). "Ligand-induced conformational changes allosterically activate Toll-like receptor 9." *Nat Immunol* 8(7): 772-779.
- Lau, Y. Y., Y. H. Chen, T. T. Liu, C. Li, X. Cui, R. E. White and K. C. Cheng (2004). "Evaluation of a novel in vitro Caco-2 hepatocyte hybrid system for predicting in vivo oral bioavailability." *Drug Metab Dispos*, 32(9): 937-942.
- Lawrence, T. (2009). "The nuclear factor NF-kappaB pathway in inflammation." *Cold Spring Harb Perspect Biol* 1(6): a001651.
- Lee, E. G., D. L. Boone, S. Chai, S. L. Libby, M. Chien, J. P. Lodolce and A. Ma (2000). "Failure to regulate TNF-induced NF-kappaB and cell death responses in A20-deficient mice." *Science* 289(5488): 2350-2354.
- Leeson, P. (2012). "Drug discovery: Chemical beauty contest." *Nature* 481(7382): 455-456.
- Li, S., H. Zheng, A. P. Mao, B. Zhong, Y. Li, Y. Liu, Y. Gao, Y. Ran, P. Tien and H. B. Shu (2010). "Regulation of virus-triggered signaling by OTUB1- and OTUB2-mediated deubiquitination of TRAF3 and TRAF6." *J Biol Chem* 285(7): 4291-4297.
- Lin, S. C., Y. C. Lo and H. Wu (2010). "Helical assembly in the MyD88-IRAK4-IRAK2 complex in TLR/IL-1R signalling." *Nature* 465(7300): 885-890.
- Lomaga, M. A., W. C. Yeh, I. Sarosi, G. S. Duncan, C. Furlonger, A. Ho, S. Morony, C. Capparelli, G. Van, S. Kaufman, A. van der Heiden, A. Itie, A. Wakeham, W. Khoo, T. Sasaki, Z. Cao, J. M. Penninger, C. J. Paige, D. L. Lacey, C. R. Dunstan, W. J. Boyle, D. V. Goeddel and T. W. Mak (1999). "TRAF6 deficiency results in osteopetrosis and defective interleukin-1, CD40, and LPS signaling." *Genes Dev* 13(8): 1015-1024.
- Lorick, K. L., J. P. Jensen, S. Fang, A. M. Ong, S. Hatakeyama and A. M. Weissman (1999). "RING fingers mediate ubiquitin-conjugating enzyme (E2)-dependent ubiquitination." *Proc Natl Acad Sci USA* 96(20): 11364-11369.
- Lu, S. and J. Wang (2013). "The resistance mechanisms of proteasome inhibitor bortezomib." *Biomark Res* 1(1): 13.
- Luong le, A., M. Fragiadaki, J. Smith, J. Boyle, J. Lutz, J. L. Dean, S. Harten, M. Ashcroft, S. R. Walmsley, D. O. Haskard, P. H. Maxwell, H. Walczak, C. Pusey and P. C. Evans (2013). "Cezanne regulates inflammatory responses to hypoxia in endothelial cells by targeting TRAF6 for deubiquitination." *Circ Res* 112(12): 1583-1591.
- Lydeard, J. R., B. A. Schulman and J. W. Harper (2013). "Building and remodelling Cullin-RING E3 ubiquitin ligases." *EMBO Rep* 14(12): 1050-1061.

- Mahoney, D. J., H. H. Cheung, R. L. Mrad, S. Plenchette, C. Simard, E. Enwere, V. Arora, T. W. Mak, E. C. Lacasse, J. Waring and R. G. Korneluk (2008). "Both cIAP1 and cIAP2 regulate TNF $\alpha$ -mediated NF- $\kappa$ B activation." *Proc Natl Acad Sci USA* 105(33): 11778-11783.
- Makarov, S. S. (2001). "NF- $\kappa$ B in rheumatoid arthritis: a pivotal regulator of inflammation, hyperplasia, and tissue destruction." *Arthritis Res* 3(4): 200-206.
- Makarova, K. S., L. Aravind and E. V. Koonin (2000). "A novel superfamily of predicted cysteine proteases from eukaryotes, viruses and *Chlamydia pneumoniae*." *Trends Biochem Sci* 25(2): 50-52.
- Makki, K., P. Froguel and I. Wolowczuk (2013). "Adipose tissue in obesity-related inflammation and insulin resistance: cells, cytokines, and chemokines." *ISRN Inflamm* 2013: 139239.
- Makley, L. N. and J. E. Gestwicki (2013). "Expanding the number of 'druggable' targets: non-enzymes and protein-protein interactions." *Chem Biol Drug Des* 81(1): 22-32.
- Marin, I. and A. Ferrus (2002). "Comparative genomics of the RBR family, including the Parkinson's disease-related gene parkin and the genes of the ariadne subfamily." *Mol Biol Evol* 19(12): 2039-2050.
- Megas, C., E. G. Hatzivassiliou, Q. Yin, E. Marinopoulou, P. Hadweh, D. A. Vignali and G. Mosialos (2011). "Mutational analysis of TRAF6 reveals a conserved functional role of the RING dimerization interface and a potentially necessary but insufficient role of RING-dependent TRAF6 polyubiquitination towards NF- $\kappa$ B activation." *Cell Signal* 23(5): 772-777.
- Meng, Q., M. Zheng, H. Liu, C. Song, W. Zhang, J. Yan, L. Qin and X. Liu (2012). "TRAF6 regulates proliferation, apoptosis, and invasion of osteosarcoma cell." *Mol Cell Biochem* 371(1-2): 177-186.
- Mevissen, T. E., M. K. Hospenthal, P. P. Geurink, P. R. Elliott, M. Akutsu, N. Arnaudo, R. Ekkebus, Y. Kulathu, T. Wauer, F. El Oualid, S. M. Freund, H. Ovaa and D. Komander (2013). "OTU deubiquitinases reveal mechanisms of linkage specificity and enable ubiquitin chain restriction analysis." *Cell* 154(1): 169-184.
- Motshwene, P. G., M. C. Moncrieffe, J. G. Grossmann, C. Kao, M. Ayaluru, A. M. Sandercock, C. V. Robinson, E. Latz and N. J. Gay (2009). "An oligomeric signaling platform formed by the Toll-like receptor signal transducers MyD88 and IRAK-4." *J Biol Chem* 284(37): 25404-25411.
- Naito, A., S. Azuma, S. Tanaka, T. Miyazaki, S. Takaki, K. Takatsu, K. Nakao, K. Nakamura, M. Katsuki, T. Yamamoto and J. Inoue (1999). "Severe osteopetrosis, defective interleukin-1 signalling and lymph node organogenesis in TRAF6-deficient mice." *Genes Cells* 4(6): 353-362.
- Namjou, B., C. B. Choi, I. T. Harley, M. E. Alarcon-Riquelme, B. Network, J. A. Kelly, S. B. Glenn, J. O. Ojwang, A. Adler, K. Kim, C. J. Gallant, S. A. Boackle, L. A. Criswell, R. P. Kimberly, E. E. Brown, J. Edberg, G. S. Alarcon, A. M. Stevens, C. O. Jacob, G. S. Gilkeson, D. L. Kamen, B. P. Tsao, J. M. Anaya, E. M. Kim, S. Y. Park, Y. K. Sung, J. M. Guthridge, J. T. Merrill, M. Petri, R. Ramsey-Goldman, L. M. Vila, T. B. Niewold, J. Martin, B. A. Pons-Estel, N. Genoma en Lupus, T. J. Vyse, B. I. Freedman, K. L. Moser, P. M. Gaffney, A. H. Williams, M. E. Comeau, J. D. Reveille, C. Kang, J. A. James, R. H. Scofield, C. D. Langefeld, K. M. Kaufman, J. B. Harley and S. C. Bae (2012). "Evaluation of TRAF6 in a large multiethnic lupus cohort." *Arthritis Rheum* 64(6): 1960-1969.
- Napetschnig, J. and H. Wu (2013). "Molecular basis of NF- $\kappa$ B signaling." *Annu Rev Biophys* 42: 443-468.

- Netea, M. G., C. Wijmenga and L. A. O'Neill (2012). "Genetic variation in Toll-like receptors and disease susceptibility." *Nat Immunol* 13(6): 535-542.
- O'Neill, L. A. and A. G. Bowie (2007). "The family of five: TIR-domain-containing adaptors in Toll-like receptor signalling." *Nat Rev Immunol* 7(5): 353-364.
- O'Neill, L. A., Golenbock D. and A. G. Bowie (2013). "The history of Toll-like receptors – redefining innate immunity." *Nat Rev Immunol* 13(6): 453-460.
- Oeckinghaus, A. and S. Ghosh (2009). "The NF-kappaB family of transcription factors and its regulation." *Cold Spring Harb Perspect Biol* 1(4): a000034.
- Oeckinghaus, A., M. S. Hayden and S. Ghosh (2011). "Crosstalk in NF-kappaB signaling pathways." *Nat Immunol* 12(8): 695-708.
- Oeckinghaus, A., E. Wegener, V. Welteke, U. Ferch, S. C. Arslan, J. Ruland, C. Scheidereit and D. Krappmann (2007). "Malt1 ubiquitination triggers NF-kappaB signaling upon T-cell activation." *EMBO J* 26(22): 4634-4645.
- Ohno, H., G. Takimoto and T. W. McKeithan (1990). "The candidate proto-oncogene bcl-3 is related to genes implicated in cell lineage determination and cell cycle control." *Cell* 60(6): 991-997.
- Ostuni, R., I. Zanoni and F. Granucci (2010). "Deciphering the complexity of Toll-like receptor signaling." *Cell Mol Life Sci* 67(24): 4109-4134.
- Overington, J. P., B. Al-Lazikani and A. L. Hopkins (2006). "How many drug targets are there?" *Nat Rev Drug Discov* 5(12): 993-996.
- Pal, D., S. Dasgupta, R. Kundu, S. Maitra, G. Das, S. Mukhopadhyay, S. Ray, S. S. Majumdar and S. Bhattacharya (2012). "Fetuin-A acts as an endogenous ligand of TLR4 to promote lipid-induced insulin resistance." *Nat Med* 18(8): 1279-1285.
- Perkins, J. R., I. Diboun, B. H. Dessailly, J. G. Lees and C. Orengo (2010). "Transient protein-protein interactions: structural, functional, and network properties." *Structure* 18(10): 1233-1243.
- Pham, L. V., H. J. Zhou, Y. C. Lin-Lee, A. T. Tamayo, L. C. Yoshimura, L. Fu, B. G. Darnay and R. J. Ford (2008). "Nuclear tumor necrosis factor receptor-associated factor 6 in lymphoid cells negatively regulates c-Myb-mediated transactivation through small ubiquitin-related modifier-1 modification." *J Biol Chem* 283(8): 5081-5089.
- Phan, T. C., J. Xu and M. H. Zheng (2004). "Interaction between osteoblast and osteoclast: impact in bone disease." *Histol Histopathol* 19(4): 1325-1344.
- Pulvino, M., Y. Liang, D. Oleksyn, M. DeRan, E. Van Pelt, J. Shapiro, I. Sanz, L. Chen and J. Zhao (2012). "Inhibition of proliferation and survival of diffuse large B-cell lymphoma cells by a small-molecule inhibitor of the ubiquitin-conjugating enzyme Ubc13-Uev1A." *Blood* 120(8): 1668-1677.
- Rahighi, S., F. Ikeda, M. Kawasaki, M. Akutsu, N. Suzuki, R. Kato, T. Kensche, T. Uejima, S. Bloor, D. Komander, F. Randow, S. Wakatsuki and I. Dikic (2009). "Specific recognition of linear ubiquitin chains by NEMO is important for NF-kappaB activation." *Cell* 136(6): 1098-1109.

- Reyes-Turcu, F. E., K. H. Ventii and K. D. Wilkinson (2009). "Regulation and cellular roles of ubiquitin-specific deubiquitinating enzymes." *Annu Rev Biochem* 78: 363-397.
- Rickert, R. C., J. Jellusova and A. V. Miletic (2011). "Signaling by the tumor necrosis factor receptor superfamily in B-cell biology and disease." *Immunol Rev* 244(1): 115-133.
- Rotin, D. and S. Kumar (2009). "Physiological functions of the HECT family of ubiquitin ligases." *Nat Rev Mol Cell Biol* 10(6): 398-409.
- Russ, A. P. and S. Lampel (2005). "The druggable genome: an update." *Drug Discov Today* 10(23-24): 1607-1610.
- Salem, K., C. O. Brown, J. Schibler and A. Goel (2013). "Combination chemotherapy increases cytotoxicity of multiple myeloma cells by modification of nuclear factor (NF)-kappaB activity." *Exp Hematol* 41(2): 209-218.
- Salmina, E.S., G.L. Rusinov, P.A. Slepukhin, R. I. Ishmetova, S. G. Tolshchina, V. A. Potemkin and M. A. Grishina (2011) "Intermolecular Interactions in Heteromolecular Crystals of Tetrazine Derivatives with Azoles." *J Struct Chem* 52(6): 1134–1138.
- Sanjuan, M. A., S. Milasta and D. R. Green (2009). "Toll-like receptor signaling in the lysosomal pathways." *Immunol Rev* 227(1): 203-220.
- Sato, S., H. Sanjo, K. Takeda, J. Ninomiya-Tsuji, M. Yamamoto, T. Kawai, K. Matsumoto, O. Takeuchi and S. Akira (2005). "Essential function for the kinase TAK1 in innate and adaptive immune responses." *Nat Immunol* 6(11): 1087-1095.
- Scheinecker, C., K. Redlich and J. S. Smolen (2008). "Cytokines as therapeutic targets: advances and limitations." *Immunity* 28(4): 440-444.
- Schmukle, A. C. and H. Walczak (2012). "No one can whistle a symphony alone - how different ubiquitin linkages cooperate to orchestrate NF-kappaB activity." *J Cell Sci* 125(Pt 3): 549-559.
- Schorpp, K., I. Rothenaigner, E. Salmina, J. Reinshagen, T. Low, J. K. Brenke, J. Gopalakrishnan, I. V. Tetko, S. Gul and K. Hadian (2013). "Identification of Small-Molecule Frequent Hitters from AlphaScreen High-Throughput Screens." *J Biomol Screen* 19(5): 715-726.
- Shembade, N., A. Ma and E. W. Harhaj (2010). "Inhibition of NF-kappaB signaling by A20 through disruption of ubiquitin enzyme complexes." *Science* 327(5969): 1135-1139.
- Shi, H., M. V. Kokoeva, K. Inouye, I. Tzamelis, H. Yin and J. S. Flier (2006). "TLR4 links innate immunity and fatty acid-induced insulin resistance." *J Clin Invest* 116(11): 3015-3025.
- Simmonds, R. E. and B. M. Foxwell (2008). "Signalling, inflammation and arthritis: NF-kappaB and its relevance to arthritis and inflammation." *Rheumatology (Oxford)* 47(5): 584-590.
- Skaar, J. R., J. K. Pagan and M. Pagano (2013). "Mechanisms and function of substrate recruitment by F-box proteins." *Nat Rev Mol Cell Biol* 14(6): 369-381.
- Skaar, J. R., J. K. Pagan and M. Pagano (2014). "SCF ubiquitin ligase-targeted therapies." *Nat Rev Drug Discov* 13(12): 889-903.

- Slepukhin, P. A., E. S. Salmina, V. A. Potemkin and M. A. Grishina (2013). "Crystal and Electronic Structure of Heteromolecular Complexes of 3,6-bis-(3,5-dimethylpyrazol-1-yl)-1,2,4,5-tetrazine with Azoles." *J Struct Chem* 54 (6): 1091-1100.
- Soucy, T. A., P. G. Smith, M. A. Milhollen, A. J. Berger, J. M. Gavin, S. Adhikari, J. E. Brownell, K. E. Burke, D. P. Cardin, S. Critchley, C. A. Cullis, A. Doucette, J. J. Garnsey, J. L. Gaulin, R. E. Gershman, A. R. Lublinsky, A. McDonald, H. Mizutani, U. Narayanan, E. J. Olhava, S. Peluso, M. Rezaei, M. D. Sintchak, T. Talreja, M. P. Thomas, T. Traore, S. Vyskocil, G. S. Weatherhead, J. Yu, J. Zhang, L. R. Dick, C. F. Claiborne, M. Rolfe, J. B. Bolen and S. P. Langston (2009). "An inhibitor of NEDD8-activating enzyme as a new approach to treat cancer." *Nature* 458(7239): 732-736.
- Spratt, D. E., H. Walden and G. S. Shaw (2014). "RBR E3 ubiquitin ligases: new structures, new insights, new questions." *Biochem J* 458(3): 421-437.
- Starczynowski, D. T., W. W. Lockwood, S. Delehoussee, R. Chari, J. Wegrzyn, M. Fuller, M. S. Tsao, S. Lam, A. F. Gazdar, W. L. Lam and A. Karsan (2011). "TRAF6 is an amplified oncogene bridging the RAS and NF-kappaB pathways in human lung cancer." *J Clin Invest* 121(10): 4095-4105.
- Staudt, L. M. (2010). "Oncogenic activation of NF-kappaB." *Cold Spring Harb Perspect Biol* 2(6): a000109.
- Stieglitz, B., R. R. Rana, M. G. Koliopoulos, A. C. Morris-Davies, V. Schaeffer, E. Christodoulou, S. Howell, N. R. Brown, I. Dikic and K. Rittinger (2013). "Structural basis for ligase-specific conjugation of linear ubiquitin chains by HOIP." *Nature* 503(7476): 422-426.
- Suhir, H. and A. Etzioni (2010). "The role of Toll-like receptor signaling in human immunodeficiencies." *Clin Rev Allergy Immunol* 38(1): 11-19.
- Sun, H., X. Li, L. Fan, G. Wu, M. Li and J. Fang (2014). "TRAF6 is upregulated in colon cancer and promotes proliferation of colon cancer cells." *Int J Biochem Cell Biol* 53: 195-201.
- Sun, H., X. B. Li, Y. Meng, L. Fan, M. Li and J. Fang (2013). "TRAF6 upregulates expression of HIF-1alpha and promotes tumor angiogenesis." *Cancer Res* 73(15): 4950-4959.
- Sun, L., L. Deng, C. K. Ea, Z. P. Xia and Z. J. Chen (2004). "The TRAF6 ubiquitin ligase and TAK1 kinase mediate IKK activation by BCL10 and MALT1 in T lymphocytes." *Mol Cell* 14(3): 289-301.
- Sun, S. C. (2012). "The noncanonical NF-kappaB pathway." *Immunol Rev* 246(1): 125-140.
- Tack, C. J., R. Stienstra, L. A. Joosten and M. G. Netea (2012). "Inflammation links excess fat to insulin resistance: the role of the interleukin-1 family." *Immunol Rev* 249(1): 239-252.
- Taganov, K. D., M. P. Boldin, K. J. Chang and D. Baltimore (2006). "NF-kappaB-dependent induction of microRNA miR-146, an inhibitor targeted to signaling proteins of innate immune responses." *Proc Natl Acad Sci USA* 103(33): 12481-12486.
- Takeuchi, M., M. Rothe and D. V. Goeddel (1996). "Anatomy of TRAF2. Distinct domains for nuclear factor-kappaB activation and association with tumor necrosis factor signaling proteins." *J Biol Chem* 271(33): 19935-19942.
- Tarantino, N., J. Y. Tinevez, E. F. Crowell, B. Boisson, R. Henriques, M. Mhlanga, F. Agou, A. Israel and E. Laplantine (2014). "TNF and IL-1 exhibit distinct ubiquitin requirements for inducing NEMO-IKK supramolecular structures." *J Cell Biol* 204(2): 231-245.

- Thomas, C., J. F. Bazan and K. C. Garcia (2012). "Structure of the activating IL-1 receptor signaling complex." *Nat Struct Mol Biol* 19(4): 455-457.
- Tokunaga, F., T. Nakagawa, M. Nakahara, Y. Saeki, M. Taniguchi, S. Sakata, K. Tanaka, H. Nakano and K. Iwai (2011). "SHARPIN is a component of the NF-kappaB-activating linear ubiquitin chain assembly complex." *Nature* 471(7340): 633-636.
- Toubi, E. and Y. Shoenfeld (2004). "Toll-like receptors and their role in the development of autoimmune diseases." *Autoimmunity* 37(3): 183-188.
- Trompouki, E., E. Hatzivassiliou, T. Tschirritsis, H. Farmer, A. Ashworth and G. Mosialos (2003). "CYLD is a deubiquitinating enzyme that negatively regulates NF-kappaB activation by TNFR family members." *Nature* 424(6950): 793-796.
- Tsukamoto, H., K. Fukudome, S. Takao, N. Tsuneyoshi and M. Kimoto (2010). "Lipopolysaccharide-binding protein-mediated Toll-like receptor 4 dimerization enables rapid signal transduction against lipopolysaccharide stimulation on membrane-associated CD14-expressing cells." *Int Immunol* 22(4): 271-280.
- Ungermannova, D., J. Lee, G. Zhang, H. G. Dallmann, C. S. McHenry and X. Liu (2013). "High-throughput screening AlphaScreen assay for identification of small-molecule inhibitors of ubiquitin E3 ligase SCFSkp2-Cks1." *J Biomol Screen* 18(8): 910-920.
- Vallabhapurapu, S. and M. Karin (2009). "Regulation and function of NF-kappaB transcription factors in the immune system." *Annu Rev Immunol* 27: 693-733.
- Vallabhapurapu, S., A. Matsuzawa, W. Zhang, P. H. Tseng, J. J. Keats, H. Wang, D. A. Vignali, P. L. Bergsagel and M. Karin (2008). "Nonredundant and complementary functions of TRAF2 and TRAF3 in a ubiquitination cascade that activates NIK-dependent alternative NF-kappaB signaling." *Nat Immunol* 9(12): 1364-1370.
- van den Berg, S. M., T. T. Seijkens, P. J. Kusters, B. Zarzycka, L. Beckers, M. den Toom, M. J. Gijbels, A. Chatzigeorgiou, C. Weber, M. P. de Winther, T. Chavakis, G. A. Nicolaes and E. Lutgens (2014). "Blocking CD40-TRAF6 interactions by small-molecule inhibitor 6860766 ameliorates the complications of diet-induced obesity in mice." *Int J Obes (Lond)*.
- VanDemark, A. P., R. M. Hofmann, C. Tsui, C. M. Pickart and C. Wolberger (2001). "Molecular insights into polyubiquitin chain assembly: crystal structure of the Mms2/Ubc13 heterodimer." *Cell* 105(6): 711-720.
- Varfolomeev, E., T. Goncharov, A. V. Fedorova, J. N. Dynek, K. Zobel, K. Deshayes, W. J. Fairbrother and D. Vucic (2008). "c-IAP1 and c-IAP2 are critical mediators of tumor necrosis factor alpha (TNFalpha)-induced NF-kappaB activation." *J Biol Chem* 283(36): 24295-24299.
- Vassilev, L. T., B. T. Vu, B. Graves, D. Carvajal, F. Podlaski, Z. Filipovic, N. Kong, U. Kammlott, C. Lukacs, C. Klein, N. Fotouhi and E. A. Liu (2004). "In vivo activation of the p53 pathway by small-molecule antagonists of MDM2." *Science* 303(5659): 844-848.
- Villoutreix, B. O., M. A. Kuenemann, J. L. Poyet, H. Bruzzoni-Giovanelli, C. Labbe, D. Lagorce, O. Sperandio and M. A. Miteva (2014). "Drug-Like Protein-Protein Interaction Modulators: Challenges and Opportunities for Drug Discovery and Chemical Biology." *Mol Inform* 33(6-7): 414-437.



- Wajant, H. and P. Scheurich (2011). "TNFR1-induced activation of the classical NF-kappaB pathway." *FEBS J* 278(6): 862-876.
- Wallach, D. and A. Kovalenko (2008). "Self-termination of the terminator." *Nat Immunol* 9(12): 1325-1327.
- Wang, C., L. Deng, M. Hong, G. R. Akkaraju, J. Inoue and Z. J. Chen (2001). "TAK1 is a ubiquitin-dependent kinase of MKK and IKK." *Nature* 412(6844): 346-351.
- Wang, D., S. Zhang, L. Li, X. Liu, K. Mei and X. Wang (2010). "Structural insights into the assembly and activation of IL-1beta with its receptors." *Nat Immunol* 11(10): 905-911.
- Weisberg, S. P., D. Hunter, R. Huber, J. Lemieux, S. Slaymaker, K. Vaddi, I. Charo, R. L. Leibel and A. W. Ferrante, Jr. (2006). "CCR2 modulates inflammatory and metabolic effects of high-fat feeding." *J Clin Invest* 116(1): 115-124.
- Wells, J. A. and C. L. McClendon (2007). "Reaching for high-hanging fruit in drug discovery at protein-protein interfaces." *Nature* 450(7172): 1001-1009.
- Wertz, I. E., K. M. O'Rourke, H. Zhou, M. Eby, L. Aravind, S. Seshagiri, P. Wu, C. Wiesmann, R. Baker, D. L. Boone, A. Ma, E. V. Koonin and V. M. Dixit (2004). "De-ubiquitination and ubiquitin ligase domains of A20 downregulate NF-kappaB signalling." *Nature* 430(7000): 694-699.
- Wertz, I. E., and V. M. Dixit (2010). "Signaling to NF-kappaB: regulation by ubiquitination." *Cold Spring Harb Perspect Biol* 2(3): a003350.
- Wiener, R., X. Zhang, T. Wang and C. Wolberger (2012). "The mechanism of OTUB1-mediated inhibition of ubiquitination." *Nature* 483(7391): 618-622.
- Wooff, J., L. Pastushok, M. Hanna, Y. Fu and W. Xiao (2004). "The TRAF6 RING finger domain mediates physical interaction with Ubc13." *FEBS Lett* 566(1-3): 229-233.
- Wu, H. and J. R. Arron (2003). "TRAF6, a molecular bridge spanning adaptive immunity, innate immunity and osteoimmunology." *Bioessays* 25(11): 1096-1105.
- Xie, P. (2013). "TRAF molecules in cell signaling and in human diseases." *J Mol Signal* 8(1): 7.
- Xie, P., Z. J. Kraus, L. L. Stunz and G. A. Bishop (2008). "Roles of TRAF molecules in B lymphocyte function." *Cytokine Growth Factor Rev* 19(3-4): 199-207.
- Xu, G., Y. C. Lo, Q. Li, G. Napolitano, X. Wu, X. Jiang, M. Dreano, M. Karin and H. Wu (2011). "Crystal structure of inhibitor of kappaB kinase beta." *Nature* 472(7343): 325-330.
- Xu, M., B. Skaug, W. Zeng and Z. J. Chen (2009). "A ubiquitin replacement strategy in human cells reveals distinct mechanisms of IKK activation by TNFalpha and IL-1beta." *Mol Cell* 36(2): 302-314.
- Xu, P., D. M. Duong, N. T. Seyfried, D. Cheng, Y. Xie, J. Robert, J. Rush, M. Hochstrasser, D. Finley and J. Peng (2009). "Quantitative proteomics reveals the function of unconventional ubiquitin chains in proteasomal degradation." *Cell* 137(1): 133-145.

- Yamamoto, M., T. Okamoto, K. Takeda, S. Sato, H. Sanjo, S. Uematsu, T. Saitoh, N. Yamamoto, H. Sakurai, K. J. Ishii, S. Yamaoka, T. Kawai, Y. Matsuura, O. Takeuchi and S. Akira (2006). "Key function for the Ubc13 E2 ubiquitin-conjugating enzyme in immune receptor signaling." *Nat Immunol* 7(9): 962-970.
- Yang, W. L., J. Wang, C. H. Chan, S. W. Lee, A. D. Campos, B. Lamothe, L. Hur, B. C. Grabiner, X. Lin, B. G. Darnay and H. K. Lin (2009). "The E3 ligase TRAF6 regulates Akt ubiquitination and activation." *Science* 325(5944): 1134-1138.
- Yasunaga, J., F. C. Lin, X. Lu and K. T. Jeang (2011). "Ubiquitin-specific peptidase 20 targets TRAF6 and human T cell leukemia virus type 1 tax to negatively regulate NF-kappaB signaling." *J Virol* 85(13): 6212-6219.
- Ye, H., J. R. Arron, B. Lamothe, M. Cirilli, T. Kobayashi, N. K. Shevde, D. Segal, O. K. Dzivenu, M. Vologodskaya, M. Yim, K. Du, S. Singh, J. W. Pike, B. G. Darnay, Y. Choi and H. Wu (2002). "Distinct molecular mechanism for initiating TRAF6 signalling." *Nature* 418(6896): 443-447.
- Ye, Y. and M. Rape (2009). "Building ubiquitin chains: E2 enzymes at work." *Nat Rev Mol Cell Biol* 10(11): 755-764.
- Yin, J., Y. Peng, J. Wu, Y. Wang and L. Yao (2014). "Toll-like receptor 2/4 links to free fatty acid-induced inflammation and beta-cell dysfunction." *J Leukoc Biol* 95(1): 47-52.
- Yin, Q., B. Lamothe, B. G. Darnay and H. Wu (2009). "Structural basis for the lack of E2 interaction in the RING domain of TRAF2." *Biochemistry* 48(44): 10558-10567.
- Yin, Q., S. C. Lin, B. Lamothe, M. Lu, Y. C. Lo, G. Hura, L. Zheng, R. L. Rich, A. D. Campos, D. G. Myszka, M. J. Lenardo, B. G. Darnay and H. Wu (2009). "E2 interaction and dimerization in the crystal structure of TRAF6." *Nat Struct Mol Biol* 16(6): 658-666.
- Yoshida, H., H. Jono, H. Kai and J. D. Li (2005). "The tumor suppressor cylindromatosis (CYLD) acts as a negative regulator for toll-like receptor 2 signaling via negative cross-talk with TRAF6 AND TRAF7." *J Biol Chem* 280(49): 41111-41121.
- Yoshikawa, A., Y. Sato, M. Yamashita, H. Mimura, A. Yamagata and S. Fukai (2009). "Crystal structure of the NEMO ubiquitin-binding domain in complex with Lys 63-linked di-ubiquitin." *FEBS Lett* 583(20): 3317-3322.
- Zarnegar, B. J., Y. Wang, D. J. Mahoney, P. W. Dempsey, H. H. Cheung, J. He, T. Shiba, X. Yang, W. C. Yeh, T. W. Mak, R. G. Korneluk and G. Cheng (2008). "Noncanonical NF-kappaB activation requires coordinated assembly of a regulatory complex of the adaptors cIAP1, cIAP2, TRAF2 and TRAF3 and the kinase NIK." *Nat Immunol* 9(12): 1371-1378.
- Zepp, J., L. Wu and X. Li (2011). "IL-17 receptor signaling and T helper 17-mediated autoimmune demyelinating disease." *Trends Immunol* 32(5): 232-239.
- Zhang, L., K. Blackwell, Z. Shi and H. Habelhah (2010). "The RING domain of TRAF2 plays an essential role in the inhibition of TNFalpha-induced cell death but not in the activation of NF-kappaB." *J Mol Biol* 396(3): 528-539.
- Zheng, N., P. Wang, P. D. Jeffrey and N. P. Pavletich (2000). "Structure of a c-Cbl-UbcH7 complex: RING domain function in ubiquitin-protein ligases." *Cell* 102(4): 533-539.

- Zhong, L., F. Cao and Q. You (2013). "Effect of TRAF6 on the biological behavior of human lung adenocarcinoma cell." *Tumour Biol* 34(1): 231-239.
- Zhu, L. J., L. Dai, D. H. Zheng, Y. Q. Mo, X. Ou-Yang, X. N. Wei, J. Shen and B. Y. Zhang (2012). "Upregulation of tumor necrosis factor receptor-associated factor 6 correlated with synovitis severity in rheumatoid arthritis." *Arthritis Res Ther* 14(3): R133.
- Zotti, T., P. Vito and R. Stilo (2012). "The seventh ring: exploring TRAF7 functions." *J Cell Physiol* 227(3): 1280-1284.

## 9 Abbreviations

Å	Ångström
AD	Activation Domain
ADME	absorption-distribution-metabolism-excretion
ALPHAScreen	Amplified Luminescence Proximity Homogeneous Assay
APC	antigen presenting cells
APPL1	adaptor protein, phosphotyrosine interaction, PH (pleckstrin homology) domain and leucine zipper containing 1
ARD	ankyrin repeat-containing domain
ATM	Ataxia telangiectasia mutated
ATP	adenosine-tri-phosphate
BAFF-R	B cell activating factor belonging to the TNF family
Bcl-XI	B cell lymphoma extra large
BCL10	B cell chronic lymphocytic leukemia/lymphoma associated 10
BCR	B cell receptor
BD	Binding Domain
C25	Compound 25
Caco-2	human colon adenocarcinoma cell
CARMA	CARD containing MAGUK protein 1
cDNA	complementary DNA
CD40/80/86	Cluster of Differentiation
ciAP	cellular inhibitor apoptosis protein
Cl	Chloride
Cl <sub>int</sub>	intrinsic clearance constant
cpm	counts per minute
C-terminal	carboxy-terminal
CV	Coefficient of Variation
CYLD	Cylindromatosis
CYP	Cytochrom
Cys	cysteine
D/DMSO	Dimethylsulfoxide
DELFI	Dissociation-Enhanced Lanthanide Fluorescence Immunoassay
DIO	diet-induced obesity
DNA	Desoxyribonucleic acid

dsRNA	double stranded RNA
DUB	deubiquitinase
ELISA	Enzyme Linked Immunosorbent Assay
EMSA	Electrophoretic Mobility Shift Assay
ERAD	endoplasmatic reticulum-associated degradation
eWAT	epidermal white adipose tissue
F	Fluor
FADD	Fas-associated death domain protein
FATCAT	flexible structure alignment by chaining aligned fragment pairs allowing twists F-box
FDA	Food and Drug Administration
FetA	FetuinA
FFA	free fatty acids
FH	frequent hitters
Fig.	Figure
for	forward
g/kg	gram/kilogram
G6Pase	Glucose-6-phosphatase
GSK3 $\beta$	Glycogen Synthase Kinase 3 $\beta$
GST	Glutathione-S-Transferase
GTT	Glucose Tolerance Test
HECT	homology to E6AP C terminus
HepG2	human hepatoma cells
hERG	human Ether-a-go-go related gene
HFD	High-fat-diet
HIF1 $\alpha$	hypoxia-inducible factor 1 $\alpha$
His	Histidine
HOIL-1	Heme-Oxidized IRP2 ubiquitin ligase 1
HOIP	HOIL-1 interacting protein
HTS	High-Throughput-Screening
IAP	inhibitor apoptosis protein
IBM	IAP-binding motif
ICAM-1	Intracellular Adhesion Molecule 1
IC <sub>50</sub>	inhibitory concentration <sub>50</sub>

IDO	Institute of Diabetes and Obesity
I $\kappa$ B	Inhibitor of kappa B
IFN	Interferon
IGF-1	insulin-like growth factor-1
IKK	I $\kappa$ B kinase complex
IL-	Interleukin-
IL-1R	Interleukin-1 receptors
IRAK	Interleukin-1 receptor associated kinase
JAMM	JAB1/MPN/MOV34 family
K63	Lysine 83
K <sub>d</sub>	dissociation constant
k <sub>el</sub>	elimination constant
LogD	distribution coefficient
LogP	partition coefficient
LPS	lipopolysaccharide
LUBAC	linear ubiquitin assembly complex
Lys	Lysine
MALT1	Mucosa associated lymphoid tissue1
MAPK	mitogen-activated protein kinases
MAPKKK	MAPK-kinase-kinase
MDM2	Mouse double minute 2 homolog
MEF	Mouse Embryonic Fibroblast
Me/CH <sub>3</sub>	methyl-
MeO	Methyl-oxide
Met	Methionine
min	minute
miR	MicroRNA
mRNA	messenger RNA
$\mu$ M/mM	Micro-/Mili-molar
$\mu$ L/mL	Micro-/Mili-litre
MST	Microscale Thermophoresis
MyD88	Myeloid Differentiation primary response gene 88
<sup>15</sup> N	<sup>15</sup> nitrogen
NAE	NEDD8 activating enzyme

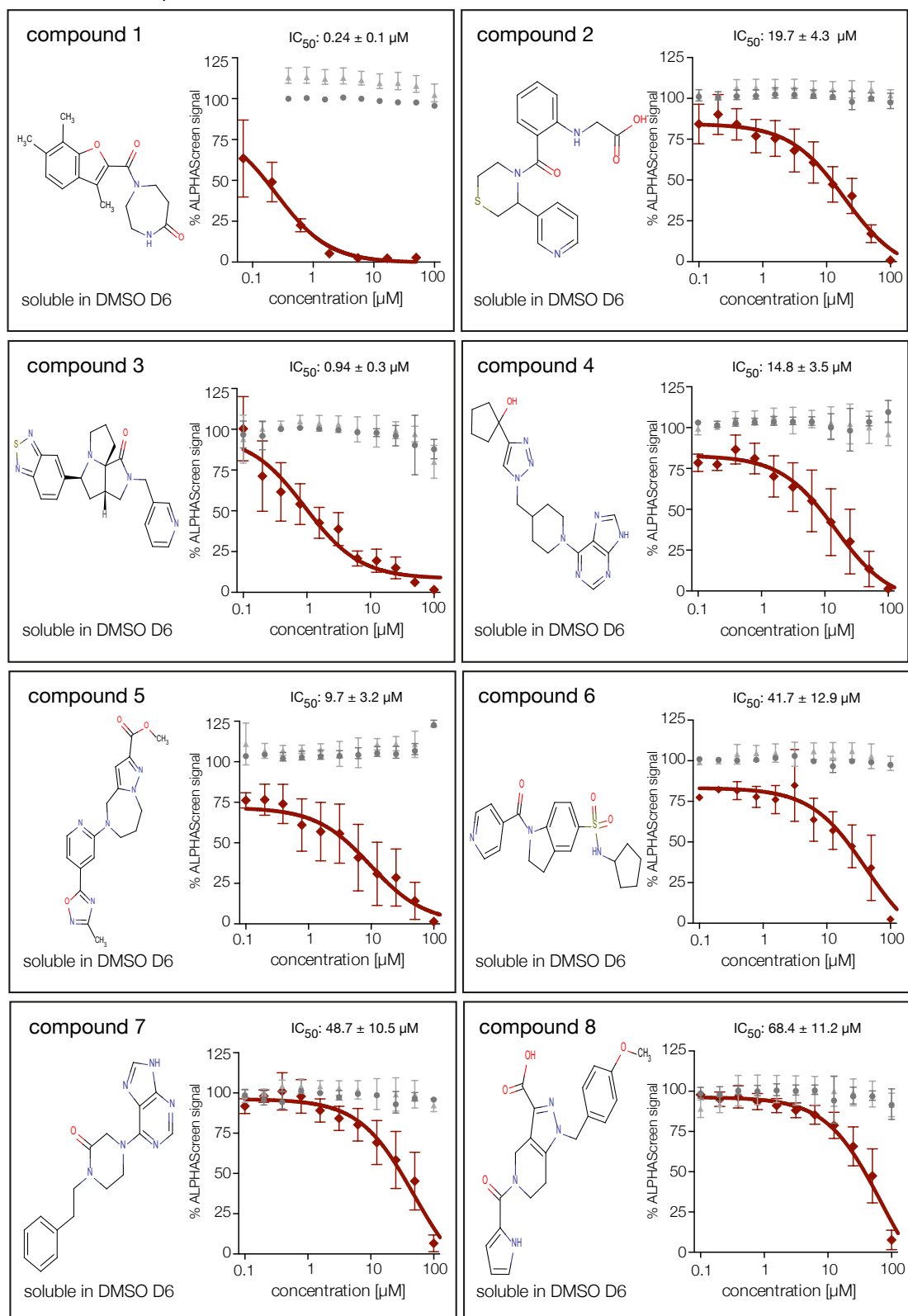
neg.	negative
NEMO	NF- $\kappa$ B essential modifier
NF- $\kappa$ B	nuclear factor “kappa-light-chain-enhancer” of activated B cells
NIK	NF- $\kappa$ B inducing kinase
nM	Nanomolar
NMR	Nuclear Magnetic Resonance
NLR	Nucleotide-binding Oligomerization Domain-like receptors
NLS	Nuclear Localization Signal
ns	not significant
N-terminal	amino-terminal
OTU	Ovarian Tumor Proteases
OTUB1	OTU deubiquitinase, ubiquitin aldehyde binding 1
OTULIN	OTU DUB with linear linkage specificity
PAMP	pathogen associated molecular pattern
PDB	Protein Data Bank
$^{32}\text{P}$	$^{32}$ Phosphorus
p-	phospho-
PAINS	pan-assay-interference-compounds
PEPCK	Phosphoenolpyruvate-carboxykinase
pM	pico-molar
pos.	positive
PPI	protein-protein interactions
qPCR	quantitative realtime polymerase chain reaction
R1/R2/R3	residue 1/2/3
RA	rheumatoid arthritis
RANK	Receptor Activator of NF- $\kappa$ B
RBR	RING-between-RING
rev	reverse
RHR	Rel homology region
RING	really interesting new gene
RIP1	Receptor-Interacting Protein 1
RLR	RIG-I-like receptors
RNA	Ribonucleic acid
RNF8	RING finger protein 8

RZ1	RING-Zincfinger1 domain
SAR	structure activity relationship
SLE	systemic lupus erythematosus
SDS-PAGE	Sodium-Duodecyl-Sulfate-Polyacrylamid-Gelectrophoresis
SNP	single nucleotide polymorphisms
SOFAST HMQC	Band-Selective Optimized Flip Angle Short Transient Heteronuclear Multiple Quantum Coherence
ssRNA	single stranded RNA
StDEV	Standard Deviation
StrepII	Strep-TagII
SW	Signal Window
T <sub>1/2</sub>	half-time
T2DM	Type 2 diabetes mellitus
TAD	C-terminal transactivation domain
TAB	TGF $\beta$ -activated kinase 1 binding protein
TAK1	TGF $\beta$ -activated kinase 1
TCR	T cell receptors
TIR	Toll/IL-1R domain
TGF $\beta$	Transforming Growth Factor $\beta$
TLR	Toll-like receptor
TNF $\alpha$	Tumor Necrosis Factor $\alpha$
TNFR1	Tumor Necrosis Factor Receptor 1
TRADD	TNFR1-associated death domain proteins
TRAF	TNFR associated Factor
TR-FRET	time resolved Förster resonance energy transfer
Ubc13	Ubiquitin-conjugating enzyme 13
Ubc13FH	Ubc13-Flag-His
UCHs	Ubiquitin COOH-terminal hydrolases
Uev1a	Ubiquitin-conjugating E2 variant 1a
UPS	Ubiquitin Proteasom System
USP	Ubiquitin specific proteases
VCAM	Vascular Adhesion Molecule
WT	Wildtype
Y2H	Yeast-Two-Hybrid assay



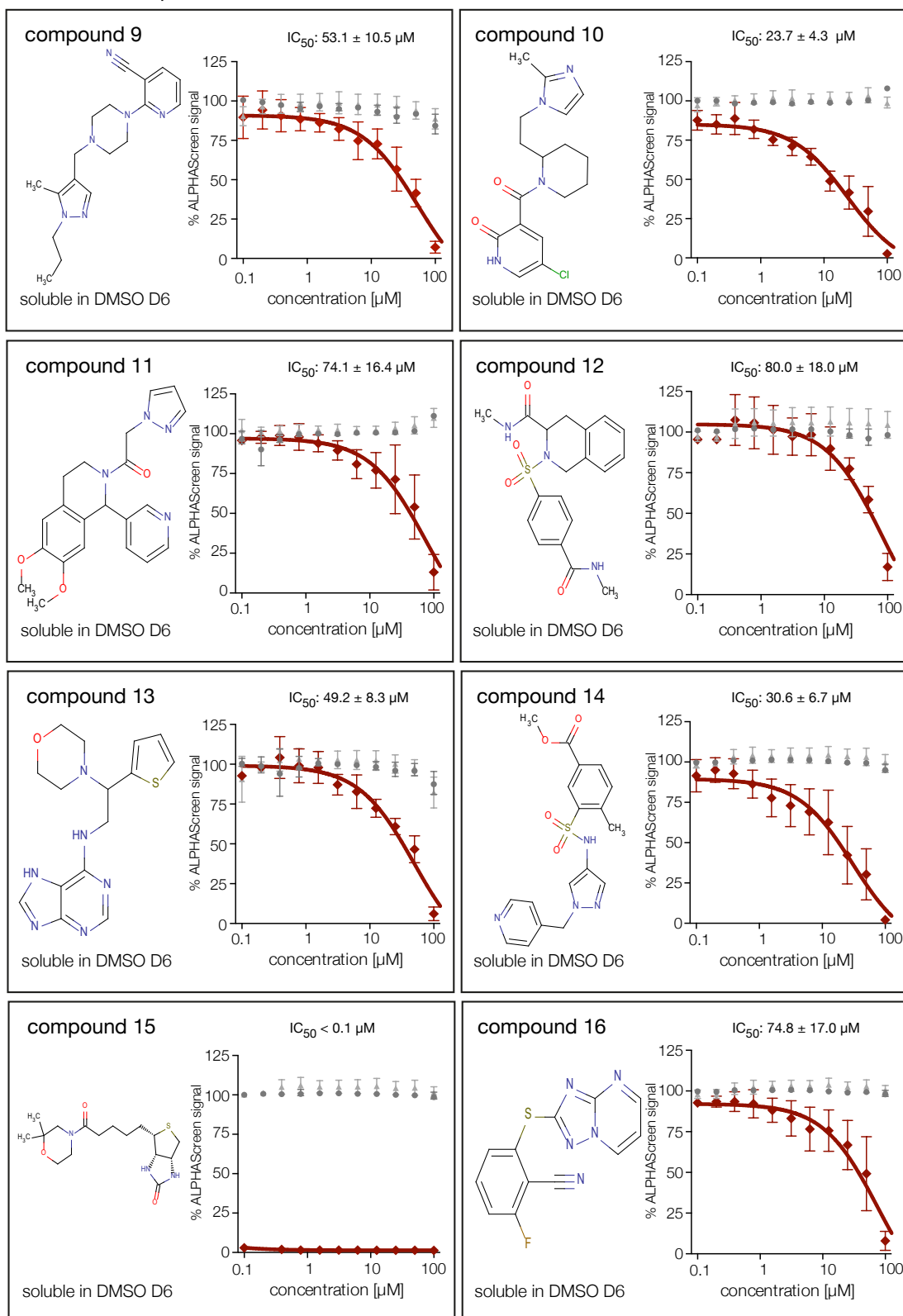
## 10 Supplement

◆ TRAF6<sub>WT</sub>StreptII - Ubc13FH    ▲ GST-OTUB1 - Ubc13FH    • GST-RNF8 - Ubc13FH



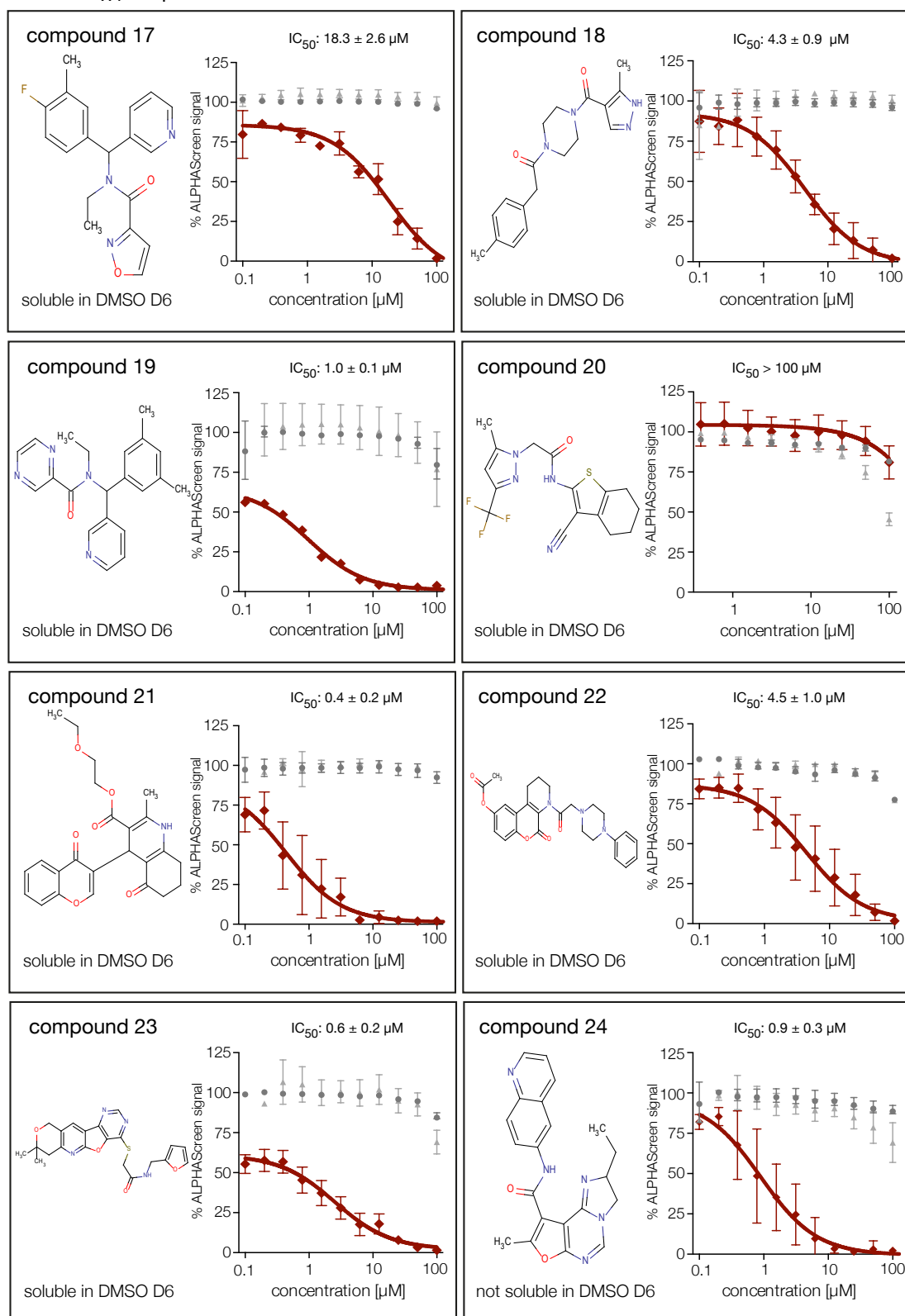
**Supplement 10.1: ALPHAScreen data of the reordered primary hit compounds 1-8.** All compounds impair the TRAF6<sub>WT</sub>StreptII-Ubc13FH interaction (displayed in red), whereas the interactions of GST-OTUB1 and GST-RNF8 to Ubc13FH remain unaffected.

◆ TRAF6<sub>WT</sub>StreptII - Ubc13FH ▲ GST-OTUB1 - Ubc13FH ● GST-RNF8 - Ubc13FH



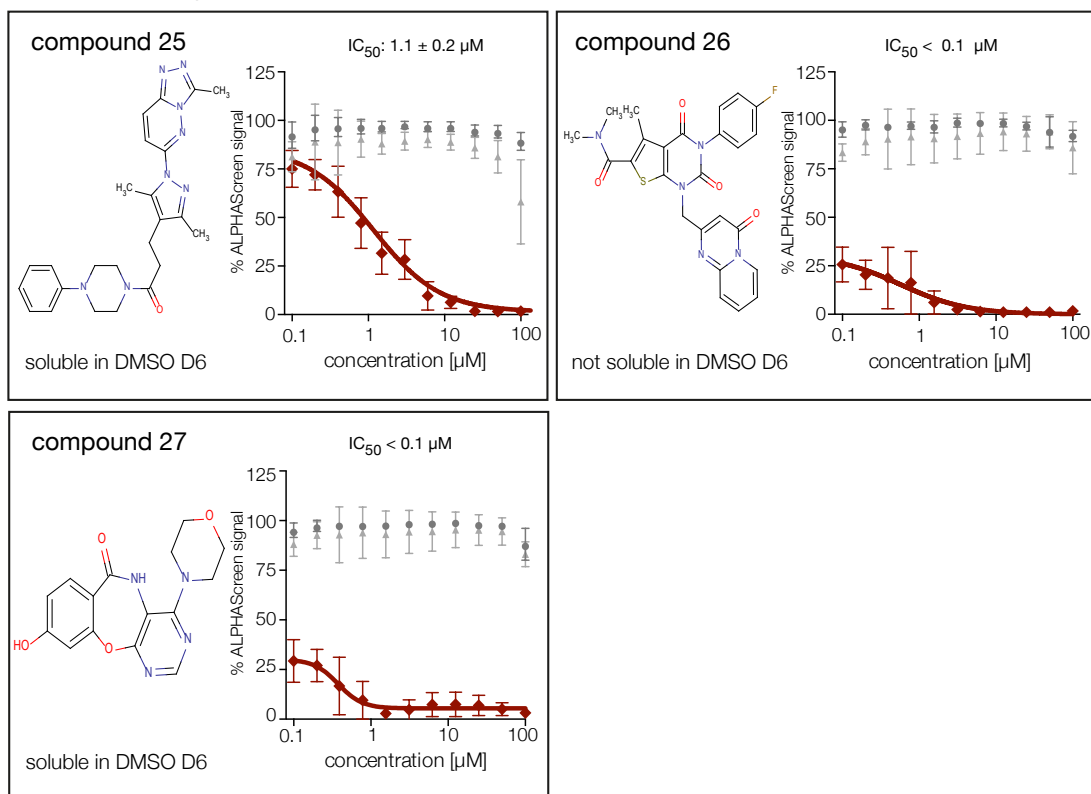
**Supplement 10.2: ALPHAScreen data of the reordered primary hit compounds 9-16.** All compounds impair the TRAF6<sub>WT</sub>StreptII-Ubc13FH interaction (displayed in red), whereas the interactions of GST-OTUB1 and GST-RNF8 to Ubc13FH remain unaffected.

◆ TRAF6<sub>WT</sub>StreptII - Ubc13FH    ▲ GST-OTUB1 - Ubc13FH    ● GST-RNF8 - Ubc13FH



**Supplement 10.3: ALPHAScreen data of the reordered primary hit compounds 17-24.** All small molecules except compound 20 impair the TRAF6<sub>WT</sub>StreptII-Ubc13FH interaction (displayed in red), whereas the interactions of GST-OTUB1 and GST-RNF8 to Ubc13FH remain unaffected (except compound 20).

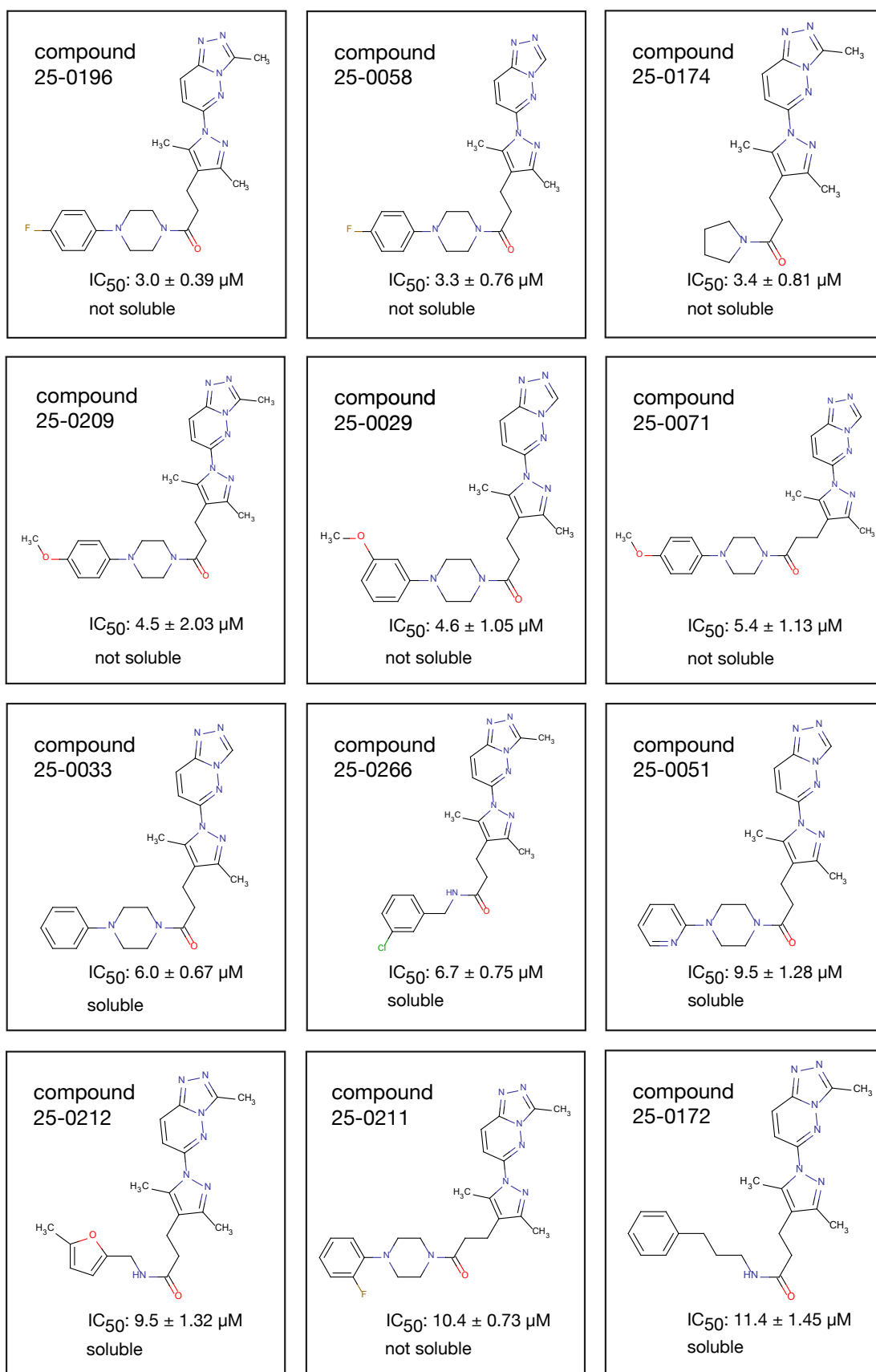
◆ TRAF6<sub>WT</sub>StreptII - Ubc13FH    ▲ GST-OTUB1 - Ubc13FH    ● GST-RNF8 - Ubc13FH



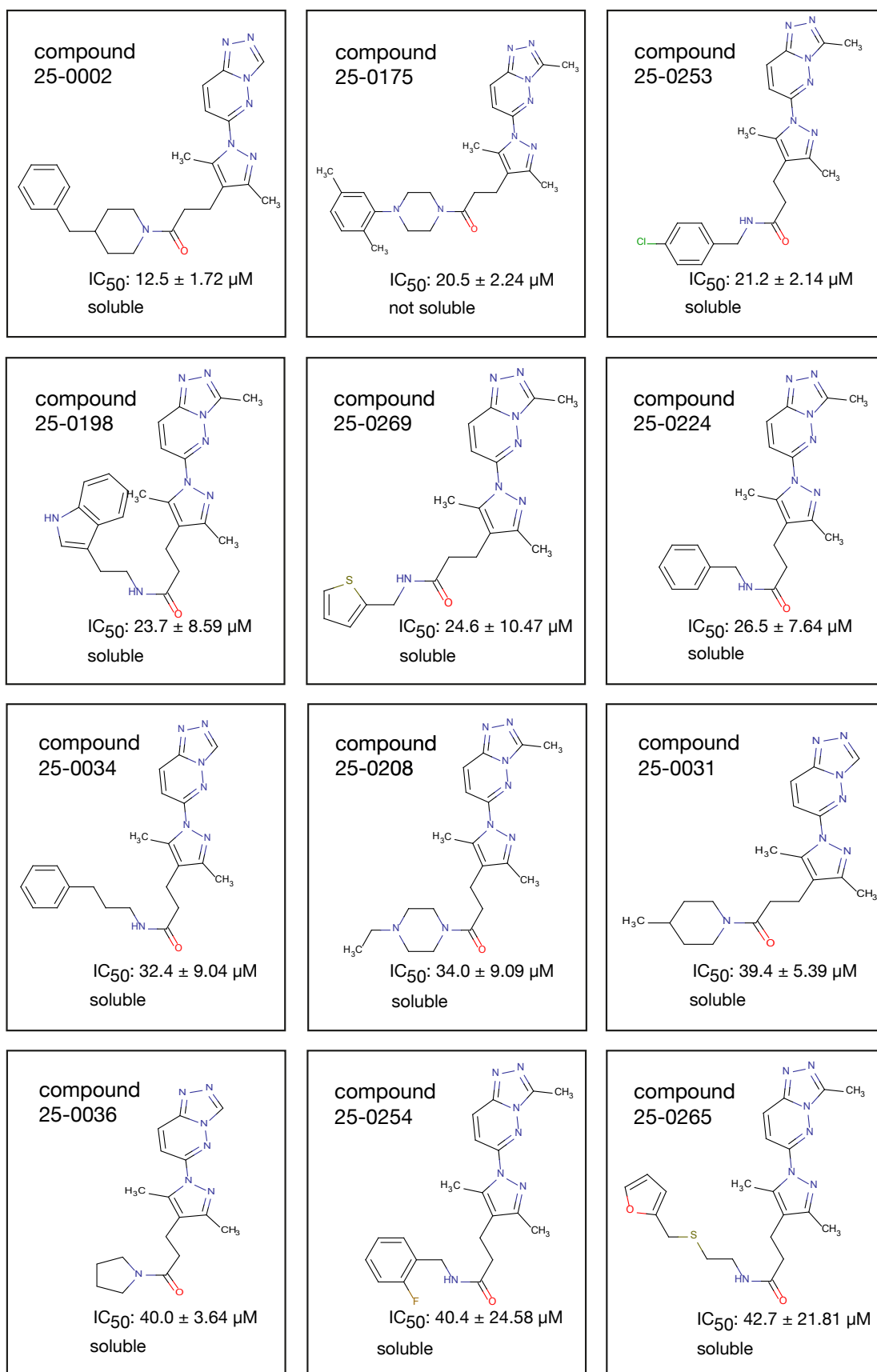
**Supplement 10.4: ALPHA Screen data of the reordered primary hit compounds 25, 26 and 27.** All compounds impair the TRAF6<sub>WT</sub>StreptII-Ubc13FH interaction (displayed in red), whereas the interactions of GST-OTUB1 and GST-RNF8 to Ubc13FH remain unaffected.

	stimulation	IL1 $\beta$		TNF $\alpha$	
	concentration [ $\mu$ M]	30,0	50,0	30,0	50,0
IRAK 1/4 inhibitor	experiment 1	78,6			
c1	experiment 1	18,8	9,7		
	experiment 2	66,9	61,1	133,3	96,5
c2	experiment 1	103,8	123,1		
	experiment 2	81,1	67,5	104,0	168,9
c3	experiment 1	96,7	122,0		
	experiment 2	79,1	66,5	129,0	102,1
c4	experiment 1	88,3	71,4		
	experiment 2	75,1	73,3	85,6	52,5
c5	experiment 1	83,2	73,2		
	experiment 2	80,4	112,6	83,5	78,1
c6	experiment 1	89,3	79,5		
	experiment 2	111,4	86,1	81,4	67,2
c7	experiment 1	85,7	83,9		
	experiment 2	86,4	75,9	115,0	114,5
c8	experiment 1	100,8	76,8		
	experiment 2	81,8	79,8	82,2	73,3
c9	experiment 1	89,5	68,6		
	experiment 2	103,8	82,8	112,5	85,5
	experiment 3	81,3	114,2	94,8	120,4
c10	experiment 1	80,2	68,2		
	experiment 2	59,6	17,6	15,7	13,1
c11	experiment 1	110,7	91,1		
	experiment 2	22,7	26,9	9,5	16,9
c12	experiment 1	80,1	94,7		
	experiment 2	74,7	52,2	81,0	110,9
c13	experiment 1	58,6	68,4		
	experiment 2	35,8	25,0	52,4	75,2
c14	experiment 1	62,3	67,6		
	experiment 2	23,7	14,5	71,7	72,2
c15	experiment 1	44,6	42,9		
	experiment 2	122,7	106,0	182,4	204,1
c16	experiment 1	53,9	68,1		
	experiment 2	79,9	126,9	91,1	70,8
c17	experiment 1	71,8	78,3		
	experiment 2	106,0	139,6	67,1	87,7
c18	experiment 1	66,8	78,3		
	experiment 2	136,2	154,2	96,9	84,2
c19	experiment 1	67,3	57,4		
	experiment 2	108,7	150,1	121,9	106,3
c20	experiment 1	101,2	100,1		
c21	experiment 1	101,0	105,0		
	experiment 2	100,6	129,5	135,7	168,4
c22	experiment 1	83,8	83,2		
	experiment 2	61,2	69,1	138,7	194,6
c23	experiment 1	86,11955	91,43879		
	experiment 2	33,4	32,5	76,9	69,8
c24	experiment 1	80,7	74,4		
	experiment 2	45,9	34,5	125,8	91,6
c25	experiment 1	46,9	43,8		
	experiment 2	33,0	24,0	125,8	95,5
c26	experiment 1	100,9	93,3		
	experiment 2	74,4	76,5	119,7	151,0
c27	experiment 1	5,9	2,1		
	experiment 2	19,8	12,0	13,8	19,6
	experiment 3	3,4	3,3		

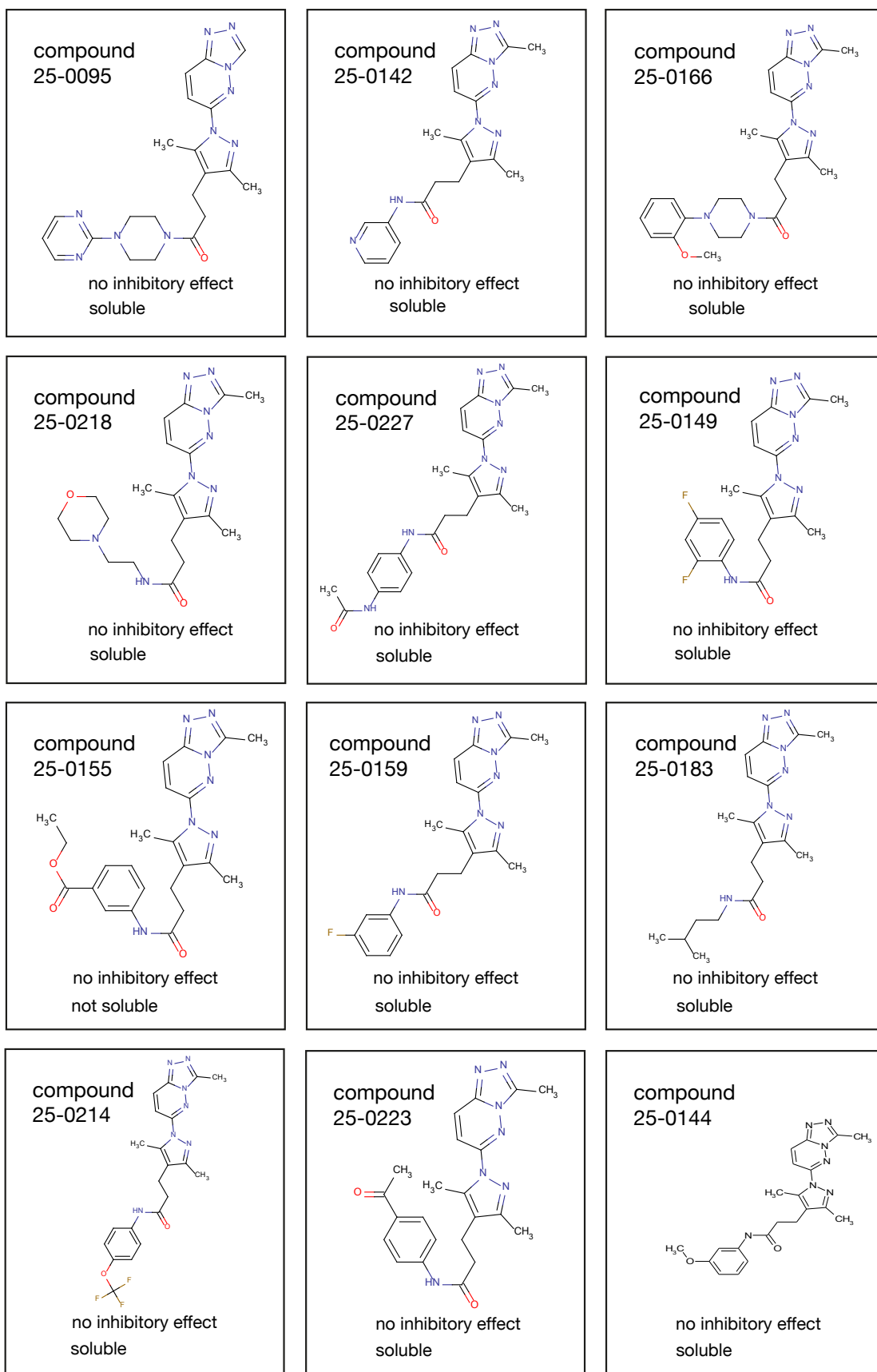
**Supplement 10.5:**  
**Quantification of NF- $\kappa$ B activation in EMSA experiment of all primary hit compounds after IL-1 $\beta$  and TNF $\alpha$  stimulation.**  
 Displayed are all single quantified EMSA experiments after IL-1 $\kappa$  and TNF $\kappa$  stimulation. Values represent % NF- $\kappa$ B activation and are normalized to DMSO treated control MEF cells. Compounds marked in light grey exhibit an IL-1 $\beta$  specific effect on NF- $\kappa$ B activation.



**Supplement 10.6: Compound structures,  $IC_{50}$  and solubility data of the SAR analysis of C25 in ALPHAScreen experiments.**  $IC_{50}$  values represent the effect of each compound on TRAF6<sub>WT</sub>StrepII-Ubc13FH interaction. Bindings of GST-OTUB1 and GST-RNF8 to Ubc13FH remain unaffected (except for 25-0212).

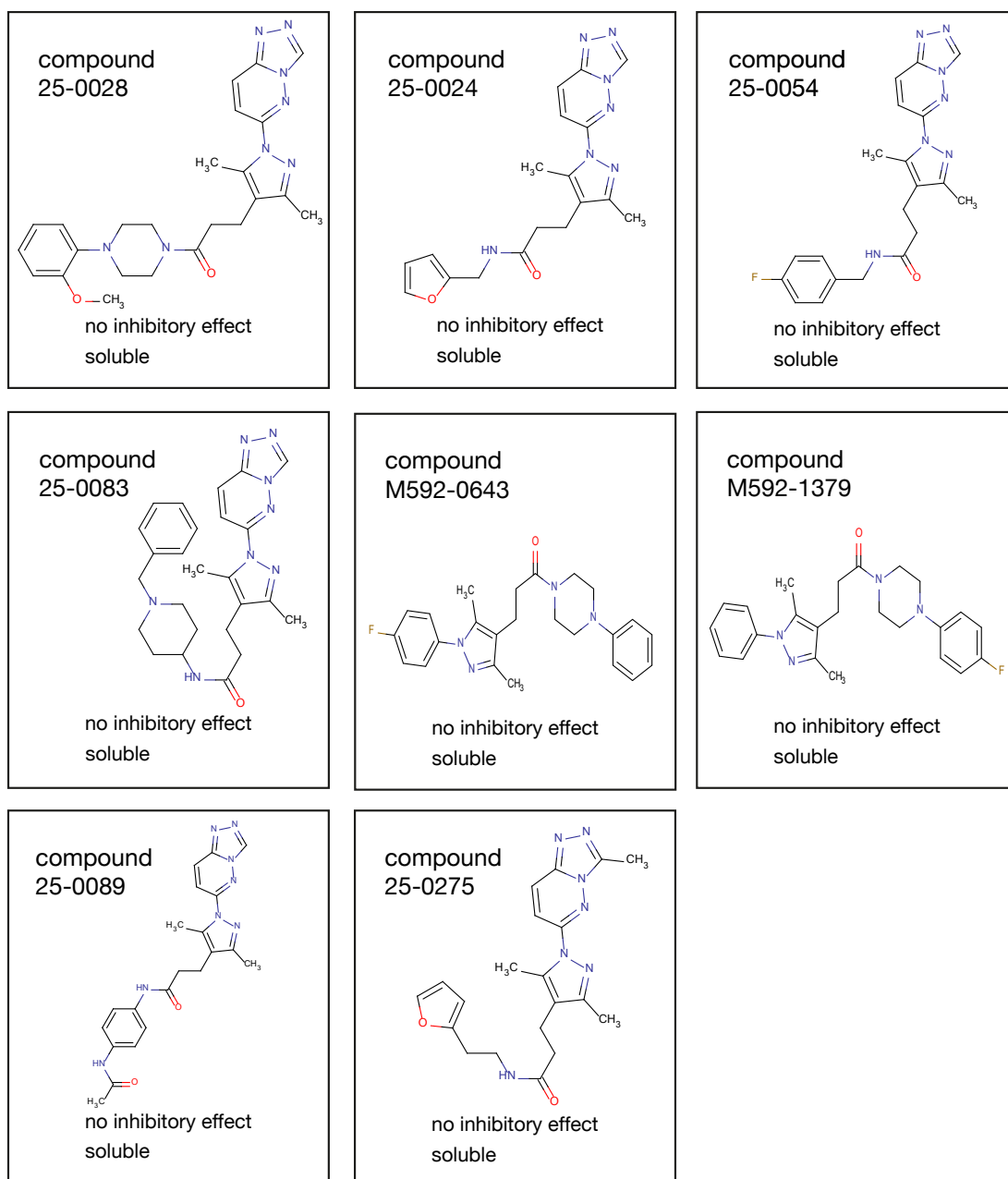


**Supplement 10.7: Compound structures, IC<sub>50</sub> and solubility data of the SAR analysis of C25 in ALPHAScreen experiments.** IIC<sub>50</sub> values represent the effect of each compound on TRAF6<sub>WT</sub>StrepII-Ubc13FH interaction. Bindings of GST-OTUB1 and GST-RNF8 to Ubc13FH remain unaffected.



**Supplement 10.8: Compound structures and solubility data of the SAR analysis of C25 in ALPHAScreen experiments.** Depicted compounds did not show inhibitory effects on TRAF6<sub>WT</sub>StrepII-Ubc13FH interaction. Bindings of GST-OTUB1 and GST-RNF8 to Ubc13FH remain unaffected as well.



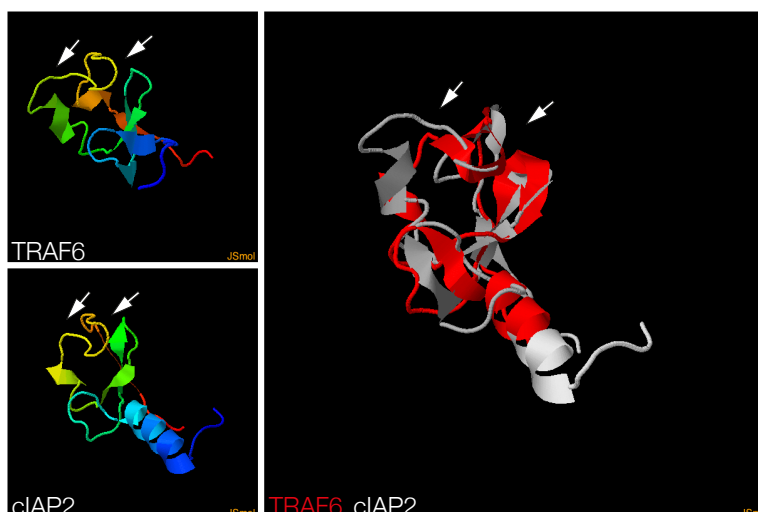


**Supplement 10.9: Compound structures and solubility data of the SAR analysis of C25 in ALPHAScreen experiments.** Depicted compounds did not show inhibitory effects on TRAF6<sub>WT</sub>StreptII-Ubc13FH interaction. Bindings of GST-OTUB1 and GST-RNF8 to Ubc13FH remain unaffected as well.

**A**

Alignment  
**TRAF6 RING**  
 (2jmd\_.pdb 63 amino acids)  
 with **ciAP2 RING**  
 (3eb5\_.pdb 65 amino acids)

alignment-length	63
Twists	0
equivalent positions	55
opt-rmsd	3.15
chain-rmsd	1.77
P-value	1.38e-02

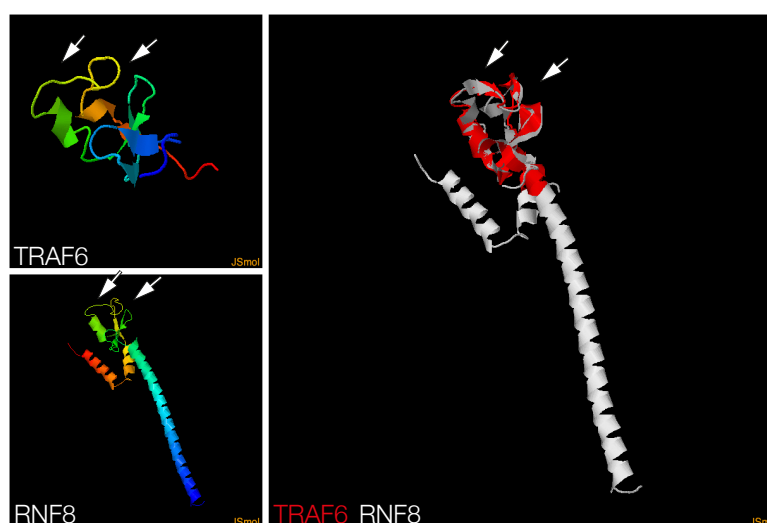
**B**

**Supplement 10.10: Structural alignment of the RING domains of TRAF6 and ciAP2.** TRAF6 (PDB: 2jmd) and ciAP2 (PDB: 3eb5) were aligned using the FATCAT software provided by the Godzik laboratory. (A) Calculations of parameters to define the similarity between the RING domains of TRAF6 and ciAP2. opt-rmsd = root mean square deviation with structural rearrangements; chain-rmsd = root mean square deviation without structural rearrangements. (B) Superposition of TRAF6 and ciAP2 RING domains in two different views.

**A**

Alignment  
**TRAF6 RING**  
 (2jmd\_.pdb 63 amino acids)  
 with **RNF8 RING**  
 (4ayc\_.pdb 136 amino acids)

alignment-length	62
Twists	0
equivalent positions	59
opt-rmsd	3.05
chain-rmsd	1.55
P-value	2.04e-04

**B**

**Supplement 10.11: Structural alignment of the RING domains of TRAF6 and RNF8.** TRAF6 (PDB: 2jmd) and RNF8 (PDB: 4ayc) were aligned using the FATCAT software provided by the Godzik laboratory. (A) Calculations of parameters to define the similarity between the RING domains of TRAF6 and RNF8. opt-rmsd = root mean square deviation with structural rearrangements; chain-rmsd = root mean square deviation without structural rearrangements. (B) Superposition of TRAF6 and RNF8 RING domains in two different views.

## **11.1 Publications**

Vincendeau, M., Nagel, D., **Brenke, J. K.**, Brack-Werner, R. and Hadian, K. (2013). „Heterogenous nuclear ribonucleoprotein Q increases protein expression from HIV-1 Rev-dependent transcripts.“ *Virology*, 10, 151.

Schorpp, K., Rothenaigner, I., Salmina, E., Reinshagen, J., Low, T., **Brenke, J. K.**, Gopalakrishnan J, Tetko I. V., Gul S. and Hadian, K. (2013). „Identification of Small-Molecule Frequent Hitters from AlphaScreen High-Throughput Screens.“ *J Biomol Screen*, 19(5), 715-726.

Manuscript in preparation:

Vincendeau, M., Hadian K., Messias A., Halander J., **Brenke J. K.**, Griesbach R., Greczmiel U., Bertossi A., Stehle R., Nagel D., Velvarska H., Niessing D., Demski K., Geerlof A., Sattler M. and Krappmann D. “Small Molecule Inhibition of NEMO-Ubiquitin binding disrupts NF- $\kappa$ B survival signaling.”

## **11.2 Curriculum Vitae**

### **Personal Details**

Name            Jara Kerstin Brenke  
Born            February 27, 1987 in Freiberg  
Citizenship    German  
Residing in    Munich, Germany

### **Education**

#### **January 2011 to present**

Dissertation at the Helmholtz Zentrum München, Institute of Molecular Toxicology and Pharmacology – Assay Development and Screening, Dr. Kamyar Hadian

„Targeting the TRAF6-Ubc13 interaction for therapeutic intervention“  
Doctoral adviser: Prof. Dr. Daniel Krappmann

#### **August to December 2010**

Internship at the University of Michigan, Ann Arbor, Department of Internal Medicine – Nephrology, Markus Bitzer, M.D, Assistant Professor

#### **October 2005 to July 2010:**

Studies in Biology at the Ludwig-Maximilians-Universität München

Degree: Diploma (final grade: 1.3)

Diploma thesis at the Institute of Virology at the Helmholtz Zentrum München, Prof. Dr. Ruth Brack-Werner: „Identification of HIV-1 Rev-interacting cellular host factors

#### **1998 to 2005:**

Geschwister-Scholl-Gymnasium Freiberg, Germany  
Degree: Abitur (final grade: 2.0)

### **11.3 Acknowledgement**

I want to thank my doctoral advisor Prof. Daniel Krappmann for providing this topic, critical reading of this thesis and the support during the last four years.

I also want to express my gratitude to the members of the thesis committee for their time reviewing my thesis: Prof. Elisabeth Weiß, Prof. Heinrich Jung, Prof. Ruth Brack-Werner and Prof. Charles David.

I gracefully acknowledge Kamyar Hadian and appreciate all his time, ideas and funding to make this work possible. It was an honor to be his first Ph.D. student. I want to thank him and Michelle Vincendeau for their great scientific and non-scientific support, encouragement and sympathy in every condition of life.

The members of my HELENA thesis committee Prof. Mathias Heikenwälder and Prof. Stefan Jentsch I want to thank for their time and the discussions contributing to my work.

Thanks to all collaboration partners for their great expertise, time and resources to perform the experiments: Dr. Manfred Rösner, Dr. Grzegorz Popowicz, Dr. Paul Pfluger, Dr. Timo Müller, Dr. Christoffer Clemmensen and Katrin Firscher.

A special thanks goes to members of the Hadian group: Stefanie Brandner, Scarlett Dornauer, Larissa Ringelstetter, Ina Rothenaigner, Kenji Schorpp and Elisabeth Weber. Thanks for the patience, constant support and discussions. Thank you all so much for making the last four years such a great experience (scientifically and non-scientifically related).

I want to thank the present and former members of the Krappmann lab (Arianna Bertossi, Miriam Bogner, Katrin Demski, Andrea Eitelhuber, Torben Gehring, Richard Grießbach, Daniela Hlala, Bernhard Kloo, Isabel Meininger, Daniel Nagel and Gisela Schimmack) as well as „Maggie“ Chia-Hua Ho and Andrea Takacs for their constant help and cooperation.

Besonderer Dank gebührt meiner Familie, die mich durch alle Höhen und Tiefen der letzten Jahre bedingungslos begleitet haben. Danke für euer Verständnis, eure Unterstützung, materiell wie auch immateriell, Liebe sowie Treue und Glauben an mich. Es ist schön zu wissen, dass wir füreinander da sind.

Meinen Mädels, egal ob nah oder fern, danke ich für ihre treue Freundschaft, Aufmunterung und Ablenkung in jeglicher Form wann immer es nötig war.



## Eidesstattliche Erklärung

Ich versichere hiermit an Eides statt, dass die vorgelegte Dissertation von mir selbständig und ohne unerlaubte Hilfe angefertigt ist.

München, den .....26.2.2015.....

Jara Brenke .....

(Unterschrift)

## Erklärung

Hiermit erkläre ich, \*

☐ dass die Dissertation nicht ganz oder in wesentlichen Teilen einer anderen Prüfungskommission vorgelegt worden ist.

☐ dass ich mich anderweitig einer Doktorprüfung ohne Erfolg **nicht** unterzogen habe.

☐ dass ich mich mit Erfolg der Doktorprüfung im Hauptfach .....  
und in den Nebenfächern .....  
bei der Fakultät für ..... der .....  
(Hochschule/Universität)  
unterzogen habe.

☐ dass ich ohne Erfolg versucht habe, eine Dissertation einzureichen oder mich der Doktorprüfung zu unterziehen.

München, den.....26.2.2015.....

Jara Brenke .....

(Unterschrift)

\*) Nichtzutreffendes streichen

